SPR-699 FEBRUARY 2018

Materials, Properties, and Optimum Geometries of the Design of Noise Walls

Arizona Department of Transportation Research Center

ADOT

Materials, Properties, and Optimum Geometries of the Design of Noise Walls

SPR-699
February 2018

Prepared by:
Paul Donavan and Carrie Janello
Illingworth & Rodkin, Inc.
1 Willowbrook Court, Suite 120
Petaluma, CA 94954

Contributing Authors:
Dana Lodico
Lodico Acoustics, LLC
355-C Inverness Drive
Englewood, CO 80112

Stephen Shaffer
Independent Consultant
Tempe, AZ

Sergey I. Voropayev
Harindra J. S. Fernando
Department of Civil and Environmental Engineering and Earth Sciences
University of Notre Dame
Notre Dame, IN 46556

Nicholas C. Ovenden
Department of Mathematics
University College London
Gower Street
London WC1E 6BT
United Kingdom

Prepared for:
Arizona Department of Transportation
206 South 17th Avenue
Phoenix, Arizona 85007
In cooperation with
U.S. Department of Transportation
Federal Highway Administration

This report was funded in part through grants from the Federal Highway Administration, U.S. Department of Transportation. The contents of this report reflect the views of the authors, who are responsible for the facts and the accuracy of the data, and for the use or adaptation of previously published material, presented herein. The contents do not necessarily reflect the official views or policies of the Arizona Department of Transportation or the Federal Highway Administration, U.S. Department of Transportation. This report does not constitute a standard, specification, or regulation. Trade or manufacturers' names that may appear herein are cited only because they are considered essential to the objectives of the report. The U.S. government and the State of Arizona do not endorse products or manufacturers.

1. Report No.	2. Government Accession No.	3. Recipient's Catalog No.
FHWA-AZ-18-699		

4. Title and Subtitle	5. Report Date
Materials, Properties, and Optimum Geometries of the Design of Noise Walls	February 2018
	6. Performing Organization Code

7. Author	8. Performing Organization Report No.
Paul Donavan, Carrie Janello, Dana Lodico, Stephen Shaffer, Sergey Voropayev, Harindra Fernando, and Nicholas Ovenden	

9. Performing Organization Name and Address	10. Work Unit No.
Illingworth & Rodkin, Inc. 1 Willowbrook Court, Suite 200 Petaluma, California 94954 Department of Civil and Environmental Engineering and Earth Sciences University of Notre Dame Notre Dame, IN 46556	11. Contract or Grant No. SPR 000-1((679) 699

12. Sponsoring Agency Name and Address	13.Type of Report & Period Covered
Arizona Department of Transportation 206 S. 17th Avenue Phoenix, Arizona 85007	Final Report, 2013-2018
	14. Sponsoring Agency Code

15. Supplementary Notes

Project performed in cooperation with the Federal Highway Administration

16. Abstract

This research addressed barrier design features that could enhance noise wall performance. It was concluded that application of a horizontal T-top to a conventional straight vertical wall was the most promising. This was established through literature review, scale model testing, and meetings with noise wall suppliers. Field measurements of noise levels and meteorological conditions were conducted over a three-period behind a noise wall exposed to traffic noise. The variation in average noise level from one session average to another was as much as 7.4 dB. Temperature was found to the primary parameter related to the variation. Wind typically increases noise level variation; however, the wind was light and not variable over the measurement period. An approach to analytically modeling the variation in noise level with meteorological conditions was developed. This included a combination of Boundary Element Modeling near the noise wall with parabolic equation methods and Computational Fluid Dynamics used for more distant locations.

17. Key Words	18. Distribution Statement	23. Registrant's Seal
Noise walls, highway traffic noise, noise measurement, sound propagation, meteorological effects	This document is available to the US public through the National Technical Information Service, Springfield, Virginia 22161	

19. Security Classification	20. Security Classification	21. No. of Pages	22. Price
Unclassified	Unclassified	164	

SI* (MODERN METRIC) CONVERSION FACTORS

APPROXIMATE CONVERSIONS TO SI UNITS

Symbol	When You Know	Multiply By	To Find	Symbol
		LENGTH		
in	inches	25.4	millimeters	mm
ft	feet	0.305	meters	m
yd	yards	0.914	meters	m
mi	miles	1.61	kilometers	km
		AREA		
in^2	square inches	645.2	square millimeters	mm^2
ft^2	square feet	0.093	square meters	m^2
yd^2	square yard	0.836	square meters	m^2
ac	acres	0.405	hectares	ha
mi^2	square miles	2.59	square kilometers	km^2
		VOLUME		
fl oz	fluid ounces	29.57	milliliters	mL
gal	gallons	3.785	liters	L
ft^3	cubic feet	0.028	cubic meters	m^3
yd^3	cubic yards	0.765	cubic meters	m^3
		NOTE: volumes greater than 1000 L shall be shown in m^3		
		MASS		
oz	ounces	28.35	grams	g
lb	pounds	0.454	kilograms	kg
T	short tons (2000 lb)	0.907	megagrams (or "metric ton")	Mg (or "t")
		TEMPERATURE (exact degrees)		
°F	Fahrenheit	5 (F-32)/9 or (F-32)/1.8	Celsius	°C
		ILLUMINATION		
fc	foot-candles	10.76	lux	lx
fl	foot-Lamberts	3.426	candela/m^2	cd/m^2
		FORCE and PRESSURE or STRESS		
lbf	poundforce	4.45	newtons	N
lbf/in^2	poundforce per square inch	6.89	kilopascals	kPa

APPROXIMATE CONVERSIONS FROM SI UNITS

Symbol	When You Know	Multiply By	To Find	Symbol
		LENGTH		
mm	millimeters	0.039	inches	in
m	meters	3.28	feet	ft
m	meters	1.09	yards	yd
km	kilometers	0.621	miles	mi
		AREA		
mm^2	square millimeters	0.0016	square inches	in^2
m^2	square meters	10.764	square feet	ft^2
m^2	square meters	1.195	square yards	yd^2
ha	hectares	2.47	acres	ac
km^2	square kilometers	0.386	square miles	mi^2
		VOLUME		
mL	milliliters	0.034	fluid ounces	fl oz
L	liters	0.264	gallons	gal
m^3	cubic meters	35.314	cubic feet	ft^3
m^3	cubic meters	1.307	cubic yards	yd^3
		MASS		
g	grams	0.035	ounces	oz
kg	kilograms	2.202	pounds	lb
Mg (or "t")	megagrams (or "metric ton")	1.103	short tons (2000 lb)	T
		TEMPERATURE (exact degrees)		
°C	Celsius	1.8C+32	Fahrenheit	°F
		ILLUMINATION		
lx	lux	0.0929	foot-candles	fc
cd/m^2	candela/m^2	0.2919	foot-Lamberts	fl
		FORCE and PRESSURE or STRESS		
N	newtons	0.225	poundforce	lbf
kPa	kilopascals	0.145	poundforce per square inch	lbf/in^2

*SI is the symbol for the International System of Units. Appropriate rounding should be made to comply with Section 4 of ASTM E380.
(Revised March 2003)

CONTENTS

LIST OF FIGURES

LIST OF TABLES

LIST OF ACRONYMS, ABBREVIATIONS, AND SYMBOLS

2D ..... Two dimensional

AASHTO ..... American Association of State Highway and Transportation Officials

ADOT ..... Arizona Department of Transportation

ARFC..... **A**sphalt rubber friction course

BEM ..... Boundary Element Model

B&K ..... Brüel and Kjaer

°C ..... Degree Centigrade

CTIM ..... Continuous-flow time-integrated method

dB ..... Decibel

dBA ..... A-weighted decibel

DD ..... Doubling of distance

Δ ..... Delta

^{o}F ..... Degree Fahrenheit

FFT ..... Fast Fourier Transform

FHWA ..... Federal Highway Administration

ft ..... Foot/feet

h ..... Hour

Hz ..... Hertz

IL ..... Insertion loss

km ..... Kilometer

L_{eq} ..... Equivalent sound level

m ..... Meter

mm ..... Millimeter

m/s ..... Meters per second

mph ..... Miles per hour

NCHRP ..... National Cooperative Highway Research Program

OB ..... Octave band

OBSI ..... On-board sound intensity

QPPP ..... Quiet Pavement Pilot Program

R^2 ..... Coefficient of determination

RTA ..... Real Time Analyzer

SLM ..... Sound level meter

TNM ..... Traffic Noise Model

U.S. ..... United States

EXECUTIVE SUMMARY

Residents of Arizona have been concerned about traffic noise from their freeway systems. This concern has been addressed by ADOT in several ways including research into quieter pavements, extensive application of asphalt rubber friction course (ARFC) as an overlay of existing and new concrete roadways as part of the Arizona Quiet Pavement Pilot Program (QPPP), the design and implementation of aesthetically appealing highway noise walls, and research into the effects of environmental conditions on sound propagation. Although the use of ARFC overlays has drawn significant favorable response from the public in the greater Phoenix area, construction of noise walls continues to be a major element of highway noise abatement for ADOT, so optimizing barrier designs for cost and noise reduction performance remains an important issue.

Research into barrier designs for enhanced insertion loss performance falls into three groupings: absorptive top edge designs of various shapes, barrier additions designed to improve the diffraction at the top edge of the barrier, and devices to create interference between sounds of different path length in the vicinity of the top of the barrier. Although many of these have demonstrated some promise in potentially improving highway noise barrier performance, it is difficult to actually evaluate each concept on an equal basis due to varying evaluation methods. As a result, there was a need to collect and consolidate published information, perform testing of the more promising technologies to produce a set of consistent and directly comparable results, and determine recommended designs for full field testing.

Another aspect of barrier design is the effect that atmospheric conditions have on ability of the barrier to reduce noise. In the metropolitan Phoenix area, residents have complained that noise reduction provided by barriers was not “effective” in the winter months. In earlier ADOT Research, It was found temperature inversions in that time of the year can produce measurable increases in traffic noise levels by as much as 10 dB. Wind is also known to affect barrier performance by creating diffraction that reduces the insertion loss creating higher noise levels for receptors normally in the barrier shadow zone. In evaluating enhanced and conventional barrier designs, prediction the performance of the barrier under a range of atmospheric conditions is of concern.

The first aspect of the research was to identify and assess design features that could enhance barrier performance. After reviewing the literature and then meeting with different barrier manufacturers to identify more novel concepts, more promising barrier configurations were evaluated using acoustic scale model testing. Model testing was an efficient method of evaluating barrier enhancing concepts with less expense than field testing. The model results led to the recommendation of further field evaluation of a T-top barrier design in which a horizontal surface is added to the top of the barrier. Other barrier treatments that rely on sound interference at the top edge of the barrier were not effective. Application of T-top designs was concluded to be most promising when the height of a barrier is constrained.

The second aspect of the research was to investigate the effects of meteorological conditions on barrier performance through field and analytical studies. The field measurements were conducted over three day period with eight sessions at different times of the day behind a 14 feet high barrier in a park adjacent to the Agua Fria Freeway. Within individual sessions, the variation in barrier performance was up to 6.8 dB while variation was up 7.4 dB between sessions. The variation correlated well with air temperature, however, the winds perpendicular to the barrier were quite low over the three days of testing. To model the effect of meteorological conditions on highway sound propagation, a hybrid modeling approach was defined. Close to the barrier, Boundary Element modeling would be used to define the acoustic field and parabolic equation methods and Computational Fluid Dynamcis would be used to examine the more distant effects meteorological conditions on sound propagation.

CHAPTER 1: INTRODUCTION

Over the past few decades, residents of Arizona have been concerned about traffic noise from their freeway systems. This concern has been addressed by ADOT in several ways, including research into quieter pavements (Donavan and Rymer 2010); extensive application of asphalt rubber friction course (ARFC) as an overlay of existing and new concrete roadways, which is part of the Arizona Quiet Pavement Pilot Program (QP3) (Scofield and Donavan 2005); the design and implementation of aesthetically appealing highway noise walls; and research into the effects of environmental conditions on sound propagation (Saurenman et al. 2005). Although the use of ARFC overlays has drawn significant favorable response from the public in the greater Phoenix area, construction of noise walls continues to be a major element of highway abatement for ADOT. For this reason, optimizing barrier designs for cost and noise reduction performance remains an important issue. Another aspect of barrier performance is the variation of noise reduction performance with varying meteorological conditions. Residents in the greater Phoenix have complained about increased traffic noise under conditions particularly in the winter months. Previous ADOT research has documented the influence of temperature inversions on increasing traffic noise, which can occur both in open conditions and behind sound walls (Saurenman et al. 2005). Similar to temperature inversions, wind gradients in downwind conditions (wind from source to receiver) is also known to increase traffic noise both with and without sound walls (Lodico and Reyff 2009). The primary objectives of this research were: 1) identify materials and designs that may have advantages over traditional, reflective noise walls; 2) measure and assess effects of meteorological conditions on barrier performance for an existing sound wall; 3) evaluate alternative sound wall designs based on the acoustic scale model testing; and 4) recommend methods for analytically assessing the effect of wind on barrier performance.

This research was conducted in two phases. In Phase I, potential innovative design information was collected and reviewed by means of a literature review and meeting with individual fabricators of sound walls. Also in the first phase, field measurements were conducted on an existing sound wall to compare with theoretical analysis and the Federal Highway Administration (FHWA) Traffic Noise Model (TNM) and to examine the effect of meteorology on barrier performance. At the end of Phase I, recommendations were developed for designs that should be considered experimentally and analytically in Phase II. The research in Phase II included quantifying the noise performance of different sound wall top edge geometries and developing a recommendation for an analytical approach to modeling the changes in barrier performance under different wind conditions.

CHAPTER 2: TECHNOLOGY REVIEW

LITERATURE SEARCH RESULTS

Enhancing the noise reducing performance of noise walls has been a topic of interest for 25 years or more. The most common approach is to add sound absorption to the traffic side of the noise wall either by barrier material selection or by the addition of material to an existing wall. Under specific conditions, such as parallel walls lining both sides of a highway and elevated receiver locations, added absorption has been calculated to provide as much as a 5 dB reduction for some receiver locations (Donavan and Lodico 2013). Many sound wall manufacturers now offer barriers with absorptive materials applied to the face of a barrier for use in an outdoor highway environment, and in some states, absorptive barriers are used routinely. A somewhat related method is to tilt the noise walls by as little as 3° to as much as 15° in order to reflect the sound upward (Pigasse and Kragh 2011). Another approach examined extensively in the literature is to add something to the top of noise wall. Many of these approaches identified and summarized as a result of a literature review reported to ADOT in FHWA-AZ-06-572 (Watson 2006), which was completed in 2006. In this report, many innovative barrier designs were identified, and their potential was assessed for implementation in Arizona. The report compared 12 general barrier types based on their acoustical performance, availability/economic considerations, and constructability. Based on this assessment, two barrier designs were recommended for consideration: T-top Barrier with absorptive material on top of the T, and a vertical barrier with absorptive material on the face. The T-top geometry has been advocated repeatedly, particularly with absorption added to the top of the "T". This configuration was one of two recommended in the literature analysis performed for ADOT in 2006 (Watson 2006), and again in another extensive literature analysis, performed by the Danish Road Institute in 2011 (Pigasse and Kragh 2011).

Additions and modifications to the top of noise walls along the lines of innovating designs fall into three groupings. These included absorptive top edge designs of various shapes (Kawai and Toyoda 2012, Kawai 2012, Hasebe 2007, Okubo and Yamamoto 2006, Domingues et al. 2010), barrier additions designed to improve the diffraction at the top edge of the barrier (Yoon, et al. 2012, Auerbach et al. 2009, Okubo et al. 2009, Boone 2009, Okubo et al. 2007, Gharabegian 2006), and devices to create interference between sounds of different path length in the vicinity of the top of the barrier (Kang et al. 2011, Kim et al. 2011). These approaches can be done separately or in combination, as illustrated in Figure 1. Most of the studies documenting the performance of these design approaches were conducted using analytical or acoustic scale modelling methods. The analytical studies were typically done using two dimensional (2D) Boundary Element Methods (BEM). The acoustic model studies were done in scales typically ranging from about 10 to 1 to full scale. All of the modeling, either analytical or scale, used only a single point source. For a single point source, the sound over the barrier even by different paths is coherent, allowing for interference effects to occur. In reality, traffic is made up of many individual, incoherent point sources that are best represented as an incoherent line source (Lyon 1973). As a result, the sound arriving at the edge of the barrier comes from many directions and is not correlated in space or time, minimizing the possibility of the destructive interference. This does not diminish the computer and scale model results in providing direction on treatments to pursue; however, predicted insertion losses from these models will likely never be realized in the field. The largest improvements in barrier performance are typically predicted by 2D BEM (up to 30 dB). Scale model studies with single point sources more typically indicate reductions of 7 to 10 dB, while full size model results can be as great as 7 dB for a point source. Actual field try-outs of wall top modifications for actual traffic noise more typically are in the range of 1 to 2 dB for improvement, compared to a conventional noise wall.

Many of the basic T-Top design have been investigated using the BEM, as described above, where the absorptive material is replaced by "wells" (a comb-like cross section) of varying depth that improve T-Top performance, essentially by interference effects (Monazzam and Lam 2005, Hasebe 2012, Hasebe

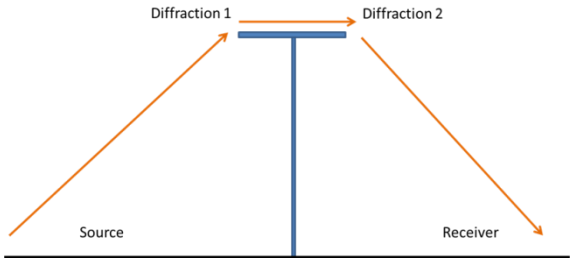

Example of performance improvement by multiple diffractions

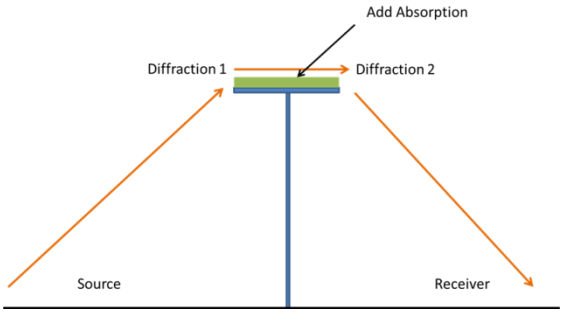

Example of performance improvement with added absorption

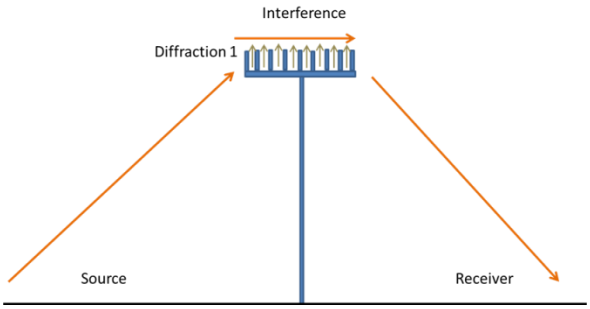

Example of performance improvement by interference of sound

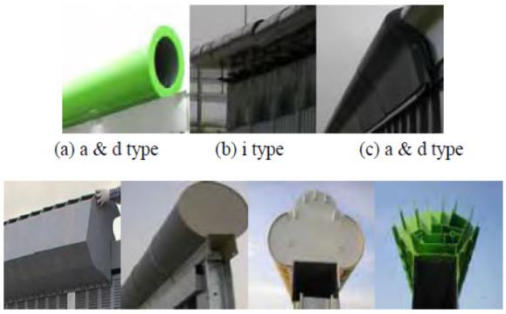

Examples of complex top additions featuring interference, diffraction, and/or absorption (Ref. 15)

Figure 1. Different Types of Barrier Top Treatments

2012), Diez et al. 2012. Scale modelling has been conducted to verify BEM models in some cases, with results generally tracking those of the BEM models. A T-Top design barrier was recently installed in Golden, Colorado, which is likely one of the first built in the U.S. Unfortunately, full-scale field measurements without and with the top were not possible; however, a reduced size experimental evaluation of the concept indicated improvements of 3 to 4 dB at distances of 1.7 to 3.5 times the wall height away (Lodico and Goldberg 2010). These tests also demonstrated that additional reductions of about 1½ dB could be made with the addition of absorbing material to the top of the T. In another study, field testing on a shaped barrier, similar to a 'T', using a traffic noise source found improvements of only .5 to 1 dB (Diez et al. 2012).

Like the T-top, many of the other most promising barrier designs include absorptive material, either on the face or top of the barrier (Donavan and Lodico 2013, Hasebe 2007, Cohn and Harris 1996). Many sound wall manufacturers now offer barriers with absorptive materials applied to the face of a barrier for use in an outdoor highway environment (Donavan and Lodico 2013). However, sound-absorbing materials placed on top of a barrier may have additional maintenance concerns, as precipitation and debris could fall directly onto the absorptive material, changing the material properties and causing difficulties with maintaining the noise reduction properties of the material. The Colorado study (Lodico and Goldberg 2010) found that fiberglass insulation installed on the top of a T-top design improved the noise reduction of the barrier but that a porous rubber material did not. Unfortunately, fiberglass

insulation is not a practical material for outdoor applications, and the porous rubber resulted in a sharp peak around 800 Hz, a primary frequency component of traffic noise. These results point to the idea that a material may be able to be tuned to eliminate peaks within the frequency range of interest to result in improved barrier performance at a reduced sound wall height. Absorptive materials currently constructed for use on the face of the barrier, such as Armtec's Durisol and CSI's SoundSorb, would likely be able to be used as absorptive top materials. Some off-the-shelf absorptive materials that are currently marketed for other uses, such as the Sound Seal Quilted Fiberglass Absorbers, the Empire Acoustical M-90 Backless Absorption Panels, or the Lamvin Soundsucker Metal Acoustical Panels, may also prove to be practical for outdoor use on top of barriers.

Some of the interference designs demonstrated some promise without the need for added absorptive material (Yin 2008). There has also been some research into the use of random and periodic "jagged" edge profiles in the upper portion of the barrier that are intended to also create interference along the top edge of the barrier (Ho et al. 1997, Sarigul-Klijn and Karnopp 2000). These designs also appear promising and may avoid the additional maintenance concerns that may be connected to the use of absorptive material.

SOUND WALL VENDOR MEETINGS

As part of the Technology Review, manufacturers and suppliers of noise walls were contacted regarding the acoustic performance for their products. Particular emphasis was placed on designs that would enhance barrier insertion loss beyond conventional noise walls and those with added absorptive treatments only. In all, eight vendors were contacted. Of these, four were interested in reviewing their products and ideas with the Research Team. The four others either did not respond at all; felt they did not have pertinent information; or were not interested in participating. Several suppliers indicated that they could build anything that was desired but had no suggestions themselves. The four remaining suppliers were interested in presenting their concepts and expertise to ADOT and the Research Team.

Presentations from the four sound wall suppliers were given to the project team on March 4, 2014. Summaries of each presentation are available in the Appendix B. Each presenter described how their product or idea might best meet the needs of this research project. Two of the presenters (Eric Humphries from Armtec and Boone Bucher from CSI) described existing absorptive products that are commercially available for use on sound walls and that could be extended as top treatment materials. Peter D'Antonio from RPG described an absorptive product and a quadratic residual diffusor product called DiffusorBlox, which is a reflection phase grating system that incorporates divided wells of different depth to uniformly scatter sound. Again, both of these products could be used for the base or top treatment of a sound wall.

Gary Figello from Faddis described the Foss Double Barrier System; an idea that has been around since the 1970's and is included in the FHWA TNM. Theoretically, two absorptive barriers, spaced 6 to 8 feet apart, would provide significant additional reduction from a single barrier. As an example, the reduction from two 12-ft absorptive barriers, spaced 6 feet apart, would be equivalent to the reduction from a single 20-ft high barrier. There were some concerns about the practicality of this system, and there is no known field data of a Foss Barrier System.

TECHNOLOGIES FOR FURTHER CONSIDERATION

Although many of these design enhancements have demonstrated some promise in improving highway noise barrier performance, it is difficult to evaluate each of these concepts on an equal basis. The studies, having been conducted by different practitioners across the world, use varying analysis and/or

measurement techniques. Some studies attempt to adjust for the added height of a device added to the top of a barrier and some do not. Most of the reduced scale and full-scale model studies use a single source noise that can magnify interference effects, as compared to distributed traffic noise sources. Most of the analytical studies do not present actual field or acoustic model results to validate their findings. For these reasons, it is difficult to develop a rank ordering of promising technologies based on objective data. The technologies that rely on inference effects are questionable; however, examining at least one or two of these with acoustic scale modeling would be useful to at least evaluate the merits of this kind of approach.

Based on the conclusions of the 2006 ADOT Report Watson 2006), the follow-up literature review of this research, and discussions with sound wall manufacturers, as presented in the previous sections, the following designs were recommended for consideration for scale-model testing:

- T-top Barrier with various absorptive materials on top and also with a QRD treatment
- T-top Barrier with a “rake” on top
- Straight barrier with absorptive material on the vertical face with a simulation of something similar to Quietstone and with QRD treatment similar to DiffusorBlox
- Foss double barrier system
- Straight barrier with a Helmholtz resonator device on top
- Straight barrier with “rake” on vertical surfaces
- Straight barrier variable flow resistance device on top

CHAPTER 3: NOISE BARRIER FIELD MEASUREMENTS

Under Phase I, noise, air quality, and meteorological measurements were conducted to document the field performance of a noise barrier. Measurements were conducted from May 11 to May 14, 2014 at Oasis Park, AZ, as shown in Figure 2. The purpose of these measurements was to generate data to compare to acoustic scale model data and analytical models developed in Phase 2. The acoustical measurement methodologies and preliminary analysis are described in more detail in Appendix C. The meteorological and air quality measurement methodologies and preliminary analysis are given in the "*Experimental setup and preliminary data summary for meteorological and air quality measurements*" report presented in Appendix D.

Figure 2. Aerial View of Measurement Site

Acoustical and traffic measurements were conducted during eight sessions, selected to represent a variety of weather conditions occurring over the three-day measurement period. Acoustical measurements were made at seven locations, using the same methodologies as those used for the QP3 measurements (Donavan et al. 2014). Two reference microphone locations were used to monitor traffic noise levels: 1) one located on the roadway side of the barrier at the approximate height of the top edge of the barrier, 95 feet from the center of the near freeway lane; and 2) one located on top of the barrier at a height of 5 feet above the barrier. In addition, five distance microphone locations were used: 1) at a distance of 50 feet from the barrier, at a height of 5 feet above the ground; 2) at a distance of 100 feet from the barrier, at a height of 5 feet above the ground; 3) at a distance of 100 feet from the barrier, at a height of 10 feet above the ground; 4) at a distance of 200 feet from the barrier, at a height of 5 feet above the ground; and 5) at a distance of 300 feet from the barrier, at a height of 5 feet above the ground. Five of the seven channels were measured in ⅓ octave bands. At the remaining two channels, noise levels were measured using sound level meters (SLM), which give only overall A-weighted levels. The SLM output signals were digitally recorded for future use. The layout of the acoustical measurement positions is shown diagrammatically in Figure 3 and overlaid on a photograph in Figure 4.

OBSI measurements, similar to Type 1 measurements used in the QP3, were also conducted on Agua Fria Freeway adjacent to the site.

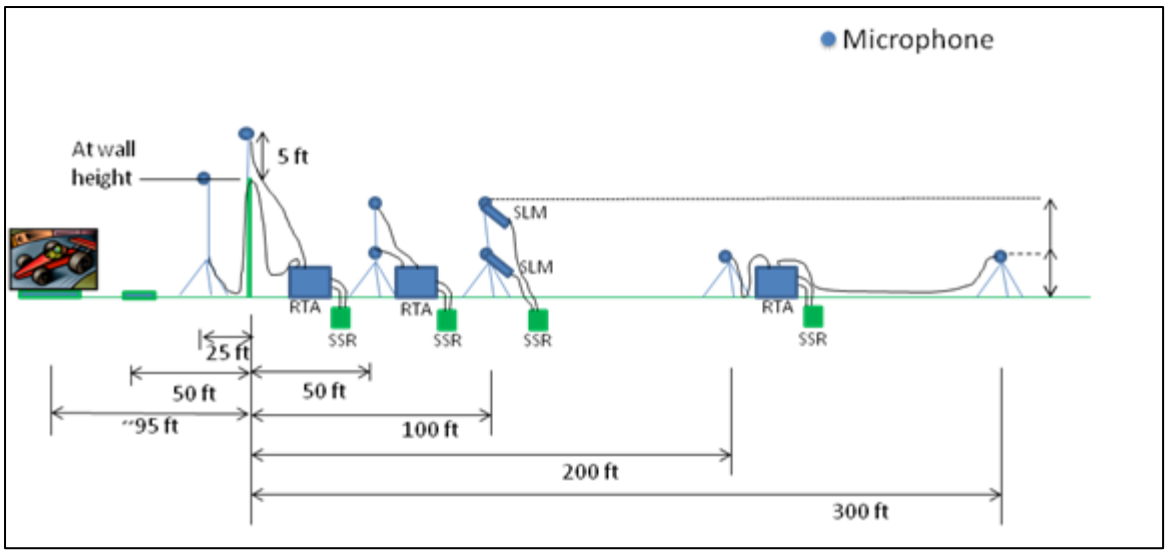

Figure 3. Acoustical Measurement Site Diagram

Figure 4. Photo of Oasis Park Site with Measurement Locations

Continuous meteorological data acquisition began at 12:45 pm on May 11, 2014 and ended at 8:00 pm on May 14, 2014. Meteorological sensors, each including a sonic anemometer, a thermocouple, and a relative humidity sensor, were attached at four locations on two towers, located at distances of 10 and 130 feet from the barrier, at heights of 6.5 and 33 feet above the ground, as shown in Figure 5. A

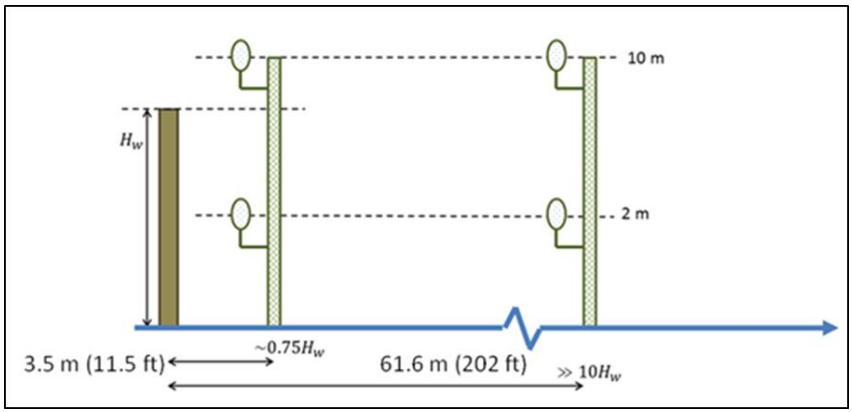

Figure 5. Meteorological and Air Quality Measurement Site Diagram

barometer and three air quality sensors were also located on the site. Meteorological and air quality measurements included wind speed and direction, temperature and relative humidity, barometric pressure, and air particulate matter concentrations. Table 1 provides the times and dates of meteorological and air quality and acoustical measurement.

Table 1. Measurement Sessions

Session Number	Date	Start Time	End Time
1	May 12	11:00 am	12:16 pm
2	May 12	2:14 pm	3:44 pm
3	May 12	7:04 pm	7:54 pm
4	May 13	5:49 am	7:13 am
5	May 13	11:38 am	1:08 pm
6	May 13	3:52 pm	5:06 pm
7	May 14	8:37 am	10:01 am
8	May 14	1:02 pm	2:41 pm

A summary of the results of the acoustical measurement data is shown in Table 2, based on five-minute raw data averages. As expected, the measurements generally indicate lower noise levels with increased

Table 2. Averages and Ranges of Measured Acoustical Data for All Sessions, dBA

	Roadside[a]	Top-of-Barrier[a]	50x5ft	100x5ft	100x10ft	200x5ft	300x5ft
Average Traffic Noise Level	77.5	74.6	59.1	58.5	59.3	57.3	56.4
Range in Traffic Noise Level	9.8	9.6	12.9	15.4	15.0	15.9	16.8

[a] Reference microphones

distance from the traffic noise source. One exception is the 100 x 10ft position, which receives less

shielding by the barrier due to the microphone height, compared to 5 feet for the other positions on the quieter side of the barrier. The range in traffic noise levels over the course of the measurements is quite large: about 10 dB for the two reference locations and 13 to 17 dB at the more distant locations. Although the range in unobstructed traffic noise is significant, Table 2 indicates that the ranges increased with distance for the microphones positioned at heights of 5 feet above the ground. Figure 6 plots an example of the one-minute sound levels at all measurement locations for Session 1. Although there are level fluctuations at the barrier and roadside locations, the levels are fairly consistent over the measurement period. At the locations behind the sound wall, the minute-to-minute fluctuations are greater, and there is a changing pattern in the results, unlike those for not shielded by the sound wall. To eliminate the variation in traffic noise sources, the results of Figure 6 were normalized by subtracting each of the measured levels from the levels measured at the top of the sound wall. The normalized results are shown in Figure 7. These data indicate that the normalized data on the freeway side of the sound wall are quite consistent. On the receiver side of the barrier, the fluctuations are greater, and there is a shifting pattern of the results with time of day. These fluctuations imply that the sound propagation varies with time, causing variation in the received noise.

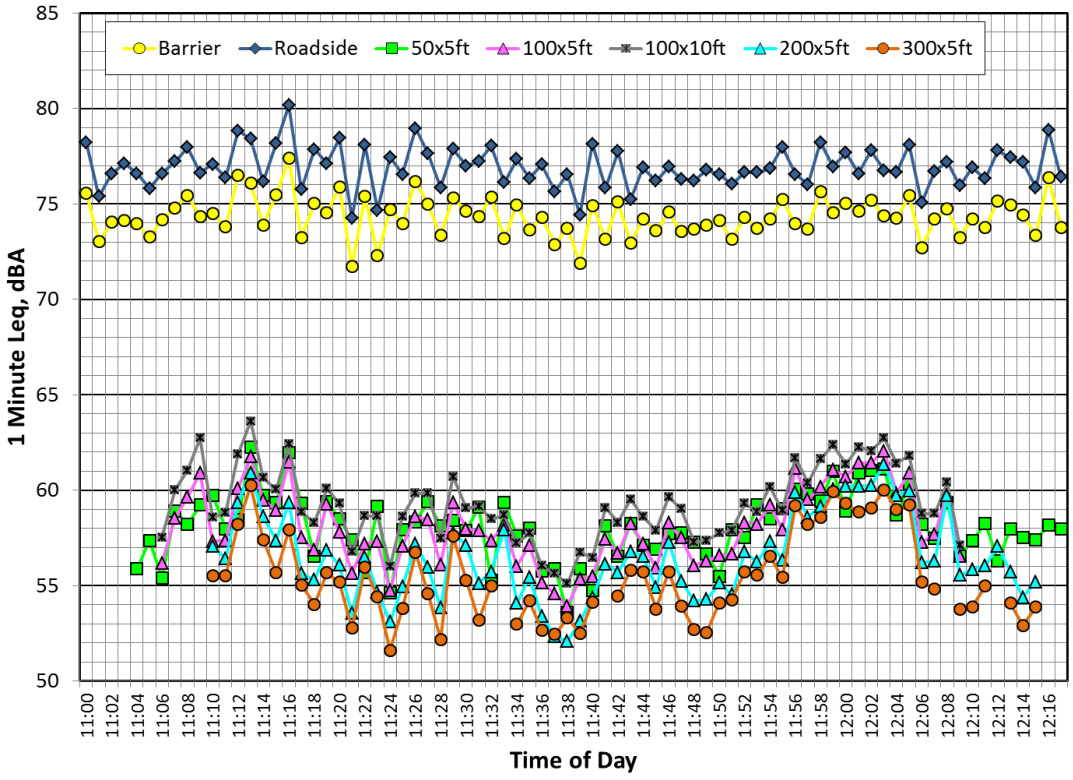

Figure 6. One-Minute Average Noise Levels Measured in Session 1

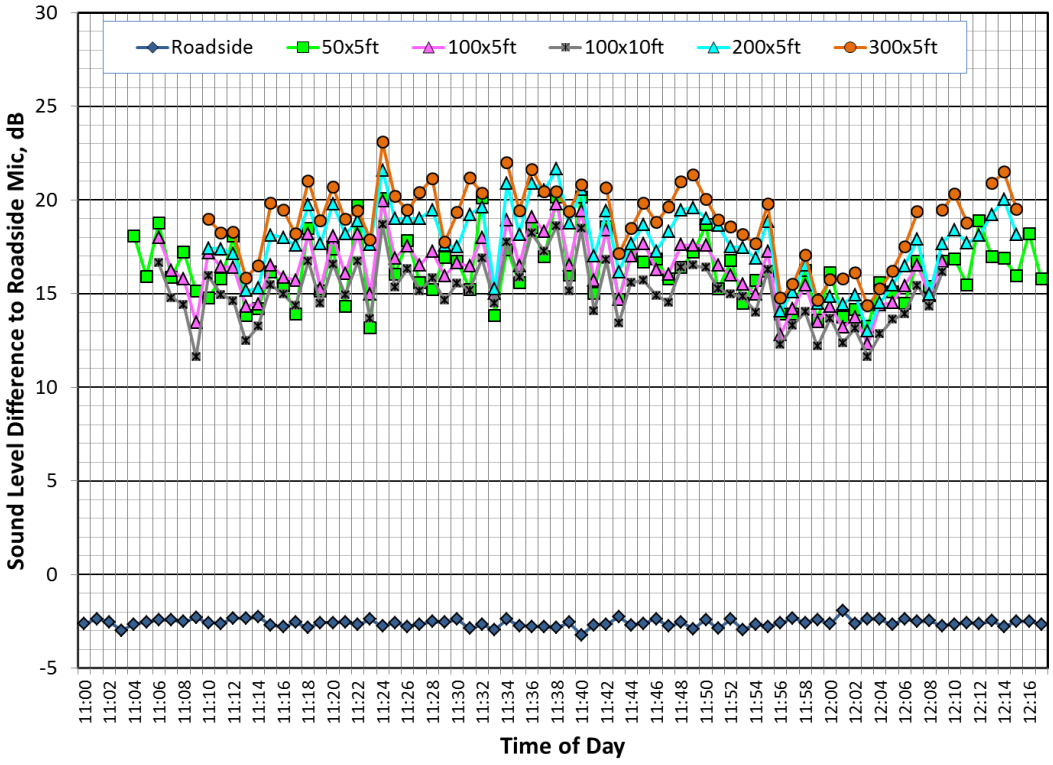

Figure 7. One-Minute Average Noise Levels Differences Relative to Top of Sound Wall Levels in Session 1

In Figure 8, the levels averaged over each session are shown for all of the measurement locations. These indicate that there are clear differences in the noise levels between sessions. Although the general ordering of noise level by location remains similar, there are some cases that are not consistent with the others. For example, during Session 7, the 100 ft x 10 ft high position has levels that are slightly lower than those at the 200-ft position, whereas under the other sessions, the 200-ft position results are typically about 1 to 2 dB higher. In Figure 9, the results are presented as level differences, in which the levels measured behind the sound wall are subtracted from the levels at the top of the wall. It should be noted that this is not barrier insertion, which is defined by the difference in level with and without the sound wall present. The values in Figure 9 inherently take into account differences in traffic noise source levels that occur from session-to-session. The noise level differences indicate considerable variation from session-to-session that are presumed to be due to differences in sound propagation caused by environmental conditions. The ranges in noise level differences for the various measurement distances range from 5.9 dB at the 50x5-ft location to 8.3 dB at the 300x5-ft location. Excluding the 10-ft position, the ranges increase with distance from the sound wall. Also included in Figure 9 are the noise level differences predicted using TNM. Generally, these display similar differences to the relationship between location and sound levels during each of the measurement sessions. For the first four sessions, the magnitudes of the differences are similar to TNM; however, for the last four sessions, the TNM values are consistently lower, typically by as much as 5 dB.

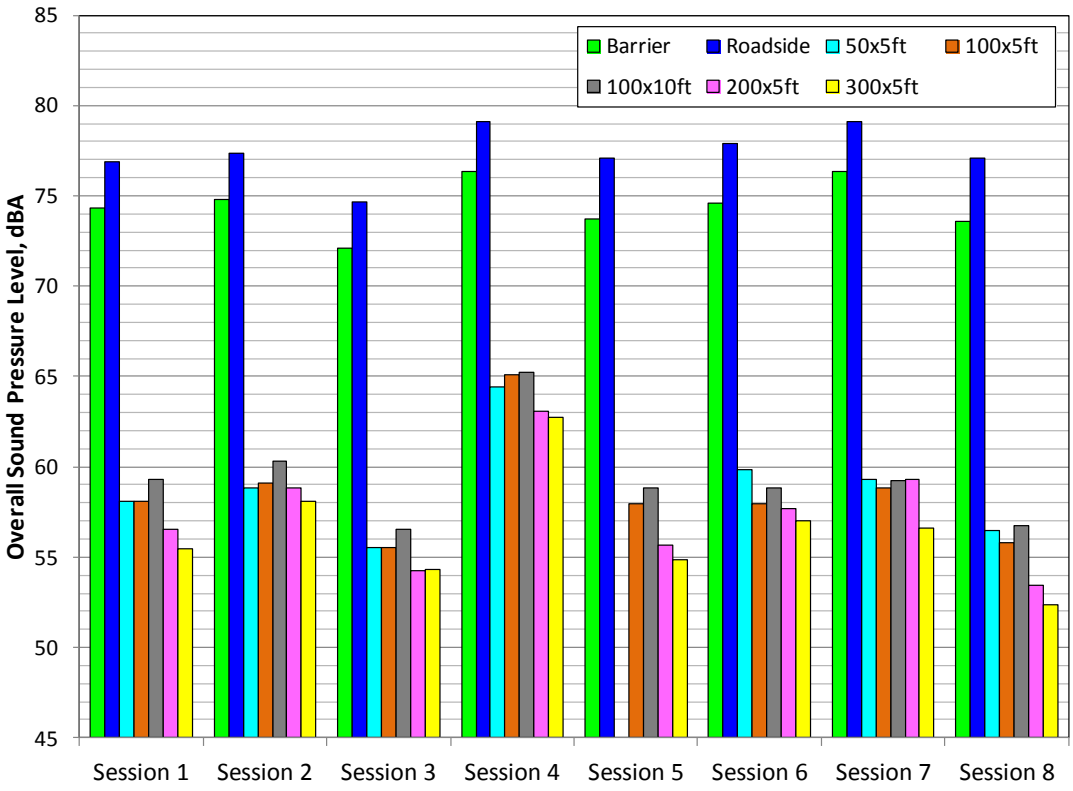

Figure 8. Session Average Measured Traffic Noise Levels

The values of Figure 9 do not represent actual barrier insertion loss performance, which is defined as the difference in level with and without the barrier present. The values of Figure 9 do not account for the difference in distance from the top of the barrier to the measurement locations, which contribute additional attenuation compared to insertion loss alone. Actual insertion loss would decrease with distance as the measurements get further out of the acoustic shadow zone of the barrier. From the TNM model results, the insertion losses are 11.2 dB at the 50x50-ft location, 9.0 dB at 100x5ft, 7.3 dB at 200x50ft, and 6.6 dB at 300x5ft.

To examine the noise and meteorological data together, Figure 10 plots the raw traffic noise levels in one-minute intervals for each of the eight measurement sessions along the same time scale as the wind speed component perpendicular to the wall and the air temperature measured at the 6.5-ft high field tower position. From the data presentation of Figure 10, there are some apparent correlations in the meteorological data and the noise data. The sound levels were consistently higher in Session 4, and the temperature in that session was lowest of any measurement session. The component of wind speed perpendicular to the sound wall was essentially 0 m/s. Throughout the sessions, the wind did not blow consistently from the west or from the east, which would have created a downwind (increased noise level) or upwind (decreased noise level), respectively. During the bulk of the measurements, the wind blew from either the north or from the south, parallel to the barrier. The session with the highest and lowest noise levels, Sessions 4 and 8 respectively, were produced at times when the temperature was lowest and highest, respectively. This trend is consistent with prior research (Donavan and Lodico 2011). To assess this correlation further, a linear regression of the normalized acoustical traffic data versus air temperature was performed for all of the sessions, yielding rates of 0.44 to 0.66 dB per decrease of degree C, depending on measurement distance from

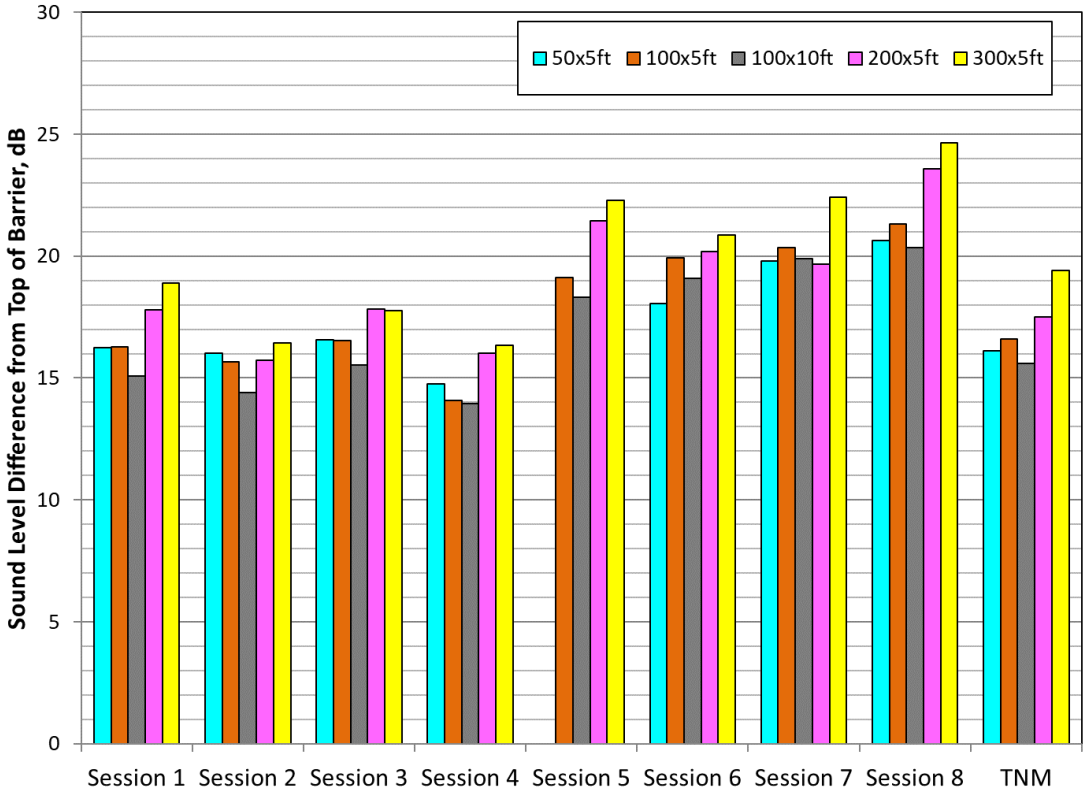

Figure 9. Values for the Noise Level Differences between the Top of the Sound Wall Measurement Location and the Microphone Locations behind the Wall

the sound wall. The coefficients of determination (R^2) ranged from were 0.68 to 0.80. For the roadside and the top of the barrier measurement locations, the temperature dependence was considerably less, 0.07 dB per degree C on the roadside and 0.12 dB per degree C at the top of the barrier. This clearly indicates that temperature had very little effect on the generation of noise. For Session 4, there was a slight inversion indicated by the temperatures at 6.5ft and 33ft, with the lower height being about 0.5 degrees C cooler. This inversion may also have contributed to the higher levels for Session 4.

Similar analysis was performed on the wind component perpendicular to the sound wall. These produce no relationship between wind speed and noise level. This result is not surprising, considering the low and inconsistent wind speeds and fluctuating directions shown in Figure 10. Downwind conditions (wind from the traffic to the receiver) are generally associated with higher levels, both for open conditions (Lodico and Reyff 2009) and locations behind a sound wall (Beranek and Iver 1992); however, this behavior could not be demonstrated wind the wind conditions that occurred during these measurements.

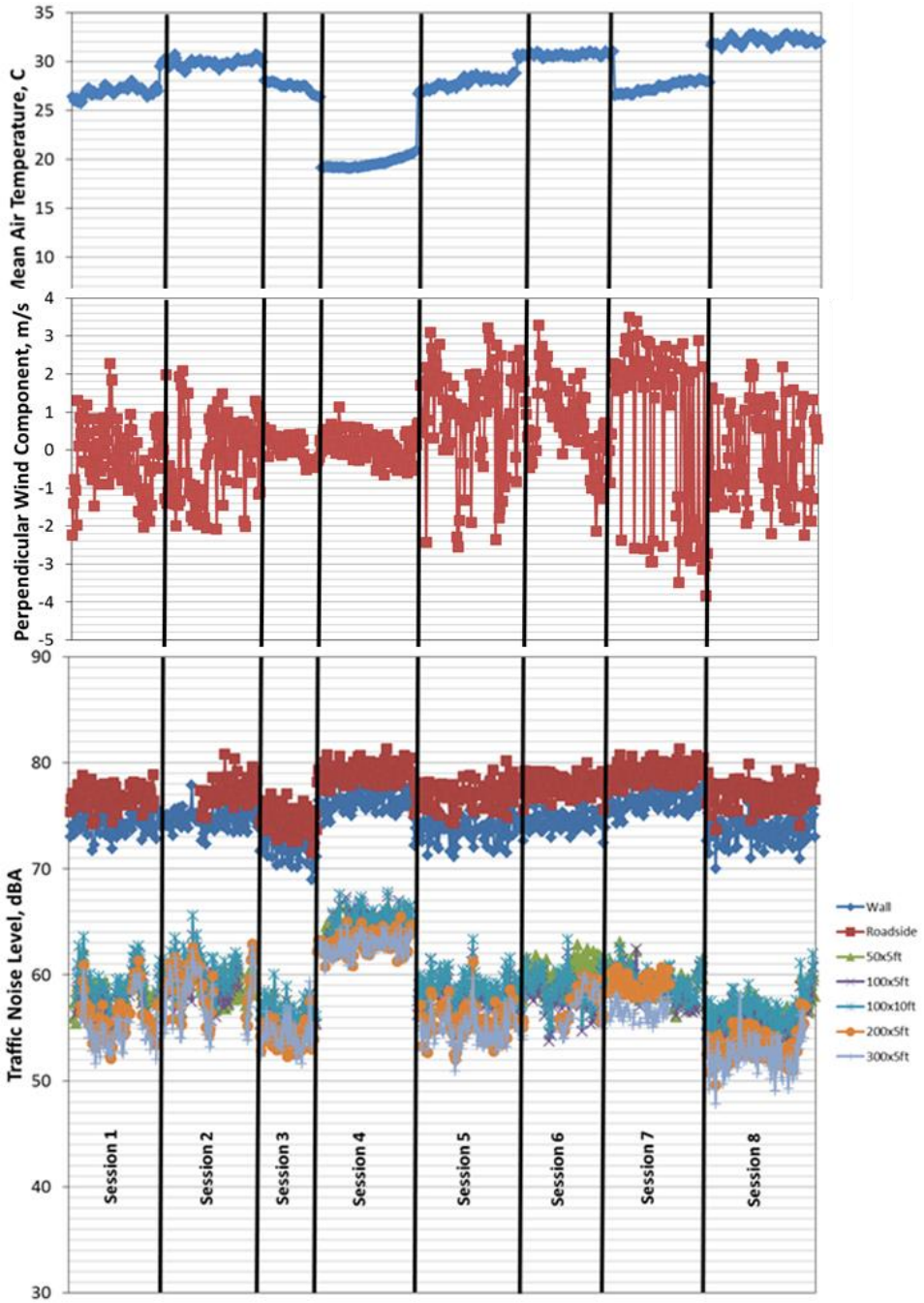

Figure 10. Measured Wind Component, Air Temperature, and Sound Pressure Levels, All Sessions

A large amount of scatter is apparent in the acoustical data for all the measurement sessions, as shown in Figures 6 and 10. Some of this scatter is to be expected due to varying traffic conditions. In Figure 7, this scatter was somewhat reduced by normalizing the data by subtracting the noise levels measured behind the barrier from the noise levels measured at the top of the barrier. Traffic noise variations that are attributable to variations in traffic volume, speed, or vehicle mix can be reduced using traffic noise

modeling. This was done using TNM applied in 15-minute intervals, generally following the procedures specified in AASHTO TP-99 (AASHTO 2013). The results of both methods are presented in more detail in Appendix A. However, even with these normalizations, some scatter continues to be present, especially in the more distant measurement locations. In Figure 11, the noise levels for each measurement location are plotted versus the levels measured at the top of barrier. The linear regression through the roadside levels

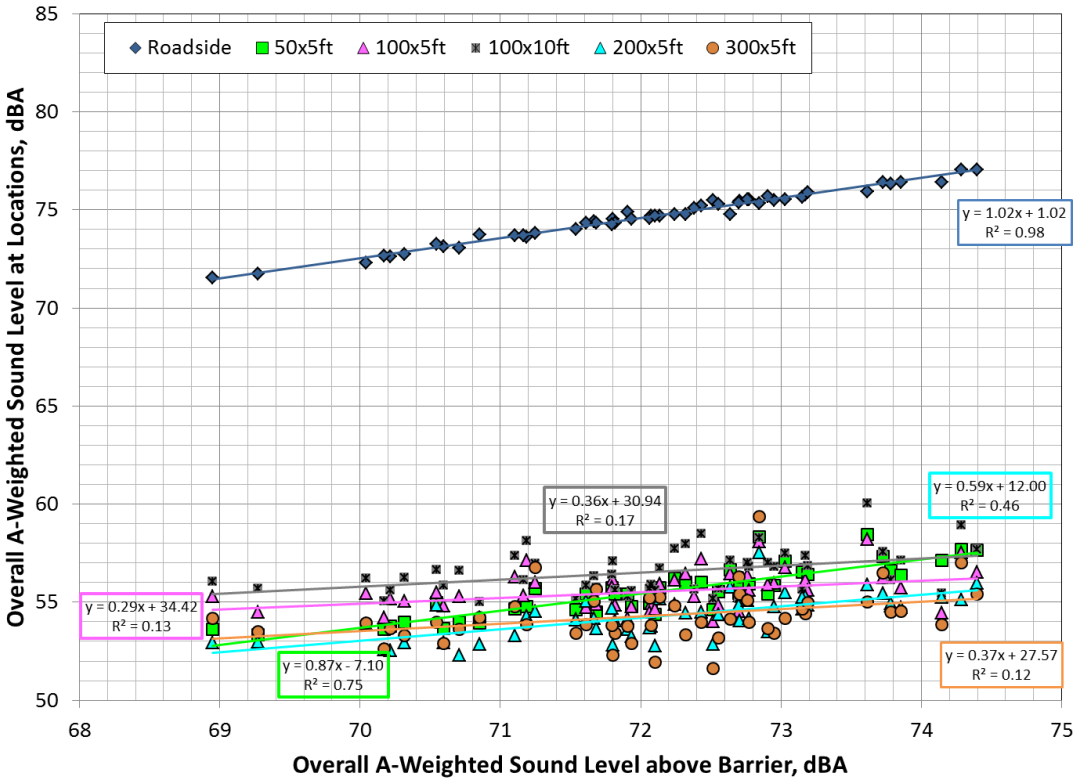

Figure 11. Sound Pressure Levels from the Roadside and behind the Sound Wall Plotted Versus Levels above the Sound Wall for Measurement Session 3

provides almost a one-to-one relationship, with a R^2 value of 0.98. The standard deviation about this line is 0.2 dB, and the range is 0.8 dB. At the closest position to the barrier on the receiver-side of the barrier, (50x5 ft) the relationship between the measured levels and the top of the barrier remains reasonably good at 0.87-to-1, with R^2 equal to 0.75. At the further distances, the relationships deteriorate, and the scatter about the regression line increases with the distance of the measurement location from the sound wall, reaching a maximum at 300 feet and having a standard deviation of 1.3 dB and a range of 7.6 dB. For locations in between (100x5, 100x10, and 200x5 ft), the standard deviations were 0.8 to 1.0 dB and the ranges from 4.0 to 4.8 dB. It is likely that this increased variability with distance is due to turbulence generated by wind and temperature variations along the sound propagation paths (Beranek and Iver 1992). From Figure 10, similar variabilities in the noise levels at the microphone locations on the receiver side were also found.

Acoustical data was successfully acquired and achieved its purpose of providing field data for comparison to the acoustic scale model measurements and ultimately to the results of analytical models

to be developed, as recommended in Phase II of the project. The data did support a conclusion that traffic noise levels increase with decreasing temperature; although, the temperature range was somewhat limited. Due to a lack of appropriate conditions, the effects of wind on barrier performance could not be assessed. The intent of this portion of the project was not to explicitly evaluate the effect of meteorological conditions on sound propagation over barriers. As a result, the correlation of various aspects of the meteorological data to measured sound levels was not examined in detail. This extensive data set could be used for this purpose and more explicitly, evaluating those factors, such as turbulence, that contribute to the sound level variation behind the sound wall. During the course of the measurement periods, the volume of heavy trucks was only 1 to 3% of the total traffic. As a result, the barrier performance indicated by these measurements should not be generalized to sites at which the heavy truck volumes approach 10% or more, as the effective source height of trucks is somewhat higher than it is light vehicles (Donavan and Janello 2017), and higher source heights reduce barrier performance.

CHAPTER 4: ACOUSTIC SCALE MODEL MEASUREMENTS OF BARRIERS

In order to quantitatively evaluate the acoustic performance of different sound wall designs, the most practical method is the use of acoustic scale models. Although the performance would ultimately need to be verified with actual field measurements, such as that performed in the first phase of this research, these field measurements are not very suitable to evaluating multiple design options. Aside from the issues of fabricating and installing modifications to the upper edge of the wall, outdoor testing is subject to uncontrollable variables, such as those noted in the earlier discussion of the field measurements. This makes comparison of one design to another problematic, especially if the expected improvement in performance is not large. Due to the dimensions of full size barriers and distances between source and receiver being large, indoor testing in a non-acoustically reflective environment is not practical. Analytical methods, such as boundary or finite element modeling in the necessary three dimensions and to the upper frequency range of interest, would be expensive and time consuming to run and would still leave questions in regard to accuracy.

Acoustic scale modeling is based on the invariance of the sound speed in air for similar field and laboratory conditions. The speed of sound equals the acoustic wavelength times the frequency. To maintain this ratio, when the length scale is reduced and the wavelength is shorter, the frequency must increase accordingly. This allows a scaled model of the barrier to mimic the performance of a real traffic barrier, when the frequency band of the laboratory sound source is increased by the same factor relative to typical frequency bands of traffic noise. The scaling is straightforward if any surfaces reacting with the measured sound are rigid, otherwise the impedance of the surfaces must also be scaled. However, for the sound wall cases to be considered, the surfaces are rigid and of high impedance. Air absorption is also a concern as it increases with increasing frequency. However, given the moderate scaling used, 10 to 1, and short distances of propagation, this effect is negligible.

MEASUREMENT METHODS

Given the scaling factor of 10 to 1, the frequency range of model measurements was 1 to 30 kHz, translating a full scale traffic noise range of 100 to 3,000 Hz. To generate a high sound level at these frequencies, a spark sound source was designed, built, and verified to perform adequately. The spark consisted of three electrodes, two that produced the main pulse and a third to trigger the pulse. The three-electrode design produced a stable and repeatable signal, as shown in Figure 12, in both the time domain (a) and the frequency domain (b). The frequency of the spark pulse is centered at about 17,000 Hz and produced an equal scaled frequency of 1,700 Hz. The spark source was measured to produce the same level within ±30 degrees of the forward-facing direction of the source and within 4.4 dB at off angles. The use of the short duration spark source has the advantage of not needing a special anechoic space for conducting the measurements. Reflections from surfaces that are to be excluded from the measurements can be eliminated in the time domain by only retaining the early arriving pulse or pulses of interest.

The signals generated by the spark source were monitored using a Brüel and Kjaer (B&K) ¼-inch Type 4939 microphone capable of measuring sound pressure from 4 to 100,000 Hz in conjunction with a B&K Type 2670 microphone preamplifier. Signals were captured with a 100 MHz digital storage oscilloscope and transferred to a computer for storage and processing using LabVIEW software and MATLAB programing. The time signals were processed into the frequency domain using a fast Fourier transform (FFT) and ⅓ octave band (OB) filters. The FFTs produced spectra from 600 to 50,000 Hz, and ⅓ OB levels

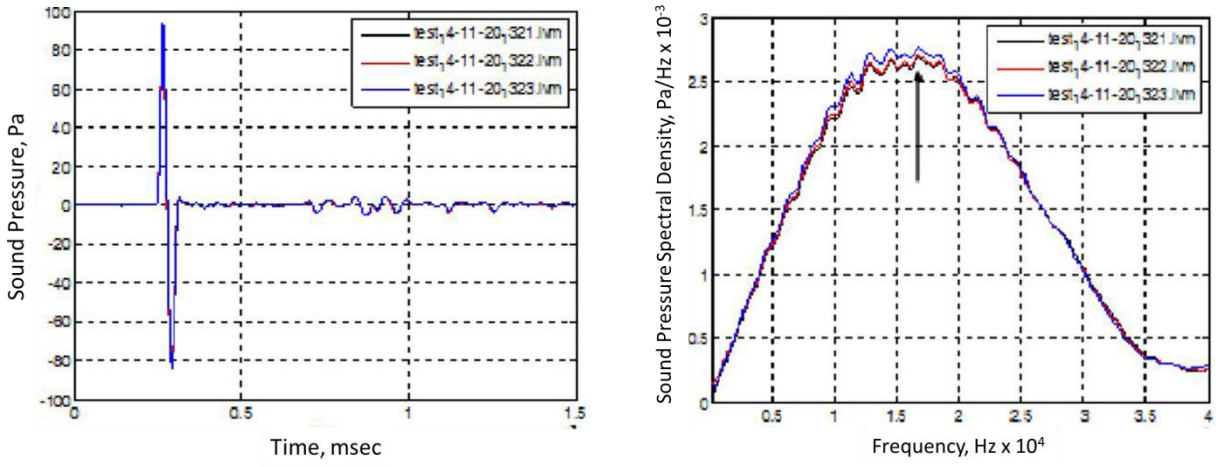

Figure 12. Spark Source Time Trace (a) and Spectrum (b)

were from bands centered at 630 Hz to 50,000 Hz. The FFT spectra were processed into sound pressure spectral densities by dividing by frequency band width so that levels are independent of the band width.

The basic measurement configuration is shown in Figure 13. The spark source (S) and the microphone (M) were positioned about a semi-circle of radius R, centered on the top of the barrier (O). For the measurements, the angles for M (θ_M) were 0, 15, 30, and 45 degrees, and angles for S (θ_S) were 15 and 30 degrees. The radius R was at either 30 or 45cm, corresponding to full scale distances of 3 and 4.5m.

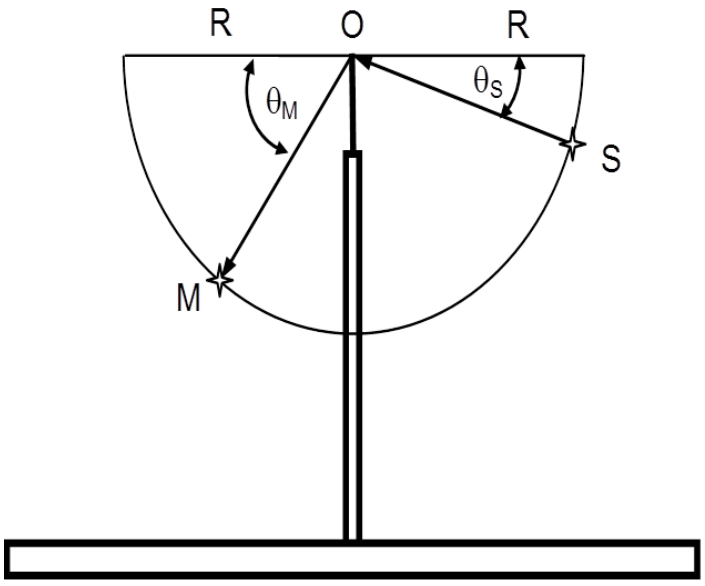

Figure 13. Geometry of Measurements with Indicated Parameter Notations

Using this coordinate system, measurements were made with and without barriers in place to determine the difference (or insertion loss, IL) in sound level. To isolate the diffracted sound only, the reflected signals from the ground plane and any other surfaces were eliminated from the time signal prior to processing. The fixture was three dimensional, with barriers extending ±60cm in the lateral

direction. The top edge of the barrier was made from aluminum plates that could be repositioned interchanged. The lower portion of barrier was wooden.

A total of six different top configurations were tested with the apparatus. Four configurations that had constant sections along the length of the barrier and their profiles are shown in Figure 14. These included a straight (S) top, corresponding to conventional sound wall designs, a T-top shape (T), an L shape, with the leg of the L in the direction away from the source (LD), and an L shape, with the leg in the

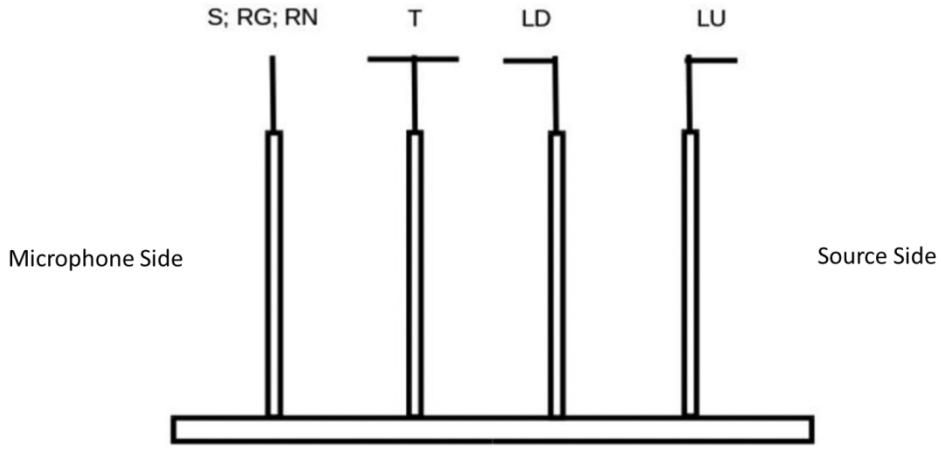

Figure 14. Top Configurations for Constant Section Designs

direction toward the source (LU). Two configurations had top configurations that varied in the lateral direction. These jagged edge designs are proposed to improve barrier performance through interference effects for sound passing over the barrier edge. One of these designs uses a regular, repeating saw-tooth jagged edge (RG), and one uses a random jagged edge (RN), as shown in Figure 15. The final barrier configuration was with the barrier completely removed (F). For the F, S, T, LD, and LU

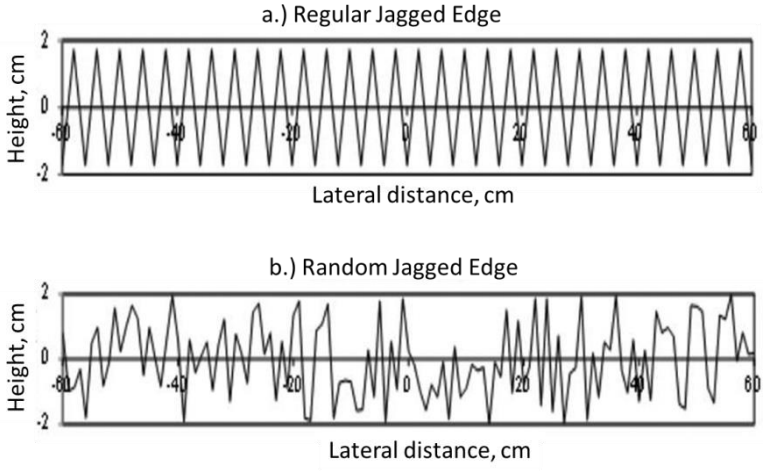

Figure 15. Top Configurations for Variable Section, Jagged Edge Designs

cases, the measurements were repeated three times and averaged for the different values of the radius, R, and microphone and source angles, θ_M and θ_S, respectively. For the RG and RN cases, since the

profile varied with lateral position, measurements were repeated at 0.5-cm increments in the lateral direction from 0 to ±4cm. The data for these 17 measurement locations were then averaged together.

MEASUREMENT RESULTS

Sound pressure spectral densities for the straight S-top and the T-top configurations are shown in Figure 16 for comparison to the no barrier spectral density of Figure 12b. The sound pressure is about 6 times

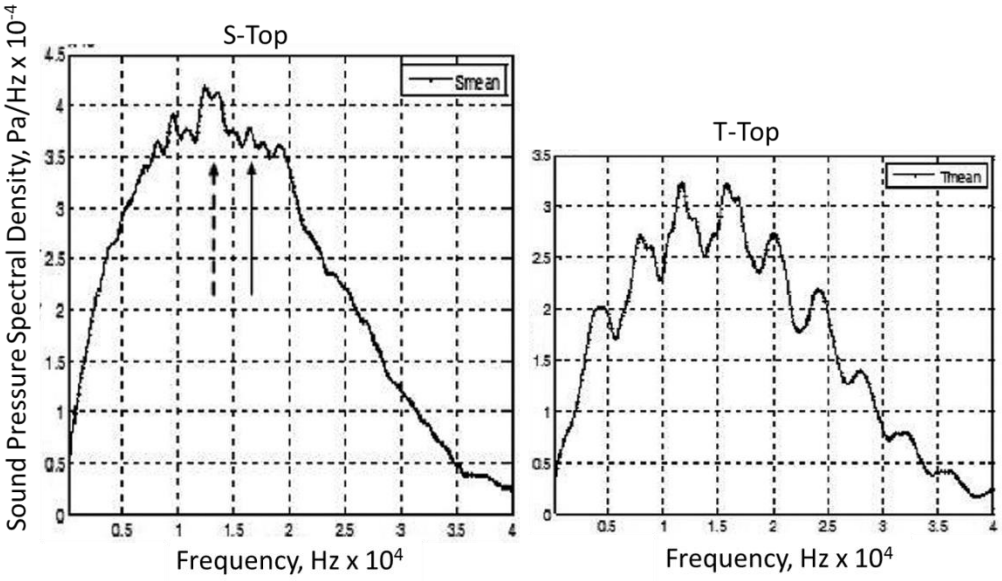

Figure 16. Frequency Spectra for the Straight (S) Top and Tee (T) Top Barrier Configurations

(~16 dB) lower for the S-top, compared to the F, no barrier case of Figure 12b. Compared to S-top, the T-top is about 1.3 times lower (~2.4 dB). The T-top also displays marked frequency content not seen in the S-top, which is presumably due to acoustic inference effects from the multiple diffracted paths over the T-top. A similar result was observed for the LU L-top. For the LD L-top configuration of Figure 17, these peaks are not so prominent, and the spectral density values are similar to the straight top

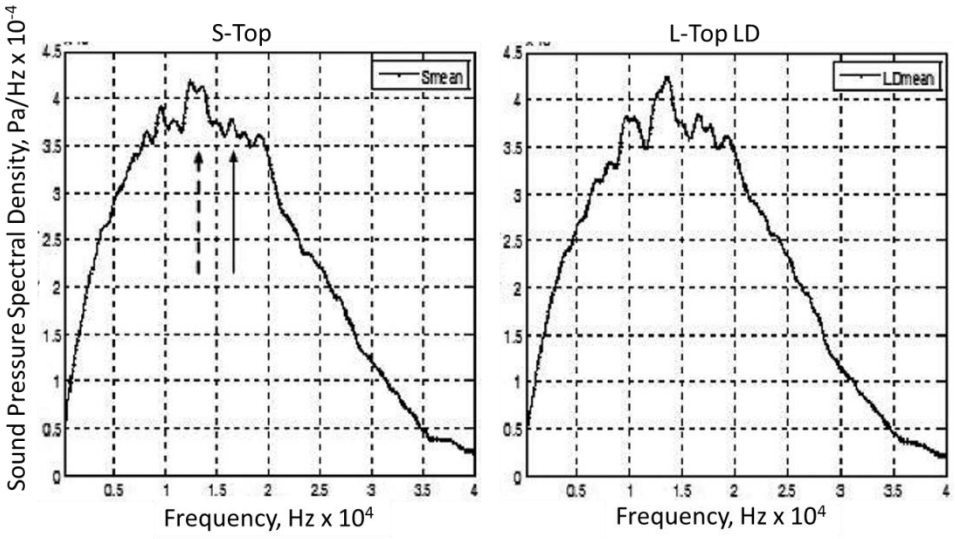

Figure 17. Frequency Spectra for the Straight (S) Top and L-Top LD Barrier Configurations

configuration in amplitude and frequency content. For the jagged tops, the uniform and random configurations are somewhat similar to the S-top, except that the uniform design produces slightly higher spectral densities, as shown in Figure 18. The random design has a spectral peak at about the same frequency and amplitude as the S-top. It is apparent that neither design produces better performance than the straight top. Past evaluations of jagged tops have typically looked at single paths over the barrier, which can produce stronger interference effects for specific orientations. However, when averaged over the length of the edge, these discrete effects appear to vanish.

The results of the measurements can also be compared to theoretical models, as well as to each other. For the straight S-top, the expression for insertion loss was developed by Maekawa as published in 1968 (Maekawa 1968). This formulation is based on the Fresnel number originally developed for electromagnetic waves passing through an aperture. Maekawa demonstrated that this number could be applied to the acoustic diffraction problem for thin screens. In terms of the nomenclature of Figure 13, the Fresnel number is a function of the angles θ_M and θ_S, R, frequency, and the speed of sound. The IL of the barrier is then a relatively simple function of the Fresnel number. This theory was further extended for finite thickness, wedge-shape barriers, the so-called geometrical theory of diffraction (Pierce 1991). In Figure 19, experimental ⅓ OB insertion loss of this research is compared to the theoretical IL calculated for four configurations, in which the source (S) was held at 15 degrees and the microphone positions were varied to θ_M=0, 15, 30, and 45 degrees with the radius R held at 30cm. There is generally good agreement (±2 dB) between the theoretical values and the measurements, and same trends are seen in both results. The geometrical theory of diffraction can be extended to diffraction over multiple wedges (Pierce 1991) to accommodate theoretical calculations that can be used with the T-top and L-top designs. In Figure 20, these are compared on a ⅓ OB basis to the Maekawa screen theory, the geometrical theory of diffraction results for an S-top design and a T-top design. Except for the above 20kHz, the measured IL results for the T-top and the LU L-top compare well to the theoretical T-top results. The straight-top S results compare closely to the geometrical theory of diffraction values throughout the entire frequency range. The LD L-top is equal to or higher than the S-top design and falls below the theoretical values for the T-top.

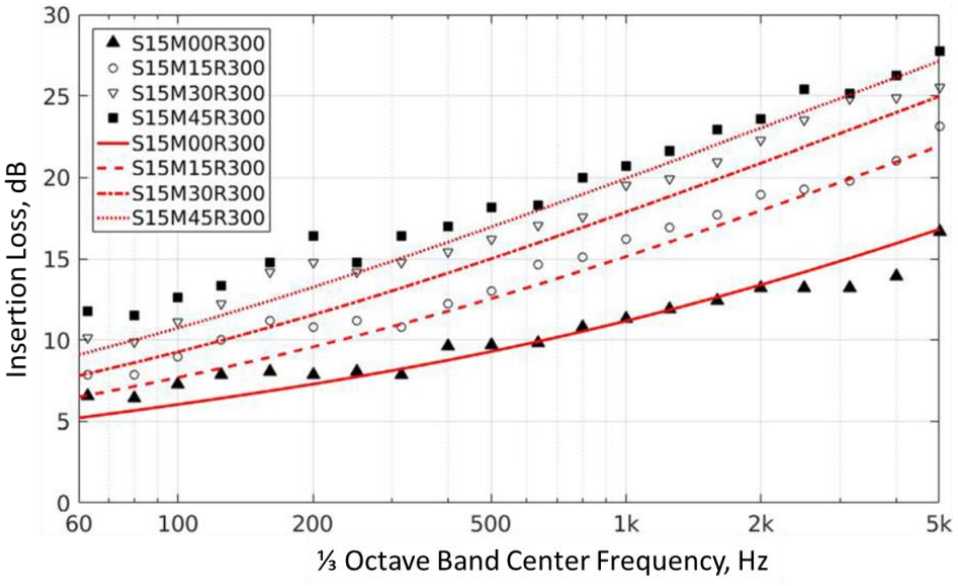

Figure 18. Comparison of Experimental and Theoretical Results (from Eqn 8) for Straight (S) Top for Source at 15° and Microphone at 0°, 15°, 30°, and 45° and a distance of 30cm

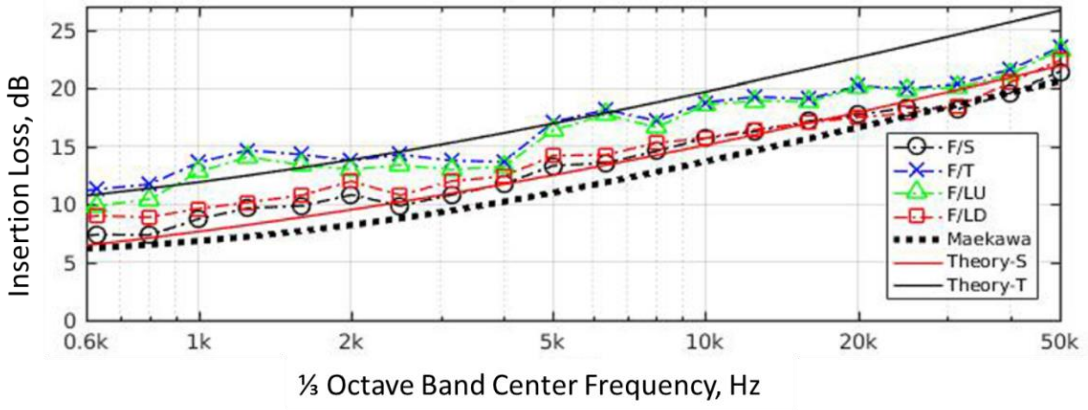

Figure 19. Comparison of Experimental and Theoretical Results for S-Top, T-Top, L-Top (LU) and L-Top LD Barrier Configurations

In order to facilitate comparison, a single number rating scale was developed based on a typical traffic ⅓ OB spectrum, defined in European standard EN 1793-3 (CEN Standard 1997). The overall A-weighted level of this traffic noise source was calculated. The insertion loss for each ⅓ OB was subtracted from the traffic noise spectrum, and these band levels were summed into an overall A-weighted level, as attenuated by the barrier. The attenuated overall level was then subtracted from the overall un-attenuated traffic noise level to obtain the insertion loss for the typical traffic noise spectrum. Using the configurations tested in the model study, traffic insertion losses are shown in Figure 21 for a full-scale R value of 9.8ft (3.0m) and a fixed source angle, of θ_S,=15° for all the barrier top configurations evaluated.

Throughout all of the θ_M microphone angles, T-top is shown to produce the highest traffic noise IL. When the microphone location is even with the top of the barrier (0°), the IL's are the smallest, with the difference between all tops being about 3 dB. The L-tops vary in rank ordering as a function of microphone angle and are both consistently below the IL of the T-top. The two jagged edge tops, RN and RG, follow the straight edge S-Top within about 1 dB, with the random edge (RN) producing slightly higher IL than the straight top and about 1 dB higher than uniform jagged edge top, RG. Compared to the S-Top, the T-Top produced increased IL of 2 to almost 7 dB, depending on microphone angle. Figure 22 shows the same rank ordering of tops for a source angle of 30° and a distance of 9.8ft (3m). Random jagged edge (RN) follows the S-Top within 1 dB or less to a microphone angle of 45° where the RN Top produces IL about 3 dB greater than the S-Top. Similar trends are shown in Figures 23 and 24 for the R value of 14.8ft (4.5m). For all cases, the T-Top produces higher IL than any of the other five barrier top configurations.

Of the four different cases, which are shown in Figures 21 through 24, Figure 23 provides the closest representation of what the performance would be in situations found in the Phoenix area. From the Quiet Pavement Pilot Program Type 2 measurements, typical distances from the closer residential measurement locations to the freeway near lane of vehicle travel were about 80ft. This was split almost equally, with 40ft between the barrier and roadway and 40ft to the measurement location. Assuming a 5-ft high receptor and a ground-level vehicle source height of tire-pavement noise, the angle to the top of a 14-ft high barrier is about 20° (θ_s) on the source side and 13° (θ_m) on the receptor side. At a microphone angle of 15°, the results in Figure 23 indicate that a T-Top would produce about 3 dB of additional IL compared to a straight wall of the same height. The T-Top has a width of 3.3ft (1m) in full size dimension. Adding this height on an existing 14-ft sound wall would increase the insertion loss by about 4 dB using the TNM source height model (Donavan and Janello 2017).

CONCLUSIONS

A one-tenth acoustic scale model was developed and tested and found to produce results similar to those calculated from existing theory. Six sound wall top configurations were experimentally evaluated, one conventional straight top, and five with varying, non-traditional top designs. The best performance was demonstrated by a T-Top design, which had a top width of 3.3ft (1m) in full size dimension. For typical ADOT highway configurations, an increase in insertion loss of about 3dB could be expected by adding the T to the top of a sound wall. However, by increasing the sound wall height by 3.3ft and leaving the top straight, the addition would produce an equivalent improvement in IL than a T-Top, if not slightly more. It appears that using a T-Top design would be limited to only cases where the sound wall height could not be increased due to other constraints. Prior to actually considering a T-Top design in a highway project, its performance should be validated with field testing. The laboratory work reported here considered only a point source of sound rather than an extended highway source along the length of the sound wall and a multi-lane geometry. Further, the modeling did not take into account ground reflections from the source and receiver sides of the sound wall.

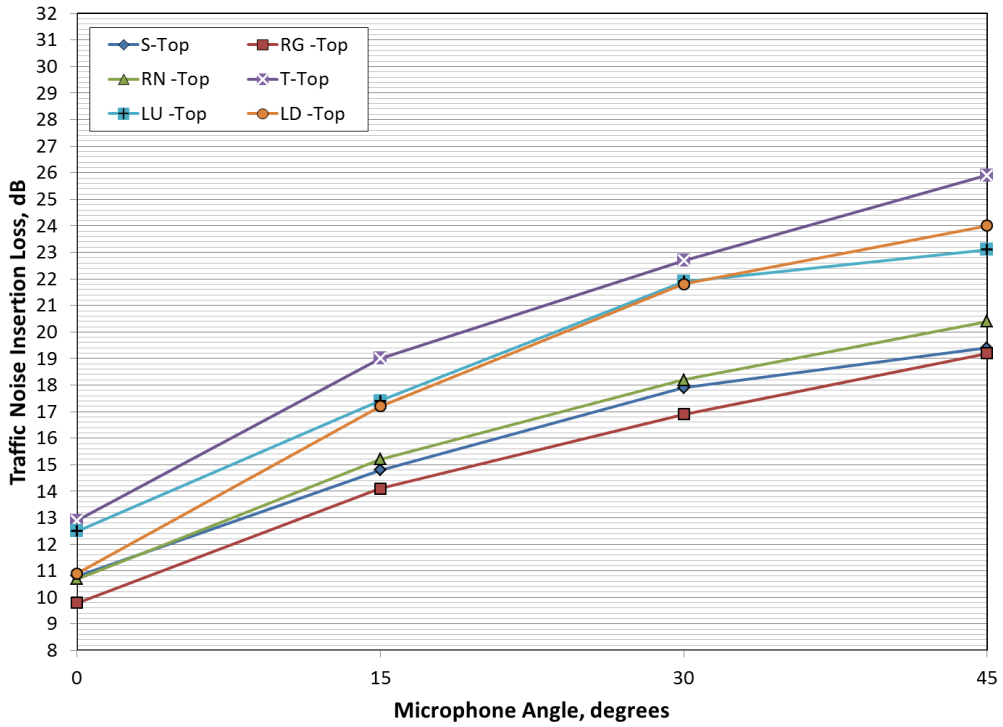

Figure 20. Traffic Noise Insertion Loss Based on Acoustic Scale Modeling Results for a Source Angle of 15° and a Full-Size R distance of 9.8ft (3m)

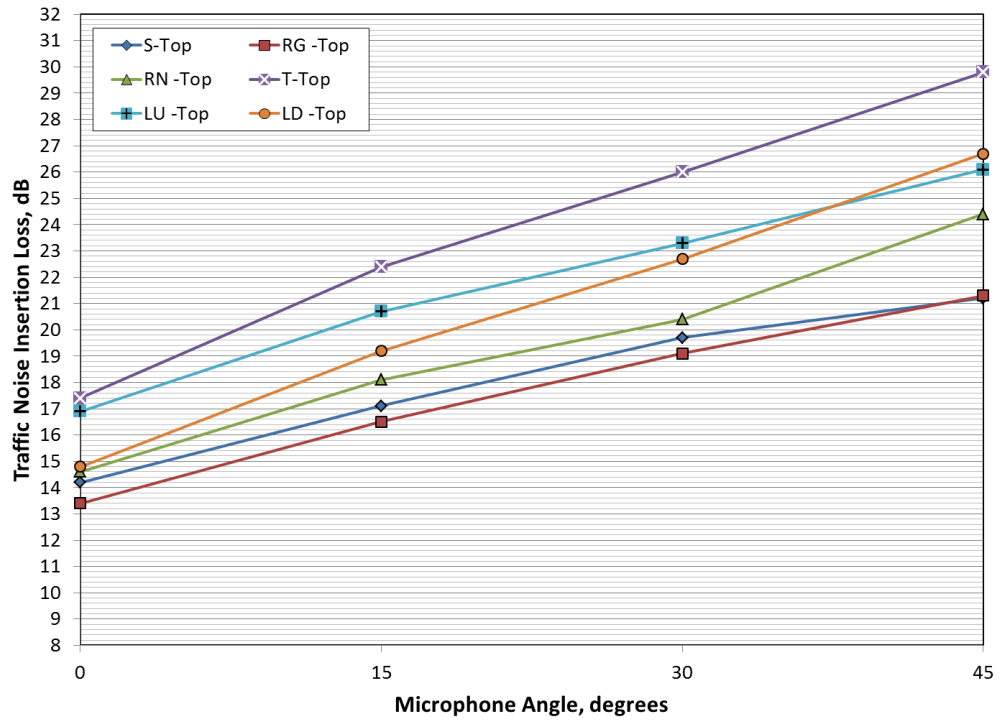

Figure 21. Traffic Noise Insertion Loss Based on Acoustic Scale Modeling Results for a Source Angle of 30° and a Full-Size R distance of 9.8ft (3m)

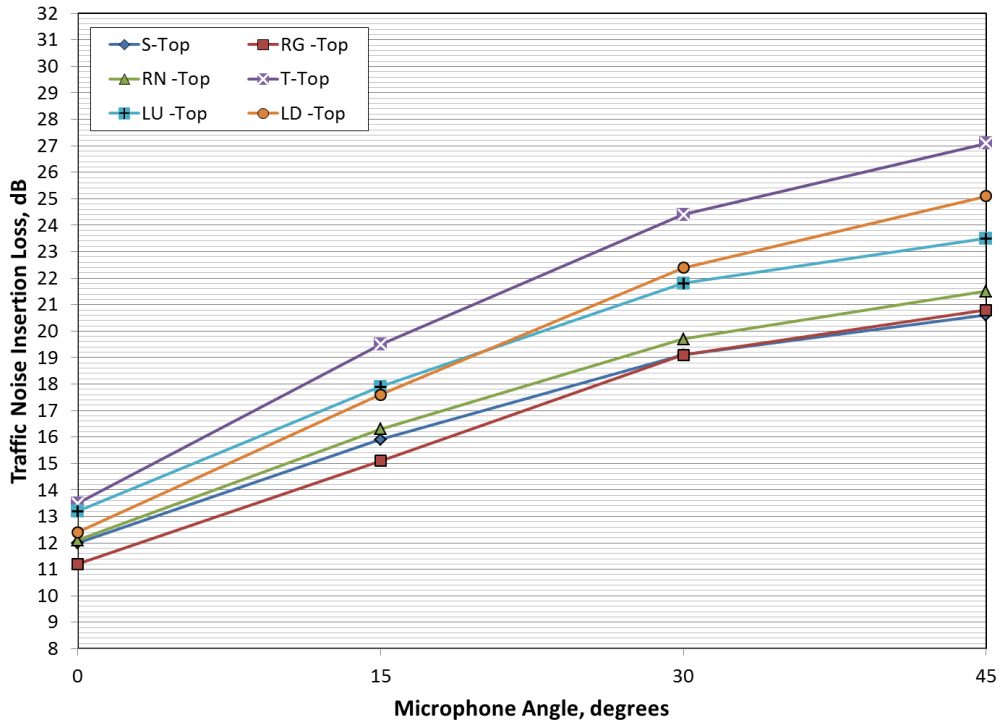

Figure 22. Traffic Noise Insertion Loss Based on Acoustic Scale Modeling Results for a Source Angle of 15° and a Full-Size R distance of 14.8ft (4.5m)

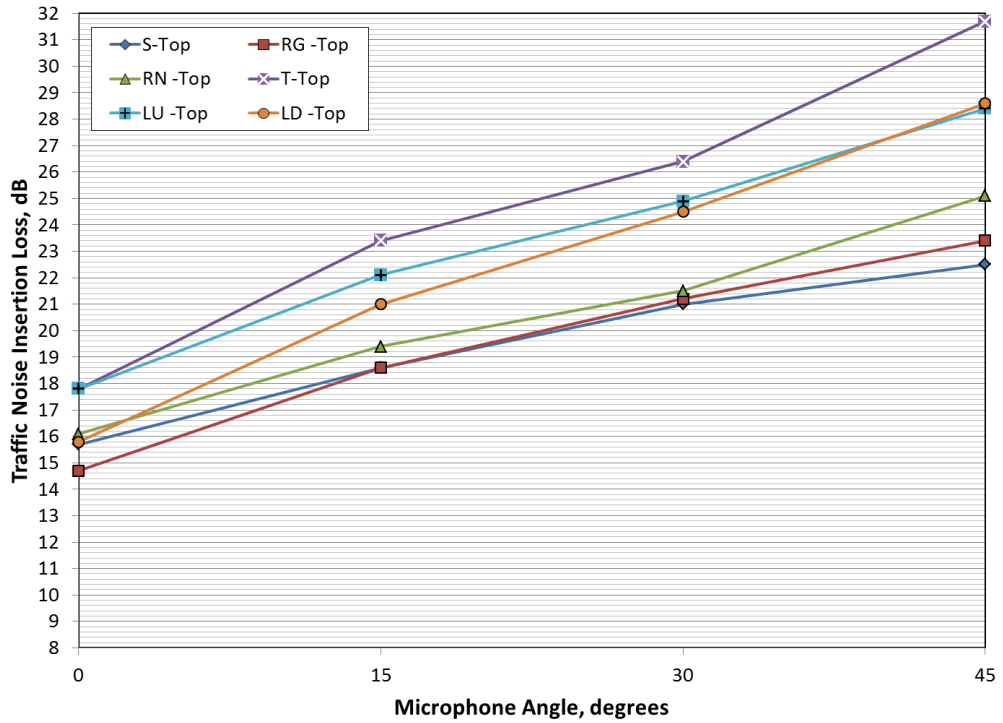

Figure 23. Traffic Noise Insertion Loss Based on Acoustic Scale Modeling Results for a Source Angle of 30° and a Full-Size R distance of 14.8ft (4.5m)

CHAPTER 5: ANALYTICAL MODELING OF BARRIER AND WIND EFFECTS

MODELING BARRIER PERFORMANCE

As discussed in Chapter 4, theoretical models have been historically developed for straight wall barriers and for double diffraction cases based on the work of Piece (Pierce 1974) for geometry shown in Figure 25. This geometry for a wide, two-edge barrier can be used in an approximation of a T-top barrier or barrier with either a source facing L-top (configuration LU) or a receiver facing L-top (configuration LD).

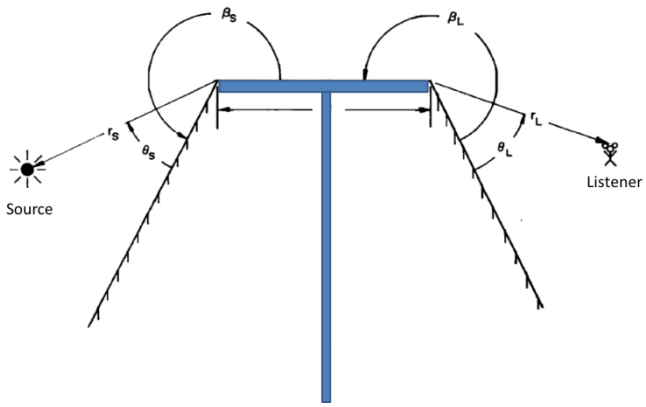

Figure 24. Representation of a T-Top barrier using wide barrier theory from Pierce

However, these approximations do not address the different overhang conditions of flat top designs, as shown in Figure 26, which were found to produce differences in the acoustic scale model results. For more complicated designs (see Figure 1), there are no theoretical models. For evaluation of more

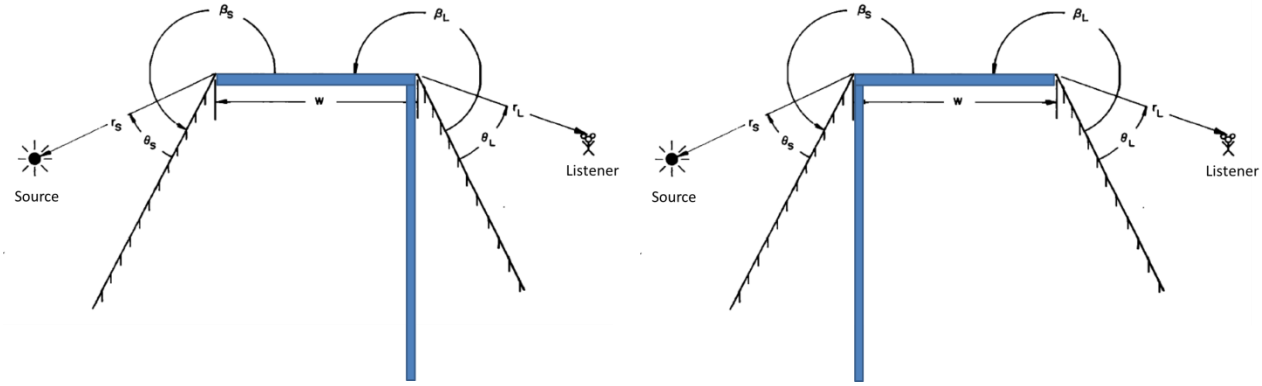

Figure 25. Representation of a L-Top barriers LU (left) and LD (right) using wide barrier theory from Pierce

complex top geometries and surface treatments that include absorption and/or scattering, computational models need to be considered. From an evaluation of different computational methods completed in this research, it was concluded that the BEM is the most promising. A variety of open source BEM models were found, and OpenBEM was selected as being applicable to the barrier calculation and easy to implement. With this tool, specific barrier geometries and surface treatments

can be modeled, and point and line noise sources can be specified. An example of the sound pressure levels computed around a simple straight wall barrier is shown in Figure 27 for 500 Hz. In this example, the source is at -5m near ground level, and the barrier is 3m in height. For this single frequency, interference from barrier

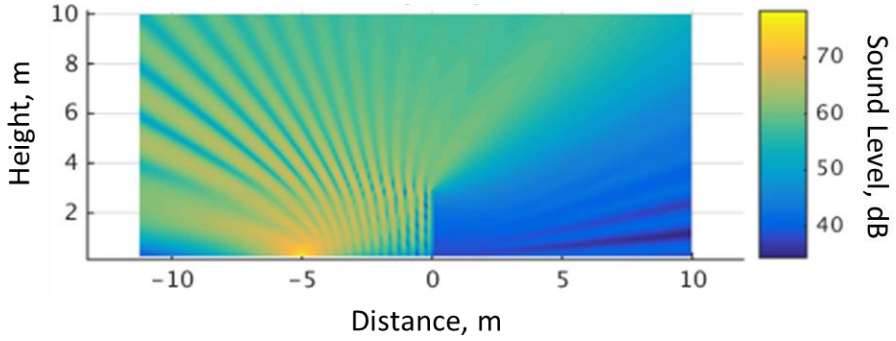

Figure 26. Calculated sound field around a 3m sound wall for a source at distance -5m using OpenBEM

reflections on the source side creates the discrete lines of higher sound level. To examine a ⅓ OB level, sound pressures from several different frequencies within the band would be calculated and averaged together, eliminating the discrete behavior occurring for the single 500 Hz frequency. In Figure 28, the insertion loss of the barrier for the same geometry is shown. As with Figure 27, lines of interference

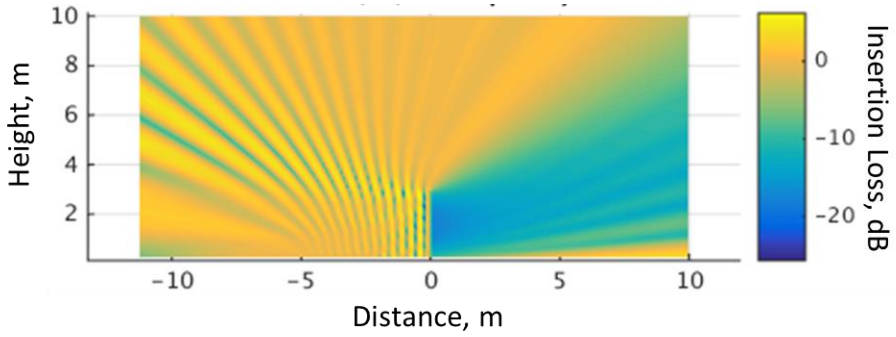

Figure 27. Calculated insertion loss around a 3m sound wall for a source at distance -5m using OpenBEM

occur because of the discrete frequency computation. However, on average, it appears that insertion loss 5m behind the barrier is about 12 dB, which is consistent with the scale model results of Figure 23.

MODELING WIND EFFECTS

The BEM approach using OpenBEM combined with ray theory can be used to compute the sound levels in the immediate vicinity of the barrier in the absence of any wind effects. For longer range calculations at distances beyond 500 to 800m, a parabolic equation approach can be used, which can also incorporate wind and temperature gradients (Ovenden et al. 2009). For open sound propagation, a downwind wind profile relative to the freeway will increase the traffic noise levels by refracting sound down and increasing sound levels near the ground. This behavior is complicated for a barrier case

because the barrier alters the wind profile near the ground. For predicting sound levels behind the barrier in this case, the alteration of the profile by the barrier needs to be taken into account. For this purpose, computational fluid dynamics (CFD) models were considered. An open source software, GERRIS, was identified and appears to be suitable for such modeling. This code was used to predict contours of mean vorticity in the vicinity of a sound wall with a T-top configuration, as shown in Figure 29 for wind approaching from the left. In this figure, the blue areas indicate regions of potential downward sound refraction and

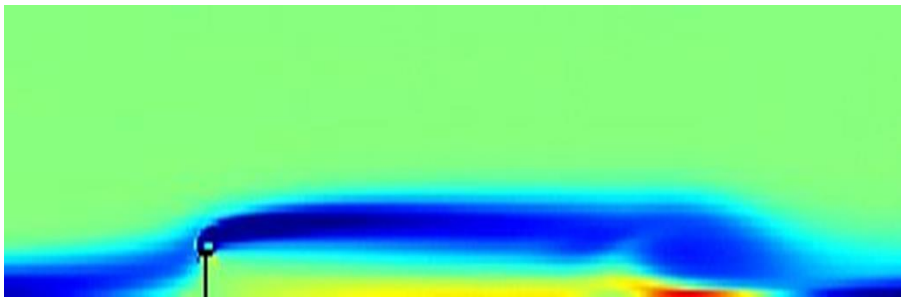

Figure 28. Computation of mean vorticity around a T-top for wind from left to right using GERRIS CFD code

increased noise levels compared to no wind. The parabolic model would then be modified using the output of the CFD model to predict sound levels behind the barrier.

In the ADOT SPR-605 project (Fernando et al. 2010, Shaffer et al. 2013), the framework used to predict sound levels out to 2,000ft is shown in Figure 30. Ray theory resulting from Green's function approximation was used near the source to define input to the parabolic equation model domain used for the longer-range calculations. For computing sound levels behind barriers and taking into account wind and temperature gradients, the more complex framework is shown in Figure 31. In this case, the sound levels close to the roadway and barrier (200ft) will be calculated using BEM, with ray theory used to determine the upper sound propagation for heights from 50 to 1,000ft. At 200ft, the parabolic equation domain using inputs from the CFD modeling will begin. The use of the BEM software will allow examination of different barrier configurations and their effect on close in and more distant sound levels.

The process for computationally evaluating different noise barrier designs would follow the steps listed:

1. A representative sound source for freeway traffic is developed and used throughout for all barriers.
2. Chosen barrier designs (geometry and surface properties) is input into OpenBEM. This is used to determine the acoustic starting field for that barrier design.
3. The barrier geometry is input into GERRIS, and the mean wind (and temperature) profiles downwind of the barrier are computed using GERRIS. A set of benchmark meteorological profiles are used as input conditions upstream.
4. Each meteorological case is input into a refined parabolic equation (PE) model that incorporates in an efficient manner changes to the near-ground wind and temperature profiles with increasing range. A spatial map of the sound pressure level is produced for each meteorological test case.
5. Steps 2-4 can be repeated for different barrier designs and near-ground sound levels can be compared to see whether any particular design performs best overall.

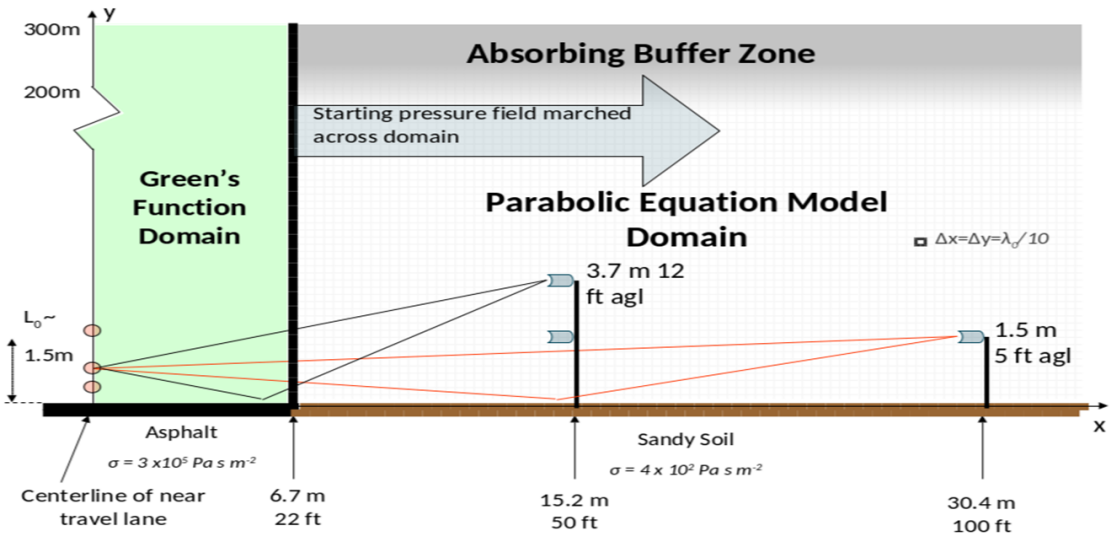

Figure 29. Geometry and calculation domains used model highway noise propagation in ADOT Project SPR-605

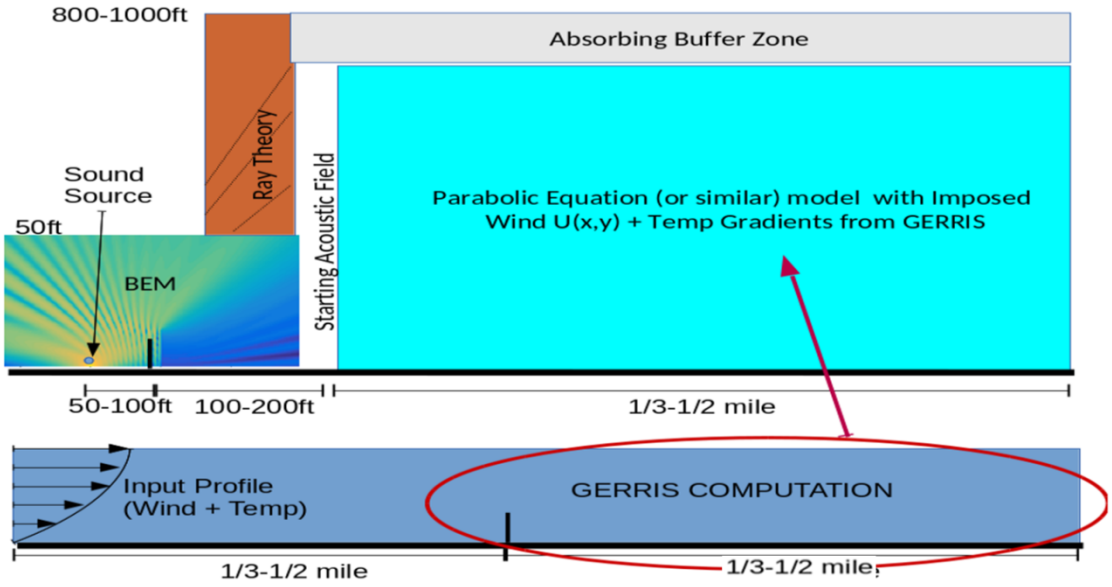

Figure 30. Numerical framework for computing the performance of different barrier designs for different meteorological conditions

CHAPTER 6: CONCLUSIONS AND RECOMMENDATIONS

CONCLUSIONS

Based on the information generated in this research, the following conclusions were developed:

- The performance of actual barrier enhancements is difficult to assess due to the various methods used for the research reported in the literature. Further, the performances of barrier tops that rely on interference effects tend to be exaggerated when single frequency sound and/or single source-receiver paths are used. This was shown by the acoustic model results in which jagged edge tops performed poorly compared to other, non-interference based top designs.

- Considerable temporal variability was observed behind the barrier, with the levels ranging from 4.7 to 6.8 dB on average over the measurement periods with traffic noise variation eliminated. The variation was greater at distances of 100ft and beyond. The cause of the variation was likely due to short-term atmospheric fluctuations over the sound propagation paths to the measurement position.

- The variation found in the measurement averages from session-to-session was 5.0 to 7.4 dB with traffic noise variation eliminated. This amount of variation would be quite discernible in the surrounding neighborhood and could be sufficient to generate complaints. The noise level variation correlated well to air temperature variation, with noise levels increasing with decreasing temperature, and possible temperature inversion effects on sound propagation. Wind speed indicated little effect on barrier performance; however, this was likely due to a lack of wind components perpendicular to the barrier.

- Acoustical scale modeling is an efficient, economical method to evaluate barrier concepts for a variety of different geometries. It is also not subject to the uncertainty due to environmental conditions, as are field measurements. Acoustical scale modeling should be considered for screening different concepts prior to actual field measurements of barrier enhancements.

- Of the concepts evaluated, the T-top concept produced the greatest insertion loss for barriers of the same height. However, the use of a T-top compared to a straight barrier with the width the T added to the height would not produce an acoustical advantage. T-top designs are best considered to be used in situations where straight wall barrier height cannot be increased.

- The effects of wind and temperature could be analytically modeled using BEM to define the acoustic field near a barrier, and then using parabolic equation methods and CFD to examine the more distant sound fields with ray acoustics used to bridge the transition between the different methods.

RECOMMENDATIONS

There are several aspects of this research that lead to further recommendations. The first is the validation and implementation of the T-top enhancement. Of the configurations evaluated, this design was the most promising in producing additional noise reductions, relative to the straight wall barrier of the same height. In order to add this option to the list of noise reduction methods that could be employed by ADOT, field verification of the performance should be completed. This could be done using an existing sound wall to which a temporary top modification could be added, such as a double layer

1-inch thick plywood. This could be tested in both a horizontal (T) configuration and in a vertical configuration as added height to the barrier. This would validate the performance compared to no top treatment and also document any acoustical advantage of the T-top versus simply added barrier height. If the T-top configuration is validated, designs of permanent T-top barriers could be developed as appropriate and placed in ADOT's "tool box" for use when shorter wall heights are required.

A second recommendation is to explore the influence of barrier design on minimizing the effect of meteorological conditions. Even with only minimal wind component in the direction perpendicular to the barrier, the noise levels behind the barrier varied by as much as 6.3 dB at 100ft and 7.4 dB at 300ft from session-to-session. At 300ft, this is more than the insertion loss (6.6 dB) predicted by TNM. Under a more complete set of wind conditions, these ranges will likely increase. The first step in exploring the effect of barrier design on minimizing these effects would be to more fully document of the variation of barrier performance in the field under a full set of different meteorological conditions. This would be completed to document the range of variation and serve as validation data for developing the analytical modeling approach developed in this research. With validated analytical techniques, a variety of barrier top designs would be evaluated to determine if there are designs that are less sensitive to meteorological conditions. As noted in this research, the wake produced by flow over the barrier may have some significance on its performance and could possibly be modified by barrier design.

REFERENCES

AASHTO TP-99-13. 2013. *Standard Method of Test for Determining the Influence of Road Surfaces on Traffic Noise Using the Continuous-Flow Time Integrated Method (dba).*

Auerbach, M., A. Bockstedte, M. Markiewicz, O. Zaleski, and O. Estorff. 2009. "Numerical and Experimental Investigations of Noise Barriers with Helmholtz Resonators", Proceedings of Inter-Noise 2009, Ottawa, Canada, August 2009 (in09_449).

Beranek, L and I. Iver. 1992. *Noise and Vibration Control Engineering.* John Wiley & Sons, Inc., New York, New York.

Boone, M. 2009. "Design of an innovative screen top based on destructive sound interference", Proceedings of Inter-Noise 2009, Ottawa, Canada, August 2009 (in09_145).

Cohn, L. and R. Harris. 1996. "Special Noise Barrier Applications, Phase III", Dept. of Civil Engineering, University of Louisville, Louisville, KY, prepared for the Washington State Department of Transportation, January 1996.

Diez, I., Pilar Fernandez, and Itziar Aspuru. 2012. "Analysis of Efficiency and Usefulness of Top Devices in Noise Barriers", Proceedings of Inter-Noise 2012, New York, New York, August 2012 (in12_1438).

Domingues, O., S. Antunes, I. Ramos, and A. Velez Grilo. 2010. "Diffraction edges perceived efficiency", Proceedings of Inter-Noise 2010, Lisbon, Portugal, June 2010 (435778).

Donavan, P. and B. Rymer. 2010. "Performance and Acoustic Longevity of Concrete Pavements of Different Surface Properties", Proceedings of Inter-Noise 2010, Lisbon, Portugal, June 2010

Donavan, P. and C. Janello. 2017. *Mapping Heavy Vehicle Noise Source Heights for Highway Analysis.* NCHRP Report 842, Transportation Research Board, Washington, D.C.: 2017.

Donavan, P. and D. Lodico. 2013. "The Influence of Quieter Pavement & Absorptive Barriers on US 101 in Marin County, California." Transportation Research Board: Journal of the Transportation Research Record 2362: 25-34.

Donavan, P., and D. Lodico. 2011. *Project 1-44(1), Measuring Tire/Pavement Noise at the Source: Precision and Bias Statement*". NCHRP Report 630, Transportation Research Board, Washington, D.C. :2011.

Donavan, P., C. Janello, and J. Reyff. 2014. *Arizona Quiet Pavement Program, Progress Report 5 for 2011: Site 1, Research Sites 3A, 3D, and 3E*, Phoenix: Arizona Department of Transportation

European Committee for Standardization. 1997. *Road traffic noise reducing devices—Test methods for determining the acoustic performance—Part 3: Normalized traffic noise spectrum*. EN1793-3. http://www.cen.eu (1997)

Fernando, H., N. Ovenden, and S. Shaffer. 2010. *Investigation of Environmental Effects on Freeway Acoustics.* SPR605(1). Phoenix: Arizona Department of Transportation.

Gharabegian, A. 2006. Improving the Performance of Highway Soundwalls, Sound and Vibration, July 2006.

Hasebe, M. 2007. “Performance of a noise barrier with acoustically soft strip”, Proceedings of Inter-Noise 2007, Istanbul, Turkey, August 2007 (in07_656).

Hasebe, M. 2011. “T-Shaped Barrier with a Controlled Series of Wells on the top Plane”, International Institute of Noise Control Engineering, Proceedings of Inter-Noise 2011, Osaka, Japan, September 2011.

Hasebe, M. 2012. “Barrier with a wedge-shaped device composed of wells on the top plane”, Proceedings of Inter-Noise 2012, New York, New York, August 2012 (in12_1555).

Ho, S., I.J. Busch-Vishniac, and D. Blackstock. 1997. “Noise Reduction by a Barrier Having a Random Edge Profile.” J. Acoust. Soc. Am. 101 (5) Pt. 1.

Kang, D., J. Lee, and J. Gu. 2011. “Performance Test of Noise Reducers Installed on the Noise Barrier”, International Institute of Noise Control Engineering, Proceedings of Inter-Noise 2011, Osaka, Japan, September 2011.

Kawai, Y. 2012. “Noise Shielding Efficiency of Edge-Effect Suppression Barriers”, Acoustical Letter, Acoust. Sci &Tech. 33, 3(2012), Acoustical Society of Japan.

Kawai, Y. and M. Toyoda. 2012. “Sound insulation performance of edge-effect suppression barriers”, Proceedings of Inter-Noise 2012, New York, New York, August 2012 (in12_170).

Kim, C., T. Chang, and D.S. Kim. 2011. “Performance Evaluation of Noise Reducing Devices Installed on the Top of Highway Noise Barriers, International Institute of Noise Control Engineering , Proceedings of Inter-Noise 2011, Osaka, Japan, September 2011.

Lodico, D. and J. Reyff. 2009. “Long-Term Noise Performance of Open Graded Asphalt Concrete (OGAC) – Results of 10-Year Long Study”, Noise Control Engineering Journal, Vol. 57, No. 2: 84-93.

Lodico, D., and H. Goldberg. 2010. “Acoustical Performance of T-Top Barrier Design on CO 93”, Presentation at the Transportation Research Board Noise and Vibration Committee ADC 40 Meeting, Denver, CO, July 2010, http://www.adc40.org/presentations/summer2010/Lodico%20TRB10.pdf.

Lyon, R. 1973. *Lectures in Transportation Noise*, Grozier Publishing Co., Cambridge MA.

M. Monazzam and Y.W. Lam. 2005. “Performance of Profiled Single Noise Barriers Covered with Quadratic Residue Diffusers.” *Applied Acoustics*, 66 (6): 709-730.

Maekawa, Z. 1968. “Noise reduction by screens,” Appl. Acoust. 1(3), 157–173.

Okubo, T. and K. Yamamoto. 2006. “Determination of intrinsic efficiency of edge-modified noise barriers”, Proceedings of Inter-Noise 2006, Honolulu, Hawaii, December 2006 (in06_400).

Okubo, T., K. Yamamoto, and O. Funahashi. 2007. “Intrinsic efficiency of edge-modified noise barriers: efficiency determination of practical products and prediction of the diffracted sound field”, Proceedings of Inter-Noise 2007, Istanbul, Turkey, August 2007 (in07_248).

Okubo, T., T. Matsumoto, K. Yamamoto, O. Funahashi, T. Okura, K. Nakasaki, and M. Yamamoto. 2009. “Noise barriers with diffraction-reducing devices on top edge: Propagation prediction applying intrinsic efficiencies determined by impulse-response measurement”, Proceedings of Inter-Noise 2009, Ottawa, Canada, August 2009 (in09_435).

Ovenden N., S. Shaffer, and H. Fernando. 2009. “Impact of Meteorological Conditions on Noise Propagation from Freeway Corridors." Journal of the Acoustical Society of America, 126(1): 25-35.

Pierce A. 1991. *Acoustics. An Introduction to its Physical Principles and Applications*. AIP, New York, 1991: 481–501.

Pierce, A. 1974. “Diffraction of Sound around Corners and over Wide Barriers”, Journal of the Acoustical Society of America 55, 941.

Pigasse, G. and J. Kragh. 2011. *Optimized Noise Barriers – A State of the Art Report: Danish Road Institute Report.* 194-2011.

Sarigul-Klijn, N. and D. Karnopp. 2000. “Random and Periodic Square Wave Barriers in Noise Control”, Institute of Noise Control Engineering, Proceedings of Noise-Con 2000, Newport Beach, California, December 2000.

Saurenman, H., J. Chambers, L. Sutherland, R. Bronsdon, H. Forschner. 2005. *Atmospheric Effects Associated with Highway Noise Propagation*. Final Report 555. Phoenix: Arizona Department of Transportation.

Scofield,L. and P. Donavan. 2005. “Early Results of the Arizona Quiet Pavement Program”, Proceedings of the 80th Meeting of the Association of Asphalt Paving Technologists, Long Beach, California, March 7-9, 2005.

Shaffer, S., H. Fernando, and N. Ovenden. 2013. *Investigations of Environmental Effects on Freeway Acoustics*. SPR605(2). Phoenix: Arizona Department of Transportation.

Watson, D. 2006. *Evaluation of the Benefits and Opportunities for Innovative Noise Barrier Designs.* FHWA-AZ-06-572. HDR Engineering, Inc., 3200 East Camelback Road, Scottsdale, AZ.

Yin, H. 2008. “The Structure Study of the Interference Sound Barrier”, International Institute of Noise Control Engineering, Proceedings of Inter-Noise 2008, Shanghai, China, October 2008.

Yoon, J., Y. Kim, K. Jang, and C. Choi. 2012. “A study on the acoustic performance prediction and evaluation of lattice type noise reducing device installed on the top of noise barrier”, Proceedings of Inter-Noise 2012, New York, New York, August 2012 (in12_496).

APPENDIX A: LITERATURE SEARCH AND REVIEW

Enhancing the noise reducing performance of noise walls has been a topic of interest for 25 years or more. The most common approach is to add sound absorption to the traffic side of the noise wall either by barrier material selection or by addition of material to an existing wall. Under specific conditions, such as parallel walls lining both sides of a highway and elevated receiver locations, added absorption has been calculated to provide as much as a 5 dB reduction for some receiver locations[1]. Many sound wall manufacturers now offer barriers with absorptive materials applied to the face of a barrier for use in an outdoor highway environment and in some states, absorptive barriers are used routinely. A somewhat related method is to tilt the noise walls by as little as 3° to as much as 15° in order to reflect the sound upward[2]. Another approach examined extensively in the literature is to add something to the top of noise wall. Many of these approaches identified and summarized as a result of a literature review reported to ADOT in FHWA-AZ-06-572[3], which was completed in 2006. In this report, many innovative barrier designs were identified and their potential was assessed for implementation in Arizona. The report compared 12 general barrier types based on their acoustical performance, availability/ economic considerations, and constructability. Based on this assessment, two barrier designs were recommended for consideration; T-top Barrier with absorptive material on top of the T, and a vertical barrier with absorptive material on the face. The T-top geometry has been advocated repeatedly, particularly with absorption added to the top of the "T". This configuration was one of two recommended in the literature analysis performed for ADOT in 2006[3], and again in another extensive literature analysis, performed by the Danish Road Institute in 2011[2].

Additions and modifications to the top of noise walls along the lines of innovating designs fall into three groupings. These included absorptive top edge designs of various shapes[4,5,6,7,8], barrier additions designed to improve the diffraction at the top edge of the barrier[9,10,11,12,13,14], and devices to create

---

[1] Donavan, P. and Lodico, D., "The Influence of Quieter Pavement & Absorptive Barriers on US 101 in Marin County, California", Transportation Research Record, Journal of the Transportation Research Board, No. 2362, Environment 2013, pp 25-34.

[2] G. Pigasse, J. Kragh, Optimized Noise Barriers – A State of the Art Report, Danish Road Institute Report 194-2011, December 2011.

[3] D. Watson, "Evaluation of the Benefits and Opportunities for Innovative Noise Barrier Designs", Report No. FHWA-AZ-06-572, HDR Engineering, Inc., 3200 East Camelback Road, Scottsdale, AZ, November 2006.

[4] Y. Kawai and M. Toyoda, "Sound insulation performance of edge-effect suppression barriers", Proceedings of Inter-Noise 2012, New York, New York, August 2012 (in12_170)

[5] Y. Kawai, "Noise Shielding Efficiency of Edge-Effect Suppression Barriers", Acoustical Letter, Acoust. Sci &Tech. **33**, 3(2012), Acoustical Society of Japan.

[6] M. Hasebe, "Performance of a noise barrier with acoustically soft strip", Proceedings of Inter-Noise 2007, Istanbul, Turkey, August 2007 (in07_656)

[7] T. Okubo and K. Yamamoto, "Determination of intrinsic efficiency of edge-modified noise barriers", Proceedings of Inter-Noise 2006, Honolulu, Hawaii, December 2006 (in06_400)

[8] O. Domingues, S. Antunes, I. Ramos, A. Velez Grilo, "Diffraction edges perceived efficiency", Proceedings of Inter-Noise 2010, Lisbon, Portugal, June 2010 (435778)

[9] J. Yoon, Y. Kim, K. Jang, and C. Choi, "A study on the acoustic performance prediction and evaluation of lattice type noise reducing device installed on the top of noise barrier", Proceedings of Inter-Noise 2012, New York, New York, August 2012 (in12_496).

[10] M. Auerbach, A. Bockstedte, M. Markiewicz, O. Zaleski, and O. Estorff, "Numerical and Experimental Investigations of Noise Barriers with Helmholtz Resonators", Proceedings of Inter-Noise 2009, Ottawa, Canada, August 2009 (in09_449)

[11] T. Okubo, T. Matsumoto, K. Yamamoto, O. Funahashi, T. Okura, K. Nakasaki, and M. Yamamoto, "Noise barriers with diffraction-reducing devices on top edge: Propagation prediction applying intrinsic efficiencies

interference between sounds of different path length in the vicinity of the top of the barrier[15,16]. These approaches can be done separately or in combination as illustrated in Figure 1. Most of the studies documenting the performance of these design approaches were conducted using analytical or acoustic scale modelling methods. The analytical studies were typically done using two dimensional (2D) Boundary Element Methods (BEM). The acoustic model studies were done in scales from typically about 10 to 1 to full scale. All of the modeling, either analytical or scale, used only a single point source. For a single point source, the sound over the barrier even by different paths is coherent allowing for interference effects to occur. In reality, traffic is made up of many individual, incoherent point sources that are best represented as an incoherent line source[17]. As a result, the sound arriving at the edge of the barrier comes from many directions and is not correlated in space or time minimizing the possibility of the destructive interference. This does not diminish the computer and scale model results in providing direction on treatments to pursue; however predicted insertion losses from these models will likely never be realized in the field. The largest improvements in barrier performance are typically predicted by 2D BEM (up to 30 dB). Scale model studies with single point sources more typically indicate reductions of 7 to 10 dB while full size model results can be as great as 7 dB for a point source. Actual field try-outs of wall top modifications for actual traffic noise more typically are in the range of 1 to 2 dB for improvement compared to a conventional noise wall.

Many of the basic T-Top design have been investigated using the Boundary Element Method (BEM), as described above, where the absorptive material is replaced by “wells” (a comb-like cross section) of varying depth that improve T-Top performance essentially

---

determined by impulse-response measurement”, Proceedings of Inter-Noise 2009, Ottawa, Canada, August 2009 (in09_435)

[12] M. Boone, “Design of an innovative screen top based on destructive sound interference”, Proceedings of Inter-Noise 2009, Ottawa, Canada, August 2009 (in09_145)

[13] T. Okubo, K. Yamamoto, and O. Funahashi, “Intrinsic efficiency of edge-modified noise barriers: efficiency determination of practical products and prediction of the diffracted sound field”, Proceedings of Inter-Noise 2007, Istanbul, Turkey, August 2007 (in07_248)

[14] A. Gharabegian, Improving the Performance of Highway Soundwalls, Sound and Vibration, July 2006.

[15] D. Kang, J. Lee, and J. GU, “Performance Test of Noise Reducers Installed on the Noise Barrier”, International Institute of Noise Control Engineering, Proceedings of Inter-Noise 2011, Osaka, Japan, September 2011.

[16] C. Kim, T. Chang, and D.S. Kim, “Performance Evaluation of Noise Reducing Devices Installed on the Top of Highway Noise Barriers, International Institute of Noise Control Engineering , Proceedings of Inter-Noise 2011, Osaka, Japan, September 2011.

[17] Lyon, R., Lectures in Transportation Noise, Grozier Publishing Co., Cambridge MA, 1973.

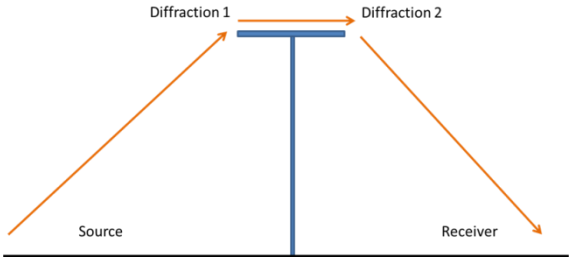

Example of performance improvement by multiple diffractions

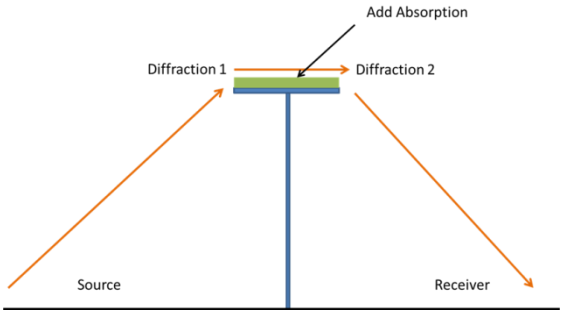

Example of performance improvement with added absorption

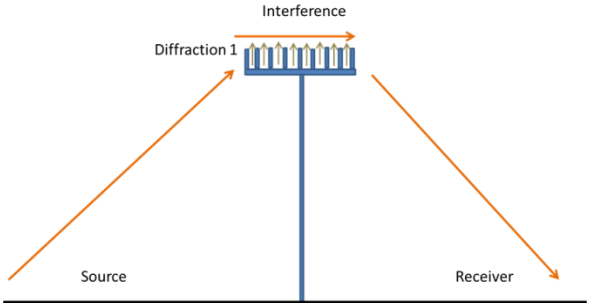

Example of performance improvement by interference of sound

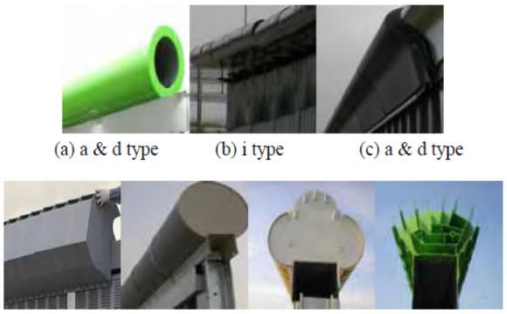

Examples of complex top additions featuring interference, diffraction, and/or absorption (Ref. 15)

Figure 1: Different types of barrier top treatments

by interference effects[18,19,20]. Scale modelling has been conducted to verify BEM models in some cases[5], with results generally tracking those of the BEM models. A T-Top design barrier was recently installed in Golden, Colorado, which is likely one of the first built in the U.S. Unfortunately, full-scale field measurements without and with the top were not possible; however, a reduced size experimental evaluation of the concept indicated improvements of 3 to 4 dB at distances of 3 to 4 wall heights away[21]. These tests also demonstrated that additional reductions of about 1½ dB could be made with the addition of absorbing material to the top of the T. In another study, field-testing on a shaped barrier, similar to a 'T' using a traffic noise source found improvements of only .5 to 1 dB[22].

Like the T-top, many of the other most promising barrier designs include absorptive material, either on

[18] M. Monazzam and Y.W. Lam, YW, 'Performance of Profiled Single Noise Barriers Covered with Quadratic Residue Diffusers' , Applied Acoustics, **66** (6), 2005, pp. 709-730.
[19] M. Hasebe, "T-Shaped Barrier with a Controlled Series of Wells on the top Plane", International Institute of Noise Control Engineering, Proceedings of Inter-Noise 2011, Osaka, Japan, September 2011.
[20] Masaki Hasebe, "Barrier with a wedge-shaped device composed of wells on the top plane", Proceedings of Inter-Noise 2012, New York, New York, August 2012 (in12_1555).
[21] D. Lodico, and H. Goldberg, "Acoustical Performance of T-Top Barrier Design on CO 93", Presentation at the Transportation Research Board Noise and Vibration Committee ADC 40 Meeting, Denver, CO, July 2010, http://www.adc40.org/presentations/summer2010/Lodico%20TRB10.pdf.
[22] Itxasne Diez, Pilar Fernandez, and Itziar Aspuru, "Analysis of efficiency and usefulness of top devices in noise barriers", Proceedings of Inter-Noise 2012, New York, New York, August 2012 (in12_1438).

the face or top of the barrier[1,6,23]. Many sound wall manufacturers now offer barriers with absorptive materials applied to the face of a barrier for use in an outdoor highway environment[24]. However, sound-absorbing materials placed on top of a barrier may have additional maintenance concerns, as precipitation and debris could fall directly onto the absorptive material, changing the material properties and causing difficulties with maintaining the noise reduction properties of the material. The Colorado study[21], found that fiberglass insulation installed on the top of a T-top design improved the noise reduction of the barrier, but that a porous rubber material did not. Unfortunately, fiberglass insulation is not a practical material for outdoor applications and the porous rubber resulted in a sharp peak around 800 Hz, a primary frequency component of traffic noise. These results point to the idea that a material may be able to be tuned be to eliminate peaks within the frequency range of interest to result in improved barrier performance at a reduced sound wall height. Absorptive materials currently constructed for use on the face of the barrier, such as Armtec's Durisol and CSI's SoundSorb, would likely be able to be used as absorptive top materials. Some off-the-shelf absorptive materials that are currently marketed for other uses, such as the Sound Seal Quilted Fiberglass Absorbers, the Empire Acoustical M-90 Backless Absorption Panels, or the Lamvin Soundsucker Metal Acoustical Panels, may also prove to be practical for outdoor use on top of barriers.

Some of the interference designs demonstrated some promise without the need for added absorptive material[25]. There has also been some research into the use of random and periodic "jagged" edge profiles in the upper portion of the barrier that are intended to also create interference on along the top of edge of the barrier[26,27]. These designs also appear promising and may avoid the additional maintenance concerns that may be connected to the use of absorptive material.

[23] L. Cohn and R. Harris, "Special Noise Barrier Applications, Phase III", Dept. of Civil Engineering, University of Louisville, Louisville, KY, prepared for the Washington State Department of Transportation, January 1996.
[24] P. Donavan and D. Lodico, "The Influence of Quieter Pavement & Absorptive Barriers on US 101 in Marin County, California", Compendium of Papers of the 92th Meeting of the Transportation Research Board, Washington, D.C., January 2013.
[25] H. Yin, "The Structure Study of the Interference Sound Barrier", International Institute of Noise Control Engineering, Proceedings of Inter-Noise 2008, Shanghai, China, October 2008.
[26] S. Ho, I.J. Busch-Vishniac, and D. Blackstock, "Noise Reduction by a Barrier Having a Random Edge Profile", J. Acoust. Soc. Am. 101 (5) Pt. 1, May 1997.
[27] N. Sarigul-Klijn and D. Karnopp, "Random and Periodic Square Wave Barriers in Noise Control", International Institute of Noise Control Engineering, Proceeding of Noise-Con 2000, Newport Beach, California, December 2000.

APPENDIX B: SOUND WALL SUPPLIER MEETINGS

March 4th, 2014, 9:00 am-4:30 pm

Panel: Dana Lodico, Paul Donavan, Christ Dimitroplos, Stephen Shaffer

Agenda:

9:00-10:00am: Eric Humphries, Armtec

10:00-10:30am: Panel Discussion

10:30am-11:30pm: Gary Figello, Faddis (web)

11:30-1:00pm: Panel Discussion and Lunch

1:00-2:00pm: Boone Bucher, CSI

2:00-2:30pm: Panel Discussion

2:30-3:30pm: Peter D'Antonio, RPG (web)

3:30-4:00pm: Panel Discussion

Armtec - Eric Humphries,

Armtec is a global infrastructure and construction materials company, headquartered in Canada, with most of their production facilities there. Their products are largely based on concrete applications for drainage products, bridges, soil retention, parking garages and other applications, including traffic noise barriers. Armtec has been active since 1977, with some installations still present from that time. The company is ISO 9002 certified and an NPCA approved precaster. Over 15-20 million ft^2 of product have been installed and they anticipate a 40+ year or greater lifetime. Supporting material includes several letters dated 2009, indicating no issues with the product. The company has approximately 1000 employees, $500 million/year of sales. They provide engineering and design (geotechnical and CAD software), enabling customization of projects. Cost minimization is best achieved with reduced project constraints, allowing more design variability by manufacturer.

Durisol was once the name of the company, but now it is a product name. It is an absorptive and non-toxic precast material made from 90% recycled wood pulp (from milling processes diverted from waste stream), mineralized and mixed with concrete. Basically any texture or design can be added to the exposed surface. The panel texture depth ranges from approximately 1.5-inch depth on the molded side and about 0.75 inch on the lid side (top of panel as cast). The panels are approximately 7.5 inches thick. Durisol comes with a 10-year warranty. There are two main types of product: Durisol Acoustic Facing - attach to existing walls, retrofit to provide absorptive quality (used widely in California and Texas); Durisol Precast Noise Barrier - precast panels typically 12-ft wide (20 inch high panels), 15-ft wide (3-ft high panels), or 20-ft wide (7-ft high panels).

Durisol can be used as a retaining wall/noise barrier (RW/NB) system by increasing the bottom panel thickness (RW panel), post size and footing diameter/depth. It can also be use along elevated roadways and has been used in applications over 20' in height on structure. It can be designed to withstand the

higher wind loads called out in the 2012 Bridge Design Manual for a 75-year service life. It has been used on past projects with wind loads of 50-57 psf in Boston. Durisol is used in many States, including CT, IN, IL, MA, NY, OH, TN and WI. The NB12 and NB15 system is absorptive on both sides with a Noise Reduction Coefficient (NRC) greater than 0.7 for a flat panel and up to 0.8 - 0.9 with a textured "stone" look. Weight of a Durisol panel is 45psf for NB15 systems and up to 90 psf for NB20. Eric did not have any information on studies looking at how dust might clog pores and change absorptive properties. The product is also available as block used primarily in the housing construction market.

Durisol has been used for the base of existing T-top shaped barriers. Constructed T-tops typically have 3.5" of absorption on one side of the barrier base, using a 12-15" overhang. It is thought that it could also be used as an absorptive material to be placed on the top of the 'T' or for a 'tilted top'. For constructed T-tops, the cost was reduced by 7% from the cost of a traditional wall with 2.25 ft additional height at the same theoretical insertion loss. The product already has peak absorption in a broad frequency range, applicable to highway noise. It may be possible to spectrally tune the wall's absorptive coefficients in relation to the roadway pavement's spectral characteristics.

They also manufacture a transparent product, which weighs 4-8 lb ft^{-2}, is self-cleaning, and has been in used in AK, CA, CT, MN, NJ, NY, OH & WI with freeze-thaw and salted road conditions. Transparent posts are thought to be too costly for barriers (they use them for hockey rinks). The product is NCHRP 350 crash tested to Test Level 4 and this system has been wind load tested to 93 psf (however, impact loads were still controlling). Another option might be to add a clear section of wall at the top of the barrier to reduce the effective visual height and to limit obscuring vistas.

Armtec also has a product called Whisper Wall. This design is a sound absorbing panel combining rubber from recycled tires and structural concrete. This material also facilitates creative surfaces that can be designed to be aesthetically pleasing.

Pre and post construction measurements may have been conducted in Texas, where field sites can be found with existing absorptive and non-absorptive walls in close proximity for comparison.

Faddis - Gary Figello

Note: Due to weather related travel problems, Gary participated in the meeting for Faddis via the web.

Faddis Concrete Products is headquartered in Pennsylvania, with 4 of its 5 plants in the state, and supplies precast concrete products for applications in transportation projects, industrial settings, security, and architectural clients, as well as noise walls. Their barrier product lines include absorptive and non-absorptive walls (AcoustaCrete), clear acrylic walls (AcoustaClear), and aluminum walls for light-weight bridge applications (AcoustAL).

For a more innovative design, Gary discussed the Foss Double Barrier system[28]. This concept was developed and demonstrated with acoustic scale testing in 1976 and the method of calculating the performance is included in the Federal Highway Administration (FHWA) Traffic Noise Model (TNM) in

[28] Foss, R., "Noise Barrier Screen Measurements, Double Barriers", Washington State Highway Department Research Program Report 24.3, Applied Physics Laboratory, University of Washington Report APL-UW 7618, August 1976.

Appendix D. As implemented in TNM, this design does not include absorptive faces for the double noise walls. Compared to a single barrier with greater equivalent height, the double barrier design could provide up to 11 dB of additional noise insertion loss. The equivalent height is at the intersection of straight lines, from the source past the top of the first wall, with line from receiver past the top of the second wall or "leaning-pole theory". This concept could be implemented with Faddis' products such as AcoustaCrete to create a Foss Double Barrier system with absorption on both faces of the inner barrier surface to provide even more attenuation.

Gary provided his spreadsheet, which calculates the Foss algorithm and compares the results to that of a single barrier. Several examples were discussed. Based on review of the spreadsheet, two 12-ft high barriers, spaced 6 feet apart, would result in the equivalent insertion loss as a single 20-ft high barrier (about 23 dB for this example).

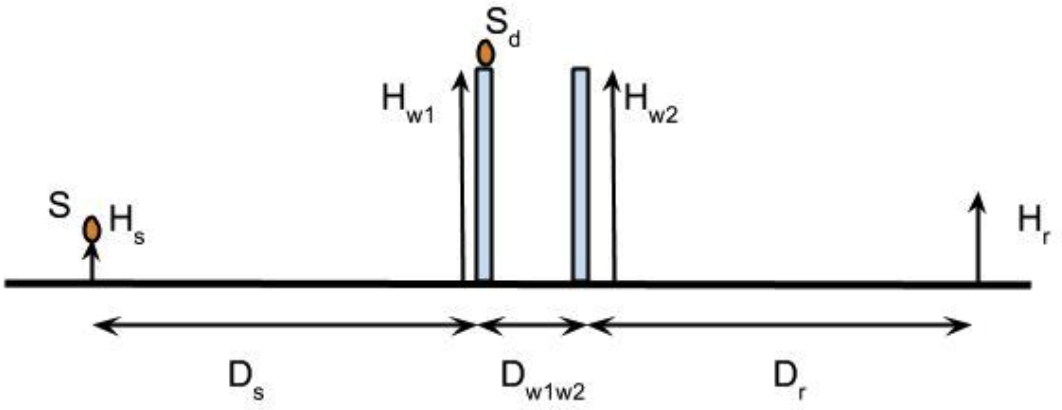

Figure 1. Schematic of type of examples worked for double wall configuration with source and receiver distances, D_s and D_r, respectively, wall separation distance D_{w1w2}, wall heights H_{w1}, H_{w2}, and source and receiver heights, H_s and H_r, respectively. The source strength is S, with a source due to diffraction atop the first wall of strength S_d.

The Foss Barrier System has many design possibilities. There are limitations in terms of the space needed for the separation distance. However, walls only need to be spaced few wavelengths for frequency of interest and Arizona often locates barriers 50 to 100 feet from the edge of pavement, so there should be plenty of space in these situations. There was also some concern of how to sell this idea to the public, as a double wall might be seen as a poor design and waste of money/resources. One option to resolve the public perception issue might be to create the first wall with an acrylic panel mounted in front of the second wall. Other options might be to tilt the primary wall, place absorptive materials (such as a gravel pit) between the two walls, or to package it as a single system. Gary did not know of any field data of Foss Barrier Systems.

Gary also provided a sample of Plaskolite from Plaskolite, Inc. headquartered in Columbus, Ohio. The specific product was OPTIX NB w/ bird shield (APL-JDW 7618). It is available in panels 0.5 inch thick ~\$10 ft^{-2}, 0.75 in for \$15 ft^{-2}, and 1 in for \$20 ft^{-2}, plus mounting cost.

CSI - Boone Bucher,

Concrete Solutions (CSI) is based in Austin, Texas. The company licenses a porous cement-based manufacturing technology, SoundSorb. Unlike other barrier companies, CSI does not produce barriers, but provides the SoundSorb technology to local concrete precast barrier manufacturers that enables their sound walls to perform as sound absorptive noise barriers. CSI licenses and trains local manufacturers to combine the mixed recycled ingredients with state approved structural concrete precast sound barrier designs, including crash barrier mounted walls and retaining wall mounted barriers, providing a sound absorptive post-less noise barrier system. The SoundSorb material is most efficient within the 450-2500 Hz range and achieves the highest possible noise reduction ratings (NRC .95- 1.0 at 3" thick application). Adding SoundSorb textures and decreasing pore size can add an additional .05+ to the NRC.

The CSI acoustical material (NRC 1.0) can be placed over existing wall faces, on the top of T-top barriers and basically applied to any surface to increase traffic noise absorption. Like concrete, this cement-based material has a long lifespan and requires 'no' maintenance. The material is free draining and can be used in a desert climate, as well as freeze/thaw conditions, and can be colorized. Hydrophobic water repellents/stains can be applied to the wall surface to colorize and cause rain to bead up and wash down the wall face. Anti-graffiti coatings can also be applied the facade. Textures (graphic art) can be stamped into the sound wall face of the CSI acoustical material, providing a lot of aesthetic design flexibility / freedom. There is no available data looking at long-term affects of dust clogging of pores; however, over the last 21 year history of SoundSorb installations, CSI has not heard of any pore clogging related issues.

SoundSorb has been tested in-situ by many transportation engineers and transportation authorities world-wide and found to be successful on many high profile highway / rail transportation projects. A research paper was provided with field data that compared four types of wall materials. All of the walls were manufactured as 14 ft high sound barriers and tested in an in-situ study. SoundSorb (NRC .95) product achieved the highest decibel reduction over all, showing a 10.8 dB for the insertion loss (IL). The standard sound reflective TXDOT concrete barrier (NRC 0.02) followed with @ 9.6 dB (IL). Durisol (using lab test results indicated NRC .80 -.85) was next, providing 8.7 dB (IL) and, lastly, Whisperwall (using lab test results NRC .70) provided the lowest decibel reduction of 6.6 dB (IL).

It was suggested that using a high NRC .95+ sound absorptive material could increase the effectiveness of a sound barrier, allowing for wall height reduction to achieve the same insertion loss and reducing the overall cost of the wall. In addition, reflections within the transportation corridor would be reduced, which could reduce traffic noise levels at receptors at locations on the highway side opposite the barrier location.

RPG - Peter D'Antonio (web)

RPG Diffusor Systems, Inc. is provider of acoustical products for several different industries with a strong emphasis in architectural acoustics. RPG offers two existing products that could be applicable to noise barrier design. The first is Diffusor Blox, a Quadratic Residue Diffusor (QRD) in the form a Concrete Masonry Unit (CMU) that functions as a cinder block with sound absorbing features. The second product is Quietstone, an absorptive panel fabricated from 96% recycled glass or stone. Both products can be used for interior or exterior applications. DiffusorBlox would be used to fabricate the noise barrier and Quietstone would be applied to the face of a noise barrier. DiffusorBlox is a reflection phase grating system, which incorporates divided wells of different depth, based on number theory to uniformly scatter sound. Included slots provide low frequency absorption and the surface finish determines the degree of high frequency absorption. The initial pattern is treated as a fundamental

domain for a fractal surface with 2-3 iterations. Patent 6,772,859 gives further details and claims: (http://www.google.com/patents/US6772859). DiffusorBlox or custom designed QRDs have been shown to provide significant IL when applied to the tops of both vertical and slanted barriers. Two-dimensional BEM calculations for determining the IL of a barrier indicate 5-12 dB IL for a barrier height of 3 m with the source located between barriers, one with a QRD top and the other with a QRD surface toward the source. With both barriers slanted, the IL improves to 16.3 dB Listed several publications (see presentation) that summarize findings. RPG may be able to send us a sample for scale modeling purposes.

Additional Suppliers Contacted

In addition to the four suppliers that presented at this meeting, several others were contacted and either did not return contact after several attempts, or declined to meet due to lack of interest or because they felt they did not have any material to present that would be of value to the project. These include; Concrete Express, Inc (CEI), Sound Fighter, MP Dory Company, and Kawasaki Quiet Edge.

Handout Materials from Meetings

Durisol performance provided by Eric Humphries from Armtec:

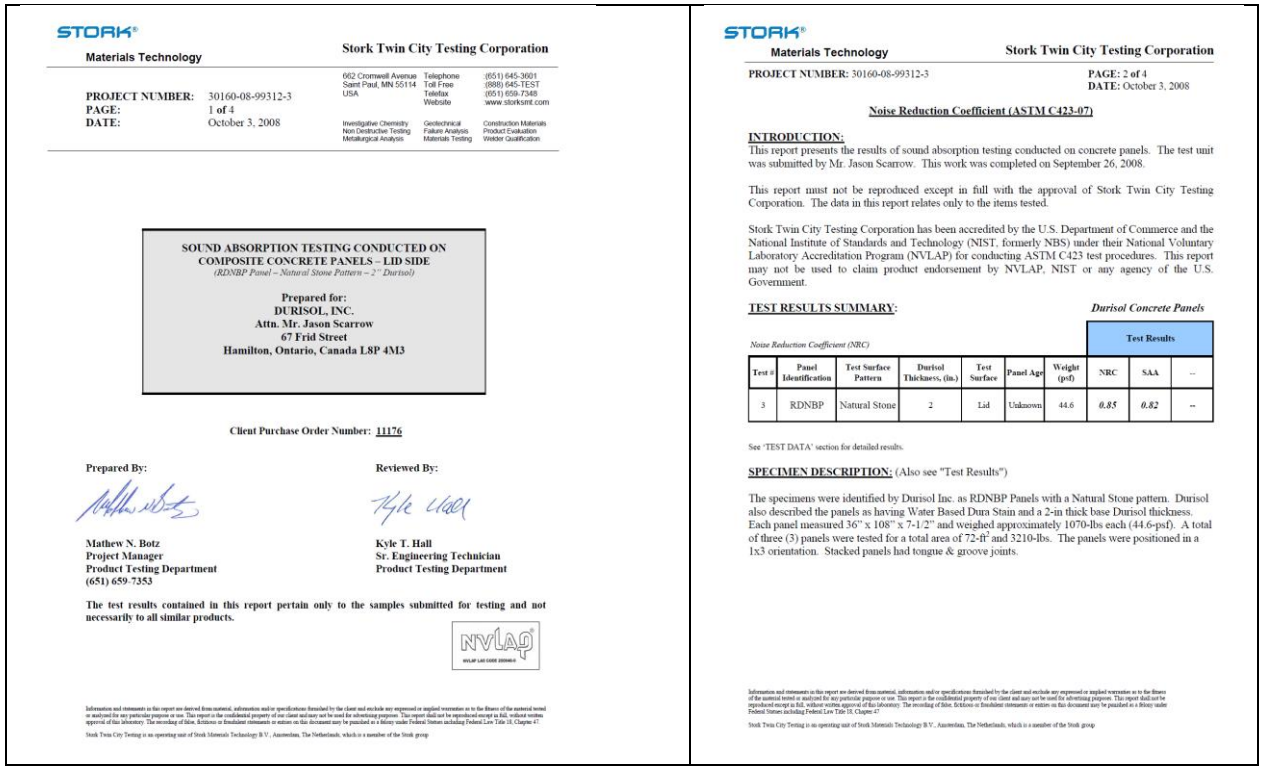

STORK®
Materials Technology

Stork Twin City Testing Corporation

662 Cromwell Avenue
Saint Paul, MN 55114
USA

Telephone :(651) 645-3601
Toll Free :(888) 645-TEST
Telefax :(651) 659-7348
Website :www.storksmt.com

Investigative Chemistry, Non Destructive Testing, Metallurgical Analysis
Geotechnical, Failure Analysis, Materials Testing
Construction Materials, Product Evaluation, Welder Qualification

PROJECT NUMBER: 30160-08-99312-3
PAGE: 1 of 4
DATE: October 3, 2008

SOUND ABSORPTION TESTING CONDUCTED ON COMPOSITE CONCRETE PANELS – LID SIDE
(RDNBP Panel – Natural Stone Pattern – 2" Durisol)

Prepared for:
DURISOL, INC.
Attn. Mr. Jason Scarrow
67 Frid Street
Hamilton, Ontario, Canada L8P 4M3

Client Purchase Order Number: 11176

Prepared By:

Mathew N. Botz
Project Manager
Product Testing Department
(651) 659-7353

Reviewed By:

Kyle T. Hall
Sr. Engineering Technician
Product Testing Department

The test results contained in this report pertain only to the samples submitted for testing and not necessarily to all similar products.

NVLAP

Information and statements in this report are derived from material, information and/or specifications furnished by the client and exclude any expressed or implied warranties as to the fitness of the material tested or analyzed for any particular purpose or use. This report is the confidential property of our client and may not be used for advertising purposes. This report shall not be reproduced except in full, without written approval of this laboratory. The recording of false, fictitious or fraudulent statements or entries on this document may be punished as a felony under Federal Statues including Federal Law Title 18, Chapter 47.

Stork Twin City Testing is an operating unit of Stork Materials Technology B.V., Amsterdam, The Netherlands, which is a member of the Stork group.

STORK®
Materials Technology

Stork Twin City Testing Corporation

PROJECT NUMBER: 30160-08-99312-3

PAGE: 2 of 4
DATE: October 3, 2008

Noise Reduction Coefficient (ASTM C423-07)

INTRODUCTION:
This report presents the results of sound absorption testing conducted on concrete panels. The test unit was submitted by Mr. Jason Scarrow. This work was completed on September 26, 2008.

This report must not be reproduced except in full with the approval of Stork Twin City Testing Corporation. The data in this report relates only to the items tested.

Stork Twin City Testing Corporation has been accredited by the U.S. Department of Commerce and the National Institute of Standards and Technology (NIST, formerly NBS) under their National Voluntary Laboratory Accreditation Program (NVLAP) for conducting ASTM C423 test procedures. This report may not be used to claim product endorsement by NVLAP, NIST or any agency of the U.S. Government.

TEST RESULTS SUMMARY: ***Durisol Concrete Panels***

Noise Reduction Coefficient (NRC)

							Test Results		
Test #	Panel Identification	Test Surface Pattern	Durisol Thickness, (in.)	Test Surface	Panel Age	Weight (psf)	NRC	SAA	--
3	RDNBP	Natural Stone	2	Lid	Unknown	44.6	*0.85*	*0.82*	--

See 'TEST DATA' section for detailed results.

SPECIMEN DESCRIPTION: (Also see "Test Results")

The specimens were identified by Durisol Inc. as RDNBP Panels with a Natural Stone pattern. Durisol also described the panels as having Water Based Dura Stain and a 2-in thick base Durisol thickness. Each panel measured 36" x 108" x 7-1/2" and weighed approximately 1070-lbs each (44.6-psf). A total of three (3) panels were tested for a total area of 72-ft^2 and 3210-lbs. The panels were positioned in a 1x3 orientation. Stacked panels had tongue & groove joints.

Information and statements in this report are derived from material, information and/or specifications furnished by the client and exclude any expressed or implied warranties as to the fitness of the material tested or analyzed for any particular purpose or use. This report is the confidential property of our client and may not be used for advertising purposes. This report shall not be reproduced except in full, without written approval of this laboratory. The recording of false, fictitious or fraudulent statements or entries on this document may be punished as a felony under Federal Statues including Federal Law Title 18, Chapter 47.

Stork Twin City Testing is an operating unit of Stork Materials Technology B.V., Amsterdam, The Netherlands, which is a member of the Stork group.

STORK®

Materials Technology — Stork Twin City Testing Corporation

PROJECT NUMBER: 30160-08-99312-3 — **PAGE:** 3 of 4 — **DATE:** October 3, 2008

TEST PROCEDURE

Sound Absorption Test

ASTM C 423-07," Sound Absorption and Sound Absorption Coefficient by the Reverberation Room Method", was followed in every respect. The panels were tested in Type A Mounting (on the floor). The panel edge/perimeter was covered with 7" tall border walls constructed from 5/8" sheetrock

NRC was calculated by rounding the sound absorption coefficients for 250, 500, 1000 and 2000 Hz to the nearest 0.05. SAA was calculated by rounding the sound absorption coefficients for the twelve frequencies from 200 Hz to 2500 Hz to the nearest 0.01.

TEST EQUIPMENT:

Manufacturer	Model	Description	S/N
Norwegian Electronics	NE830	Real Time Analyzer	11511
Brüel & Kjær	3923	Rotating Microphone Boom	815424
Norsonic (Source Rm)	1230	Pressure Condenser Microphone	26361
Brüel & Kjær (Term Rm)	4192	Pressure Condenser Microphone	2360314

REMARKS:

The test sample will be retained for a period of **15-days** and then discarded unless notified by the client.

F:\Product\MMFILES\MNB\2008 REPORTS MNB\99312-Durisol-3.doc

STORK®

Materials Technology — Stork Twin City Testing Corporation

PROJECT NUMBER: 30160-08-99312-3 — **PAGE:** 4 of 4 — **DATE:** October 3, 2008

TEST RESULTS:

Filename: TEST #3

ASTM C423 - Sound Absorption

Client	Product	Model #	Quantity	Comment
Durisol Inc.	Concrete Panels	RDNBP	1	Natural Stone Pattern

Sample Size - Wt.: 100.0 in x 96.0 in x 7.5" - 3210 lbs

Sample Description: Durisol Inc.: RDNBP Panel, Lid Side - 2" Base Durisol Thickness @7RC031 - Tag #) :

Time Stamp: Fri, Sep 26, 2008 - 11:11 AM

Total Sample Area: 72.0 ft²

F (Hz)	Absorption Coefficient	Absorption (Sabins)*
100	0.15	11.03
125	0.27	19.27
160	0.25	18.17
200	0.43	30.84
250	0.62	44.65
315	0.77	55.51
400	0.97	69.76
500	1.05	75.57
630	0.95	68.73
800	0.86	61.72
1000	0.77	55.70
1250	0.80	57.58
1600	0.88	63.70
2000	0.87	62.81
2500	0.86	61.93
3150	0.86	62.20
4000	0.87	62.36
5000	0.84	60.16

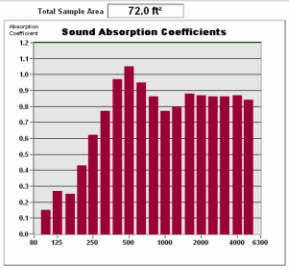

Temp (°C): 22.4 — R.H. (%): 54 — ATM (mbar): 995

* total absorption based on 72.0 ft²

SAA = 0.82 NRC = 0.85

Material provided by Gary Figello of Faddis:

Faddis
Concrete Products

AcoustaCrete®

Noise from electric transformers, reactors, and industrial equipment are abated by the installation of AcoustaCrete noise barriers.

Faddis Concrete Products
1805 Horseshoe Pike
Honey Brook, PA 19344
610 269-4685
610 942-2629 fax
www.faddis.com
info@faddis.com

Faddis
Concrete Products

AcoustaCrete®

available in a wide variety of patterns and colors, e.g., brick , field stone, tree bark, graphics, fluted, ashlar stone

Faddis Concrete Products
1805 Horseshoe Pike
Honey Brook, PA 19344
610 269-4685
610 942-2629 fax
www.faddis.com
info@faddis.com

Faddis
Concrete Products

AcoustaCrete®

Over 4,000,000 square feet of sound absorptive AcoustaCrete walls have been constructed to eliminate reverberation between walls and reflection from noise barriers.

Faddis Concrete Products
1805 Horseshoe Pike
Honey Brook, PA 19344
610 269-4685
610 942-2629 fax
www.faddis.com
info@faddis.com

Foss Double wall calculation spreadsheet from Gary Figello of Faddis:

Foss Double Barrier Analysis

feet		
30	S	horizontal distance from source to first (left) wall along reference line
100	W	horizontal distance between walls along reference line
100	M	horizontal distance from second (right) wall to receiver along reference line
230	T	horizontal distance from source to receiver along reference line
4	H1	vertical height of source
7	H2	vertical height of first (left) wall above reference line
12	H3	vertical height of second (right) wall above reference line
11	H4	vertical height of receiver

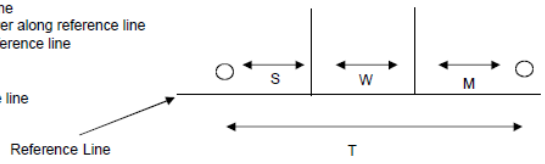

calculate Fresnel number for left wall

0.083	D = a + b - c											
30.150	a		9	900								
200.040	b		16	40000								
230.106	c		49	52900								
									1128			
		c			1128	1128	1128	1128	1000	1128	1128	1128	1128
		f			31.5	63	125	250	500	1000	2000	4000	8000
		Wave Length Feet			35.810	17.905	9.024	4.512	2.000	1.128	0.564	0.282	0.141
		N			0.005	0.009	0.018	0.037	0.083	0.147	0.295	0.590	1.179
		sqrt 2piN			0.2	0.2	0.3	0.5	0.7	1.0	1.4	1.9	2.7
		tanh			0.2	0.2	0.3	0.4	0.6	0.7	0.9	1.0	1.0
		sqrt/tanh			1.0	1.0	1.0	1.1	1.2	1.3	1.6	2.0	2.7
		20log			0	0	0	1	1	2	4	6	9
	Fresnel	Theor Ae			5.1	5.2	5.3	5.6	6.4	7.2	8.8	11.1	13.8
	safe	Barrier IL (dB)			2.1	2.2	2.3	2.6	3.4	4.2	5.8	8.1	10.8
	N=>1.2	16+10logN			0.0	0.0	0.0	0.0	0.0	0.0	0.0	0.0	0.0
	1.2<N<0	5.8+10.4(N)^0.41			6.949	7.327	7.822	8.487	9.551	10.544	12.103	14.174	16.927
	0<=N<-0.22	6-12sqrt(abs(N))			0.0	0.0	0.0	0.0	0.0	0.0	0.0	0.0	0.0

calculate Fresnel number for right wall

0.144	D = d + e - c											
130.246	d		64	16900								
100.005	e		1	10000								
230.106	c		49	52900								
									1128			
		c			1128	1128	1128	1128	1000	1128	1128	1128	1128
		f			31.5	63	125	250	500	1000	2000	4000	8000
		Wave length feet			35.810	17.905	9.024	4.512	2.000	1.128	0.564	0.282	0.141
		N			0.008	0.016	0.032	0.064	0.144	0.256	0.512	1.024	2.049
		sqrt 2piN			0.2	0.3	0.4	0.6	1.0	1.3	1.8	2.5	3.6
		tanh			0.2	0.3	0.4	0.6	0.7	0.9	0.9	1.0	1.0
		sqrt/tanh			1.0	1.0	1.1	1.1	1.3	1.5	1.9	2.6	3.6
		20log			0	0	1	1	2	3	6	8	11
	Fresnel	Theor Ae			5.1	5.3	5.6	6.1	7.2	8.4	10.6	13.2	16.1
	safe	Barrier IL (dB)			2.1	2.3	2.6	3.1	4.2	5.4	7.6	10.2	13.1
	N=>1.2	16+10logN			0.0	0.0	0.0	0.0	0.0	0.0	0.0	0.0	19.1
F values dB	1.2<N<0	5.8+10.4(N)^0.41			7.241	7.715	8.336	9.170	10.504	11.749	13.705	16.303	19.755
	0<=N<-0.22	6-12sqrt(abs(N))			0.0	0.0	0.0	0.0	0.0	0.0	0.0	0.0	0.0

Set up the example so that the N of the right wall is greater than the N of the left wall
Now, calculate Fresnel number assuming a point source at top of the more attenuative wall and calculate the new Nj for remaining wall

0.029	D = a + f - g											
30.150	a		9	900								
100.125	f		25	10000								
130.246	g		64	16900								
									1128			
		c			1128	1128	1128	1128	1000	1128	1128	1128	1128
		f			31.5	63	125	250	500	1000	2000	4000	8000
		Wave length feet			35.810	17.905	9.024	4.512	2.000	1.128	0.564	0.282	0.141
		N			0.002	0.003	0.006	0.013	0.029	0.051	0.102	0.203	0.406
		sqrt 2piN			0.1	0.1	0.2	0.3	0.4	0.6	0.8	1.1	1.6
		tanh			0.1	0.1	0.2	0.3	0.4	0.5	0.7	0.8	0.9
		sqrt/tanh			1.0	1.0	1.0	1.0	1.1	1.1	1.2	1.4	1.7
		20log			0	0	0	0	0	1	2	3	5
	Fresnel	Theor Ae			5.0	5.1	5.1	5.2	5.5	5.9	6.6	7.9	9.8
	safe	Barrier IL (dB)			2.0	2.1	2.1	2.2	2.5	2.9	3.6	4.9	6.8
	N=>1.2	16+10logN			0.0	0.0	0.0	0.0	0.0	0.0	0.0	0.0	0.0
J values	1.2<N<0	5.8+10.4(N)^0.41			6.542	6.786	7.106	7.536	8.223	8.864	9.871	11.209	12.987
	0<=N<-0.22	6-12sqrt(abs(N))			0.0	0.0	0.0	0.0	0.0	0.0	0.0	0.0	0.0

Assume right wall N is greater than left wall N

		31.5	63	125	250	500	1000	2000	4000	8000
F		7.241	7.715	8.336	9.170	10.504	11.749	13.705	16.303	19.115
J		6.542	6.786	7.106	7.536	8.223	8.864	9.871	11.209	12.987
W		100	100	100	100	100	100	100	100	100
T		230	230	230	230	230	230	230	230	230
W/T		0.435	0.435	0.435	0.435	0.435	0.435	0.435	0.435	0.435
		3.125	3.125	3.125	3.125	3.125	3.125	3.125	3.125	3.125
		-1.300	-1.300	-1.300	-1.300	-1.300	-1.300	-1.300	-1.300	-1.300
		0.962	0.966	0.971	0.977	0.984	0.988	0.993	0.996	0.998
Total Attenuation dB		12.028	12.737	13.669	14.922	16.931	18.809	21.763	25.693	30.279
Improvement over single barrier		4.786	5.022	5.333	5.752	6.427	7.060	8.059	9.390	11.164

EXAMPLE RESULT IS 16.96 (ROUNDING)

Note: For the actual working spreadsheet, contact the authors of this report. Other available materials include WSDOT research reports on absorptive single wall barrier and the Foss double wall.

Material from Peter D'Antonio of RPG on Diffusor Block:

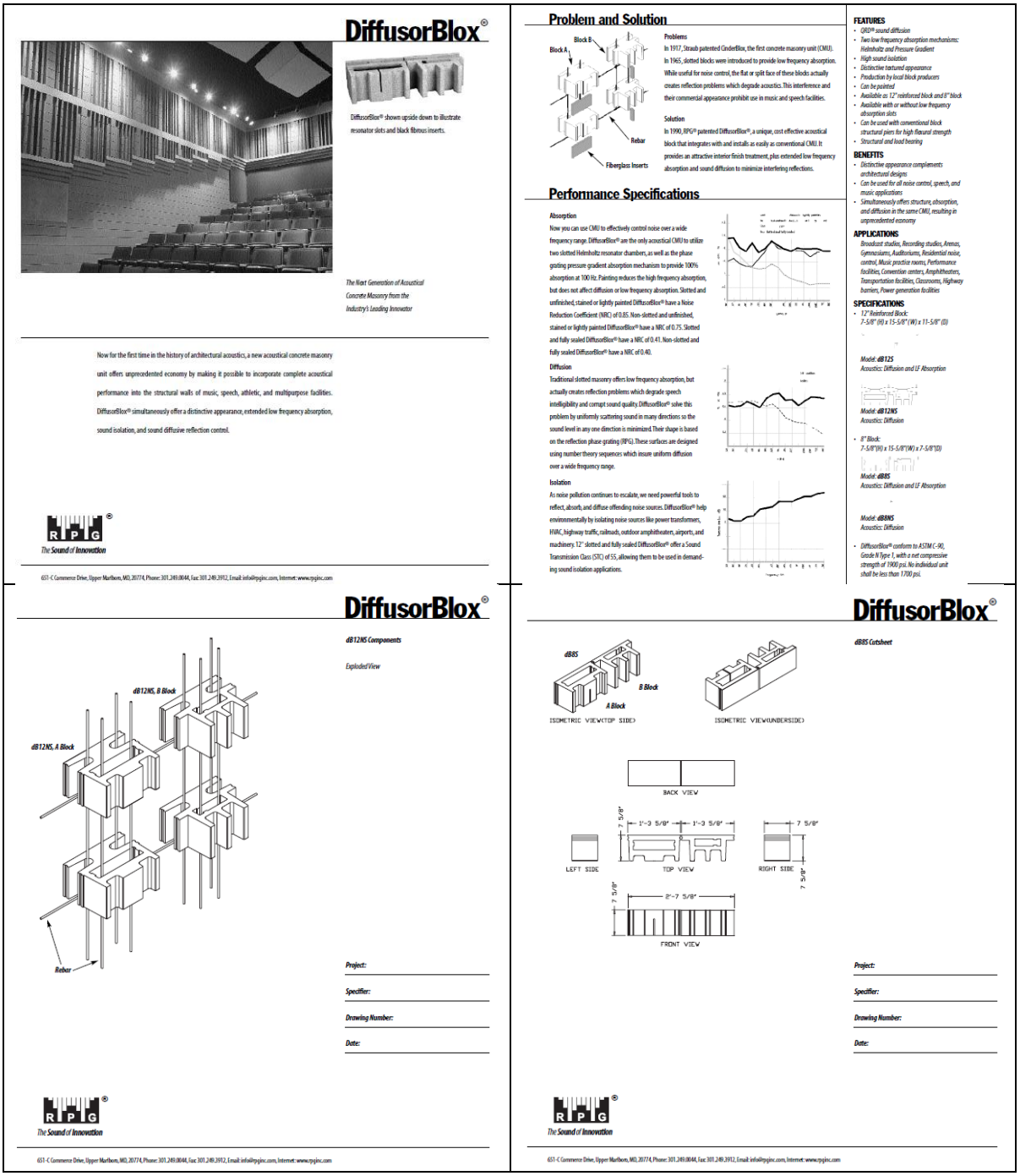

DiffusorBlox®

DiffusorBlox® shown upside down to illustrate resonator slots and black fibrous inserts.

The Next Generation of Acoustical Concrete Masonry from the Industry's Leading Innovator

Now for the first time in the history of architectural acoustics, a new acoustical concrete masonry unit offers unprecedented economy by making it possible to incorporate complete acoustical performance into the structural walls of music, speech, athletic, and multipurpose facilities. DiffusorBlox® simultaneously offer a distinctive appearance, extended low frequency absorption, sound isolation, and sound diffusive reflection control.

RPG *The Sound of Innovation*

651-C Commerce Drive, Upper Marlboro, MD, 20774, Phone: 301.249.0044, Fax: 301.249.3912, Email: info@rpginc.com, Internet: www.rpginc.com

Problem and Solution

Problem

In 1917, Straub patented UnderBlox, the first concrete masonry unit (CMU). In 1965, slotted blocks were introduced to provide low frequency absorption. While useful for noise control, the flat or split face of these blocks actually creates reflection problems which degrade acoustics. This interference and their commercial appearance prohibit use in music and speech facilities.

Solution

In 1990, RPG® patented DiffusorBlox®, a unique, cost effective acoustical block that integrates with and installs as easily as conventional CMU. It provides an attractive interior finish treatment, plus extended low frequency absorption and sound diffusion to minimize interfering reflections.

Performance Specifications

Absorption

Now you can use CMU to effectively control noise over a wide frequency range. DiffusorBlox® are the only acoustical CMU to utilize two slotted Helmholtz resonator chambers, as well as the phase grating pressure gradient absorption mechanism to provide 100% absorption at 100 Hz. Painting reduces the high frequency absorption, but does not affect diffusion or low frequency absorption. Slotted and unfinished, stained or lightly painted DiffusorBlox® have a Noise Reduction Coefficient (NRC) of 0.85. Non-slotted and unfinished, stained or lightly painted DiffusorBlox® have a NRC of 0.75. Slotted and fully sealed DiffusorBlox® have a NRC of 0.41. Non-slotted and fully sealed DiffusorBlox® have a NRC of 0.40.

Diffusion

Traditional slotted masonry offers low frequency absorption, but actually creates reflection problems which degrade speech intelligibility and corrupt sound quality. DiffusorBlox® solve this problem by uniformly scattering sound in many directions so the sound level in any one direction is minimized. Their shape is based on the reflection phase grating (RPG). These surfaces are designed using number theory sequences which insure uniform diffusion over a wide frequency range.

Isolation

As noise pollution continues to escalate, we need powerful tools to reflect, absorb, and diffuse offending noise sources. DiffusorBlox® help environmentally by isolating noise sources like power transformers, HVAC, highway traffic, railroads, outdoor amphitheaters, airports, and machinery. 12" slotted and fully sealed DiffusorBlox® offer a Sound Transmission Class (STC) of 55, allowing them to be used in demanding sound isolation applications.

FEATURES

- *QRD® sound diffusion*
- *Two low frequency absorption mechanisms: Helmholtz and Pressure Gradient*
- *High sound isolation*
- *Distinctive textured appearance*
- *Production by local block producers*
- *Can be painted*
- *Available as 12" reinforced block and 8" block*
- *Available with or without low frequency absorption slots*
- *Can be used with conventional block structural piers for high flexural strength*
- *Structural and load bearing*

BENEFITS

- *Distinctive appearance complements architectural designs*
- *Can be used for all noise control, speech, and music applications*
- *Simultaneously offers structure, absorption, and diffusion in the same CMU, resulting in unprecedented economy*

APPLICATIONS

Broadcast studies, Recording studios, Arenas, Gymnasiums, Auditoriums, Residential noise, control, Music practice rooms, Performance facilities, Convention centers, Amphitheaters, Transportation facilities, Classrooms, Highway barriers, Power generation facilities

SPECIFICATIONS

- *12" Reinforced Block: 7-5/8" (H) x 15-5/8" (W) x 11-5/8" (D)*

Model: dB12S
Acoustics: Diffusion and LF Absorption

Model: dB12NS
Acoustics: Diffusion

- *8" Block: 7-5/8"(H) x 15-5/8"(W) x 7-5/8"(D)*

Model: dB8S
Acoustics: Diffusion and LF Absorption

Model: dB8NS
Acoustics: Diffusion

- *DiffusorBlox® conform to ASTM C-90, Grade N Type I, with a net compressive strength of 1900 psi. No individual unit shall be less than 1700 psi.*

DiffusorBlox®

dB12NS Components

Exploded View

Project:

Specifier:

Drawing Number:

Date:

RPG *The Sound of Innovation*

651-C Commerce Drive, Upper Marlboro, MD, 20774, Phone: 301.249.0044, Fax: 301.249.3912, Email: info@rpginc.com, Internet: www.rpginc.com

DiffusorBlox®

dB8S Cutsheet

Project:

Specifier:

Drawing Number:

Date:

RPG *The Sound of Innovation*

651-C Commerce Drive, Upper Marlboro, MD, 20774, Phone: 301.249.0044, Fax: 301.249.3912, Email: info@rpginc.com, Internet: www.rpginc.com

Note: Full brochure is available from the authors of this report

Material from Peter D'Antonio of RPG on Quietstone:

QUIETSTONE
Innovative acoustics

Quietstone®
Durable, versatile sound absorber.

Truly multi functional sound absorbers.

Rigid, durable sound absorption panels with a unique aesthetic appeal.

Quietstone is made from specially bonded aggregates. This produces a porous panel with excellent sound absorption capabilites. They also have a unique aesthetic appeal to compliment modern architecture.

Advantages

- High sound absorption
- Non combustible - class 1 of BS476: Part 6, class 0 of BS476: Part 7
- Weather resistant - impervious to frost and rain
- Durable - high impact resistance and can be easily cleaned
- Attractive - aesthetically pleasing finish can be pigmented to suit surroundings

Applications

- Train stations
- Tunnel lining
- Sports halls
- Swimming pools
- Bars/nightclubs/restaurants
- Healthcare buildings
- Schools
- Airports
- Road/rail noise barriers
- Police interview rooms

Close up

RPG Diffusor Systems, Inc.
651-c Commerce Drive, Upper Marlboro, MD 20774
P: 301-249-0044 | info@rpginc.com

Quietstone®
Durable, versatile sound absorber.

Bespoke

- We are able to make bespoke solutions if you give give us a clear indication of what you need. This has included designing custom finishes for nightclubs, Bespoke mounting systems for high impact areas and working with our partners in bespoke barriers, Van Campen Aluminium on environmental noise projects. We welcome any innovative ideas you may have.

Installation

- Because of the durability and manufacturing flexibility, there are many different installation methods from invisible mounting to the rear of the panels with an aluminium frame, to simply mounting on timber batterns with cementicious adhesive. Visit the website for more detailed examples.

Finish options

- Below are some samples made for swimming pools. We can match nearly any RAL colour.

Physical properties

Standard thickness:	26mm
Width:	500mm
Length:	500mm
Other sizes are available on request	
Weight:	40Kg/m²
Compression Strength:	10.5x103 kN/

Fire Safety

- Quietstone meets the requirements of class 1 of BS476: Part 6: 1989 and class 0 of BS476: Part 7:1997.

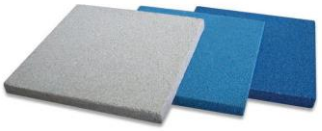

Acoustic performance

- Data provided by the University of Salford and the TNO, Delft. Please contact us should you require copies of results. BS EN ISO 354: 2003

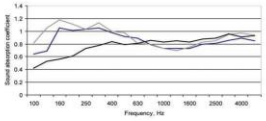

Test 1: 30mm panel, 50mm Rockwool, 40mm air gap.

Test 2: 30mm panel, 50mm Rockwool, 100mm air gap.

Test 3: 30mm panel, 50mm air gap, 50mm Rockwool.

	Sound absorption coefficients, α_p						EN-ISO 11654 α_w
	125 Hz	250Hz	500Hz	1000Hz	2000Hz	4000Hz	
Test 1	0,80	1,05	0,95	0,75	0,80	0,85	0,80 (L); class B
Test 2	1,00	1,10	0,95	0,75	0,80	0,95	0,85 (L, H); class B
Test 3	0,50	0,70	0,80	0,85	0,85	0,95	0,85; class B

RPG Diffusor Systems, Inc.
651-c Commerce Drive, Upper Marlboro, MD 20774
P: 301-249-0044 | info@rpginc.com

QUIETSTONE
Innovative Acoustics

FR30
Fire resistant sound absorption panels

Durable sound absorbers with high fire safety.

The new Quietstone FR30 panels are a world's first product combining high sound absorption, durability and heat resistance. These panels can be used in external settings and are particularly suited to controlling transport noise, even passing the stringent requirements of European tunnel lining safety. The testing for which required high impact resistance, moisture and frost resistance and a fire test which exposed the panels to 1150°C for 2 hours. Add to this high sound absorption, up to α_w 1.12 at 1000Hz and the advantages are clear.

Panels are typically mounted on a steel framework which leaves a space for all services in a tunnel and improves acoustic performance. Panels are pigmented in a range from an off-white through to black for aesthetically pleasing designs.

Key features:

- High sound absorption even at low frequencies
- High fire resistance - replaces fire safety panels
- High impact strength
- Frost and moisture resistance
- Long lifespan
- Available in a range of colours
- Passes current European tunnel lining standards
- Purpose designed mounting system available

Technical properties

Physical properties

Width	600mm
Length	1000mm
Thickness	30mm
Interlocking lips for added strength and heat insulation	
Weight	37.5kg/m²,
Weight	1,250kg/m³
Flexural strength	1.6 MPa
Compressive strength	3 MPa

Fire resistance

Tested by Efectis Nederland BV for tunnel fire safety. The test involves exposure of a full wall construction to 1150°C for 2 hours and panels must not disintegrate or exceed 250°C in the rear cavity

Impact resistance

EN 1794-1 "Road traffic noise reducing devices - non acoustic performance - Impact of stone": "Elements appear to show no visual damage."

Freeze / thaw resistance

EN 1338 - Class 0

Colours (Colours may vary from those depicted)

1 2 3 4 5 6 7 8

Acoustic performance

Tested in accordance with BS EN ISO 354: 2003 at TNO, Holland with typical tunnel lining construction.

Mounting parameters:

Test 1 - 190mm total buildup; 30mm panel, 90mm air gap, 70mm Rockwool.

Test 2 - 190mm total buildup; 30mm panel, 30mm Rockwool, 60mm air gap, 70mm Rockwool.

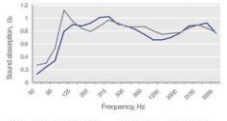

	125Hz	250Hz	500Hz	1kHz	2kHz	4kHz	EN-ISO11654 α_w	EN1793-1 DL_α	RMR2006 $DL_{\alpha,rail}$
Test 1	0,85	1,00	0,85	0,70	0,80	0,85	0,80(L); class B	7dB(A); cat A2	7dB(A)
Test 2	0,95	0,90	0,90	0,80	0,80	0,85	0,85(L); class B	8dB(A); cat A3	8dB(A)

RPG Diffusor Systems, Inc.
651-c Commerce Drive, Upper Marlboro, MD 20774
P: 301-249-0044 | info@rpginc.com

Excerpts from presentation by Peter D'Antonio of RPG on Quadratic Residual Diffusors for noise barriers:

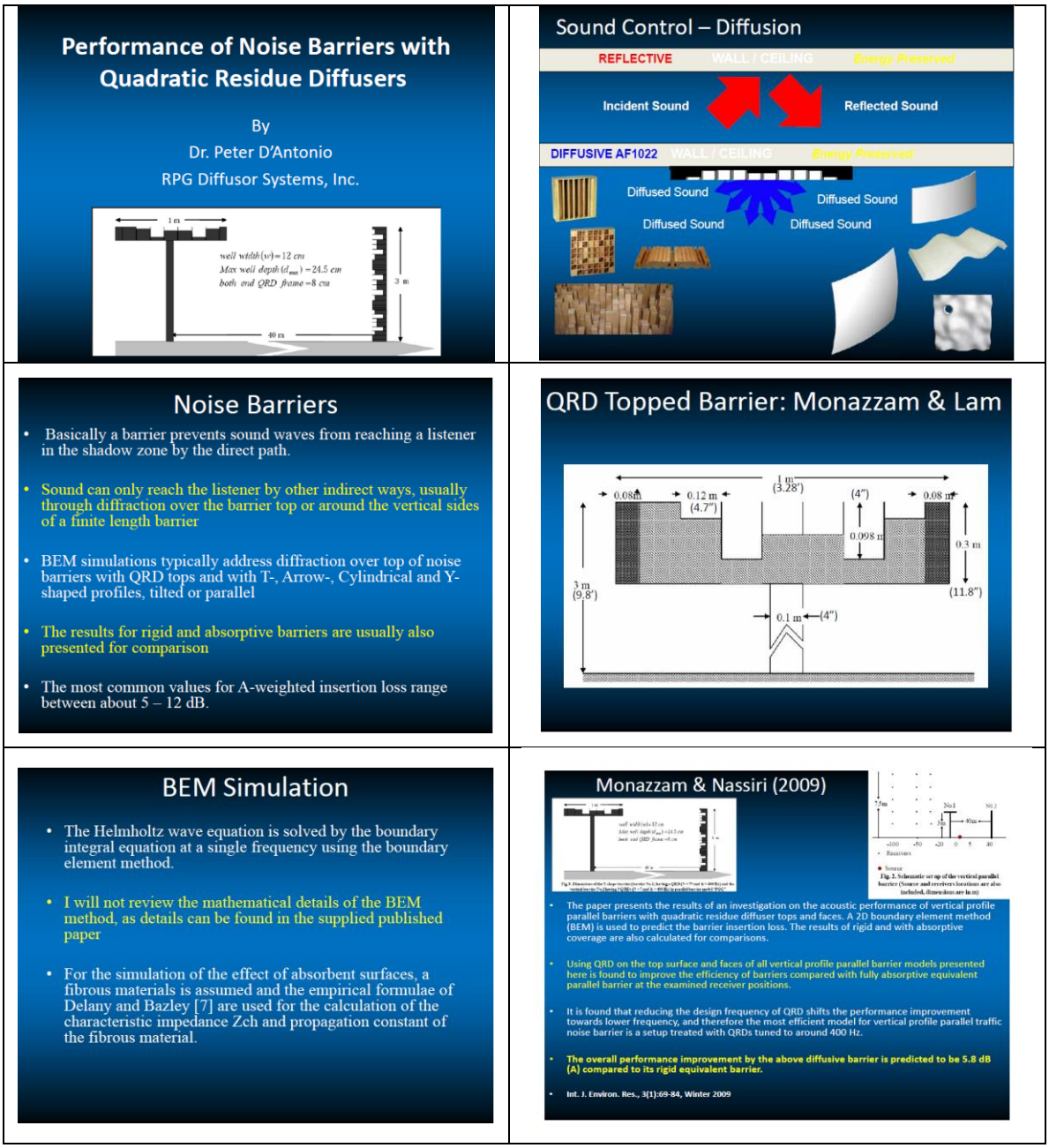

Note: Full presentation is available from the authors of this report

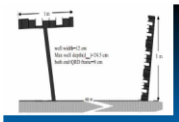

Monazzam & Nassiri: Tilted QRD Barriers

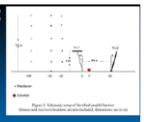

- This paper presents the results of an investigation on the acoustic performance of tilted profile parallel barriers with quadratic residue diffuser (QRD) tops and faces. A 2D boundary element method (BEM) is used to predict the barrier insertion loss.
- Applying a QRD with frequency design of 400 Hz on 5 degrees tilted parallel barrier improves the overall performance of its equivalent rigid barrier by 1.8 dB(A).
- Increase in the treated surfaces with reactive elements shifts the effective performance toward lower frequencies. It is found that by tilting the barriers from 0 to 10 degrees in parallel set up, the degradation effects in parallel barriers is reduced but the absorption effect of fibrous materials and also diffusivity of the quadratic residue diffuser is reduced significantly.
- In this case all the designed barriers have better performance with 10 degrees tilting in parallel set up. The most economic traffic noise parallel barrier which produces significantly high performance, is achieved by covering the top surface of the barrier closed to the receiver by just a QRD with frequency design of 400 Hz and tilting angle of 10 degrees.
- The average A-weighted insertion loss in this barrier is predicted to be 16.3 dB (A).
- Iran. J. Environ. Health. Sci. Eng., 2009, Vol. 6, No. 4, pp. 271-284

Summary

- BEM simulations indicate QRD topped barriers provide additional insertion loss over reflective and absorptive T-shaped barriers
- It seems worthwhile to experimentally measure scaled versions to verify these findings
- And to explore possibly better solutions using the improvements in number theory technology over the past 30 years
- 3D printing can be used to easily fabricate scale models for testing
- The RPG Goniometer apparatus can be used for the evaluations

Summary

- Following experimental verification, full scale diffusive topped models can be tested
- 1:1 testing can begin with DiffusorBlox since they are readily available

"Quiet" Stone System:

Quietstone: Bonded recycled stone aggregate

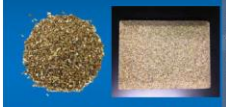

Quietstone Light: Bonded recycled glass beads

- Durable
- Recycled
- Impervious to weather
- Non combustible
- Standard or custom sizes
- Impact resistant
- Mechanically mounted or bonded to a substrate
- Sustainable
- Long lifespan
- Non fibrous
- Cost effective

Quietstone Light:
- Can be painted
- Easily worked on site

Applications

Applications

noise barriers - can be bonded directly to preformed concrete or timber battens

tunnel lining - now replaces Reapor for outdoor settings

pavilions - pavilions, generators, facades, plant enclosures

sportsfields - high impact resistance

wall cladding - light weight and cutting can be done on site

swimming pools - will not sag or stain with moisture exposure

healthcare - non-fibrous, can be washed with any detergents including sterilizers

APPENDIX C: RESULTS FROM BARRIER FIELD MEASUREMENTS

Description of Measurements

Noise, air quality, and meteorological measurements were conducted in Oasis Park, AZ, on May 11-14, 2014 for the purpose of validating Notre Dame's developmental model using acoustical and meteorological field data behind a noise wall. An aerial of the site is shown in Figure 1. The accumulated data indicates interesting potential trends between the various noise and meteorological variables. The effects of varying meteorological conditions on traffic noise as heard at locations behind a noise wall is described in a preliminary manor in this memo. Further analysis of this data is recommended and could lead to some valuable insights within the traffic noise community; however, this additional analysis was outside of the scope and budget of this project and was, therefore, not conducted.

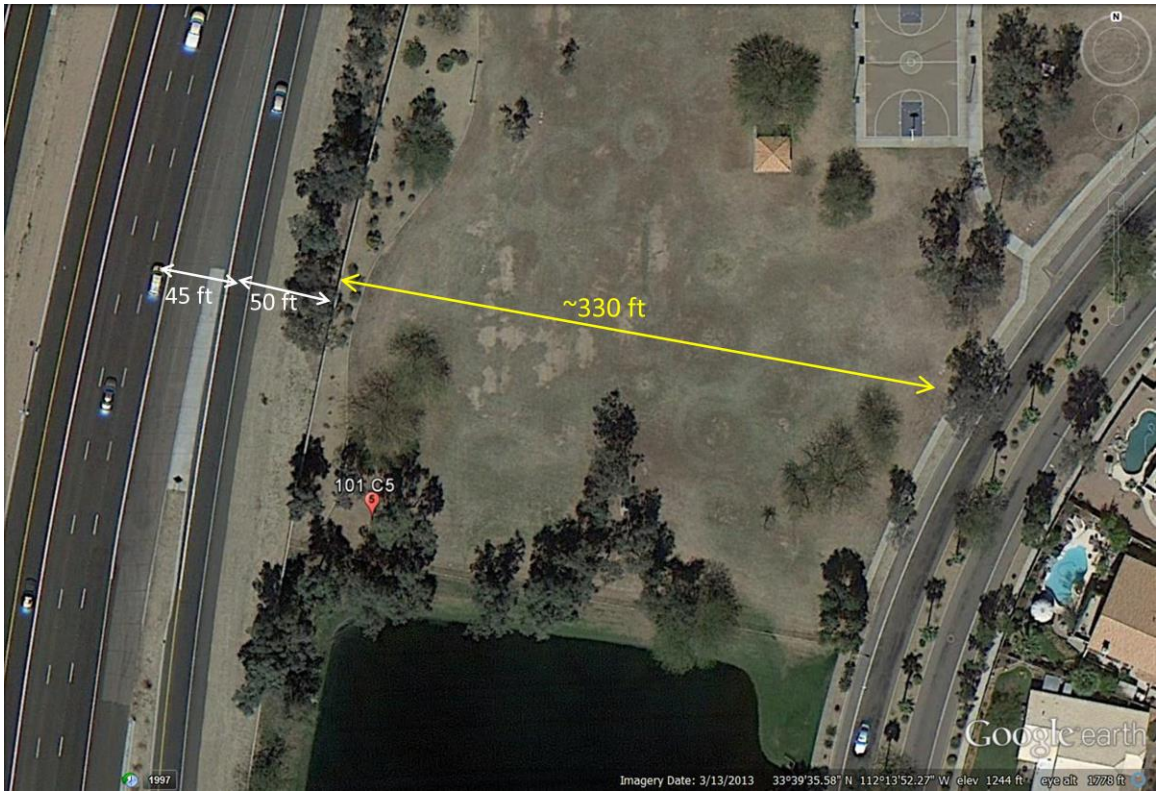

Figure 1: Aerial View of Measurement Site

Site Information

At the Oasis Park measurement site, traffic noise was clearly audible behind the barrier at all noise measurement locations. Some extraneous noise did occur over the time of the measurements, primarily local traffic and noise from the basketball court or other areas in the park when in use. Care was taken to record notable extraneous noise on the data sheets and to remove the associated data periods when contamination was thought to occur.

The terrain on both the traffic and field side of the site was relatively flat, with relatively homogeneous ground type on the field side (field grass). The barrier that shields Oasis Park from Highway 101 is 14 ft high on the field side and 15 ft 9 in high on the road side, with an 8 inch increase in height occurring just north of the measurement line. The area behind the barrier is open to a distance of about 330 ft. The

barrier extends horizontally in both directions far enough distance to eliminate noise flanking around the edges of the barrier. There are a few trees in the microphone path, and, although they are not dense, it is possible that some sound scattering could have occurred. Additionally, as seen in Figure 1, the highway has a slight horizontal curve at this location. Traffic noise modeling in SoundPLAN 7.3 indicated variations of 0.3 dB or less due to this curve as compared to a completely perpendicular roadway section under calm wind conditions. It is unknown how this horizontal curved configuration may have affected the results during higher perpendicular wind conditions.

Measurement Locations

Acoustic measurements were made at seven locations, using the same methodologies as those used for the QP3 measurements[29]. A photograph of the site, showing the acoustics and meteorological measurement locations, is shown in Figure 2.

Figure 2: Photo of Oasis Park Site with Measurement Locations

Two reference microphone locations were used, 1) one located on the roadway side of the barrier at the approximate height of the barrier and 25 ft from the center of the near lane, 2) one located on top of the barrier at a height of 5 feet above the barrier. In addition, five distance microphone locations were used; 1) distance of 50 feet from the barrier at a height of 5 feet above the ground, 2) distance of 100 feet from the barrier at a height of 5 feet above the ground, 3) distance of 100 feet from the barrier at a height of 10 feet above the ground, 4) distance of 200 feet from the barrier at a height of 5 feet above the ground, and 5) distance of 300 feet from the barrier at a height of 5 feet above the ground. A site diagram is indicated in Figure 3. Five of the seven channels were measured in 1/3 octave bands in real time using Larson Davis 2900 and 3000+ RTAs. At the remaining two channels, both of the 100 foot distances, noise levels were measured using sound level meters, which give only overall A-weighted levels, and digitally recorded for future use, should octave band data be of interest. OBSI measurements were also conducted at the site under two difference meteorological conditions, similar to Site 1 measurements from the QP3.

Traffic, meteorological and air quality measurements were conducted concurrent to the acoustic measurements. Traffic counts and speed measurements were made from the Union Hills Drive Overpass. Meteorological sensors, each including a sonic anemometer, a thermocouple, and a relative humidity sensor, were attached at four locations on two towers, located at distances of 10 and 130 feet from the barrier at heights of 6.5 and 33 feet above the ground, as shown in Figure 4. A barometer and three air quality sensors was also located on the site. Meteorological and air quality measurements included wind speed and direction, temperature and relative humidity, barometric pressure, and air

[29] Arizona Quiet Pavement Program, Progress Report 5 for 2011: Site 1, Research Sites 3A, 3D, and 3E, Prepared for ADOT, Prepared by Illingworth & Rodkin, Inc, May 22, 2014.

particulate matter concentrations. Detailed information on the locations and data resulting from the meteorological and air quality sensors is given in the *"Experimental setup and preliminary data summary for meteorological and air quality measurements"* report[30].

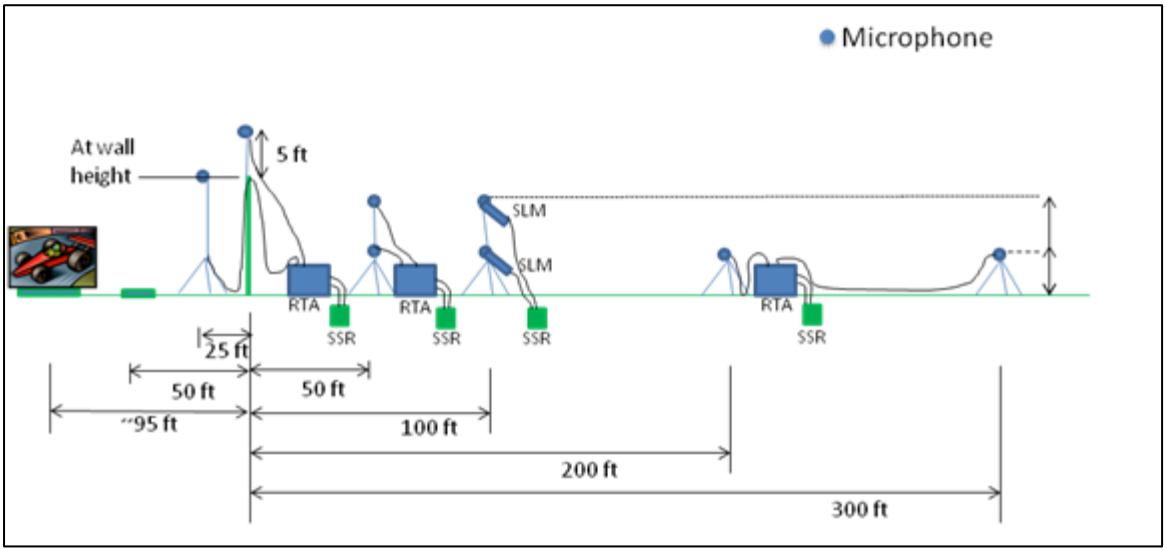

Figure 3: Acoustic Measurement Site Diagram

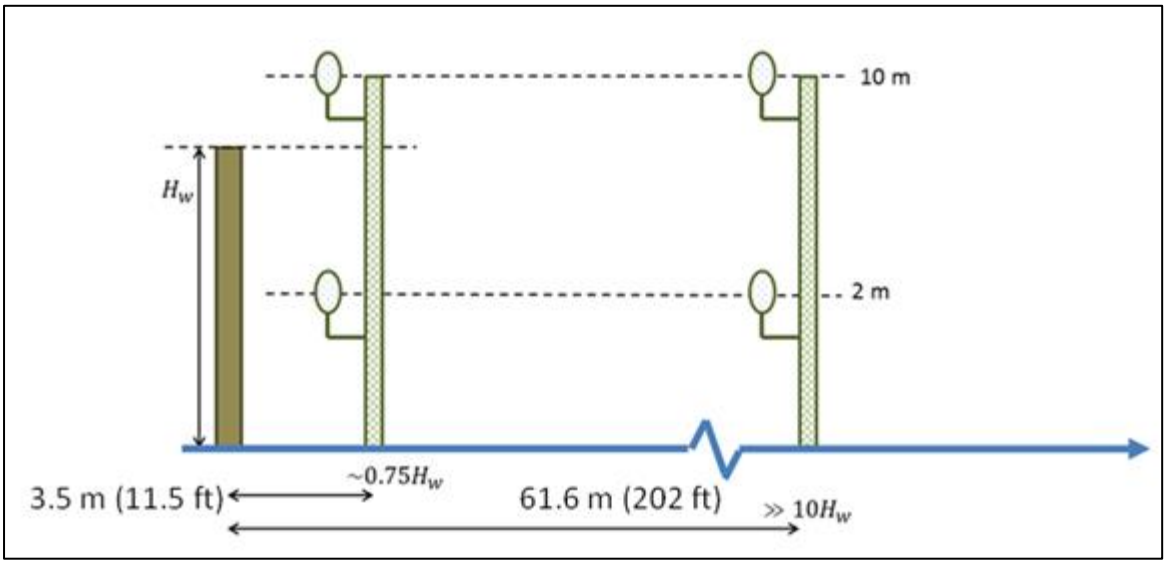

Figure 4: Meteorological and Air Quality Measurement Site Diagram

All measurements were conducted in 1-minute intervals. Continuous meteorological data acquisition began at 12:45 pm on May 11th, 2014 and ended at 8:00 pm on May 14th, 2014. Acoustical measurements were conducted during 8 sessions, selected to represent various weather conditions occurring over the 3-day measurement period. Measurement sessions are indicated below:

- Session 1: May 11, 11:00am to 12:16pm
- Session 2: May 11, 2:14pm to 3:44pn

[30] "*Experimental setup and preliminary data summary for meteorological and air quality measurements*", Field experiment 1, Shaffer, June 9, 2014.

- Session 3: May 11, 7:04pm to 7:54pm
- Session 4: May 12, 5:49am to 7:14am
- Session 5: May 12, 11:38am to 1:08pm
- Session 6: May 12, 3:52pm to 5:06pm
- Session 7: May 13, 8:37am to 10:01am
- Session 8: May 13, 1:02pm to 2:41pm

Results

The raw acoustical data for each of the eight measurement sessions is shown in Figures 5 to 12. As expected, the measurements followed the same general trend with distance from the traffic noise source, with the roadside and top-of-barrier measurements resulting in the highest noise levels, and the most distant location (300 ft from the barrier and 5 ft high) resulting in the lowest noise levels. One exception is the 100 ft distance and 10 ft high position, which resulted in noise levels that were slightly higher than both the 50 and 100 ft distance and 5 ft high positions due to the reduced barrier shielding occurring at the higher position.

Figure 13 shows the raw measured traffic noise levels in 1-minute intervals, plotted for each measurement session on a single graph. It is apparent from Figure 13 that even with the data scatter, some clear trends between data sets occur. Session 4, for example, exhibits measured noise levels that are up to 10 dB higher than the levels for the other sessions at the distant locations.

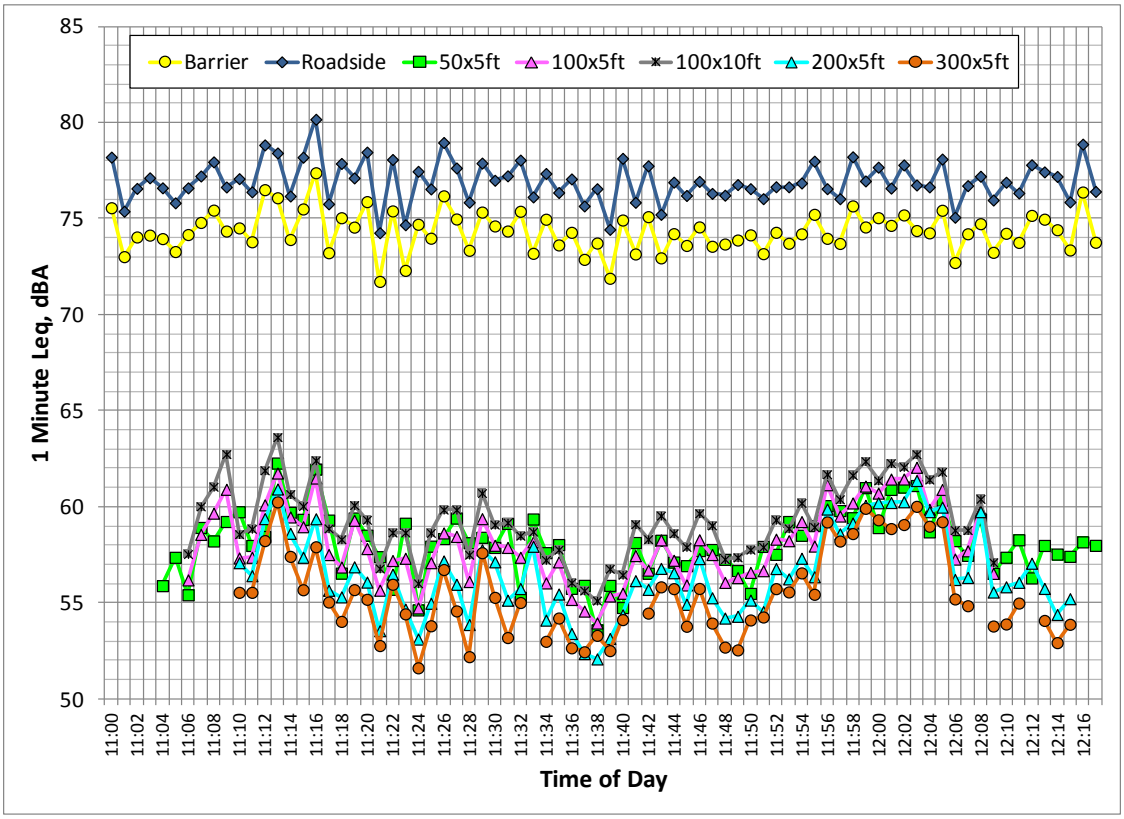

Figure 5: Measured Sound Pressure Levels for Session 1

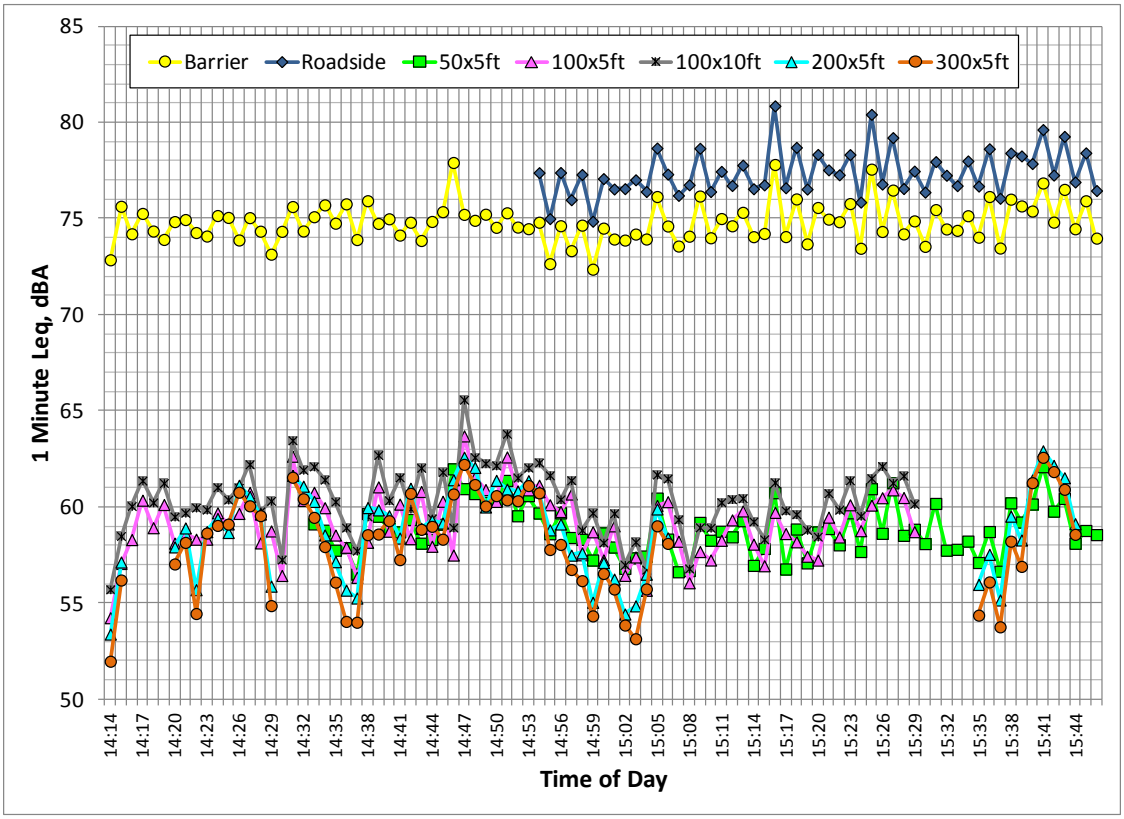

Figure 6: Measured Sound Pressure Levels for Session 2

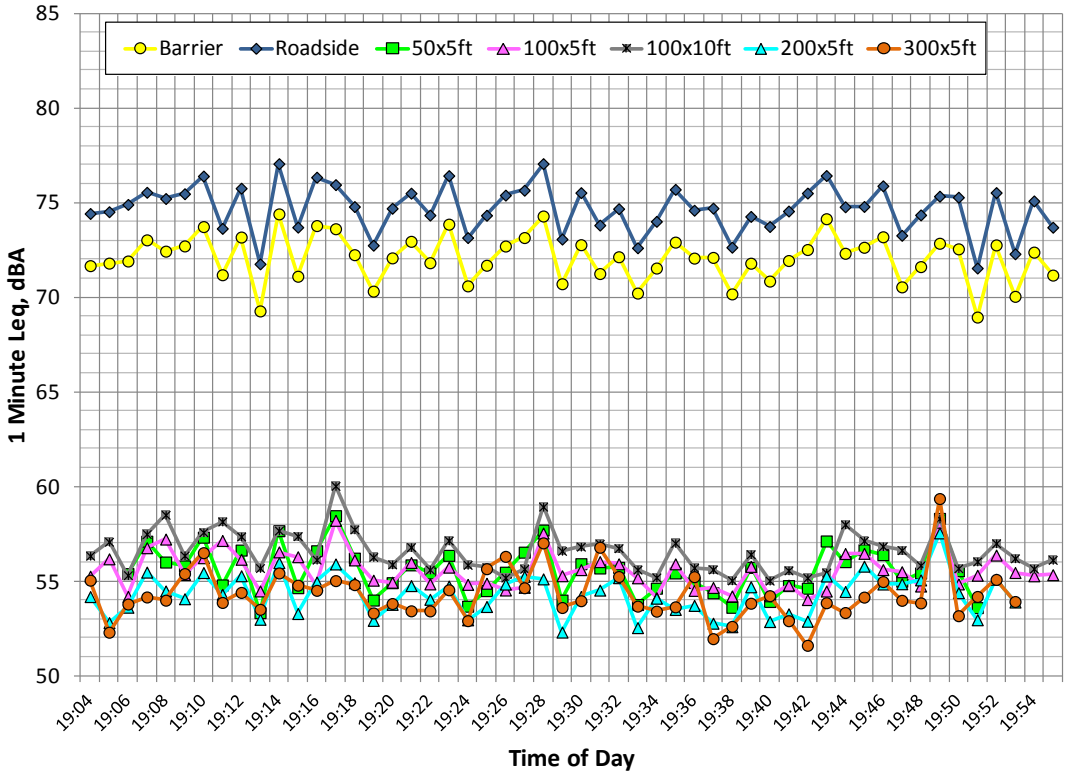

Figure 7: Measured Sound Pressure Levels for Session 3

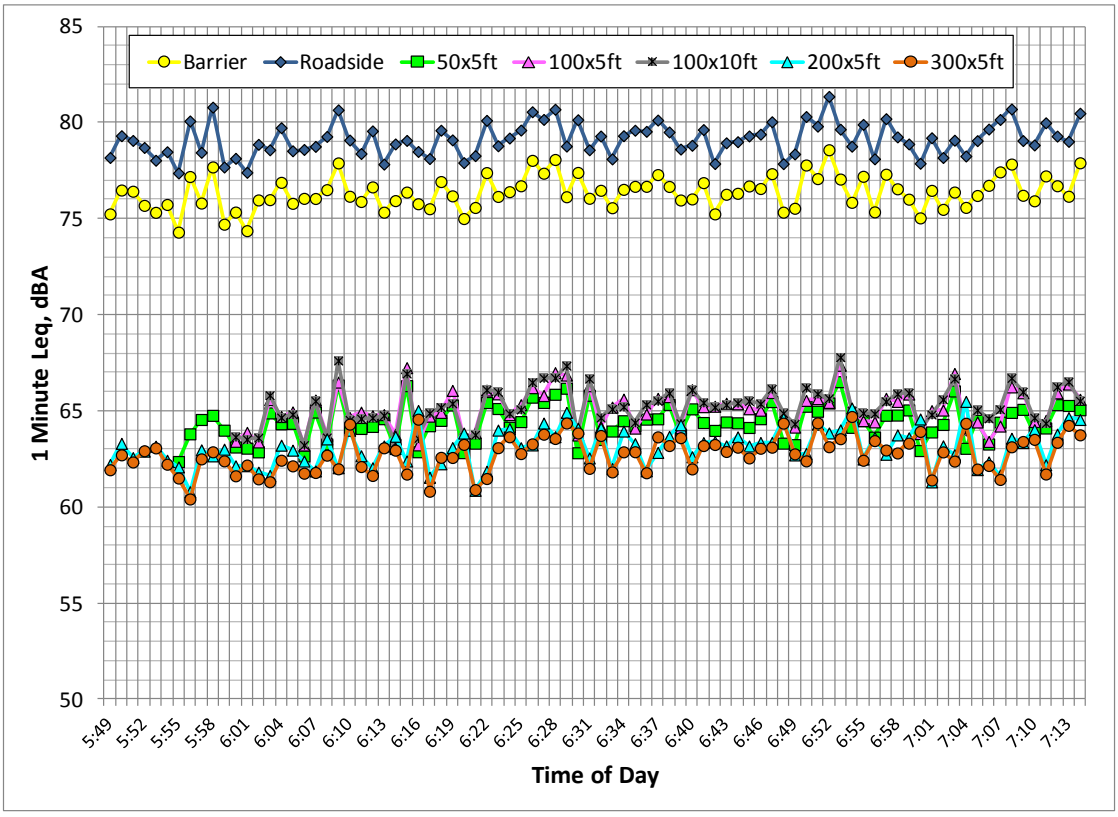

Figure 8: Measured Sound Pressure Levels for Session 4

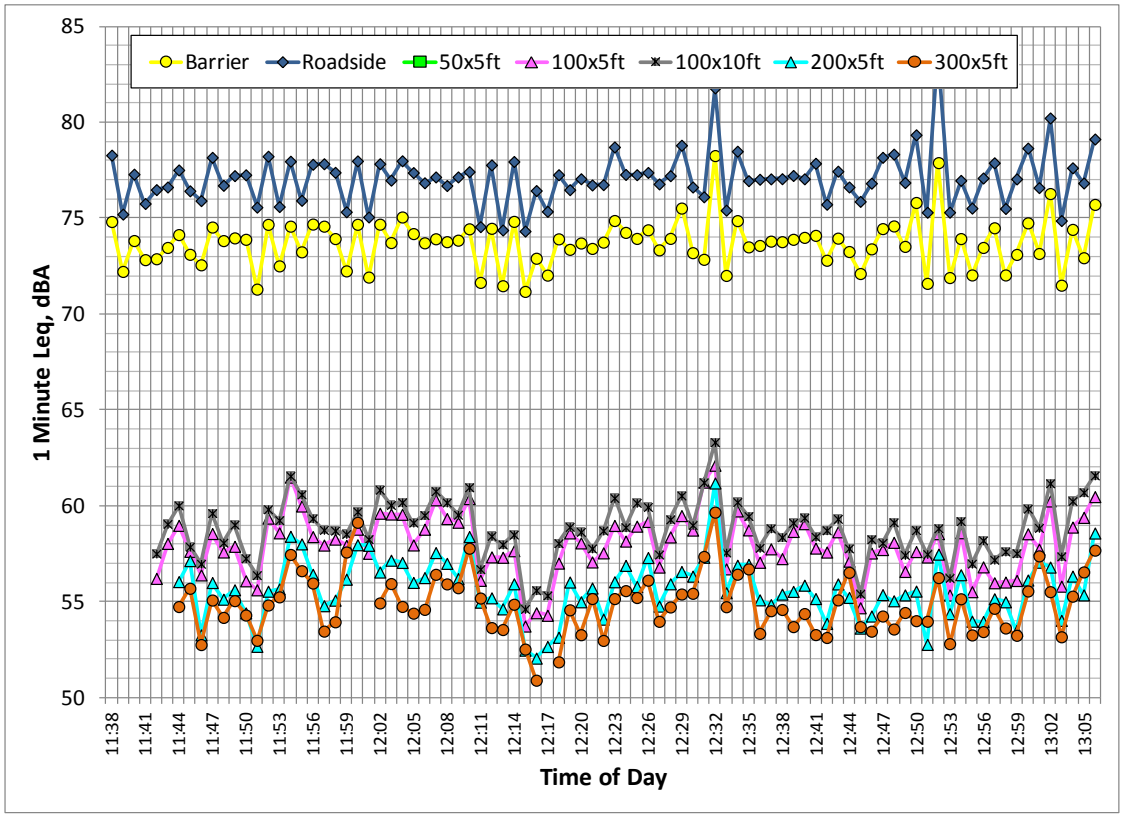

Figure 9: Measured Sound Pressure Levels for Session 5

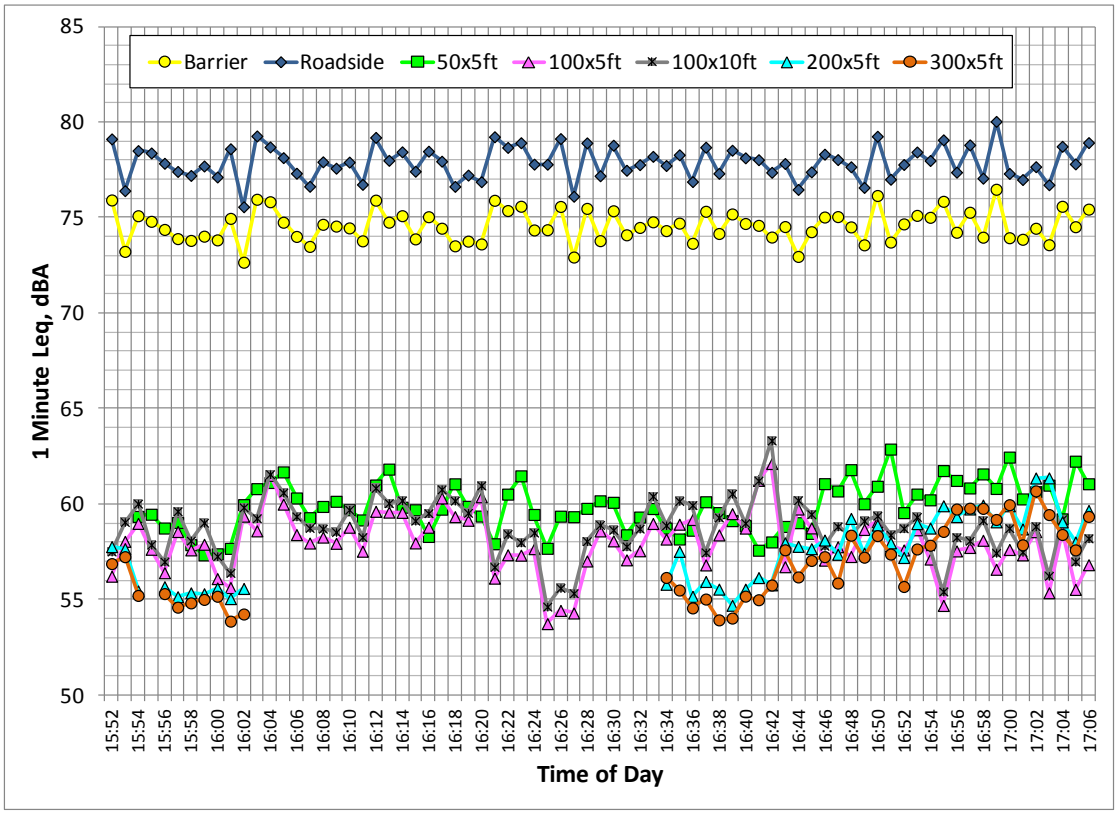

Figure 10: Measured Sound Pressure Levels for Session 6

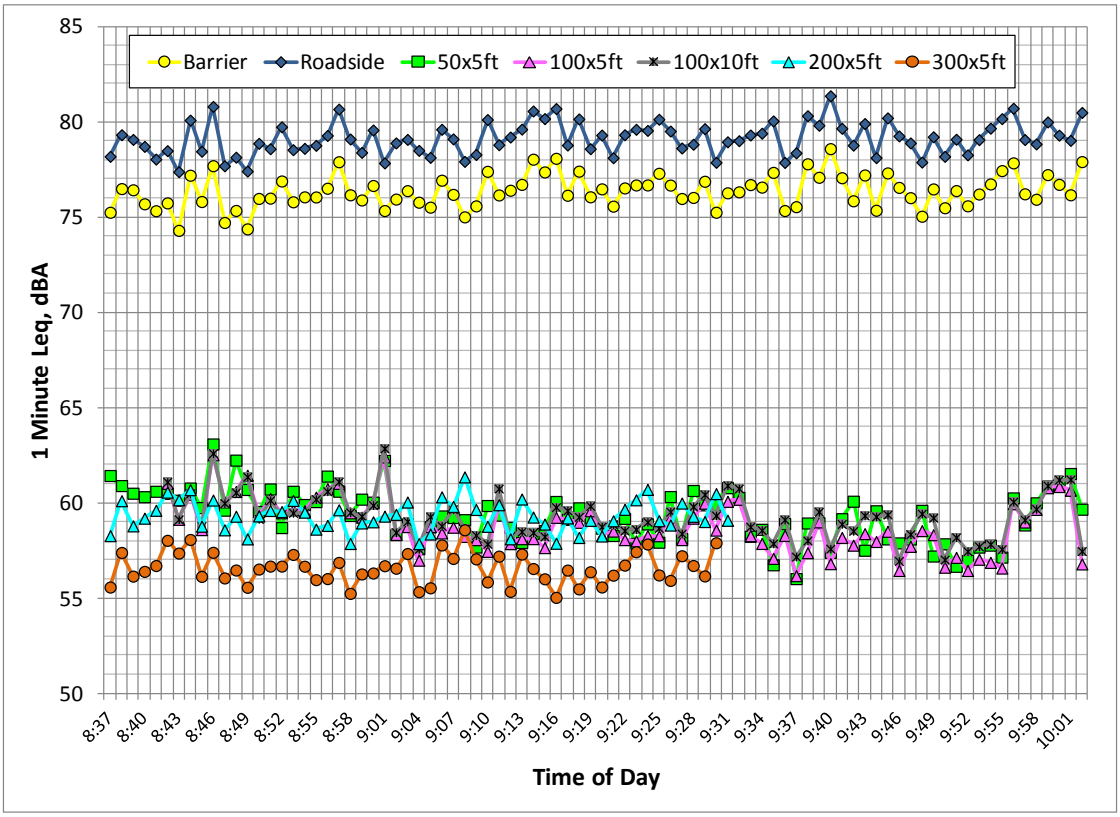

Figure 11: Measured Sound Pressure Levels for Session 7

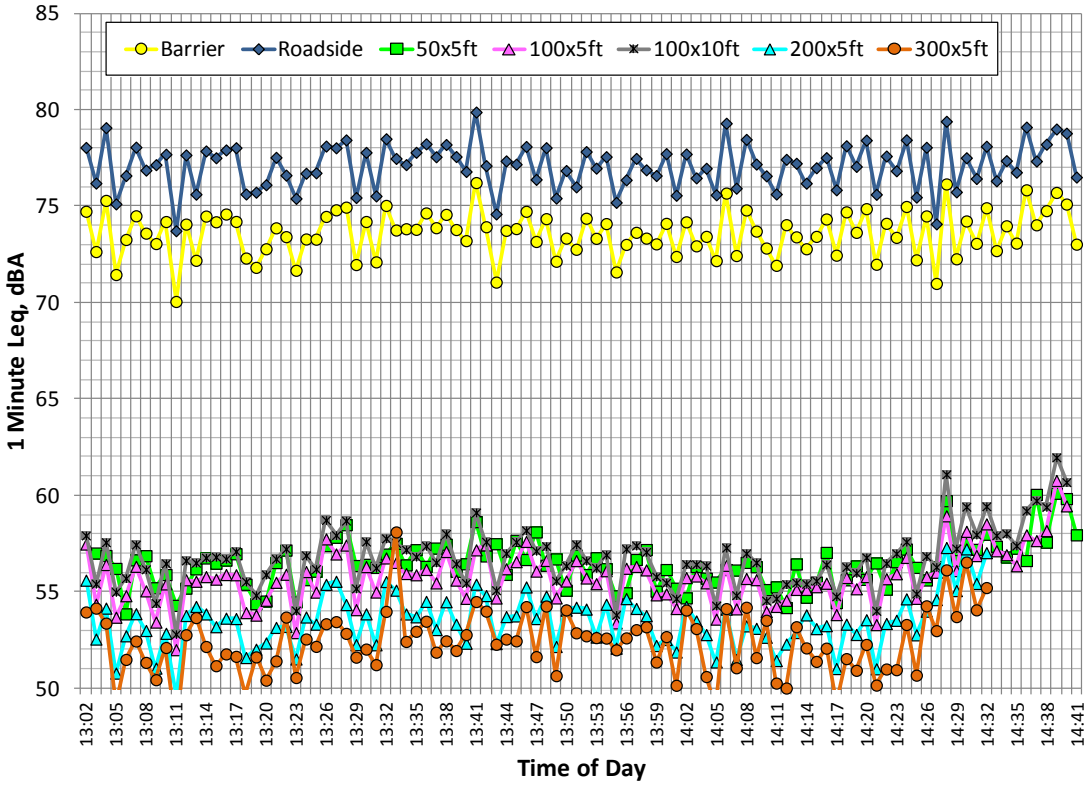

Figure 12: Measured Sound Pressure Levels for Session 8

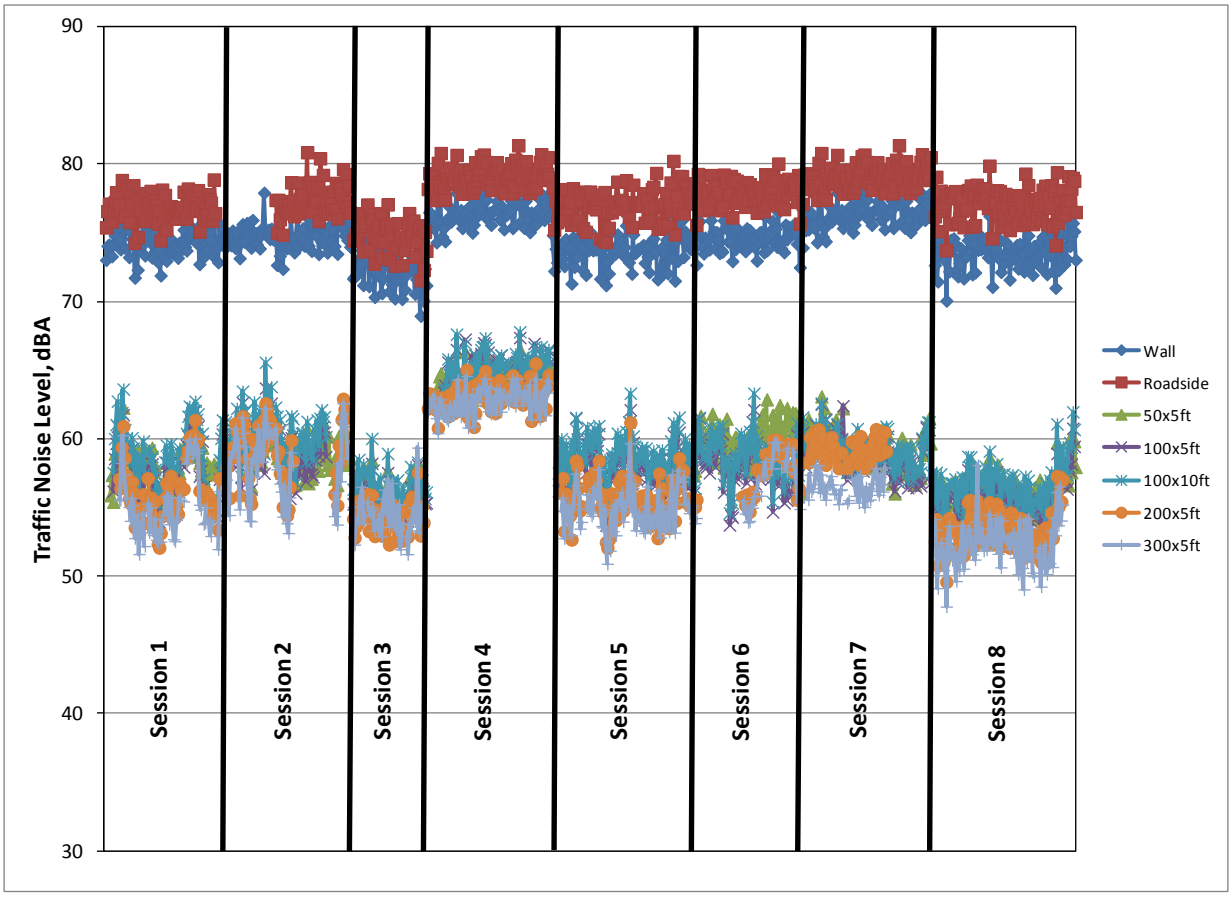

Figure 13: Measured Sound Pressure Levels, All Sessions

Figure 14 shows the overall average noise level by session for each of the seven measurement positions. Review of this figure indicates that there are clear differences in noise level between sessions. Although the general ordering of noise level by location remains similar, there are some cases that are not consistent with the others. For example, during Session 7, the 100 ft/10 ft high position has levels that are slightly lower than those at the 200 ft position, whereas under the other session, the 200 ft position results are typically about 1 to 2 dB higher.

As shown in Figures 5 to 13 large amount of scatter is apparent in the acoustical data. This is typical of these types of measurements. Some factors that might affect noise levels include varying traffic and meteorological conditions. Traffic noise variations that are attributable to variations in traffic volume, speed, or vehicle mix have been thoroughly studied and several methods of normalizing for traffic variations are common practices in the acoustics community. One method of normalizing for traffic variations is to calculate the difference in noise levels (or insertion loss, IL) between a reference location, located close to the noise source, and the more distant locations during concurrent measurement periods. It has been shown that meteorological effects on noise levels are generally minimal at locations within about 50 feet of a highway noise

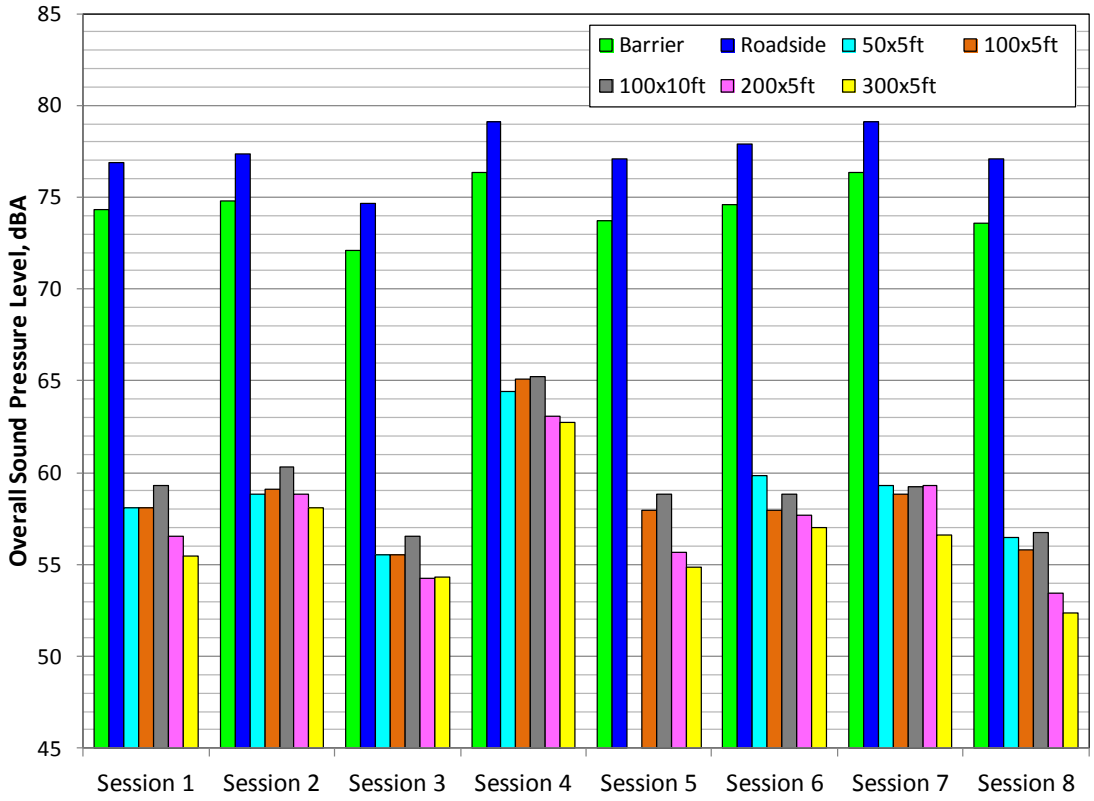

Figure 14: Session Average Measured Traffic Noise Levels

source[31], so the IL between reference and distance measurements conducted concurrently for the same noise source should theoretically normalize for traffic conditions. Figure 15 plots an example for Session 3 of the traffic noise levels for each of the measurements versus the levels measured at the top-of-barrier locations.

As seen in Figure 15, the roadside location shows a large reduction in scatter and correlates with the barrier locations rather well (R^2 = .98). More scatter is still apparent at the distant locations. The insertion loss, IL, for each measurement session between the top-of-barrier measurement location and all other locations are shown in Figures 16 to 23.

Figures 16 to 23 show similar results to Figure 15. Scatter is reduced considerable at the roadside location, but the distant locations continue to exhibit a great deal of variation in level. The session average noise reduction from the top-of-barrier location for each of the five distant measurement positions is shown in Figure 24.

[31] Lodico, Dana M., and Reyff, James A., "Long-term noise performance of open graded asphalt concrete (OGAC) - Results of 10-year long study", Noise Control Engineering J., Volume 57, Issue 2, pp. 84-93 (March 2009).

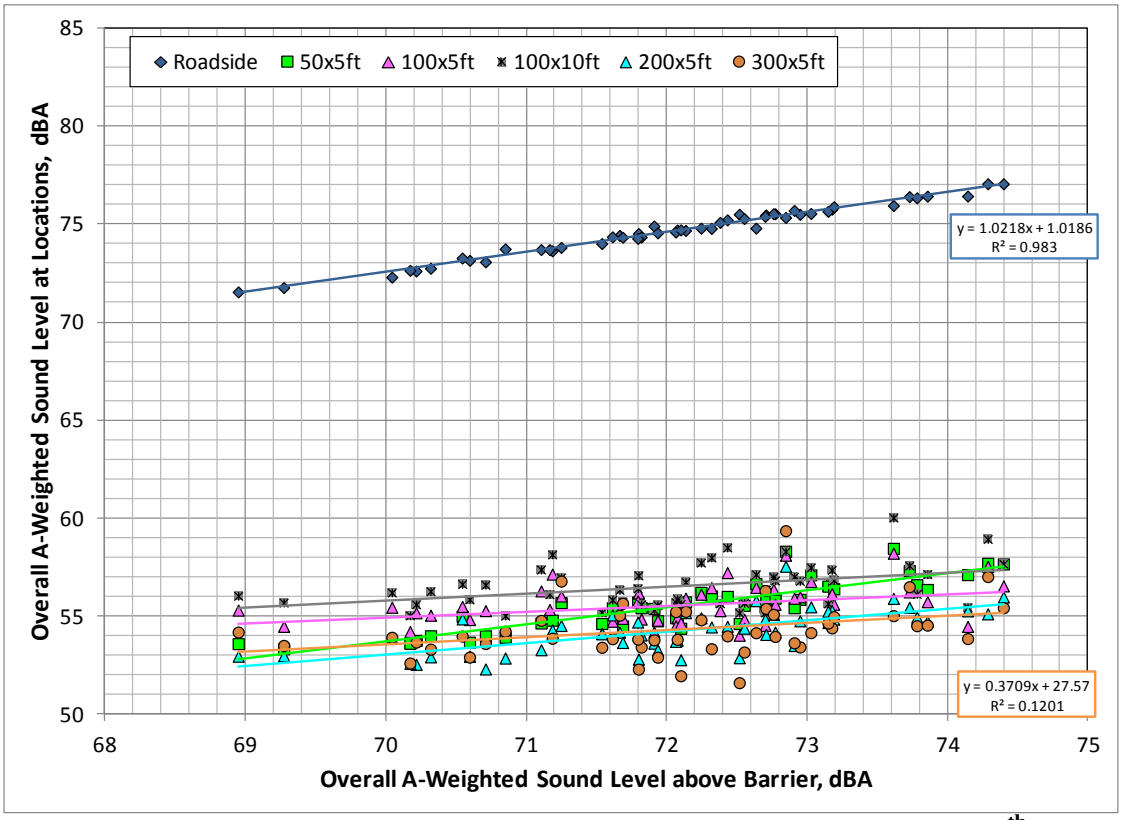

Figure 15: Roadside and Distance Comparison – Session 3, May 14th

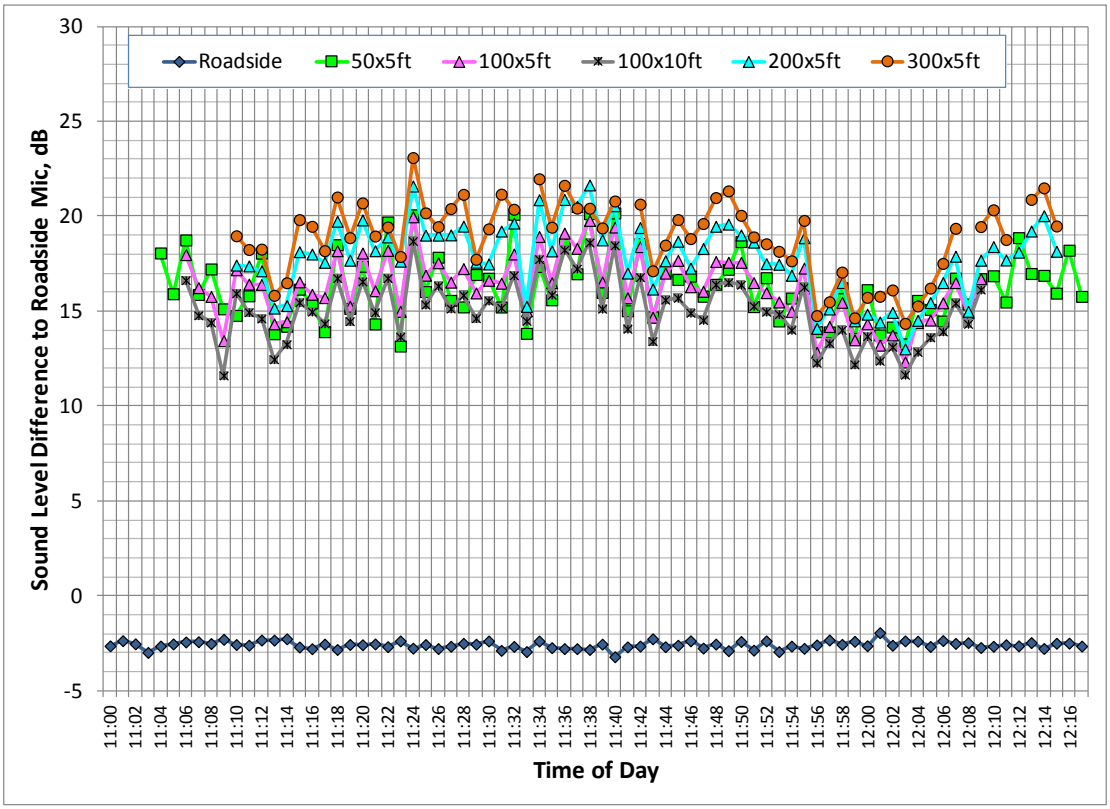

Figure 16: Noise Reduction from Top-of-Barrier Location, Session 1

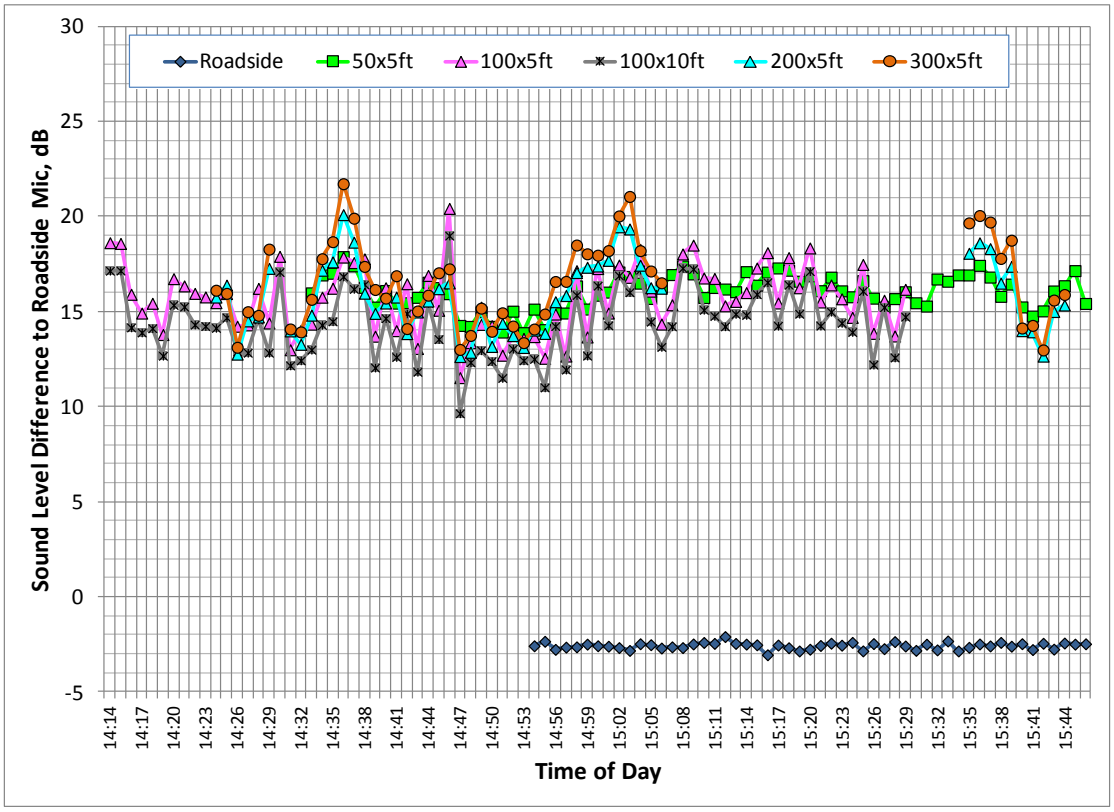

Figure 17: Noise Reduction from Top-of-Barrier Location, Session 2

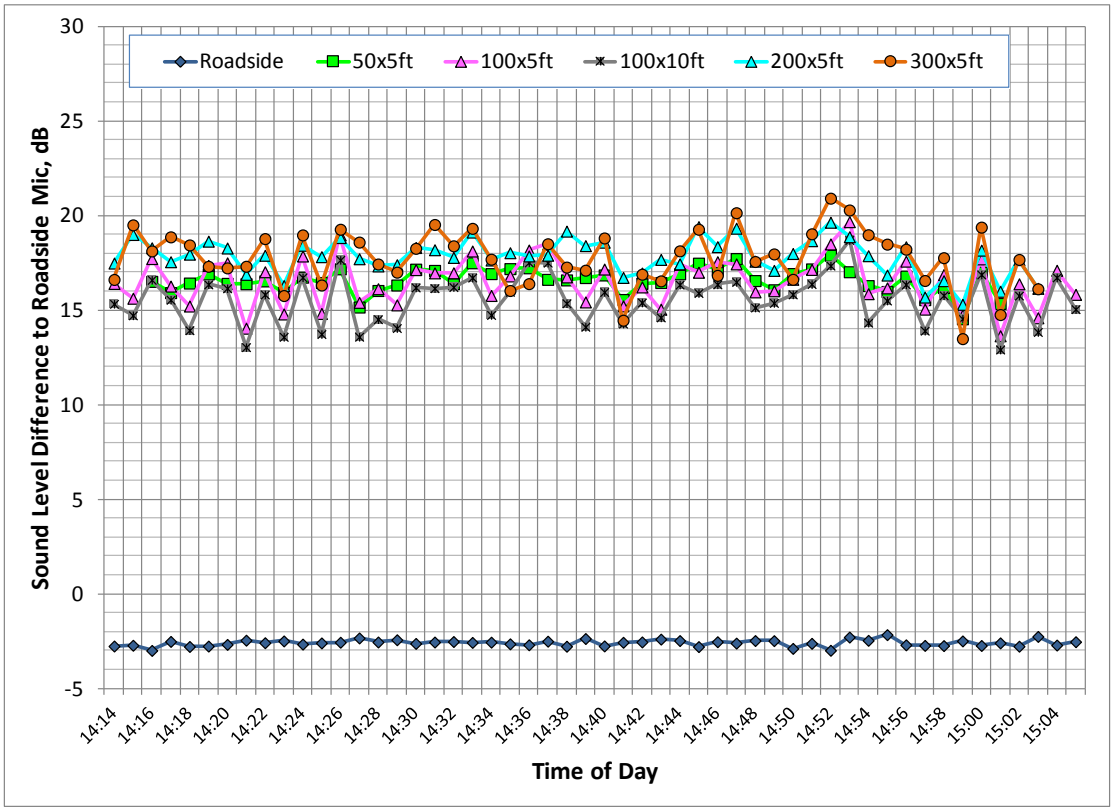

Figure 18: Noise Reduction from Top-of-Barrier Location, Session 3

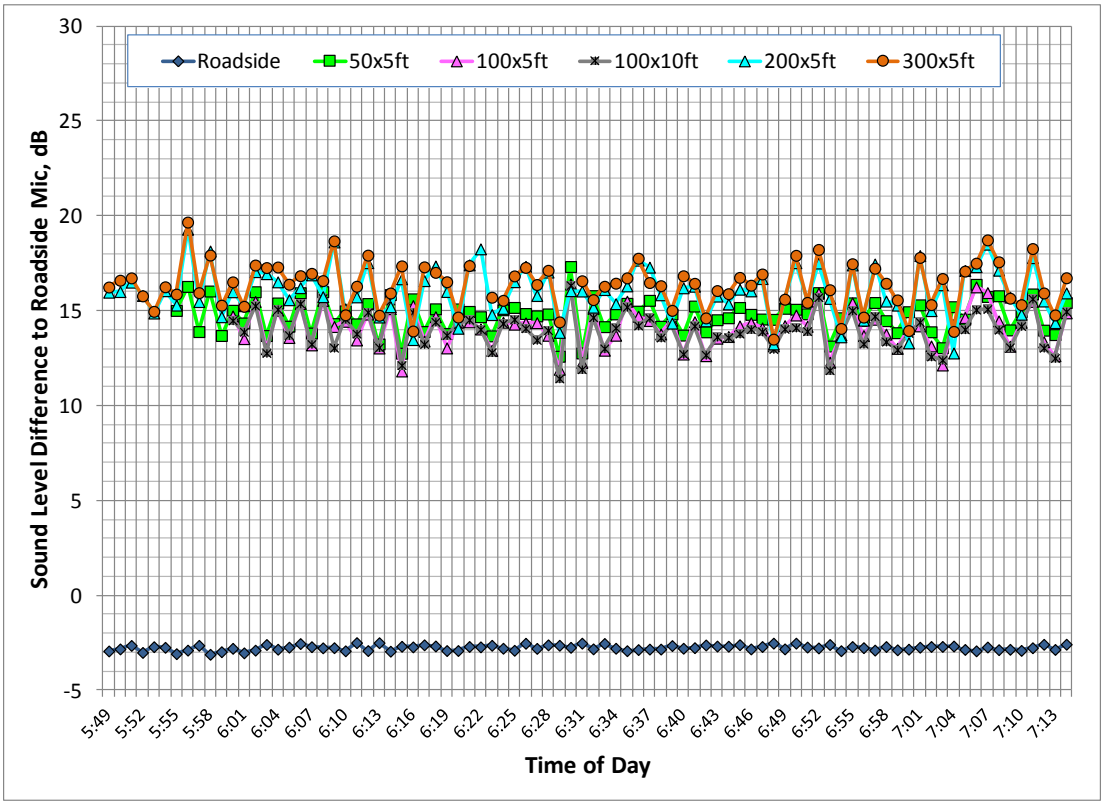

Figure 19: Noise Reduction from Top-of-Barrier Location, Session 4

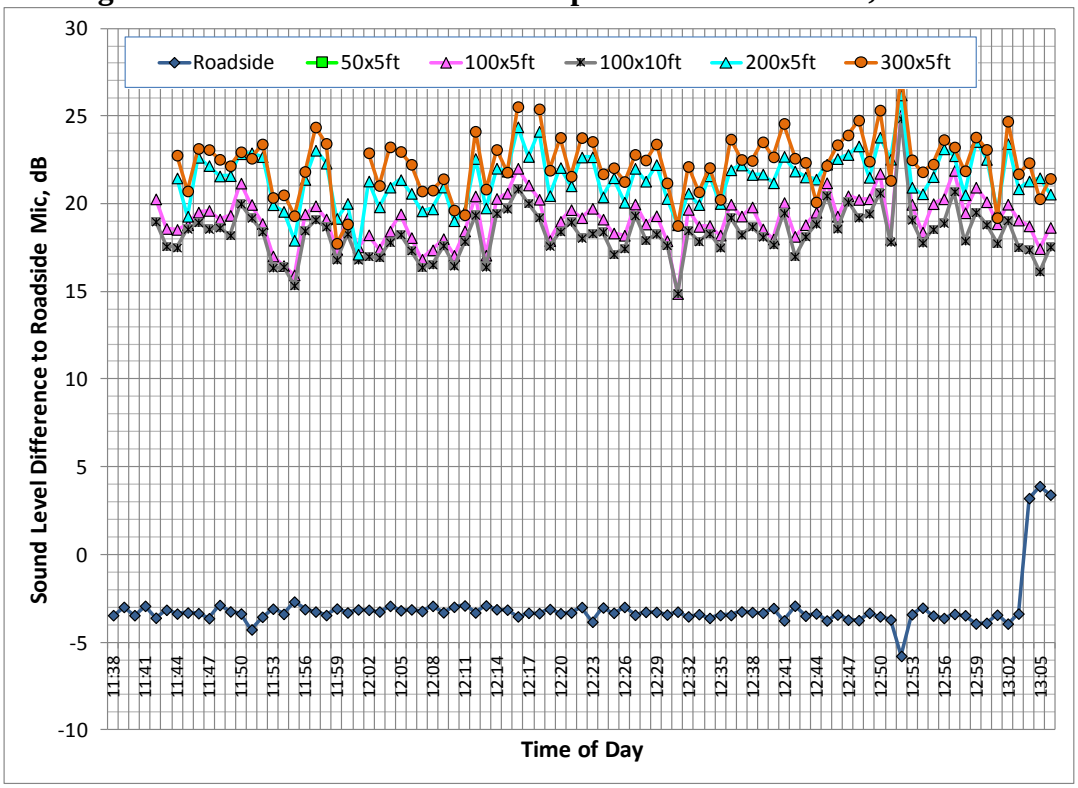

Figure 20: Noise Reduction from Top-of-Barrier Location, Session 5

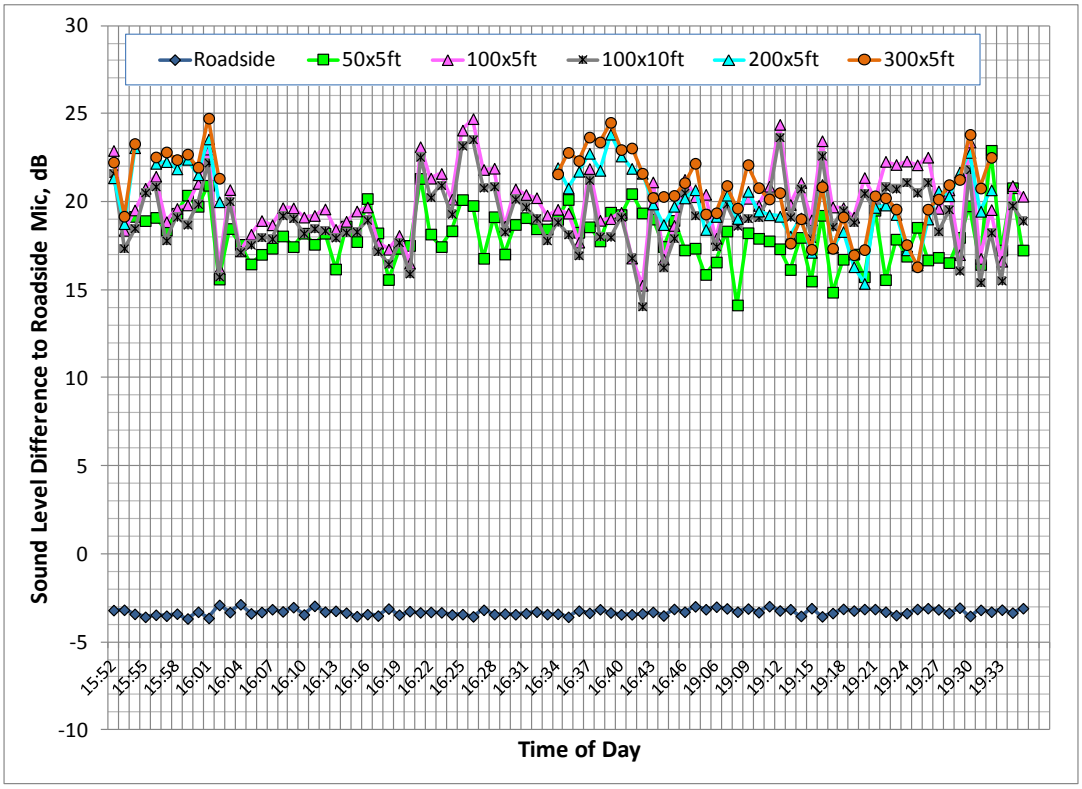

Figure 21: Noise Reduction from Top-of-Barrier Location, Session 6

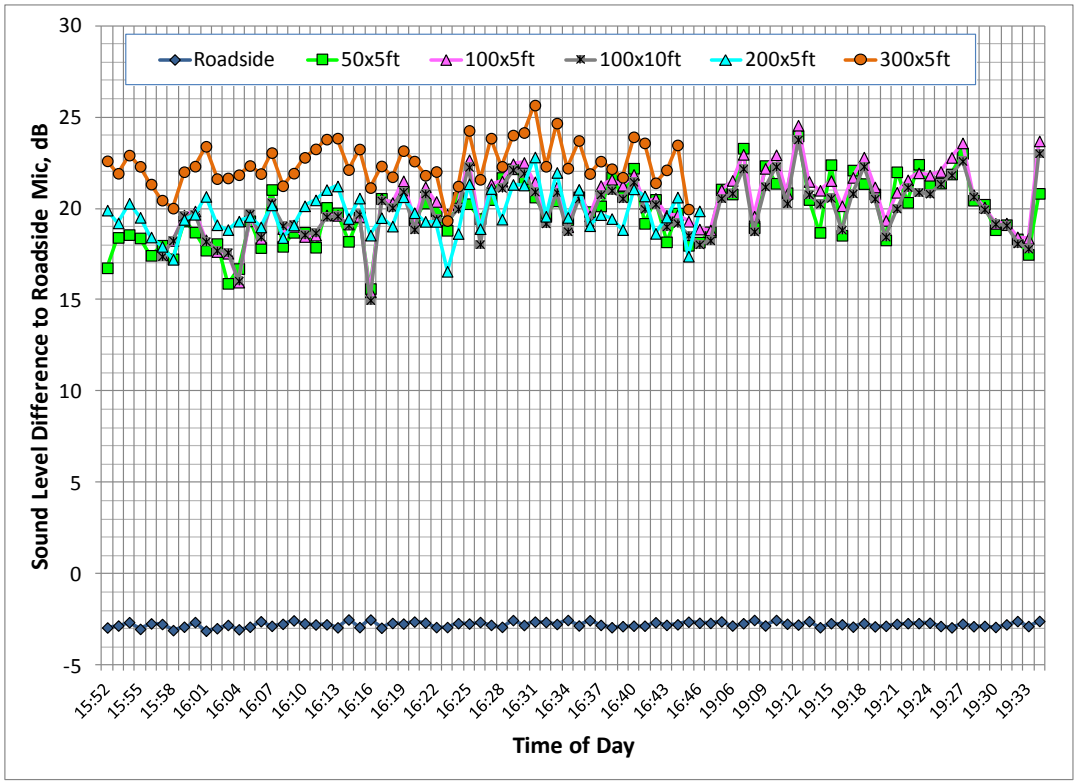

Figure 22: Noise Reduction from Top-of-Barrier Location, Session 7

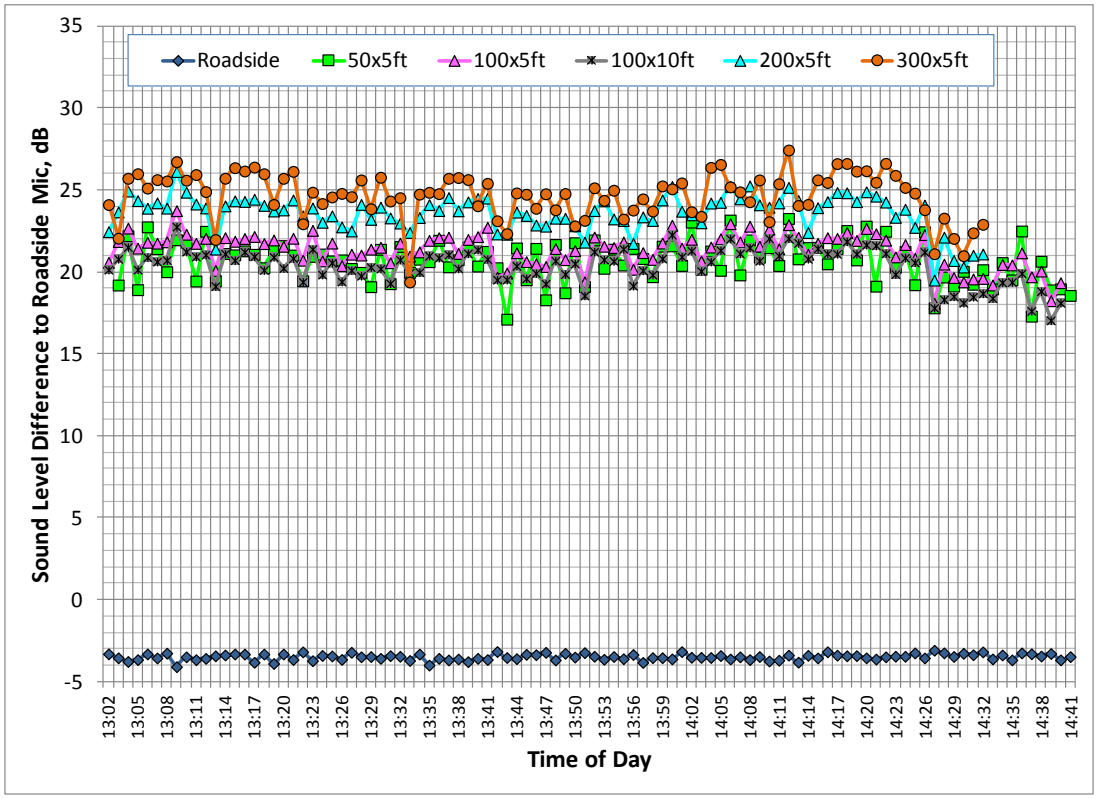

Figure 23: Noise Reduction from Top-of-Barrier Location, Session 8

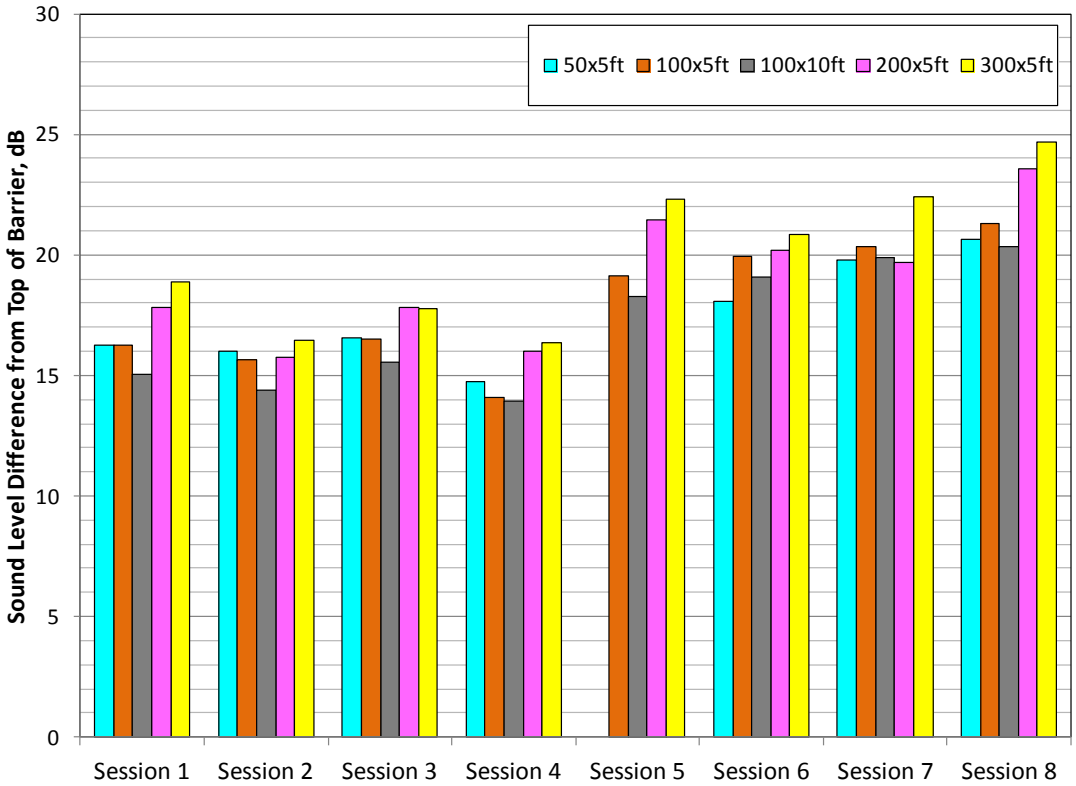

Figure 24: Session Average Insertion Loss from Barrier Position

A second commonly used method of normalizing for traffic variations is through traffic noise modeling. The Federal Highway Administration's Traffic Noise Model (TNM) was used for this purpose, generally following the procedures specified in AASHTO TP-99, *Standard Method of Test for Determining the Influence of Road Surfaces on Traffic Noise Using the Continuous-Flow Time Integrated Method (CTIM)*[32]. Traffic and geometrical data were input into the model, resulting in modeled traffic noise levels at each of the seven measurement positions. Wind variation is not an option within the TNM model. Model sensitivity to humidity and temperature occurring on a session by session basis resulted in differences in modeled levels of up to about 1 dB. To normalize for traffic conditions only, a standard temperature of 85 degrees F and 10% humidity was used for all sessions within the model. Due to time and budget constraints, data was modeled in 15-minute increments. To normalize the measured (raw) data, the average overall modeled noise level for each measurement position was calculated and subtracted from the modeled noise level for each interval by measurement position. This difference +/- the average modeled level was then subtracted from the measured level to result in the normalized level. Figures 25 to 26 show 15-minute raw and normalized averages, respectfully.

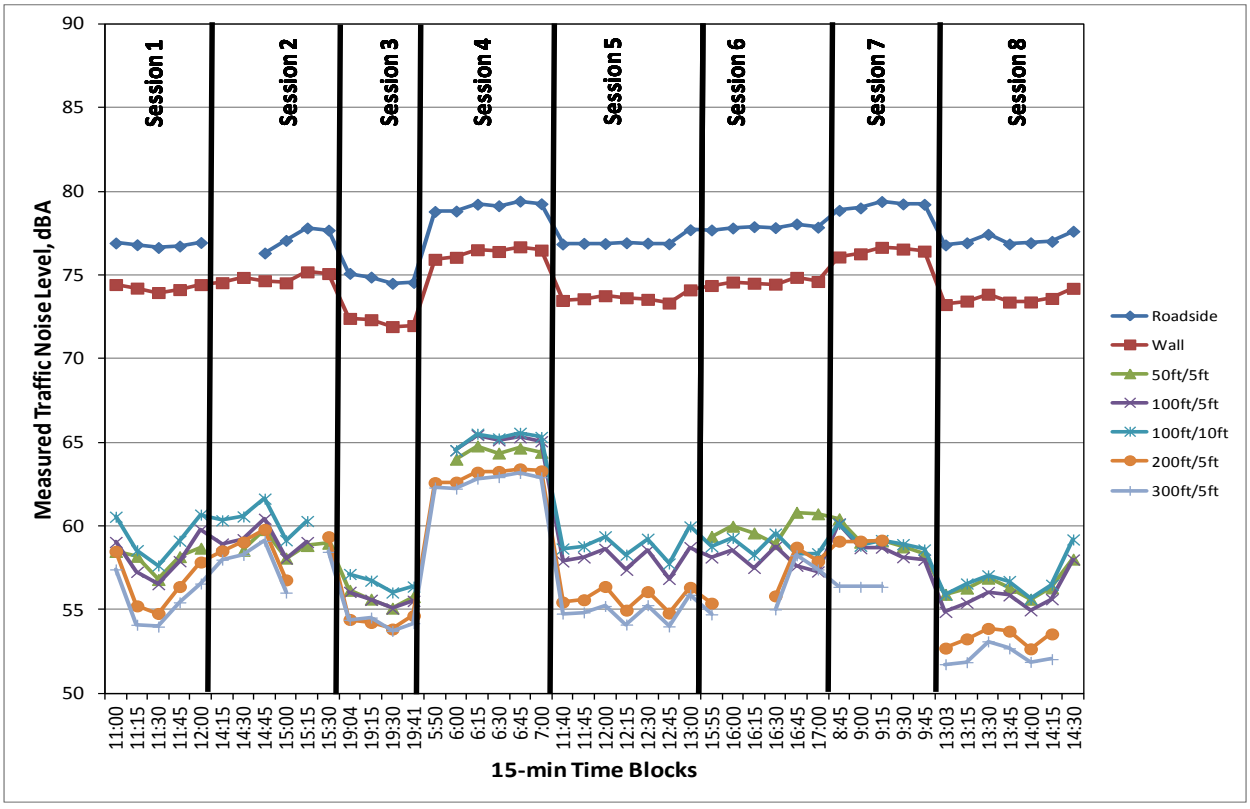

Figure 25: Measured Traffic Noise Levels, 15-Minute Averages

[32] AASHTO TP-99-13, *Standard Method of Test for Determining the Influence of Road Surfaces on Traffic Noise Using the Continuous-Flow Time Integrated Method (CTIM).*

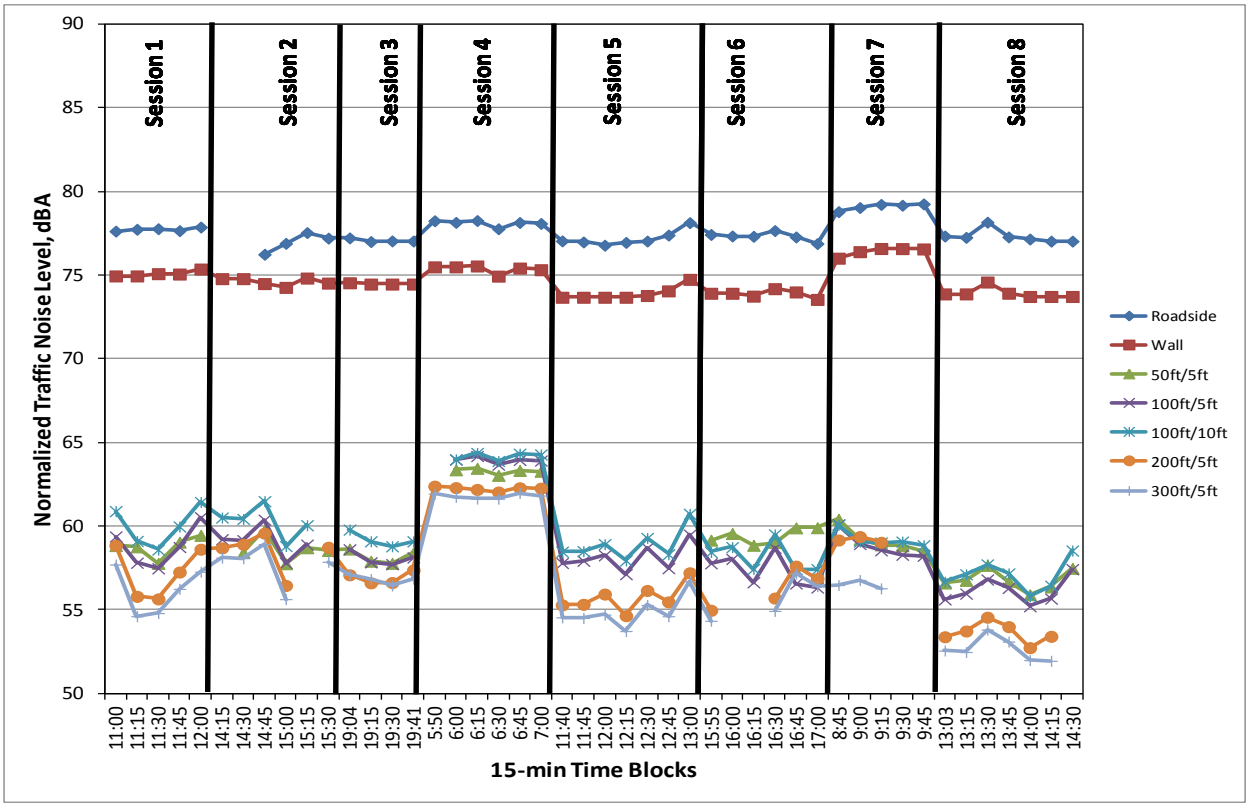

Figure 26: TNM Normalized Traffic Noise Levels, 15-Minute Averages

Comparison between these Figures and the prior ones indicate that scatter is primarily reduced due to the averaging of the data. However, there is some clear improvement between Figures 25 and 26. For example, the raw data for Session 3 (an evening measurement with lower than average traffic volumes) indicates traffic noise levels that are about 2 to 4 dB lower than those from Session 2; traffic normalized levels indicate only about a 0 to 1 dB difference between the two session. However, some scatter continues to be present, especially in the more distant measurement locations.

It is apparent from Figures 13 and 26 that even with the data scatter, some clear trends between data sets occur. Session 4, for example, exhibits measured noise levels that are up to 10 dB higher than the levels for the other sessions at the distant locations (Figure 13) and normalized levels that are up to about 8 or 9 dB higher (Figure 26). To assess the effects of meteorological conditions on the traffic noise levels, Figures 27 and 28 plot the raw traffic noise levels along the same time scale as the wind speed component perpendicular to the wall and the air temperature measured at the 6.5 ft high field tower position. Note that a (+) wind component indicates that the wind was coming from the road towards the measurement locations and a (-) wind direction indicates that the wind was coming from the measurement locations towards the road.

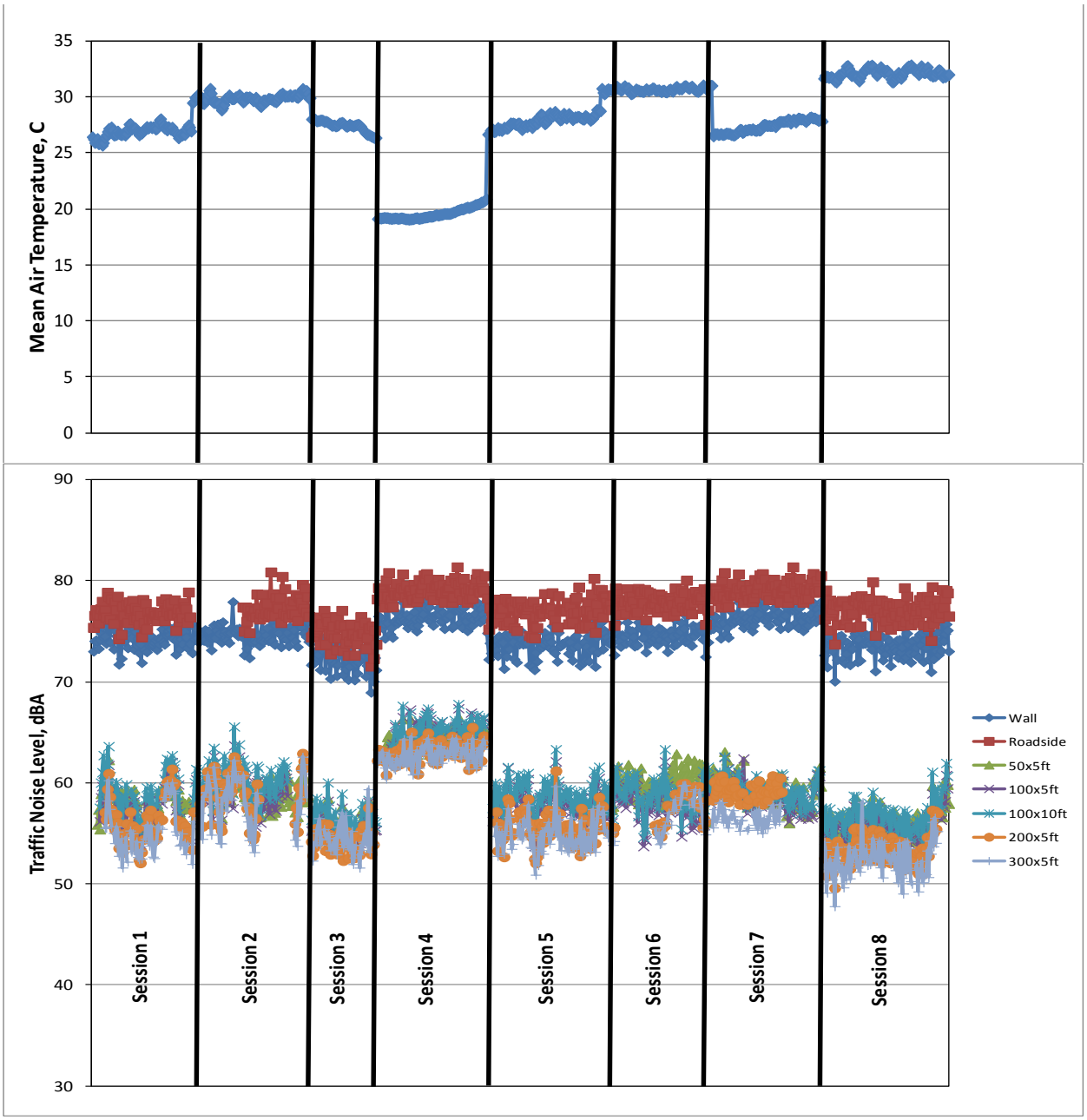

Figure 27: Measured Air Temperature and Sound Pressure Levels, All Sessions

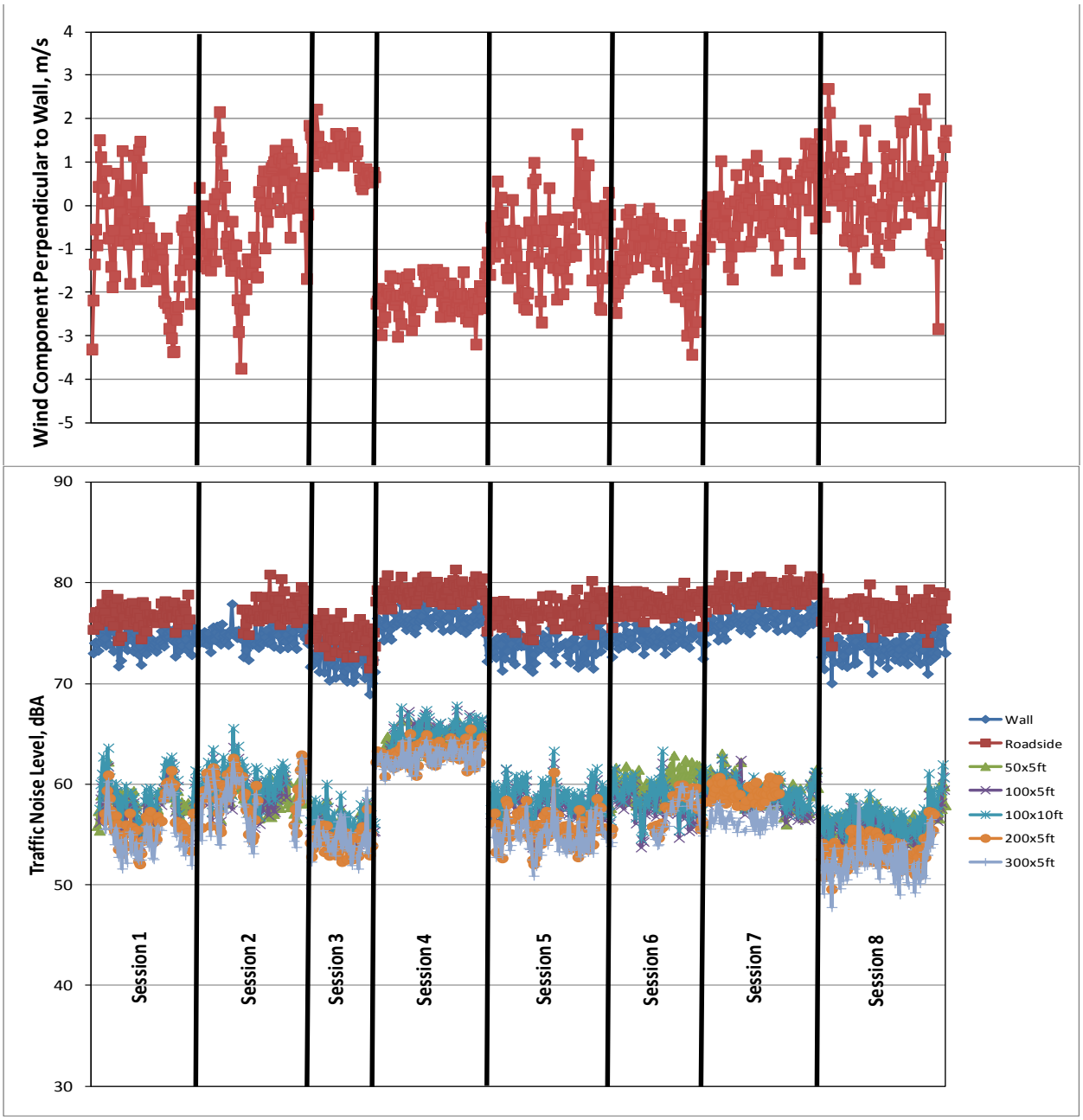

Figure 28: Measured Wind Component and Sound Pressure Levels, All Sessions

From Figures 27 and 28, some general trends can be observed; lower wind conditions and lower air temperatures are associated with higher noise levels. For air temperature, this trend is consistent with prior research[33]. For the wind component, this is counterintuitive and in conflict with prior research[3], since it would be expected that noise levels would increase when wind is blowing from the noise source toward the noise measurements. To further assess the correlation

[33] Donavan, Paul R., and Lodico, Dana M., "Project 1-44(1), Measuring Tire/Pavement Noise at the Source: Precision and Bias Statement", NCHRP Report 630, July 14, 2011.

between air temperature and wind component and the acoustical data, the acoustical data was normalized for traffic condition. In Figures 29 and 30, the traffic normalized levels shown in Figure 26 are plotted against the 15-minute average temperature and wind components measured at the 6.5 foot high field tower location, respectfully.

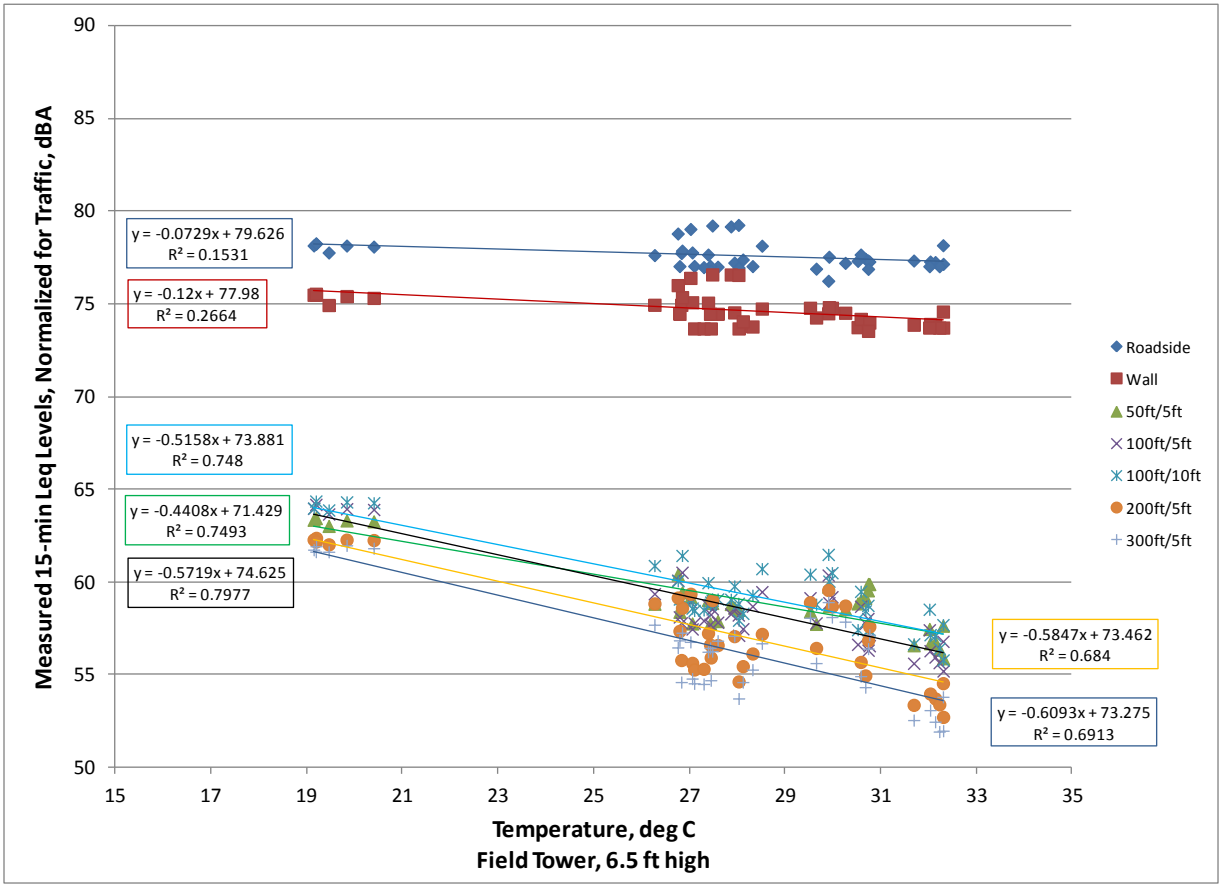

Figure 29: Traffic Normalized Noise Level vs. Air Temperature

From Figure 29, a trend of higher air temperature associated with lower noise levels can be observed more clearly. Some scatted continues to be present, with the trendlines resulting in varying R^2 values and rates for each measurement location. Rates of 0.44 to 0.66 dB/degC are indicated for the five distant measurements with R^2 values ranging from 0.68 to 0.80. As expected, smaller trends are indicated at the reference locations.

Little dependence of the noise levels on the perpendicular wind component is apparent from Figure 30. In this case, R^2 values exceed 0.5 at only the 50 foot position. As this is only a brief glance into the correlation between wind and noise levels, it would be extremely presumptuous to draw any conclusions here, particularly since field observation (auralizations) and prior research has found correlations between noise level and wind condition. Additionally, the wind component perpendicular to the wall was relatively small in these measurements. Further analysis using different components of the wind vector and the data from the other three meteorological data positions could shed more light on this topic.

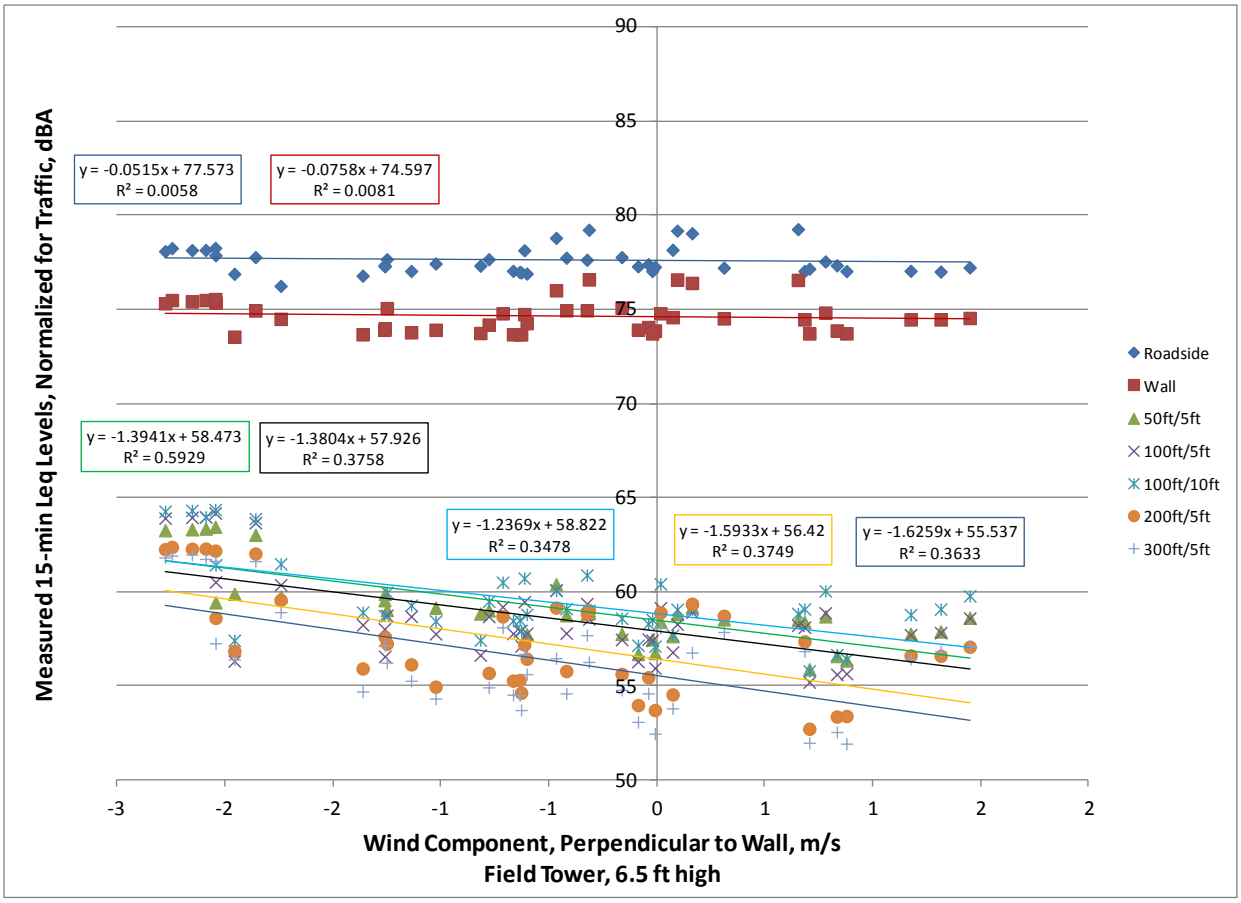

Figure 30: Traffic Normalized Noise Level vs. Wind Component Perpendicular to Barrier

Summary

Acoustical data was successfully acquired for the purposes of validating Notre Dame's developmental model. A summary of the results of the acoustical measurement data is shown in Table 1, based on 5-minute averages.

Table 1: Summary of Acoustical Data Results

(dBA)	Roadside	Top-of-Barrier	50x5ft	100x5ft	100x10ft	200x5ft	300x5ft
Ave. Traffic Noise Level	77.5	74.6	59.1	58.5	59.3	57.3	56.4
Range in Traffic Noise Level	9.8	9.6	12.9	15.4	15.0	15.9	16.8

As expected, traffic noise levels decrease with increased distance from the roadway. The exception to this is the 100x10ft position, which resulted in noise levels that were slightly higher than both the 50 and 100 ft distance and 5 ft high positions due to the reduced barrier shielding occurring at the higher position. The range in traffic noise levels over the course of the measurements is quite large; about 10 dB for the two reference locations and 13 to 17 dB at the more distant locations. In addition, a large amount of scatter was apparent in the acoustical data. This is to be expected and is typically attributed

to varying traffic and meteorological conditions.

Traffic normalization reduced this scatter somewhat. Preliminary analysis with respect to the relationships between the traffic noise levels and temperature and wind conditions did not satisfactorily explain the remaining data scatter. As described above, the data indicates interesting potential trends between the various noise and meteorological variables. Further analysis of this data is recommended and could lead to some valuable insights within the traffic noise community.

APPENDIX D: EXPERIMENTAL SETUP AND PRELIMINARY DATA SUMMARY FOR METEOROLOGICAL AND AIR QUALITY MEASUREMENTS

Contents

Description of Shared Files:

Folder **Distribute/** contains:

Photos/ - photographs of site setup, some included herein

Processed_Data_Met_1min_and_PM/ - data files and a subdirectory of figures in both .png and Matlab .fig format (which contains raw and averaged data)

Main data files:

- **AllMergedData_1min** All meteorological observations have been time-averaged to 1 minute, with standard deviation included. The mean values of horizontal wind speed and horizontal wind direction for all four sonic anemometers are also included. The .dat file is an ascii table printed from the .mat matlab file.
- **all_DustTRAK_data.mat** a Matlab file with the contents of ascii files
- **DT<x>_config<y>.txt** raw DustTRAK data in ascii format, for instrument <x> and configuration <y>. For config1, all were at “field” tower, and for config2, DT1=”roadside”, DT2=”wall”, DT3=”field”

Atmospheric and Particulate/Air Quality Measurements, Implemented Work Plan

May 9, Friday

- Obtain DustTRAK equipment from ASU

Day 1: May 11, Sunday

- Obtain rental truck and retrieve equipment from storage. Arrive at site (~2 pm).
- Identify precise final setup configuration on site.
- Assemble field and wall towers in parallel at the field tower location, relocate wall tower to final location.
- Install sensors on field tower and perform final check on data collection system.
    - Test all equipment for a 5-10 minute asynchronous collection period and check data on laptop.
    - Ensure synchronization of timestamp on datalogger as being UTC with minute and second coordinated to local time
    - set all instruments into collection mode.
- Data collection began ~15 minutes apart while both towers were on the ground after the system check and the datafile was verified on laptop.
- Raise field tower and commence measurements. Completed at ~0630 on 5/12.
- Repeat install and raise steps for wall tower. Completed at ~0730 on 5/12.
- Run experimental configuration 1 for DustTRAK sensors: at 2 m height on field tower. Started ~ 1245 on 5/12.
- Take photos of complete setup

Day 2-4: May 12-14, Monday - Wednesday, primary observational period

- Clean and rezero DustTRAK sensors and install for configuration 2, one each at 2 m AGL at field and wall tower, and on a 2 m pole on road side at .75 H_w from the wall.
- Re-zero DustTRAK at least once per day, batteries 8-12 hours, interrupts data collection.
- Monitor equipment, provide security presence during night.
- Attempt retrieving data from DustTRAK to check quality of data.
- Swap batteries and CF card on towers - no interruption in power or data collection
    - data stored in 2 periods for each tower to be merged in post-processing

Day 4: May 14

- Re-check instrument IDs and location before breaking down.
- Stop sonics at field tower last.
- Wall tower stopped around 2000, field tower around 2200
- The wall tower DustTRAK was relocated to a 2 m pole while wall tower was broken down. However, it may be possible that activities related to disassembling the wall tower may have increased PM values for this last collection period.

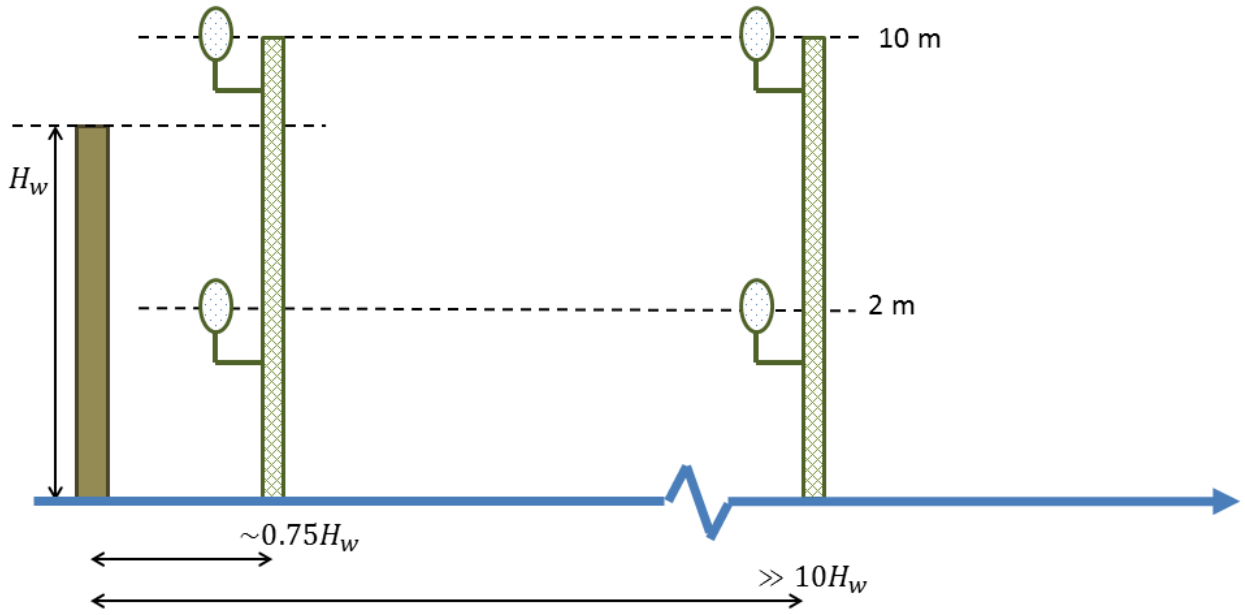

Figure 1. Schematic of ADOT SPR-699 basic experimental setup for two 10-meter towers with 2 sonic anemometers each, at 2 and 10 meters above ground level. The tower separation and placement depend upon wall height (H_w), measured from the wall position, which is also a fixed distance from the roadway.

A few research questions:

Q1: How important is the flow perturbation by the presence of the wall on the sound field?

Q2: How important is the temperature of the roadway and wall on the perturbed flow and sound field? Extended field experiments make use of FLIR camera, otherwise, temperature profiles and turbulent heat flux source area inferred by sonics and simulation.

Q3: What influence does the presence of trees with heights $H_{tree} > H_W$ have on the flow, and sound field? (if we get sites with and without trees, or include them with modified drag coefficient within the CFD model) in relation to other aspects of site heterogeneities: wash on opposite (NW) side of freeway, two recessed water recharge ponds and basketball courts (heterogeneous heat flux within source area at 10 meter height) adjacent to site; versus larger scale heterogeneities: land use and land cover changes, intersection of neighborhood, irrigated park, open desert, wash, and freeway, particularly for various mean “inlet” wind directions. Alternately, what errors would a coupled flow and acoustic propagation model incur by neglecting such effects?

Figure 2. Google Maps overview of Oasis Park (top) with schematic of setup measurement lines and distances for a few features (bottom) used during May 2012 experiment. See text for description.

The basic research guidelines used for configuring the experimental setup are illustrated by the schematic in Figure 1. The experimental plan was to place two 10 m tall towers at distances from the wall dependent upon the wall height, with one at 0.75 H_{wall}, and one >10 H_{wall}, with sensors at 2 m and 10 m AGL. The tower at ~0.75 H_W can be used to validate a CFD model by measuring wake deficit due to the wall with the lower sonic, and wall-induced sublayer jet with the upper sonic. The CFD requirements presume that H_W< 10 m allows for positioning of the upper sonic above the wall, also that the incident flow is perpendicular to the wall (for simplified 2D models). The tower away from the wall should measure free stream flow. The field tower data will be useful for validating WRF mesoscale model surface flux and stability classification. Also, these data provide values from which a

profile can be derived as inflow condition for CFD calculation, assuming similarity theory holds, or that there is uniform land use and land cover in the testing area.

Shown in Figure 2, are images from Google Maps providing an overview of Oasis park (image data dated 2014, accessed 5/2014) with approximate instrument locations denoted. Also indicated on Figure 2 are measured distances for a few key features, also given in Table 4. The wall (green dotted lines) has a slight curvature along it's length and is approximately 9 degrees east of north where the wall tower was located. The meteorological line (yellow dashed) was aligned perpendicular to the wall, approximately midway between trees and bushes near the wall on the field side, and 5.0 m south (along wall) from where the microphone line (white dashed) intersects the wall.

Along the wall, on the field side, are xeric bushes and gravel ($\leq$1 cm diameter), before transitioning to "mesic", though very dry and patchy, grass (did not measure length, suppose < 3 cm where present). Along the meteorological line, the xeric distance is 4.3 m, and mesic distance to the tower is 56.5 m. The xeric distance along the microphone line is 5.1 m. At it's largest excursion from the wall, 30.0 m north of the meteorological line, also where a light post is located, the xeric ground cover is 14.3 m wide. There is also a ~0.5 m tall ~11 m diameter gradual berm along with increased density of bushes and trees in the xeric section between the light pole and the wall.

The sprinklers were turned off at the beginning of the experimental period and remained off for the duration. Normal nightly patchwork staggered irrigation occurs between 10 pm and 730 am (Eugene Kraus, Park Manager, Private Communication), with the last occurrence before the experimental period being on the night of 5/10/2014 into morning of 5/11/2014. Sprinklers just south of the park turned on at 1:30am for several hours (and there was noise from the sprinkler water hitting the metal fence on the south side of the park).

The wall height is 4.3 m on the field side and 4.8 m on the road side, with an increase of 0.2 m just north of the wall normal line due to an added row of bricks. Measured at the wall top, the wall width is 0.31 ± 0.02 m with texture $\leq$.02 m on the fascade. Measurement details are summarized in Table 3.

There are some trees in the image which were not present at time of measurements or are the shadow of tall trees closer to the fence line (green X lines in Figure 2). An escarpment is present along the aquifer recharge basin, both at the north (not shown in Figure 2) and south end of the field (green dash-dot denotes top of escarpment). See Table 4 for a summary of measurement details shown in Figure 2.

Both the wall tower and roadside DustTRAK were situated 3.5 m from the wall (to 2 m AGL sampling volume), and the field tower is 60.8 m from the wall. Instruments were mounted on the towers so that sampling heights were located at 2 m and 10 m AGL (precise details in Table 2). The exception being that the upper temperature and relative humidity probe was located at 9.00 m (~29.5 ft) to avoid influencing the 10 m sonic via a wake, being affixed to the upper tower segment mast as shown in Figure 18. The 2 m AGL sonics were placed on arms which separated the sonic from the tower to reduce wake effect, with values summarized in Table 1.

Table 1. Summary of various measurements

tower	Instrument	measurement description	value [m]
wall	2m sonic	center of sampling volume height AGL	2.11

wall	2m sonic	center of sampling volume from tower center	1.58
field	2m sonic	center of sampling volume height AGL	2.08
field	2m sonic	center of sampling volume from tower center	2.08
wall	2m HygroClip	sampling height	1.97
field	2m HygroClip	sampling height	2.00
roadside	DustTRAK	configuration 2 inlet height AGL	1.98
wall	DustTRAK	configuration 2 inlet height AGL	1.91
wall	DustTRAK	config 2 inlet height AGL during tower breakdown	1.88
field	DustTRAK	configuration 2 inlet height AGL	2.00
field	DustTRAK	configuration 1 inlet heights AGL	2.00
field,wall	10m sonic	power wire length	15.2
field	10m sonic	data wire length	26.65
field,wall	2m sonic	power wire length	7.2
field	2m sonic	data wire length	19.22
wall	10m sonic	data wire length	24.8
wall	2m sonic	data wire length	24.5

.

Summary of Meteorological Equipment:

Table 2. Basic setup with two essentially identical 10 meter tall towers, with:
- 2 ultra sonic anemometers (2 and 10 meters), wired via differential voltage method
- 2 HygroClip temperature and relative humidity Sensors (2 and 10 meters)
- 1 thermocouple for soil temperature at 2 cm depth (not deployed last minute change)
- 1 Barometer located in the weather resistant enclosure with the data logger
- 1 CR3000 data logger with the data saved to a compact flash card.

Quantity	Part	Description
2	"Sonic"	RM Young 81000 Ultra Sonic Anemometers
1	HC2S3-L50	Rotronic HygroClip2 temperature and relative humidity probe, 50 ft cable per probe
1	HC2S3-L80	Rotronic HygroClip2 temperature and relative humidity probe, 80 ft cable per probe
1	CS106	Vaisala PTB110 Barometer (500 - 1100 hPa), 30 inch cable
1	CR3000-ST-SW-RC	Campbell Scientific Micrologger
1	CFM100-ST-SW	Campbell Scientific Compact Flash Module
1	29796-1	Power Supply 24Vdc 1.67A Output, 100-240Vac 1A Input,
1	DCDC18R	12Vdc to 18Vdc Boost Regulator

Power for the data logger and all of the equipment was provided by deep cycle marine batteries configured to run the datalogger in a continuous manner without interruption in data collection. Datalogger, barometer, power supply, DCDC converter, and CF module, were housed inside a Campbell Scientific 14-16 environmental enclosure which was left on the ground adjacent to the tower.

Table 3. Summary of measurements related to the wall height, width, and horizontal distances for measurements from the base of the wall. The wall fascade texture appeared to be a separate material bonded to an inner cement brick layer

Measurement Description	Value [m]
wall height, park side low	4.3
wall height, park side high	4.5
wall height, road side	4.8
top brick layer vertical height	0.20
wall width at top	0.31 ± 0.02
wall fascade texture depth	$\leq .02$
Distance from wall base to “wall” tower	3.5
Distance from wall base to “field” tower	61.6
Distance from wall base to “roadside” DustTRAK	3.5

.

Table 4. Summary of measurements of field features and escarpment. Escarpment measurements were made to be level with the field and aligned north-south with the line to the field tower. Top of the escarpment was defined as where the slope began to change. Tree numbers refer to Figure 2.

Measurement Description	Value [m]
escarpment top horizontal to fence	3.5
escarpment top horizontal to tree	4.9
escarpment top horizontal to water edge	9.6
escarpment top vertical to base of tree	1.3
escarpment top vertical to water surface	2.2
field tower to road edge along wall normal line	40.0
field tower to tree 1, and canopy radius along line	30.0, 4
field tower to tree 2, and canopy radius along line	31.0, 7

Particulate/Air Quality Measurements

Prof. Anderson (at ASU), lead author of FHWA-AZ-06-495, kindly allowed us to use 3 TSI DustTRAK aerosol monitoring instruments for measuring particulate matter concentrations segregated by size PM 1, 2.5, 10 micron inlet lowpass filters. We test their deployment in an un-calibrated state for PM10, with the aim to use these data for future experiment proposal purposes rather than publication. Cost estimate to calibrate is ~$500 each, with a several week turnaround time for shipping (added cost) along with time required for TSI to perform cleaning and calibration. New instruments are between $3-5k. The model used can only sample single channel.

Additional motivation is that FHWA-AZ-06-495 only examined a flat terrain no-wall case (seemingly the 101 site 3E), which we could extend. There seems to be no field data for settings typical of AZ with barriers adjacent to freeways. There is a bit of literature on flow and circulation and pollution within canyons, but seemingly for different geometries (more European "canyon") than we encounter in AZ. There is also the Maricopa County air quality and related PM issues which such a study could contribute toward fine scale modeling and perhaps improving emission inventory modeling, in coordination with our already planned fine scale flow modeling, and extending by adding PM transport (e.g. see: http://dx.doi.org/10.1063/1.4729453 but adjacent to freeway with a wall and with our planned field measurements). The effect of noise barriers on local air quality is also a controversial issue in California, and likely other arid regions.

Following experiment, it was noted that the timestamp for the sensors varied by about 1 minute between all three instruments. The data were time-averaged in log mode to 5 minutes with a 10 second time constant. It is recommended that future deployment reduce the time averaging to 60 or 30 seconds, with post-processing to 5-minutes, since the clock accuracy is within 1 minute.

Configuration 1

Since annual calibration of instruments has lapsed for several years, this configuration is designed to examine systematic and random bias between each instrument. All three instruments were configured at the same location, 2 m AGL on the field tower, as shown in Figure 26. We aim to analyze the systematic and random bias of each sensor with respect to the mean of all three, which may be useful to correct for the second configuration. Basic time series of these data are shown in Figure 12.

Configuration 2

Subsequent days of measurement had the sensors relocated to 2 m AGL at the field and wall tower, and on a 2 m tall pole on the roadway side of the wall, also at 3.5 m from the wall as with the wall tower, shown in Figures 26 and 27. Placing each DustTRAK near a sonic would enable looking at dust concentration in relation to wind speed and Reynolds stresses, to see if PM accumulates in the lee of the wall until a gust passes. Locations are summarized in Table 1. Also of interest is how concentrations change when wind is parallel to the wall.

Shown in Figure 13 and 14 are quick figures made with matlab and TSI TrakPro software, respectively. These figures show 5-minute averaged PM10 values (10 sec sampling time constant) for configuration 2. In Figure 14, inlet at 2 m AGL for "roadside" (top figure, at 3.5 m from wall on traffic side, xeric trees, leaf litter and gravel, DustTRAK "DT1"), "near wall" (middle figure, at 3.5 m from wall on field side, xeric bushes, gravel, DustTRAK "DT2"), and "field" (bottom figure, 60.8 m from wall, mesic grass, daily irrigation suspended during study period, DustTRAK "DT3"). Each test denotes changing of batteries, cleaning, and re-zeroing instrument when needed.

Instrument timestamp was checked again after the experiment and were found to vary from local standard time by: DT1 + ~10 sec, DT2 + ~45 sec, DT3 + ~60 sec. For future deployment it is suggested to average to 30 or 60 sec in situ, despite concerns with sample noise, and to post process to desired (5 minute) value. Doing so would enable to account for some of the time error. This issue arises because only the time can be set only as precise as the minute, but investigating the output file, the internal processor does track seconds.

Preliminary figures showing observed data and 1-minute time-average

Time series of 1-minute averaged meteorological variables

For all of the following figures, the blue points are raw observations at sensor sampling rate and the black curves denote the 1-minute time-averaged values in the accompanying data file. Note that LaTeX rendering was turned on for the ordinate axis label so an "_" caused the following letter to become a subscript. Also, the scales are not coordinated between each panel - these figures are intended to give a quick overview of the data. The abscissa is local MST=UTC-7 time in all cases. There were some connection issues which produced erroneous data during the first 4 minutes of collection from the hygrometer 1 Hz wall tower sensors for both 2 m and 10 m, these data have been excluded from the following figures.

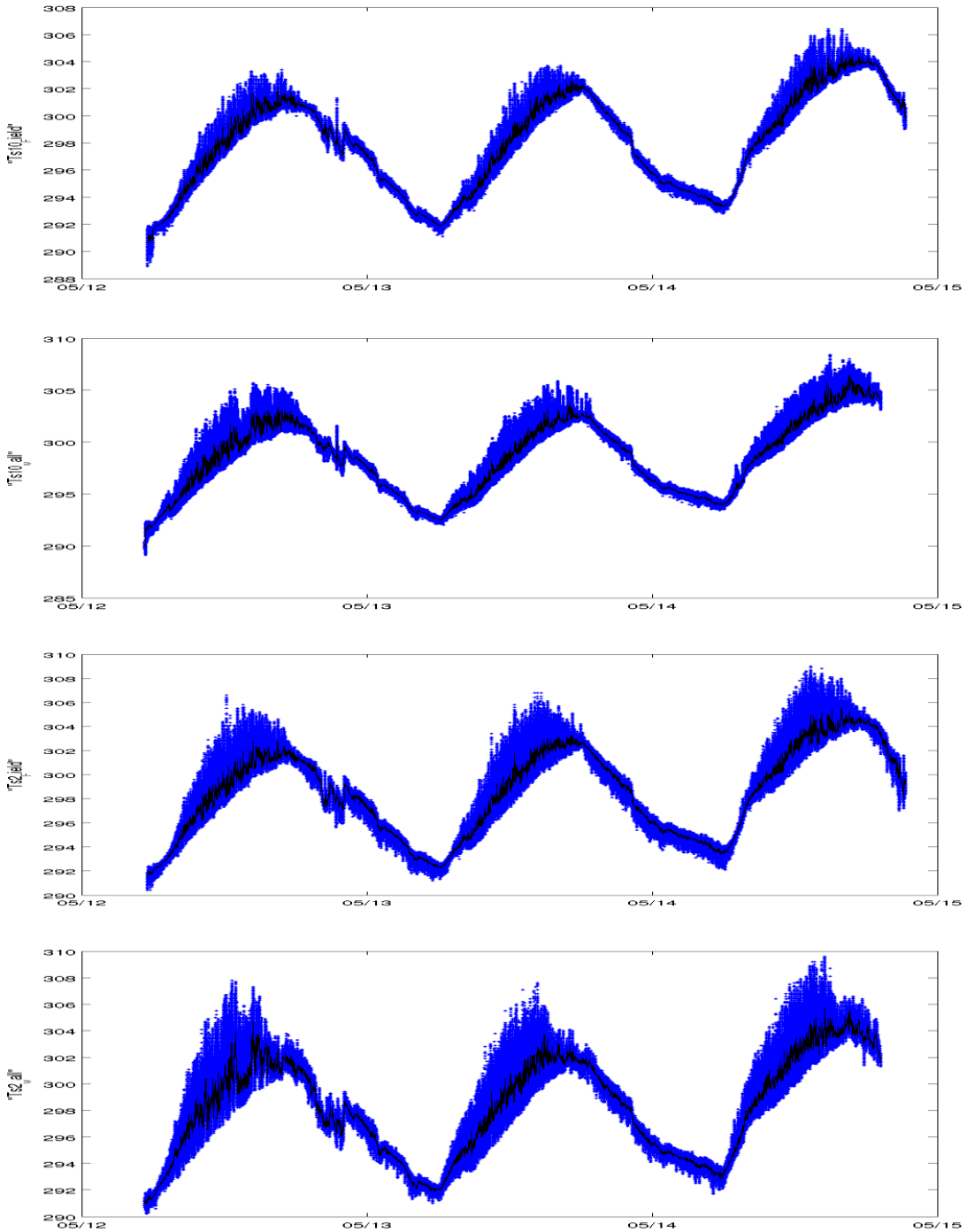

Figure 3. Virtual potential temperature measured by the sonic anemometer located at 10 m AGL field tower (top), 10 m AGL wall tower (second row), 2 m AGL field tower (third row), and 2 m AGL wall tower (bottom). Blue points are 20 Hz observations, black line is 1 minute time-average. Note that vertical scales are all different

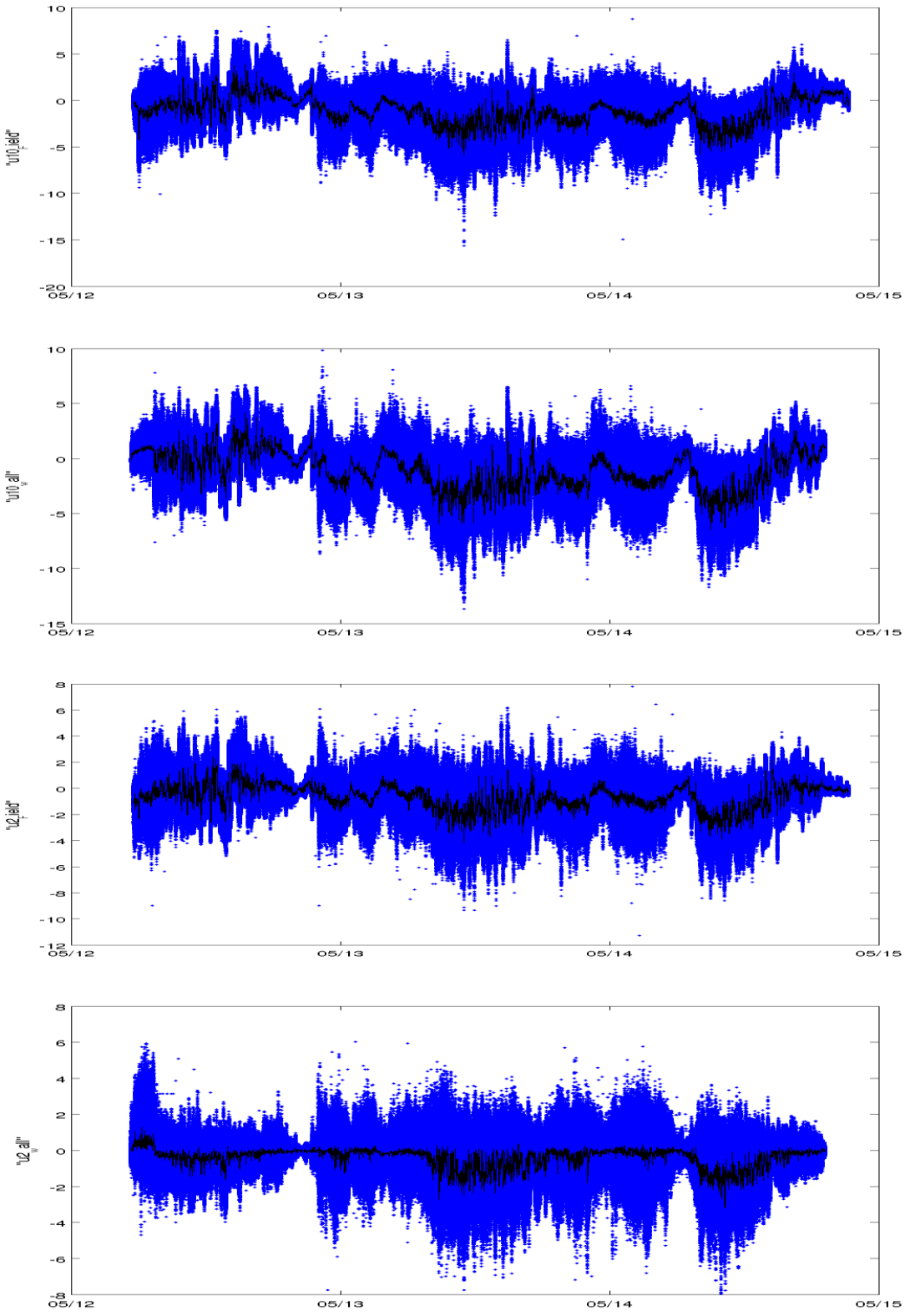

Figure 4. Same as for Figure 3 but for sonic u velocity component (u>0 is east)

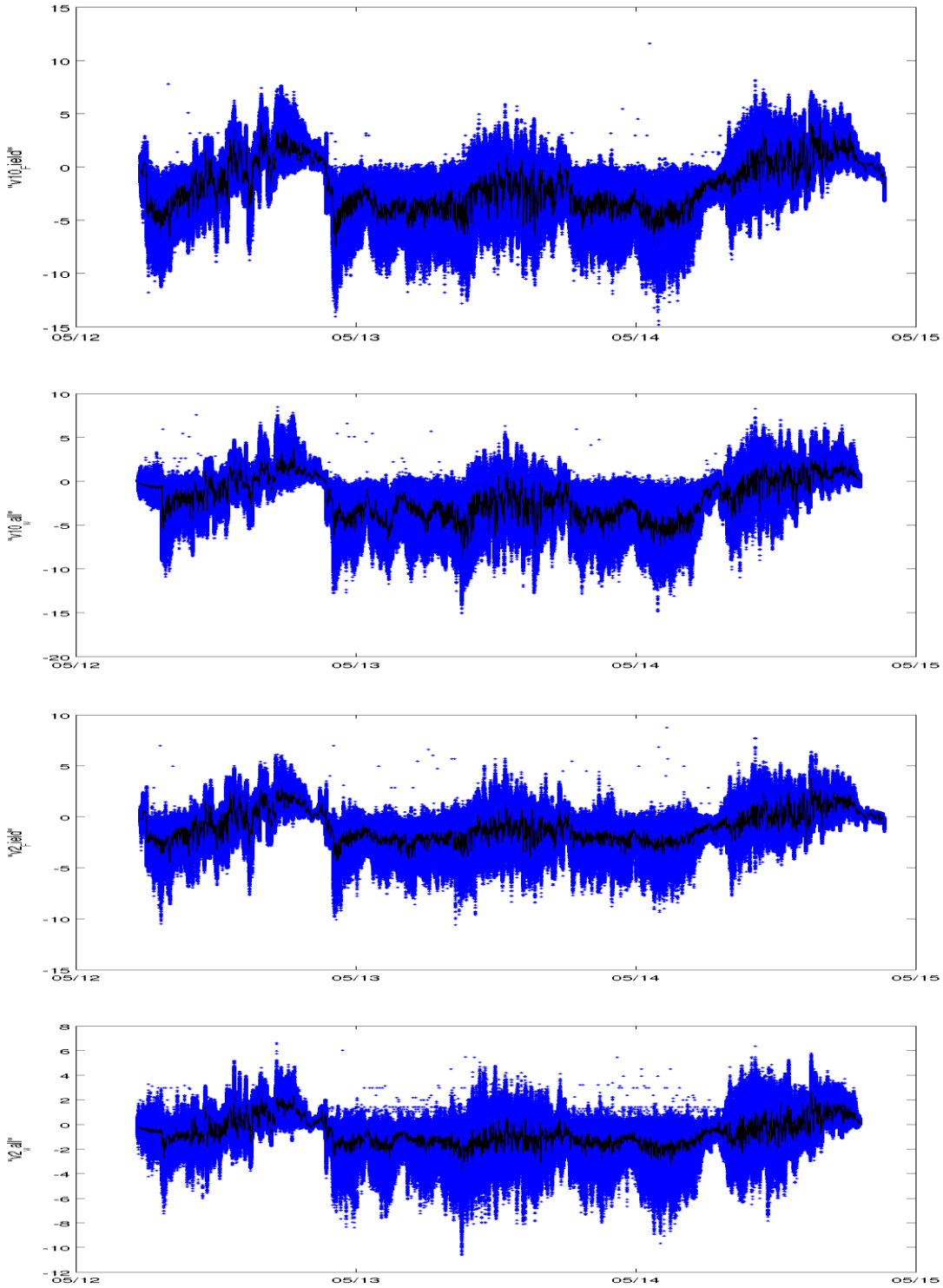

Figure 5. Same as for Figure 3 but for sonic v velocity component (v>0 is north).

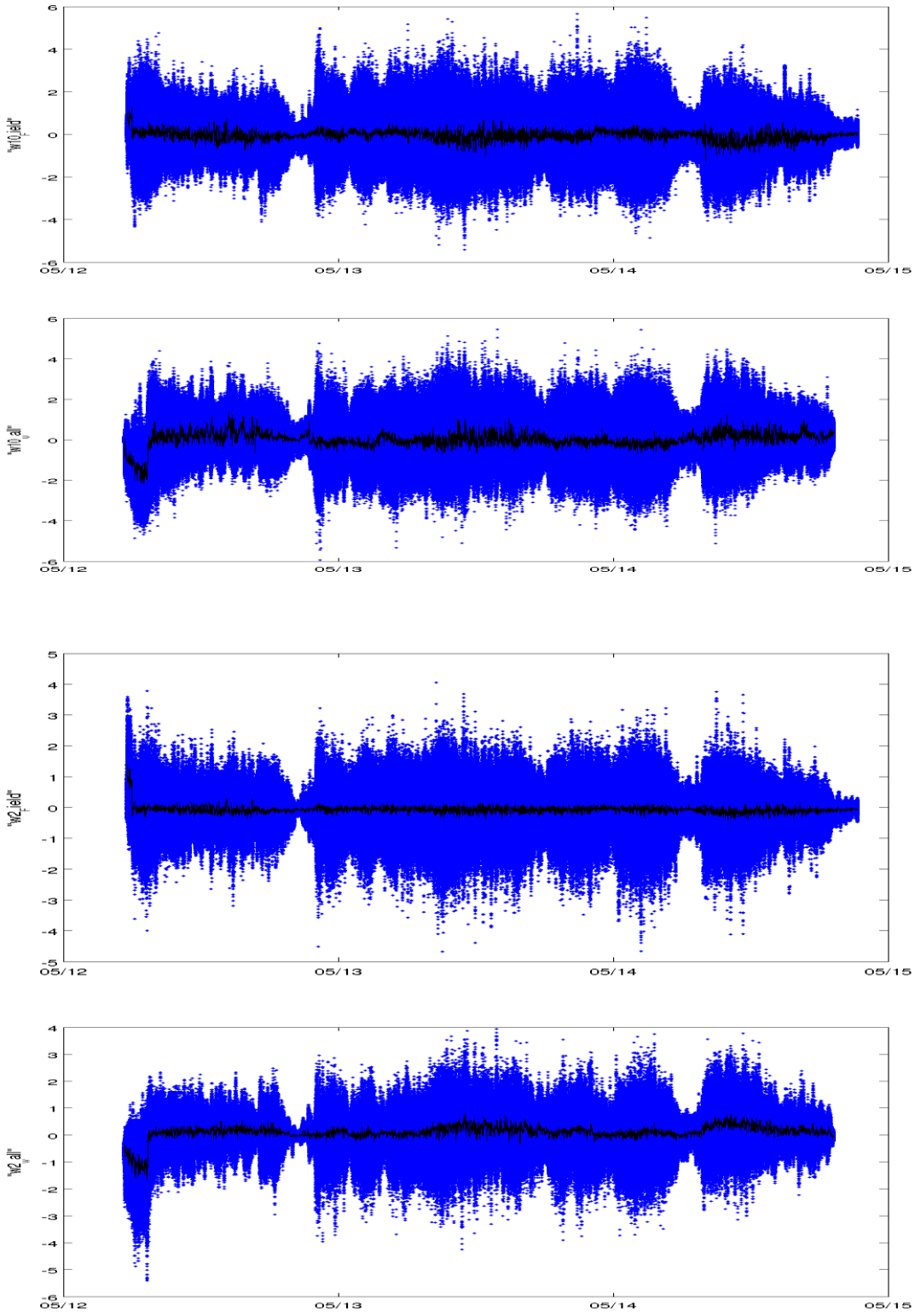

Figure 6. Same as for Figure 3 but for sonic w velocity component (w>0 is up).

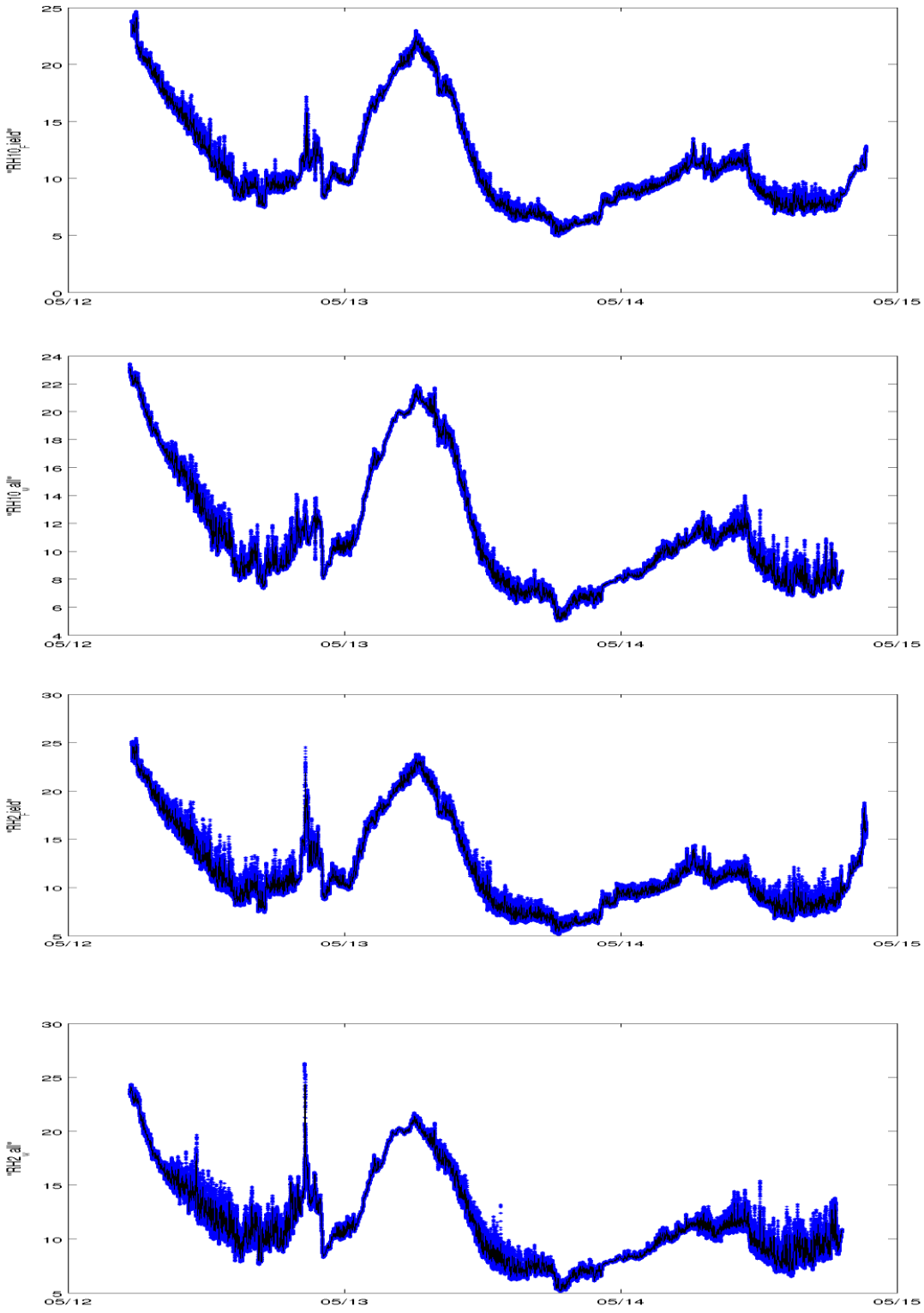

Figure 7. Same as for Figure 3 but for hygroclip relative humidity sampled at 1 Hz.

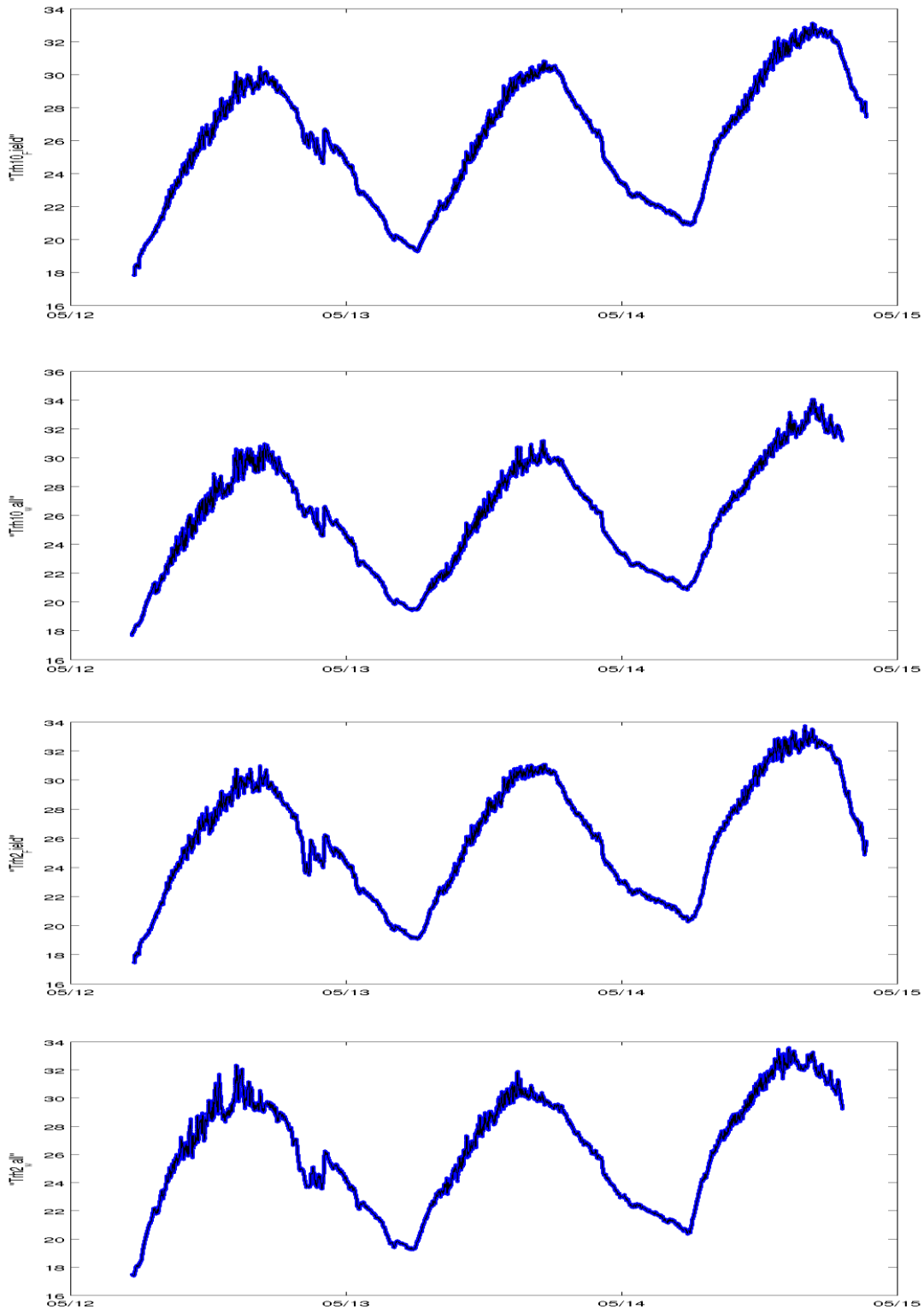

Figure 8. Same as for Figure 3 but for hygroclip temperature sampled at 1 Hz.

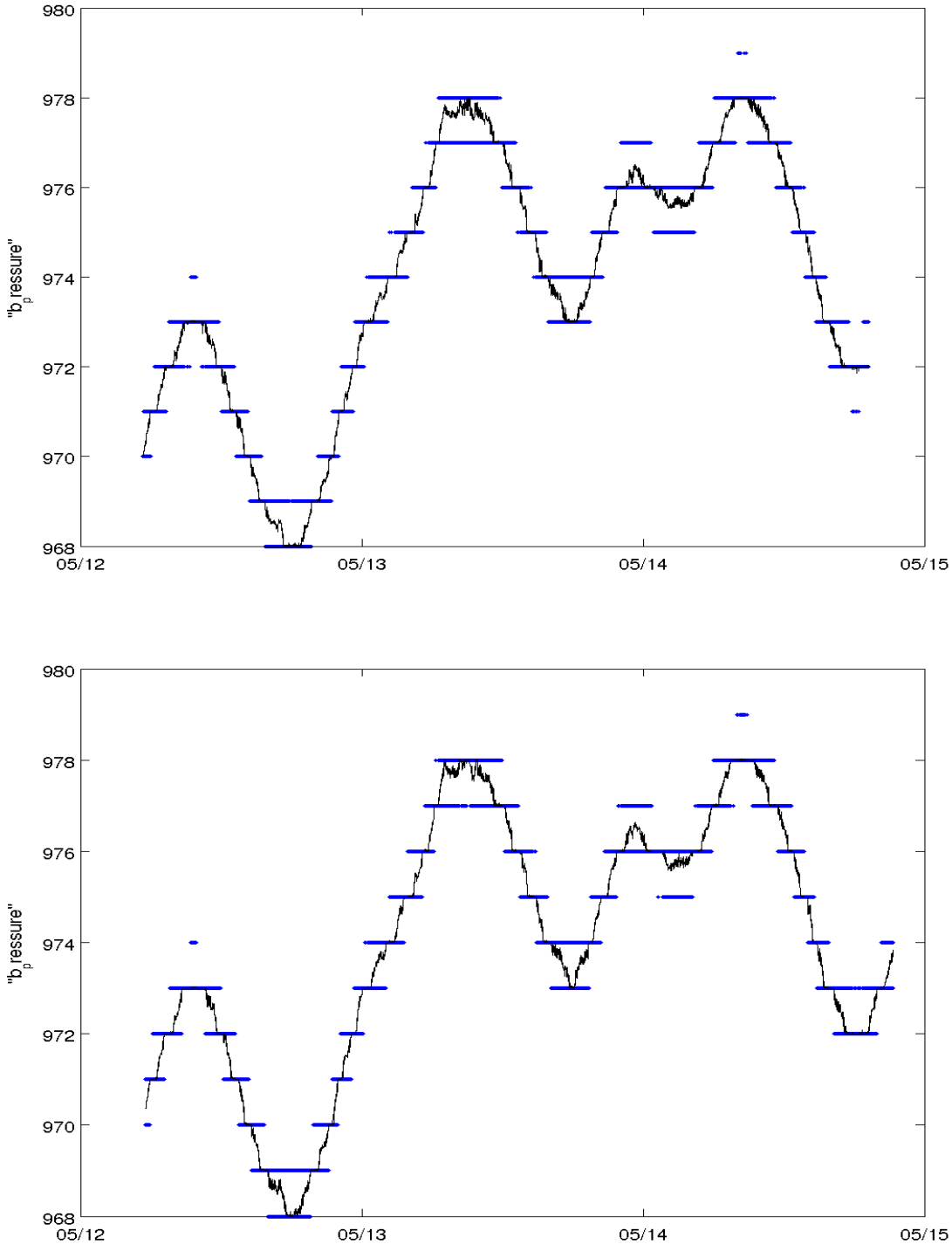

Figure 9. Barometric pressure sampled at 1 Hz (blue), averaged to 1 minute (black), for field tower (top) and wall tower (bottom).

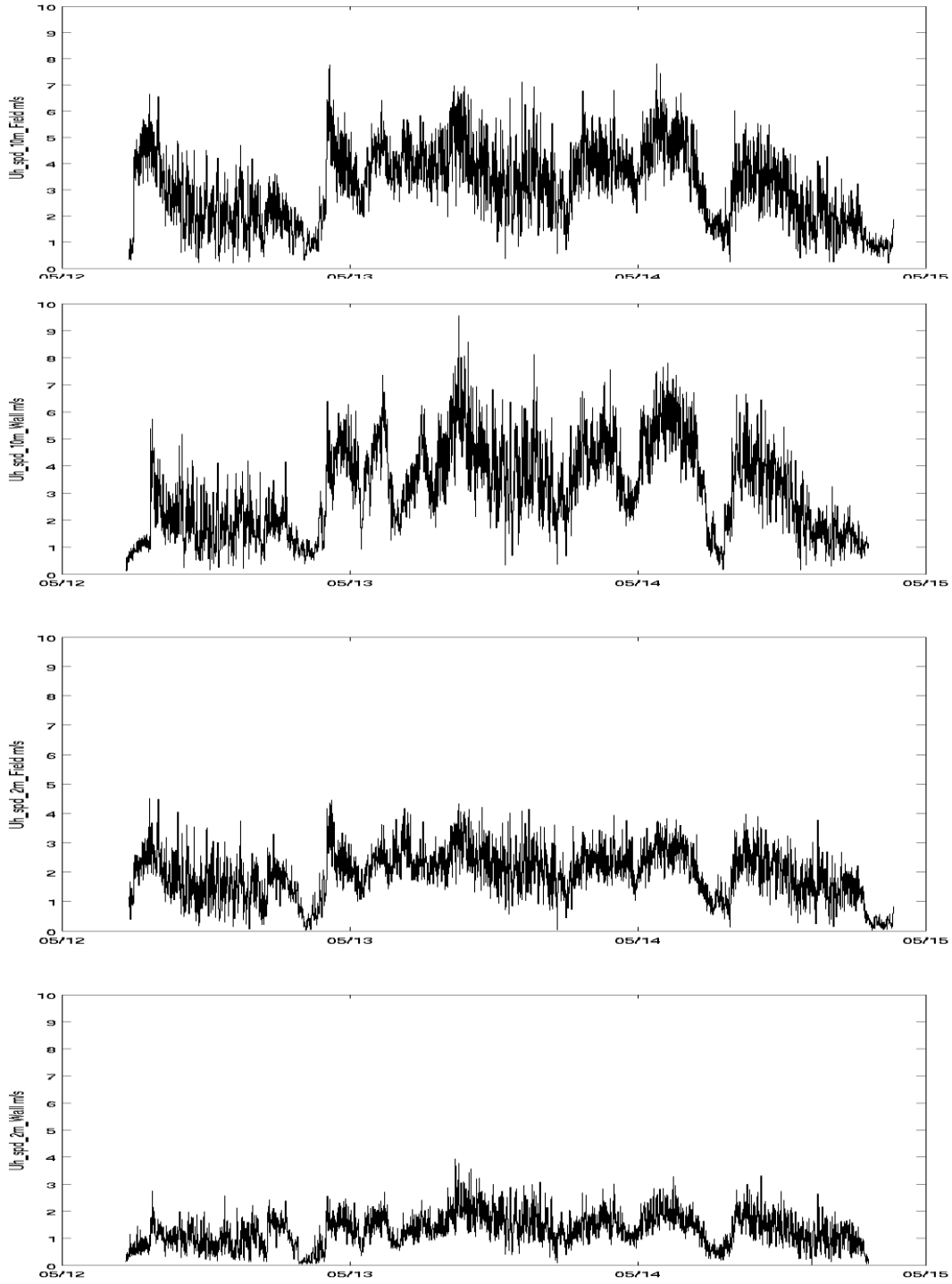

Figure 10. Same as for Figure 3 but for horizontal wind speed and just showing 1-minute averaged values.

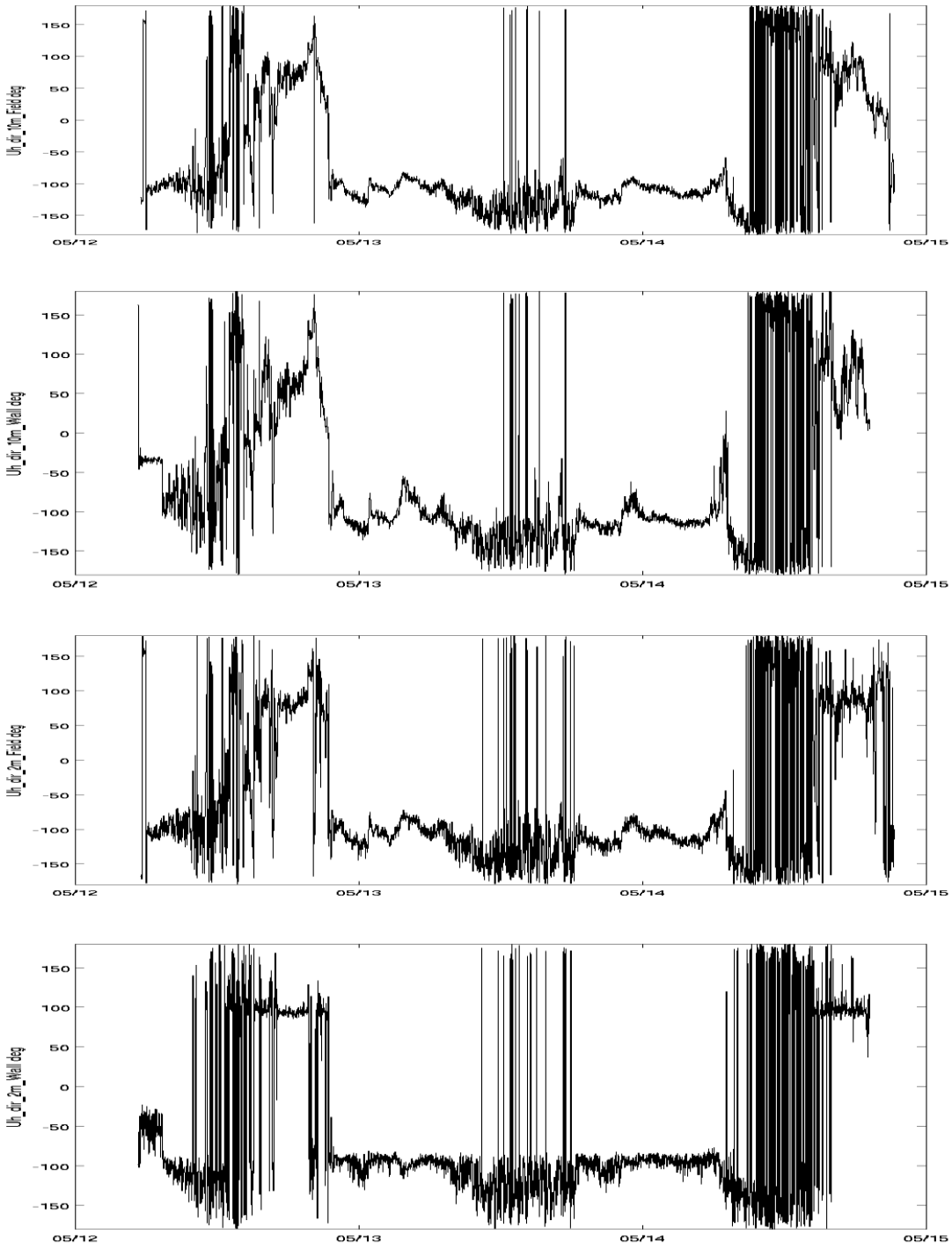

Figure 11. Same as for Figure 3 but for horizontal wind direction in degrees (0 deg is east, 90 deg is north) and just showing 1-minute averaged values. Note that the wall is approximately 9 degrees east of north, so desired incident wind direction perpendicular to wall from the road direction would be near -9 deg. The many vertical lines are typically due to wind direction near +/- 180 degrees and points being connected with lines.

PM_{10} observations, configuration 1

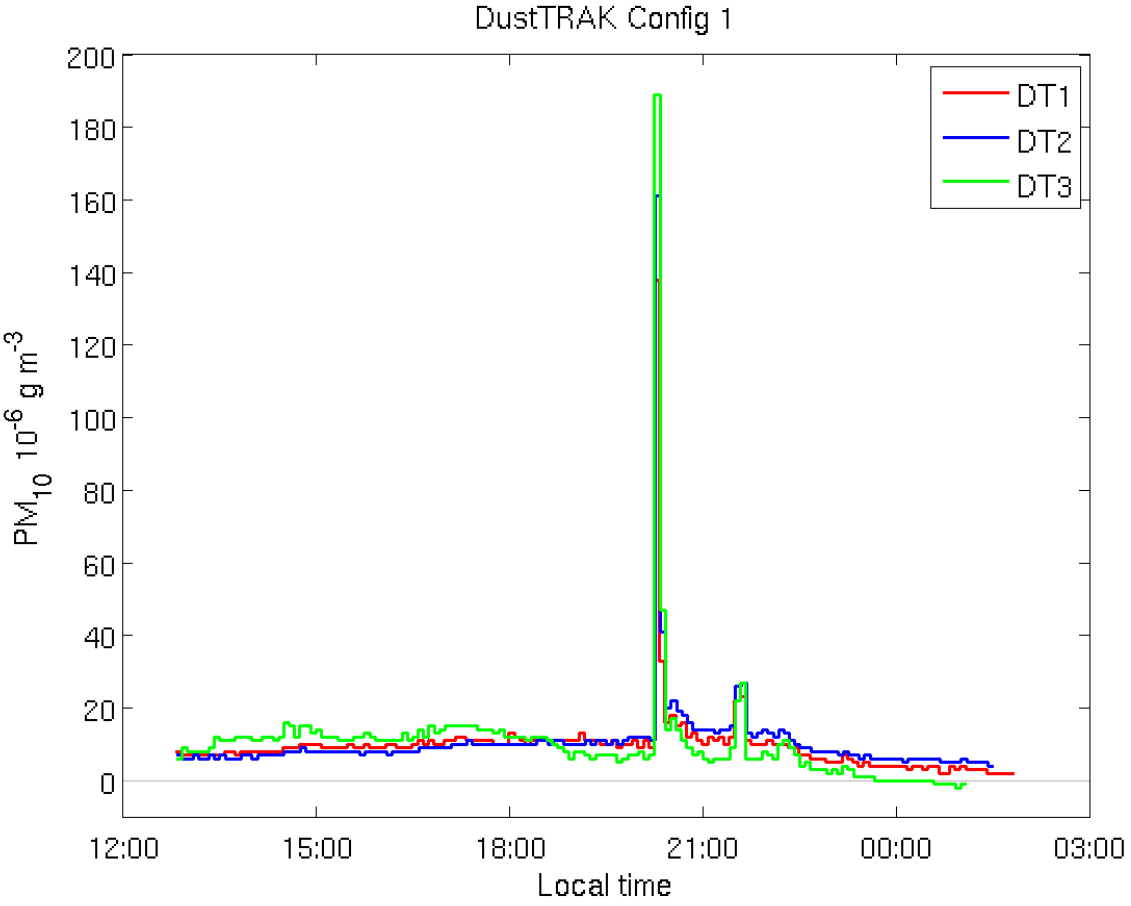

Figure 12. PM_{10} observations for configuration 1, co-located at 2 m AGL on field tower, for DustTRAK DT1 (red), DT2 (blue), and DT3 (green).

PM_{10} observations, configuration 2

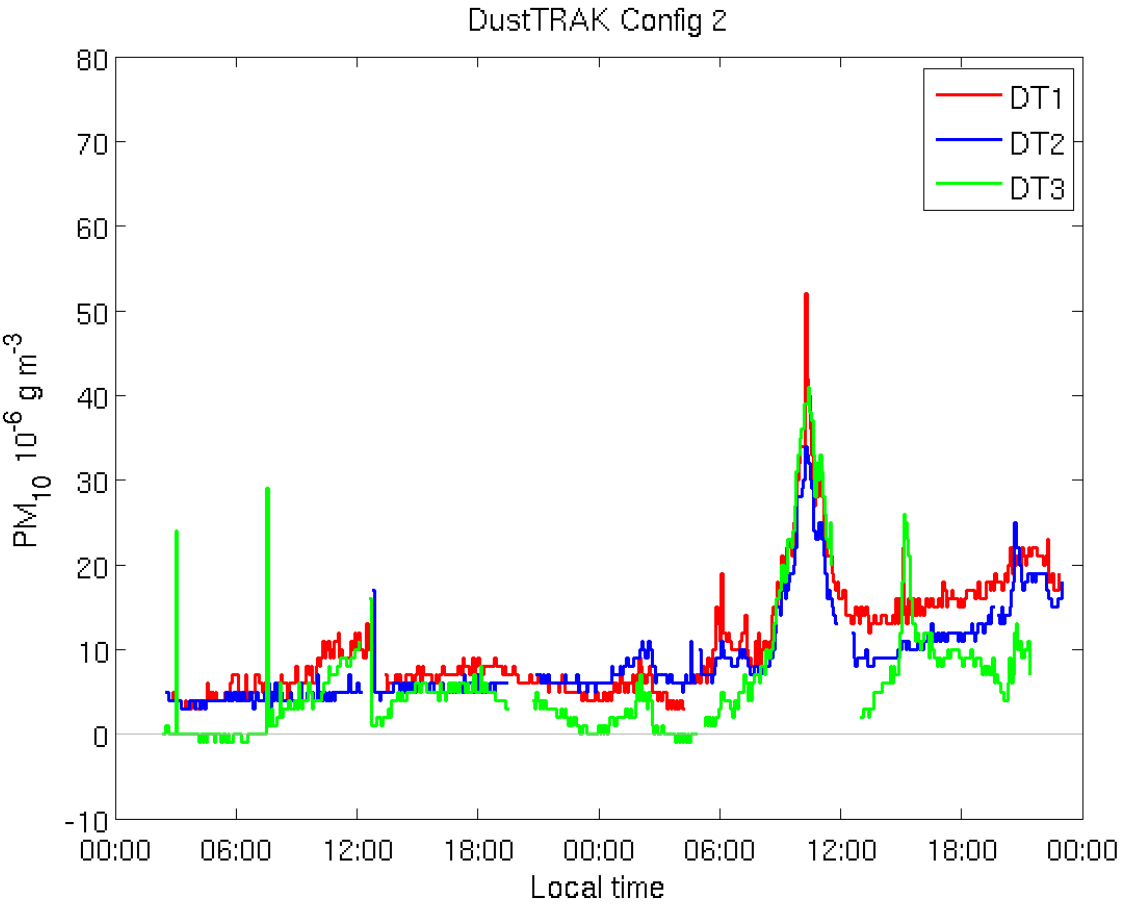

Figure 13. Observations of PM_{10} for configuration 2 for the DustTRAK sensor positioned 2 m AGL and roadside (red, DT1), on the wall tower (blue, DT2), and field tower (green, DT3).

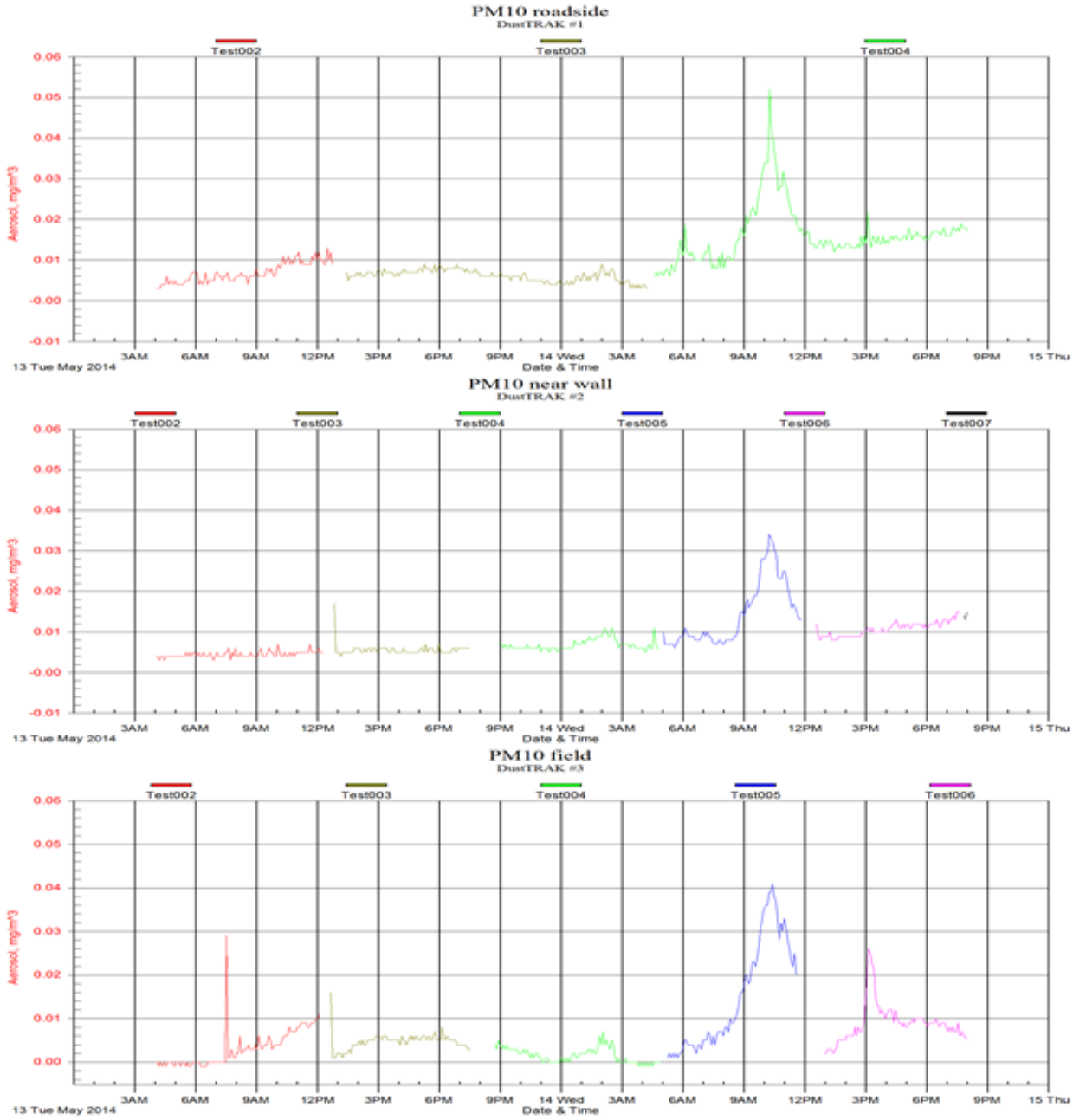

Figure 14. Quick figures made with TSI TrakPro software, viewing 5-minute averaged PM10 values (10 sec sampling time constant) for configuration 2: inlet at 2 m AGL for "roadside" (top figure, at 3.5 m from wall on traffic side, xeric trees, leaf litter and gravel, DustTRAK ID1), "near wall" (middle figure, at 3.5 m from wall on field side, xeric bushes, gravel, DustTRAK ID2), and "field" (bottom figure, 60.8 m from wall, mesic grass, daily irrigation suspended during study period, DustTRAK ID3). Each test denotes changing of batteries, cleaning, and recalibrating/zeroing instrument when needed.

Photographs of experimental setup

Higher resolution .jpg images are available in an attached folder, including many images not shown in this document. Note that aspect ratio was not always preserved when including images.

Figure 15. Images of equipment being assembled in the middle of the field. Both with a similar view atop a tripod looking toward northwest.

Figure 16. Images of (top) panoramic near southwest corner looking north with towers and microphone stands in place; (bottom left) along wall showing detail of wall texture and microphone above wall top, taken from intersection of tower line and wall looking north; (bottom right) same as bottom left but looking east into the field, wall tower is in the foreground.

Figure 17. Images of various equipment: (top left) wall tower data logger box; (top right) microphone equipment on field tripod; (bottom left) partial apparatus for mounting and taking On-Board Sound Intensity measurements; (bottom right) more acoustics equipment.

Figure 18. Images of various equipment: (top left) TSI DustTRAK; (top right) microphone; (bottom) detail showing mounting of 10 m sonic and "10 m" hygroclip which is at the top of the 3rd 10 ft tower section to reduce possible wake from the radiation shield (bottom left) on ground when disassembling (bottom right) on field tower during the observation period.

Figure 19. Images taken from between field tower and wall tower (top) looking west at wall tower (bottom) looking east toward field tower.

Figure 20. Images of field looking southwest from northeast corner of the field.

Figure 21. Image of field looking west toward the wall, from a position south of where the images shown in Figure 18 were taken, which is just out of the view on the right of this image.

Figure 22. Nearly 170 degree horizontal field of view panoramic images of the field from north of the microphone line looking south (top two), and from under the shade tree progressing from being centered toward the south, southeast, and east (bottom three).

Figure 23. Panoramic images from various locations and angles: (top two) east of field tower with view centered near west into the field and toward the wall; (third and fourth row) looking toward north and south, respectively, closer to the wall; (bottom) looking south toward field near sunset.

Figure 24. Panoramic images of (top two) field looking south, and (third row) near wall centered near west; (bottom left) looking west toward wall tower in background with field tower in foreground left; (bottom right) compass view of field tower looking due east.

Figure 25. Images of some personnel and visitors to the site.

Figure 26. Images of DustTRAK configuration 1 field tower (top left), and configuration 2 for the: field tower (top right) wall tower (bottom left) and wall tower during disassembly of wall tower (bottom right).

Figure 27. Images of roadside DustTRAK setup looking north (top) and south (bottom).

Figure 28. Images of near the wall looking south (top) and looking south toward southern aquifer recharge pond showing sloping terrain adjacent to 79th Ave on left of image.

Figure 29. Images of field tower. The blue fold-up chair was positioned due east of wall tower and due north of field tower, and is used in several images to indicate cardinal direction.

Figure 30. Image of additional wind profile measuring apparatus.

APPENDIX E: ACOUSTIC SCALE MODEL STUDY

I. Introduction

Traffic noise barriers are widely used to reduce exposure to traffic noise in neighbouring residential areas. In the presence of a barrier, the noise at a receiver location on the opposite side of the barrier from a source is due to two sound pathways: the transmitted pathway through the barrier and the diffracted waves emanating from the top of a barrier. Barriers are usually built with solid materials that should effectively block direct sound propagation. However, it is known that poorly fitted panels and other defects can lead to *sound leaks* that significantly reduce barrier performance in the field[1]. Such construction-related performance issues and the transmitted pathway are not considered in this paper. A solid barrier's performance is thus limited by the diffracted sound which is highly dependent on (i) source frequency, (ii) relative source and receiver positions and (iii) the barrier top geometry[2].

The simplest way to improve barrier performance at a given receiver location is to increase its height. However, aesthetic problems, as well as cost and safety issues usually prevent the transportation authorities from increasing the height of barriers above a certain limit[3]. Since different barrier top geometries modify the diffracted waves, various barrier shapes have been investigated in an attempt to achieve the same performance as a higher vertical screen . By finding an improved barrier top design it may be possible to keep the same barrier performance with a reduced barrier height.

In recent decades, numerous modifications to barrier design have been proposed to improve barrier performance and there are now a number of different designs of barrier top used in practice. For instance, in Japan alone there are approximately 20 types of devices that modify the edge shape of the noise barrier and are distributed as commercial products[4;5]. Shapes of different barrier tops have included T-shaped, L-shaped, Y-shaped, as well as arrow, cylindrical, multiple and random edge configurations.

Different methods are used to study top-modified barriers. They include field and large scale measurements, theoretical/numerical simulations and scaled laboratory experiments. Field measurements are complicated, expensive, have poorly controlled background conditions and are usually difficult to repeat[6;7], while large scale experiments require huge anechoic laboratories which are expensive to build and run. The main problem in three-dimensional simulations is the long calculation time, especially for barriers with complicated tops and so, often, the calculations are carried out using a two-dimensional model. Two-dimensional boundary element methods have been used to estimate the insertion loss of noise barriers. Numerical models have been developed to calculate barrier efficiency, to assess the acoustic performance of a range of barrier designs and for optimization of the acoustic performance of barriers[8;9;10]. Finite-element methods are also used to calculate the insertion loss of different noise barrier designs[11]. The computational cost for these two-dimensional numerical simulations is not significant but the cost increases significantly for fully three-dimensional calculations and for higher frequencies. The calculation time depends also on some other parameters, *e.g.* the chosen frequency range[12;13].

While some of the difficulties in conducting field experiments have been addressed by the new European procedure EN 1793-4:2015 (previously CEN/TS 1793-4)[14], an experimental method in which scaled experiments are used offers an attractive alternative[15;16]. The main idea of this approach is based on the invariance of the sound speed in air for similar field and laboratory conditions. This allows a scaled model of the barrier to mimic the performance of a real traffic barrier, when the frequency band of the laboratory sound source is increased by the same factor relative to typical frequency band of traffic noise. The scaling is straightforward if any surfaces reacting with the measured sound are rigid, otherwise the impedance of the surfaces must also be scaled. The scaled

approach is readily adopted in the present communication as we focus purely on the optimal diffractive properties of various barrier top geometries, which are assumed to be rigid throughout.

The main purpose of this present work is to develop a universal methodology for obtaining the diffractive characteristics of different top barrier designs and, by comparison, identify geometries that may have performance advantages over traditional thin screen barriers. Our proposed method is to use scaled laboratory experiments and an impulsive point sound source. If the duration of the sound pulse is sufficiently short, the primary signal that takes the shortest most direct route diffracts above barrier and arrives at the receiver much earlier than any secondary signal that has been reflected or diffracted by the surroundings. These latter signals are easily separated from the primary signal infomation and only the information from the primary signal is analysed. Such an approach eliminates the need to build an expensive acoustic anechoic chamber for experiments, thus paving a new avenue for conducting acoustic experiments in the laboratory. The apparatus is placed in the laboratory on a dense, thick wood table that serves as the ground plane. The typical frequency range of the sound source (1–30 kHz) is 10 times the typical frequency range of traffic noise (100–3000 Hz). Thus the experiments can be considered as 1:10 scaled experiments of a real traffic noise barrier top.

The barriers top designs considered in this paper can be divided into two groups: (i) barriers with homogeneous tops that maintain the same height and geometry along the entire barrier length and (ii) barriers with heterogeneous tops that have variable height and geometry along the barrier length. Typical examples of homogenous tops include a thin vertical screen and T-shape tops. Typical examples of heterogeneous tops are so-called jagged tops which have a regular or random variation of height and geometry. Naturally, the acoustic diffractive characteristics of the homogeneous barrier tops remain uniform

along the barrier, while for heterogeneous barriers it changes along the barrier and this complicates the measurements and interpretation (see below).

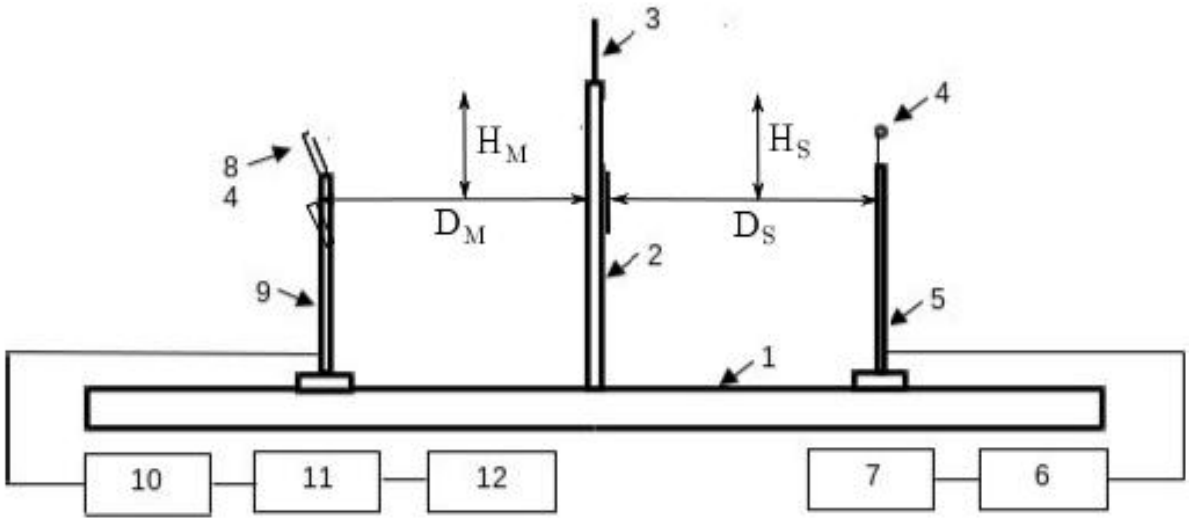

Figure 1: Experimental schematic and instruments.1 - large solid wood table, 2 - vertical wooden barrier, 3 - removable aluminum top attached to the barrier, 4 - impulsive sound source fixed to support 5, 6 - high voltage source for main electrodes, 7 - high voltage source for trigger electrode, 8 - microphone with preamplifier fixed under grazing angle to support 9, 10 - microphone conditioning amplifier, 11 - 100 MHz digital storage oscilloscope, 12 - computer with LabVIEW software.

II. Experimental set-up and method

A. Experimental schematic and instrumentation

Experiments were conducted in a laboratory in air at room temperature; see Fig. 1 for a schematic. The experimental apparatus consists of: (1) a large solid wooden table, (2) a vertical wooden barrier (2.5cm × 60cm × 120cm) with (3) removable aluminum plates

(0.15cm × 15cm × 120cm) with different top geometries, (4) an impulsive sound source fixed to a support (5), (6) a high voltage source for the main electrodes, (7) a high voltage source for the trigger electrode, (8) a Brüel & Kjær (type 4939-A-011) 1/4" free-field microphone with preamplifier 2670 and TEDS fixed below the grazing angle to support (9), (10) a Brüel & Kjær (type 2690-A-0S1) microphone conditioning amplifier, (11) a Tektronix (type 2230) 100 MHz digital storage oscilloscope, (12) a computer with LabVIEW software to analyze and store the measured signals. After each experiment the measured signals were post processed using the custom built MATLAB software described in appendix A.

B. Laboratory sound source

In experiments related to scaled acoustic modeling, different methods are used to model an impulsive point source with a short spherical acoustic wave of high intensity. Gun shots, the discharge of shot-shell primers, ultrasonic air-jet whistles, very powerful impulse lasers and spark dischargers have all been used to produce short N-shaped spherical sound waves[17;18;19;20;21]. The most popular method to generate an N-shaped sound wave is to use a spark discharger and there are a number of descriptions of different spark dischargers in the literature. These descriptions, however, are only schematics that omit the important details required to build such a device[22;23]. As a consequence, we designed and constructed our own device taking into account the following main requirements: relative simplicity, short duration, small size, omnidirectionality and most importantly - high stability. To satisfy these requirements and by taking into account that two-electrode devices are typically not stable, a three-electrode triggered spark discharger was built, as shown in Fig 2.

The electrodes are made from tungsten rods with pointed ends. Two main electrodes (diameter 0.3 cm) and a third triggering electrode (diameter 0.15 cm) are fixed to three bronze holders (diameter 0.5 cm, length 15 cm) on a plastic support and attached to a

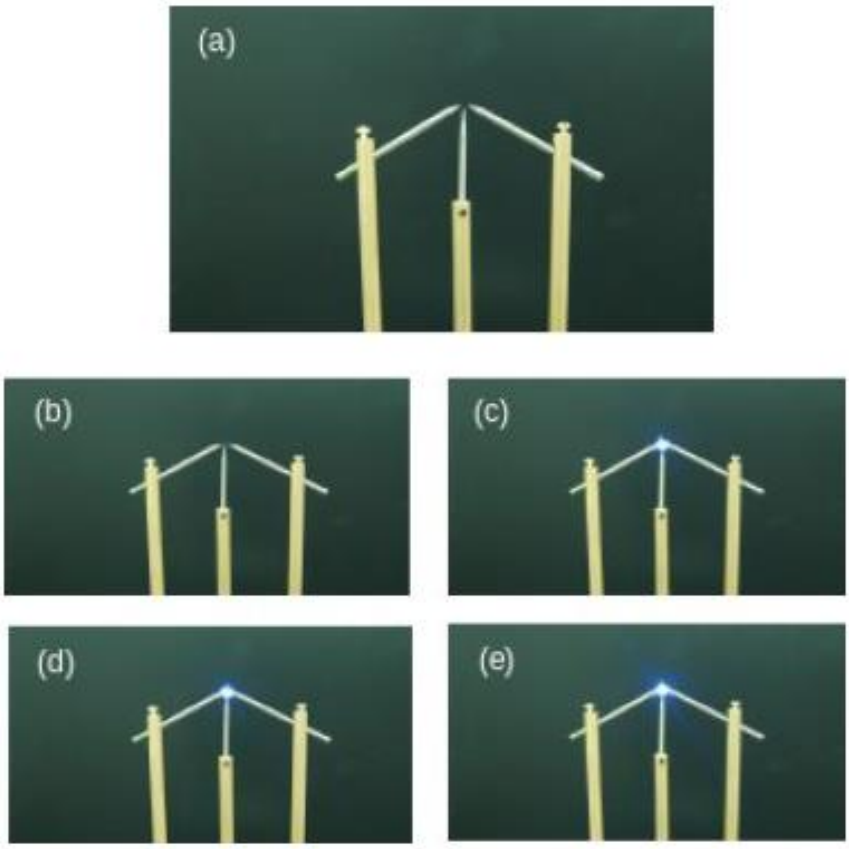

Figure 2: The sound source: (a) – three spark discharger electrodes on bronze supports are shown, the central smaller trigger electrode is between two main electrodes; (b) – a small trigger spark between trigger (central) and two main electrodes; (c) the main single spark between two main electrodes; (d) – two and (e) – four sparks at one exposure. Good spark repeatability is obvious. In this example the electrode gap is 0.3 cm and a high voltage 3 kV is used.

tripod. The gap between main electrodes (0.0-1.0 cm), as well as the position of trigger electrode, can be adjusted.

The sparks were generated by first applying a high voltage (3-5 kV depending on the gap) between the two main electrodes. This voltage was produced by a variable six stage Cockcroft-Walton voltage multiplier circuit and was kept lower than the breakdown voltage of the gap. After that, a short impulse of smaller voltage (1-2 kV depending on the trigger electrode position) was applied to the third trigger electrode placed between two main electrodes to provide an initial ionization of the air necessary to cause the spark breakdown and subsequent discharge of the capacitors in the voltage multiplier. After the spark was discharged, the capacitors were recharged and after a short time the next spark was able to be generated. Voltage measurements were made with a high-voltage probe (1000:1) placed on the high-voltage electrodes and showed high stability ($\pm 0.03\%$ variability) with time (see appendix B for further details).

The most important sound source characteristics are: (i) repeatability of sound wave duration and intensity, and (ii) approximate omnidirectionality at the very least. These properties were confirmed for our spark discharger by our measurements. Test measurements were made for two microphone orientations - normal to the sound wave front and at grazing angle. Comparison showed that although the microphone sensitivity is higher in the normal position, its transitional characteristics and omnidirectionality are improved when in the grazing position. This is in agreement with available data and is related to the specific construction of condenser microphones. In addition, the microphone safety grid generates a diffracted signal that contaminates the measured signal in the normal microphone position. Taking this into account, the grazing position was chosen as the primary microphone position in all measurements.

Typical traces of the recorded pressure $P(t)$ (measured in Pascals) as a function of

time, t, for the grazing microphone position are given in Fig. 3(a). These data were obtained with an interval between traces of about 1 min in the absence of a barrier (the free, F, signal) at a distance of 90 cm between the microphone and sound source. All seven signals recorded practically collapse onto a single curve and thus very good short-time stability and trigger synchronization are observed. The long-time stability was also satisfactory. After hundreds of sparks the signals remain practically indistinguishable from the data shown in Fig. 3 and no electrode cleaning was necessary.

The data for free signal shown in Fig. 3(a) gives an estimate of $T = 60\mu$s for the typical signal duration and thus the dominant frequency is determined as $f_0 = 1/T \approx 17$kHz. At normal atmospheric conditions this gives an estimate of $L = 2$cm for the typical wave length, which may be used as a characteristic length scale,*e.g.*, for the lateral variations in the jagged barrier top profiles (see below). The distance between the main electrodes (0.3 cm) is much less than L and so the sound source can be regarded as a point source at the typical distances of about 60-90 cm which were used between the microphone and sound source in our experiments. The azimuthal distribution of the sound intensity for the grazing microphone position is shown in Fig. 3(b) and the distribution appears to be approximately omnidirectional.

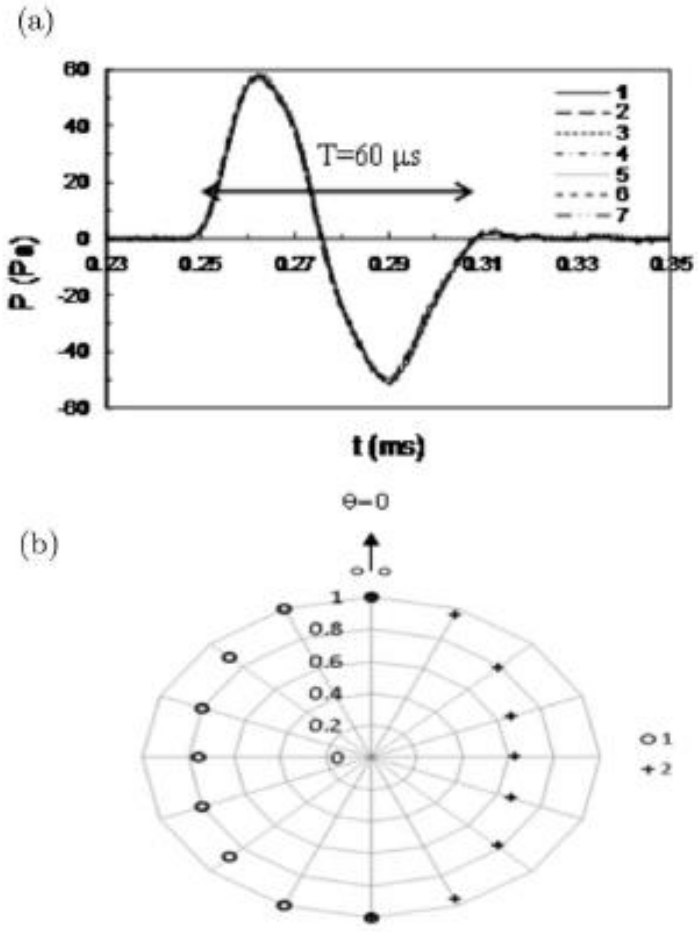

Figure 3: (a) the sound pressure, $P(t)$, in the absence of barrier (free, F, signal) as a function of time, t, for grazing microphone position at a distance of 90 cm between the microphone and sound source. Seven records are shown (see legend). In this example, the electrode gap is 0.3 cm and the high voltage is 3 kV. The typical signal duration is $T = 60\mu s$. (b) normalized azimuthal distributions of the maximum positive (1) and negative (2) sound pressure for the grazing microphone position. Direction $\theta = 0$ is shown by the arrow, and main electrodes are shown by two small circles near the arrow.

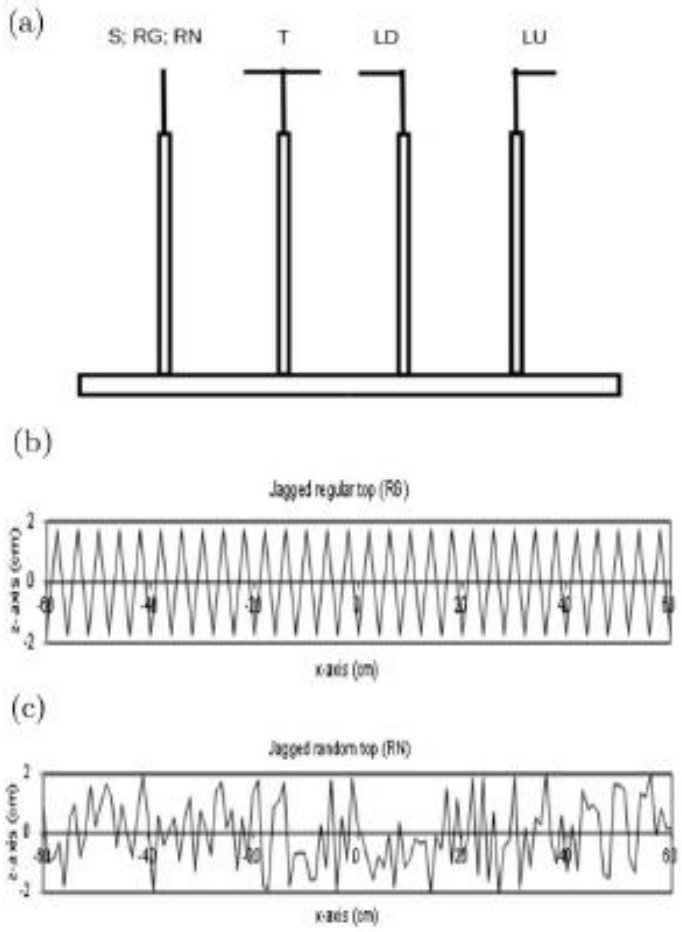

Figure 4: (a) The barrier top geometries used in the experiments: thin vertical screen (S), jagged regular (RG), jagged random (RN), T-shape (T), L-shape extending away from the sound source (LD), L-shape extending towards sound source (LU). The source is located to the right of the barrier and the microphone is to the left; (b) the jagged regular barrier top lateral profile (RG); (c) the jagged random (RN) barrier top lateral profile. All other geometries (S), (T), (LD) and (LU) simply coincide with the line $z = 0$.

C. Measurements procedure

In experiments, the large solid wooden table (5cm × 150cm × 450cm) served as the ground. A vertical barrier was fixed rigidly to the table and various removable aluminum tops, all of which could be moved accurately along the barrier, were attached to the barrier. Six different tops were used in this study as shown in Fig. 4: a thin vertical screen with a straight top (S), jagged regular (RG), jagged random (RN), T-shape (T), L-shape down (LD) extending away from the source, and L-shape up (LU) extending towards the source. All tops were made from aluminum and were considered to be acoustically rigid and non-absorbing.

For the jagged regular geometry (RG) a system of identical triangles with equal horizontal, Δx, and vertical, Δz, spacing was used; the jagged random geometry (RN), on the other hand, had a piecewise profile with fixed horizontal spacing, Δx, but with a randomly generated vertical spacing of mean value Δz. These geometries are shown in Fig. 4(b) and 4(c) respectively. The choice of spacing, 2 cm, was dictated by the characteristic wave length of the sound source. For L-shape and T-shape profiles, one or two aluminum 5×5 cm L-shape corners were attached to the vertical aluminum plate. Hence, the T-shape top had a 10 cm long horizontal section and each L-shape top had a 5cm long horizontal section. The mean vertical top position (set at $z = 0$) was identical for all top profiles.

The microphone and sound source positions relative to the barrier are shown in Fig. 5. In experiments the distance R from the barrier top (30 or 45 cm) was fixed, but angles, θ_S and θ_M, were varied. For the microphone four different angles were used, $\theta_M = 0°$, 15°, 30°, 45°, and two different angles were used for the sound source, $\theta_S = 15°$, 30°. Thus, for each of the six top geometries (S, T, LU, LD, RG, RN) shown in Fig. 4 and for one set with the free (F) signal (no barrier), eight sets of experiments with different θ_S and θ_M values were conducted at two values of distance R; thus, in total, $7 \times 8 \times 2 = 112$

experiments were performed. All measurements were made with the vertical plane passing through both the microphone and sound source lying normal to the barrier. For convenience, the notation S−−M−−R−− is used below for the various source-microphone positions. For example, S15M00R30, means that $\theta_S = 15°$, $\theta_M = 0°$ and $R = 30$cm.

In experiments where the top geometry did not vary along the barrier (homogeneous tops), three measurements at each microphone-source position were made and averaged data were used for processing. In experiments using RG and RN, where the top geometry varied along the barrier, a set of measurements performed at different barrier locations was conducted by sliding the aluminium top along the upper part of the wooden barrier between recordings. A fine ruler permitted us to measure accurately the change in barrier position x between recordings as shown in Fig. 4(b) and 4(c). Overall for RG and RN, seventeen measurements were made at $x = 0, \pm 0.5, \pm 1.0, \ldots \pm 4.0$ cm for each top.

The experiments were conducted as follows. The microphone and sound source were fixed at a selected position as in Fig. 5. Firstly, the free (F) direct signal (with no barrier) was measured three times to check repeatability. After that, the barrier was installed with the microphone and sound source remaining in the same positions, although the microphone was slightly corrected to the new grazing angle relative to the barrier top. Then, different removable aluminum tops were attached to the barrier: thin vertical screen (S), T-shape (T), L-shape up (LU), L-shape down (LD), jagged regular (RG) and then jagged random (RN) tops were used in succession and the data on the diffracted signals were obtained.

As schematically shown in Fig. 1, the free signal or diffracted signal from the barrier top arrives at the microphone with preamplifier and goes to the conditioning amplifier with variable amplification and frequency window 0.1–10^5 Hz. The typical signal amplitude is of the order of 3–6 V. This signal is displayed on the 100 MHz digital storage oscilloscope

screen and digitized at a selected frequency. In all measurements this frequency was set to $f_S = 2$ MHz, which enabled 4000 data points to be stored with the time interval $\Delta t = 0.5\mu$s. To omit the secondary diffracted/reflected signals that arrive at later times ($t > 1.5$ms) reflected from the barrier sides, ground and room ceiling/walls, only the first $N_0 = 3000$ data points were used.

A series of sixteen experiments with different sound source-microphone positions (see Fig. 5) were conducted. For each position the following set of 7 experiments was made: (i) - free signal (F) was measured 3 times; (ii) - diffracted signal from homogeneous tops (S, T, LU, LD) was measured 3 times, (iii) - diffracted signal from jagged tops (RG, RN) was measured 17 times at different x-positions, as explained above. After visual analysis, the digital data from the oscilloscope memory were transported to the computer with LabVIEW software and stored in separate files.

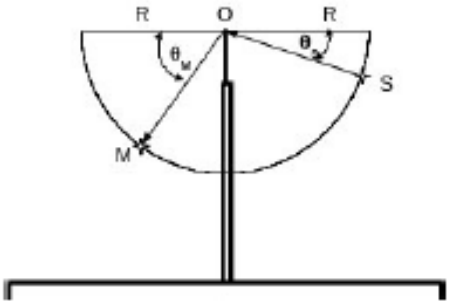

Figure 5: Schematic showing microphone, M, sound source, S, and angles, θ_M and θ_S, relative to the horizontal line passing through the origin, O, which coincides with the top of the barrier. The microphone and the sound source are at the same distance, $R = 30$ or 45 cm, from the origin and the angles used are: $\theta_S = 15°, 30°$, $\theta_M = 0°, 15°, 30°, 45°$.

D. Post-processing procedure

After each experiment, the measured sound pressure signals stored by the LabVIEW software were post processed using custom-built MATLAB software (see Appendix A). Methods of spectral analysis were used in the data processing. First, the pressure frequency spectra were calculated from the initial sound pressure data. After that, additional functions were used to calculate insertion losses for different tops as functions of the frequency and of the source and microphone positions. Using the insertion loss functions, the results were rescaled to spatial dimensions comparable to a full-size noise barrier and frequencies were rescaled to values typical for traffic noise sources. Single number ratings of the traffic barrier performance were then calculated and directivity diagrams obtained.

Two different methods were used to calculate the frequency spectra, namely, a standard fast Fourier transform (FFT) and a 1/3rd octave filter. In the FFT method, to improve the resolution, the spectral window width was reduced by using standard zero padding and thus an additional 17000 points were added to the original $N_0 = 3000$ data points; thus, in total, $N_T = 20000$ points were used in the FFT calculations. For the spectral window width this yields the estimate $\Delta f = f_S/N_T = 100$Hz, which remains constant across the entire frequency band. Calculations were made only in the frequency range 600–50000 Hz which are the scaled frequencies relevant for traffic noise. In the 1/3rd octave filter method we used a spectral filter developed by Couvreur[24], which was modified to cover a higher frequency band (up to 80 kHz). Calculations of insertion losses were made with standard central frequencies in the range 630–50000 Hz and the window width increasing with frequency. Note that the calculation here is not the same as averaging the FFT calculations over 1/3rd octave windows. Instead, a completely different direct filter method was used and the results obtained by standard FFT with a constant window width and the 1/3 Octave filter are compared below.

In the FFT method, first, the complex frequency spectrum of the sound pressure is calculated and the spectral density amplitude $S(f)$ is then determined by the magnitude of this frequency spectrum, where $f = 600, 700, 800, \ldots, 50000$ Hz. In the 1/3rd octave filter method the spectral density amplitude $S(f)$ is calculated directly at the standard 1/3rd octave central frequencies $f = 630, 800, 1000, \ldots, 50000$ Hz.

Using the spectral density amplitudes, the values of the insertion loss functions may be calculated as

$$IL(f) = 10 \log_{10} |S_0(f)/S(f)|, \tag{1}$$

where S_0 is the spectral density amplitude of the free (F) signal and $S(f)$ is the spectral density amplitude obtained when one of the barrier types is positioned between the source and microphone. Note that the definition of insertion loss gives the *relative* sound attenuations for different frequencies and these attenuations *do not* depend directly on the characteristics of the sound source used in the experiment. This permits the use of short sound pulses in testing barrier performance alone as mentioned in the introduction.

Because the sound pressure of the diffracted signal is a function of many parameters, the spectral density amplitude and insertion loss are also functions of those parameters. Thus,

$$IL = IL(f, R, \theta_S, \theta_M, A, x), \tag{2}$$

where R, θ_S, θ_M describe the source and microphone positions, A is the barrier top type (S,T,LD, LU, etc.) and x is the dependence on the lateral barrier position for the non-homogeneous tops RG and RN. In this way, insertion losses for the different barrier top geometries can be calculated and their performance compared.

Naturally, the main purpose of such scaled experiments is to measure the actual insertion loss functions for full size noise barriers. If the typical sound source frequency in the experiments is N times the frequency of the traffic noise (in our case $N = 10$, see

below), the experiments can be considered as a $1:N$ scaled experiments. The frequency of the laboratory measured insertion loss function is simply rescaled from the laboratory frequency f to the traffic noise frequency as $F = f/N$. Then, using the rescaled insertion loss function and proper estimates for the free traffic noise spectrum, the characteristics of the diffracted traffic noise behind a barrier with a rescaled length scale can be estimated. In particular, a single number rating for the traffic barrier performance can be estimated and the directivity diagrams obtained for different barrier tops.

III. Diffraction theory

The insertion loss function for the simplest case of the thin vertical screen straight top barrier can be parameterized in terms of the Fresnel number, $\mathcal{F}_N$. This number is the most important dimensionless parameter affecting the diffracted signal in the considered geometry (Fig. 5) and can be defined for our case as

$$\mathcal{F}_N = \frac{4Rf}{C}\left(1 - \sqrt{\frac{1+\cos(\theta_M+\theta_S)}{2}}\right)\cos\left(\frac{\theta_M-\theta_S}{2}\right) \tag{3}$$

where C is the ambient speed of sound. Based on the experiments reported by Maekawa[25], the following empirical parameterization for the insertion loss (in dB) of vertical thin screens is proposed[26;27]:

$$\mathrm{IL} = a_0 + 20\log_{10}\frac{\sqrt{2\pi\mathcal{F}_N}}{\tanh\sqrt{2\pi\mathcal{F}_N}}, \tag{4}$$

where a_0 is an empirical constant. Maekawa's estimate (4) for a thin vertical screen is shown as a dotted line in some plots of insertion loss presented in Section V.

A more accurate validation of the experimental results obtained in the laboratory is to compare the measured insertion losses obtained for each 1/3rd octave frequency band to those obtained using the so-called geometrical theory of diffraction. The analytical solution adopted for this purpose is that of wave diffraction by a wedge[28;29]. We adopt the input

parameters as shown in Fig. 5. Unlike other insertion loss calculations for noise barriers[30;31], here we only take into consideration the primary signal from the shortest ray of distance $2R$. The contributions of all other possible rays that are reflected at least once off the ground or off some other object are ignored. This assumption is valid given the shortness of the incident pulse as discussed in the previous section. For a point source of frequency f in a non- refracting atmosphere of constant sound speed C, the pressure field measured at the microphone situated behind a thin vertical screen is

$$p_{\text{mic}} = \frac{\mathrm{e}^{+\mathrm{i}\pi/4}}{\sqrt{2}} \left[A_D\left(\sqrt{\frac{2kR}{\pi}}\cos\left(\frac{\theta_S - \theta_M}{2}\right)\right) + A_D\left(\sqrt{\frac{2kR}{\pi}}\sin\left(\frac{\theta_S + \theta_M}{2}\right)\right)\right] \frac{\mathrm{e}^{+\mathrm{i}k2R}}{2R}, \quad (5)$$

where $k = 2\pi f/C$ and the function $A_D(X)$ governing the diffraction behaviour[28] can be written as the integral

$$A_D(X) = \frac{1}{\sqrt{2}\pi} \int_{-\infty}^{+\infty} \frac{\mathrm{e}^{-u^2}\,\mathrm{d}u}{\left[X\sqrt{\pi/2} - \mathrm{e}^{-\mathrm{i}\pi/4}\,u\right]}. \quad (6)$$

For calculation purposes, it is more convenient to express $A_D(X)$ in terms of the auxiliary Fresnel functions, $f(X)$ and $g(X)$ (Abramowitz and Stegun 1964, p300, eqns 7.3.5 and 7.3.6), as follows:

$$A_D(X) = \mathrm{sgn}(X)\left[f(|X|) - \mathrm{i}g(|X|)\right], \quad (7)$$

Plots and asymptotes of the functions $f(X)$ and $g(X)$ can be found in Pierce[28], which demonstrate their most important properties that $f(0) = g(0) = 1/2$, $f'(X)$, $g'(X) < 0$ for $X > 0$ and $f(X) \sim (\pi X)^{-1}$ and $g(X) \sim \pi^{-2}X^{-3}$ for large X; practically, these asymptotes are accurate so long as X is larger than 2. The theoretically obtained insertion loss for our thin vertical screen straight top (S) can now be derived analytically as

$$\mathrm{IL}_{\text{th}}(\theta_S, \theta_M, f, R, C) = -20\log_{10}\left|\frac{\sqrt{1+\cos(\theta_S+\theta_M)}}{2}\left[A_D\left(\sqrt{\frac{4fR}{C}}\cos\left(\frac{\theta_S-\theta_M}{2}\right)\right)+A_D\left(\sqrt{\frac{4fR}{C}}\sin\left(\frac{\theta_S+\theta_M}{2}\right)\right)\right]\right|. \quad (8)$$

We note here that the important response of insertion loss to distance R, sound speed C and frequency f only appears as the product fR/C, confirming the ability of our scaled lab experiments to reproduce the effect of a full size non-absorbing barrier. The consequence also highlights the fact that increasing the distance of the microphone and point source from the top of the barrier by some factor achieves an equivalent increase in insertion loss that would occur by increasing the frequency of the point source by the same factor.

The same analytical theory can also be applied to the other homogeneous tops (T, LD and LU) by adopting the theory of double-edge diffraction over multiple wedges and, in this paper, the theoretical insertion loss for the T-top is calculated using Eqs. (20) to (25) of Pierce[28] where β_S and β_L are set to 2π for the T-top. These theoretical insertion loss functions are compared directly in Section V. to the results obtained from our laboratory experiments.

IV. Results of selected experiments and general sound characteristics

In this section we consider some results from the laboratory measurements. Initially, we present the results obtained in a set of experiments conducted with the geometry S30M00R30 (see Fig. 5). Typical free and diffracted sound pressure signals as well as their spectra and insertion loss functions are presented. We consider first experimental data for the homogeneous barrier tops (S, T, UL, UD) and compare them to the case of the free signal (F). After that similar data for the heterogeneous jagged tops (RG, RN) are considered. In both cases the results obtained by using both Fourier analysis and a 1/3rd Octave filter are presented and compared.

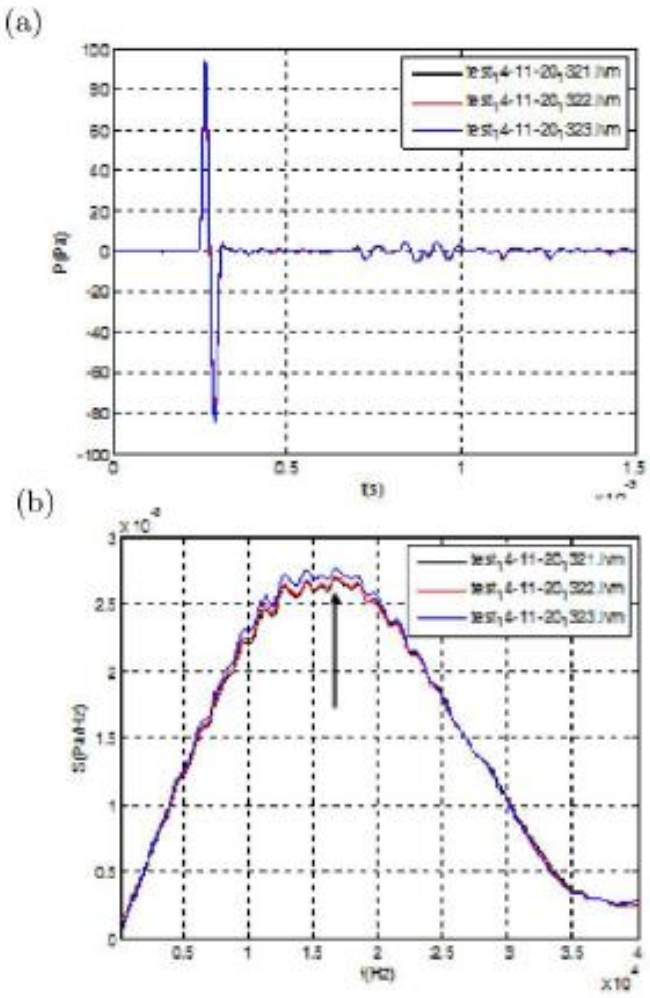

Figure 6: (a) A succession of three recordings of the sound pressure signal, $P(t)$, as a function of time, t, for three free (F) signals (see the legend) in the S30M00R30 configuration. All three signals practically coincide, and resemble the so called N-wave with a weak tail. (b) spectral density amplitude, $S(f)$, as a function of frequency, f, for the three free (F) signals. As can be seen, all three spectra also practically coincide. The arrow shows the dominant frequency, which was estimated from the data to be $f_0 = 17$kHz.

A. Free signal (F)

Three recordings of pressure, $P(t)$, measured at the microphone as a function of time, t, for three free (F) signals are shown in Fig. 6(a). All three signals practically coincide, and resemble the so-called N-wave with a weak tail; this is a profile that is typically used in acoustics to model explosions. The main signal excursion is about 80 Pa and its duration is about 60μs, suggesting an estimate of $f_0 = 17$kHz for the characteristic frequency. Three frequency spectra, calculated using a fast Fourier transform (FFT) on the three signals shown in Fig. 6(a), are shown in Fig. 6(b). The estimated characteristic frequency is shown here by the arrow and lies close to the frequency of the spectral maximum. The dominant frequencies of the signal are an order of magnitude higher than the dominant frequencies of typical traffic noise[10;32]. Thus, in our experiments the scaling factor[16] of 1:10 seems appropriate. The spectrum obtained from an average of the pressure recordings taken for the free (F) case is used below to calculate the barrier insertion losses as functions of frequency.

B. Homogeneous tops (S, T, LU, LD)

The spectral density of the mean diffracted signal for the barriers with homogeneous tops in the configuration S30M00R30 are shown in Fig. 7. For the thin vertical screen (S), the max amplitude of the recorded diffracted signal is about 15 Pa, which is approximately six times less than the free (F) signal measured with no barrier (Fig. 6). In addition, the spectral maximum amplitude for diffracted signal for the thin vertical screen (S) top is 4 kHz lower compared to the recorded free (F) signal. The spectrum of the mean diffracted signal for the T-shape (T) top is shown in Fig. 7(b). The signal is not only significantly reduced in amplitude compare to the thin vertical screen, but a noticeable secondary N-wave is present in the pressure recording. The secondary N-wave is shifted compare to the main one by approximately 0.25ms, which results in the characteristic harmonics of the

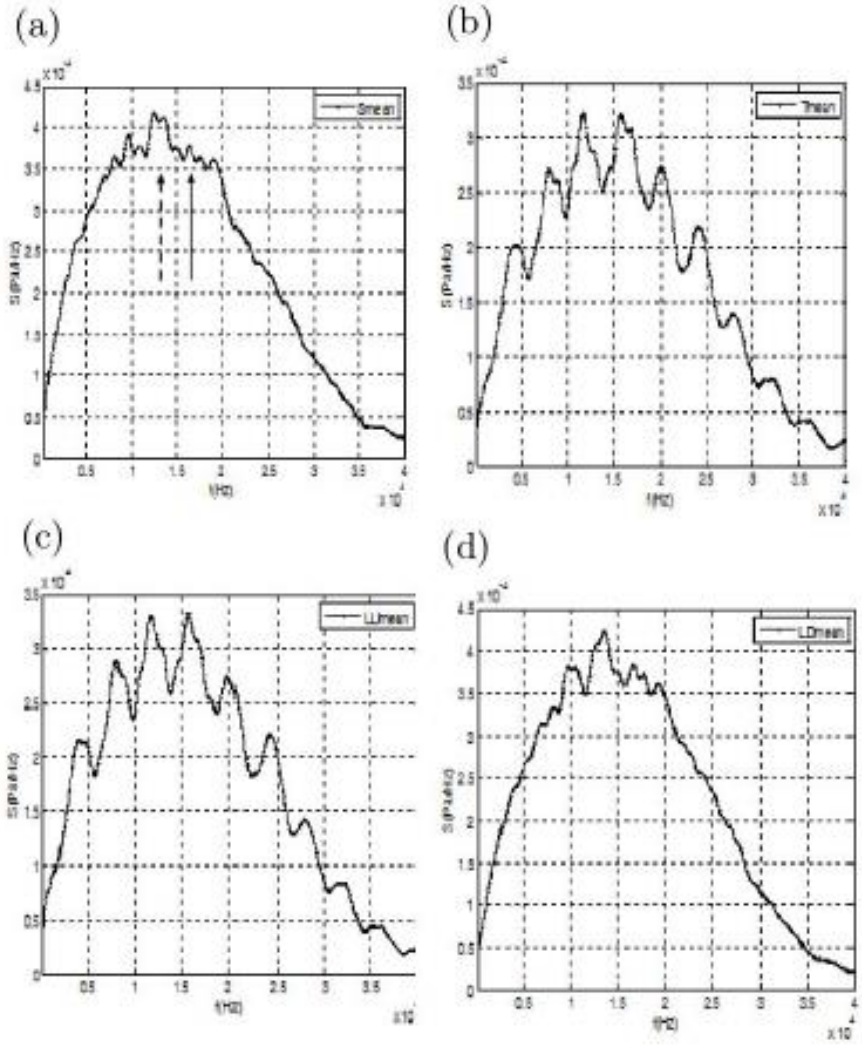

Figure 7: Spectrum density amplitudes for the mean diffracted pressure signal for the following homogeneous barrier tops: (a) thin vertical screen (S), (b) T-shaped top (T), (c) L-shaped (LU) top and (d) L-shaped (LD) top. The solid arrow shows the estimated characteristic frequency of the free signal and the dashed arrow shows the approximate position of the spectral maximum.

main frequency 1/(0.25 ms)=4 kHz that can be observed in the spectrum.

For further comparison, the spectra of the mean diffracted sound signals for the L-shape tops extending towards the source (LU) and away from the source (LD) are shown in Figs. 7(c) and (d) respectively. The spectrum for the LU top is qualitatively very similar to the spectrum shown in Fig. 7(b) for the T top. More detailed analysis shows that the LU top pressure data, for signal as well as for spectrum, are somewhat higher than similar data for the T top. On the other hand, the spectrum for the LD top is qualitatively very similar to that of the thin vertical screen (S) top in Fig. 7(a). These similarities are likely to be caused by the fact that, in the case shown, the microphone is located at the same height as the barrier top ($\theta_D = 0$) and so the main diffractive effect arises from the shape of the edge facing the source.

C. Heterogeneous tops (RG, RN)

In contrast to the diffracted signals from the homogeneous tops, the diffracted signals from the heterogeneous (jagged) tops depend strongly on the along-barrier position. As mentioned above, the diffracted signals from the heterogeneous tops, which include jagged regular (RG) and jagged random (RN) top geometries, were measured at 17 different lateral positions for each heterogeneous top. Strong amplitude and phase variability of signals (as well as the resulting spectra) is apparent from the pressure recordings $P(t)$ at each lateral position (not shown). These signals not only have different amplitudes of the leading N-waves, but positions of the following local extrema are also different. However, taking into account that the typical length scale of the barrier top variation is relatively small, in practice, compared to the distance from the barrier top to the source and microphone, the exact sound characteristics at specific locations relative to the along-top coordinate are not very important. Of more practical interest is the averaged, over this relatively small length scale, sound characteristics. As the averaging of all recorded

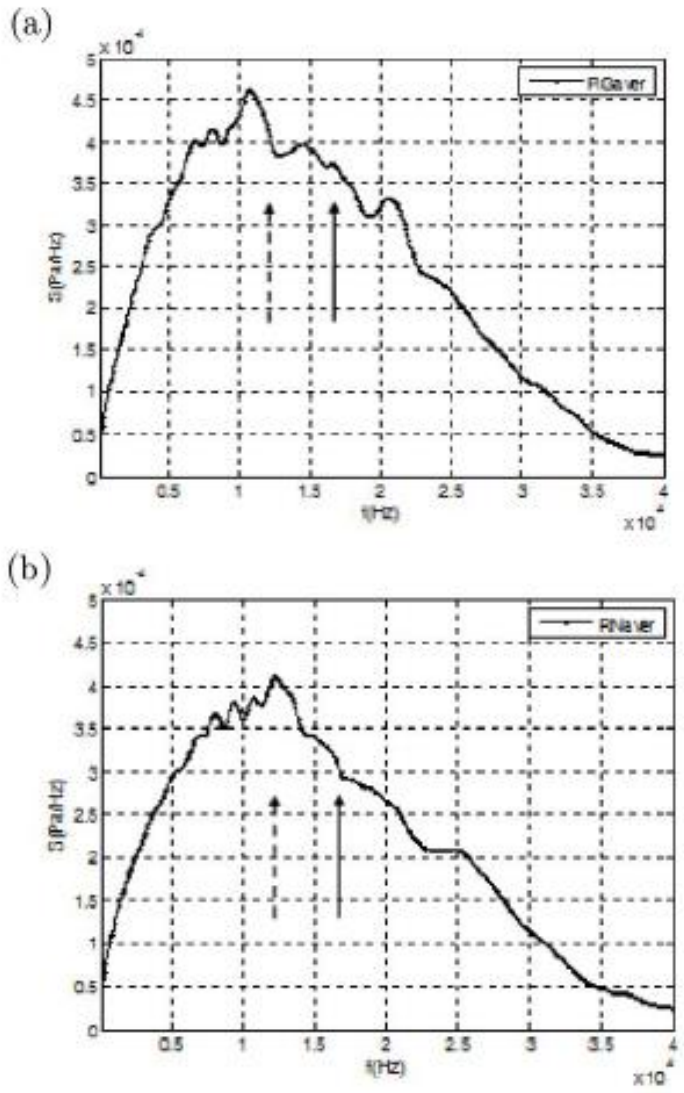

Figure 8: Spectrum density amplitudes for the mean diffracted pressure signal for (a) the RG jagged regular barrier top and (b) the RN jagged random barrier top. The mean is based on 17 measurements at different lateral positions as described in the text. The solid arrow shows the estimated characteristic frequency of the free (F) signal and the dash arrow shows the approximate position of the spectral maximum in each case.

pressure signals masks the individual frequency content and spectrum, instead, for each pressure signal the corresponding spectrum was calculated and an average of the 17 spectra was calculated for RG and RN barrier tops. These average spectra are shown in Fig. 8. In both cases, RG and RN, the approximate spectral maximum amplitude is approximately 12 kHz lower than the estimated characteristic frequency f_0 of the free (F) signal. From the preliminary analysis above, the following hierarchy of the increasing barrier top efficiency may be expected: S, LD, LU, T for homogeneous tops and RG, RN for jagged tops. More accurate estimates are given below.

V. Barrier efficiency

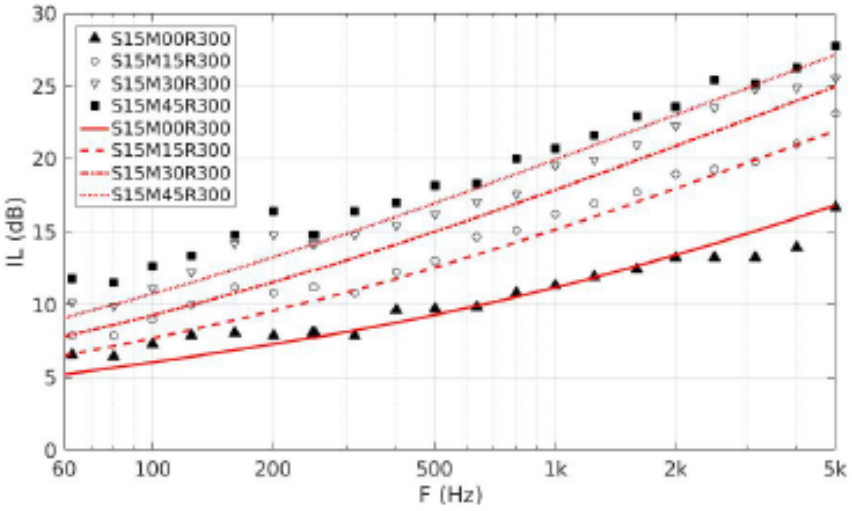

Figure 9: Symbols - Insertion losses calculated from 1/3rd-octave lab experimental data for a thin vertical barrier with a straight top (S) for four cases with different microphone positions. Red Lines - Insertion losses calculated from the analytical expression (8) using geometrical theory of diffraction.

A. Insertion loss functions for different tops

Using the spectral density amplitudes, obtained for the free and for the diffracted signals, insertion losses were calculated using (1) and typical insertion losses as functions of frequency for different top geometries are discussed briefly below. To validate our laboratory results, a plot of the insertion losses calculated from laboratory measurements for the S type barrier top lab versus the analytical expression given in (8) is shown in Fig. 9; the agreement is very good.

As a further example of the data obtained, insertion loss, IL, as a function of laboratory frequency, f, for all the laterally homogeneous barriers (S,T,LU and LD) relative to the free signal (F) for the configuration S30M00R30 is shown in Fig. 10. The results obtained from FFT calculations are shown in the top graph whereas the results of the 1/3rd octave filter calculations are shown on the bottom graph. Some variability in the FFT data at high frequencies is related to the constant spectral window width, 100Hz, which becomes small at high frequencies and the resulting 'noise' is noticeable. In the 1/3rd octave filter calculations the window width is proportional to the central filter frequency and increases with the frequency and, thus, there is no such *noise*. Despite this, both FFT and 1/3rd octave filter calculations remain satisfactorily in agreement with important details including numerous local maximums and minimums lying within ±2 dB at similar frequencies.

To compare with theory, the thick dotted line in Fig. 10 shows Maekawa's estimate (4) and the two thin solid lines in the same figure show the predictions from the geometrical theory of diffraction for a thin vertical screen and a T-top shaped barrier. As observed in Fig. 9, the agreement of both FFT and 1/3rd octave filter calculations for the thin screen S-type barrier with the geometrical theory of diffraction prediction $\mathrm{IL_{th}}$ given by (8) is excellent, especially in the range $f = 5$–25 kHz that represents the most crucial

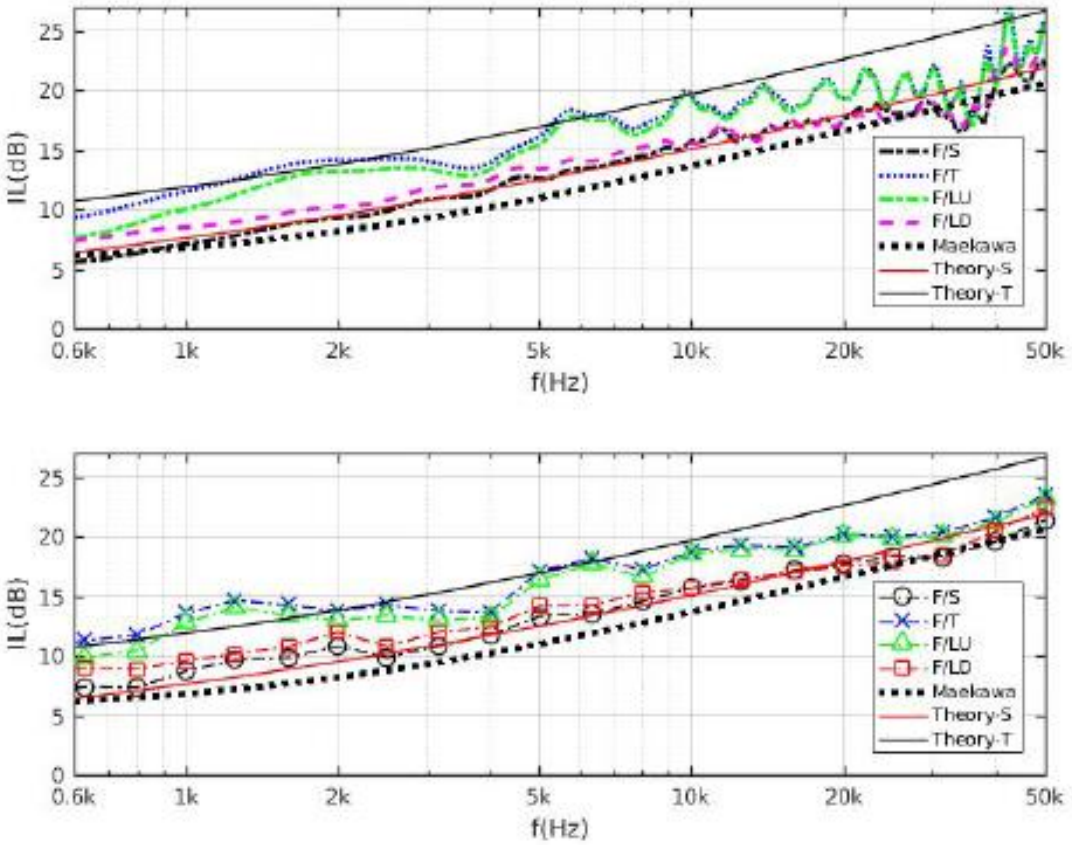

Figure 10: Insertion loss, IL, as a function of laboratory frequency f for the laterally homogeneous barriers including a thin screen (S), a T-shaped top (T) and L-shaped tops (LU and LD) relative to the free signal (F). Top - results from FFT computations. Bottom - 1/3rd octave filter calculations. The predictions from Maekawa's IL estimate for a thin screen and geometrical theory of diffraction results for a thin screen and T-top are also shown.

range of full size frequencies for traffic noise (500Hz to 2.5kHz). We note that Maekawa's estimate, while qualitatively similar, tends to underpredict the insertion losses measured in the lab by 1-2dB. For the T-top barrier, the comparison between geometrical theory of diffraction and experiments is reasonably good, but not as good as the agreement for the thin vertical screen. Both the FFT and 1/3rd octave spectra for the T-top barrier appear to undulate by roughly ±2dB above and below the theoretical line with the theoretical model tending to overestimate the insertion loss at the higher end of the spectrum.

A visual comparison of the insertion loss spectra for different barrier types in Fig. 10 and across the other tested configurations clearly indicate the T-top providing the best performance, closely followed by the LU-type barrier. The LD-type barrier performance aligns more closely with that of the thin vertical screen (S). The relative efficiency of these barrier types relative to a thin-screen S-type barrier in three different configurations is shown in Fig. 11. In all three configurations, the T-top clear has the highest efficiency followed by LU and then LD and S. Interestingly enough the LU only becomes comparable in performance to the T-top in the M00 case, where the microphone is at the same height as the barrier. The LU top's efficiency is reduced considerably for the two other cases where the microphone lies below the barrier top. For S30M00R30, geometrical theory of diffraction predicts an increase in insertion loss of 4-5dB at all the frequencies for the T-top relative to the thin screen (S) but the lab experiments suggest the performance improvement varies between +2 and +5dB across the chosen frequency range.

Typical data for the insertion loss functions for heterogeneous (RG, RN) tops relative to the thin vertical screen (S) for two particular source-microphone configurations are also shown in Fig. 11. These configurations, along with the other configurations, appear to show that the RG-top barrier does not appear to significantly improve barrier performance compared to the thin vertical screen. Some slight improvements, mainly within +1 dB but

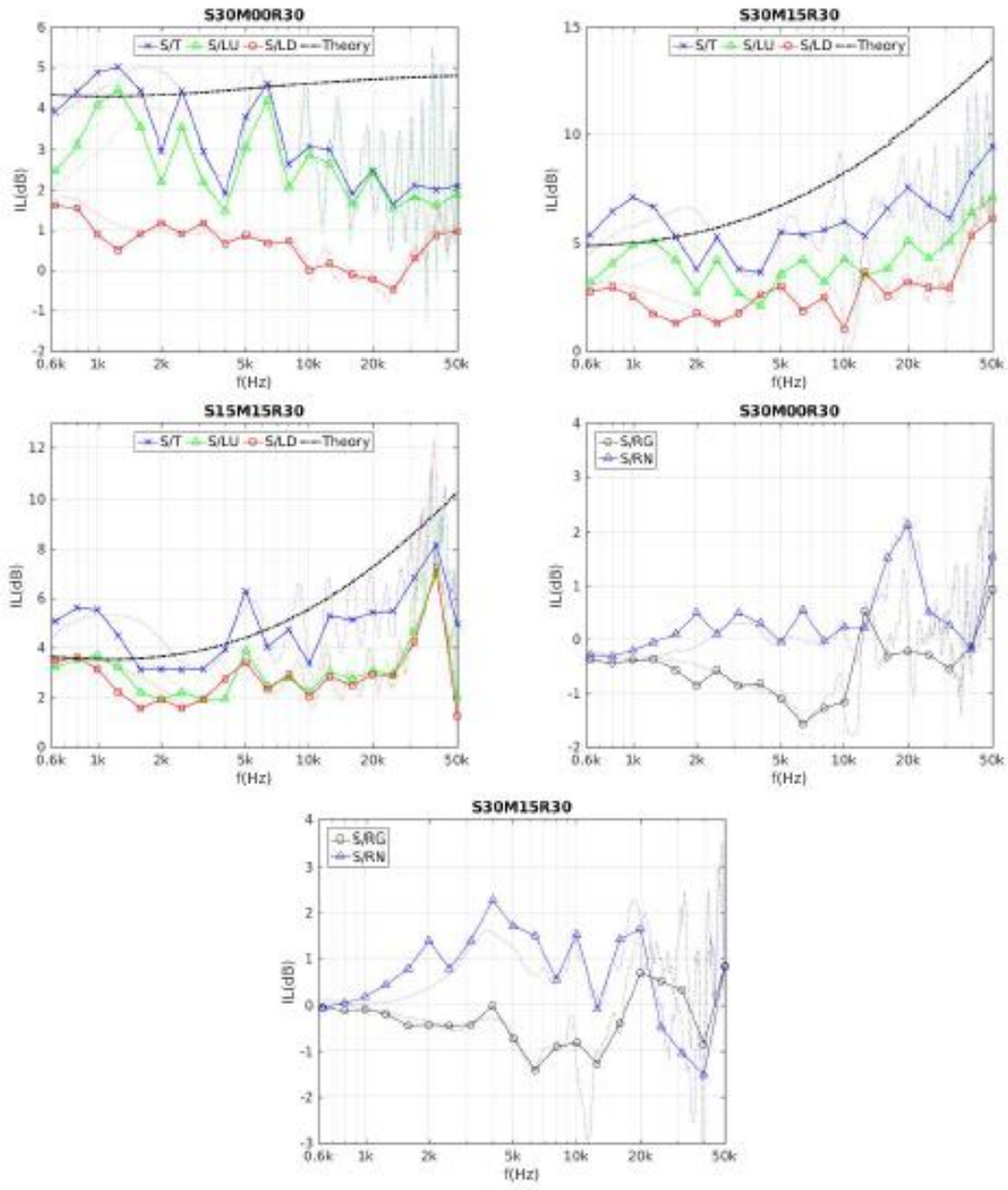

Figure 11: Insertion loss, IL, as a function of laboratory frequency f for the T-shaped top (T), the L-shaped tops (LU and LD) and the laterally heterogeneous tops (RG and RN) relative to the thin screen barrier (S) for different configurations of source and microphone positions. Faint lines show FFT results. Predictions from the geometrical theory of diffraction for the relative insertion loss of a T-top barrier relative to a thin screen are also shown.

up to 2dB for some higher frequencies, are observed for the RN top but its performance remains far below that achieved by the T-top barrier.

For all sixteen source and microphone configurations considered, similar results were obtained (see Table 1 below). A qualitative analysis, similar to that used above, suggests that the agreement between FFT and 1/3 Octave filter calculations remains satisfactory in all configurations and that the most effective barrier type tested appears to be the homogeneous T-top barrier. Furthermore, both laterally heterogeneous jagged barriers appear less effective than the T-top, with the RN-top performing somewhat better than the RG-top. To arrive at a more quantitatively definitative conclusion on barrier efficiency from the insertion loss spectra alone, however, is problematic because, in general, the insertion loss functions (2) depend on too many external parameters: in particular on the lateral position x and the frequency f. There is already an averaging of the diffracted spectra over the lateral x-axis for jagged tops, thus excluding x from the external parameters. However, a further reduction of parameters is needed. The use of a form of weighted-frequency averaging allows us to additionally exclude the frequency f from the external parameters and characterize the barrier efficiency by a so-called single number insertion loss rating. A derivation of this single number insertion loss rating is discussed below in the next section.

B. Single number insertion loss rating

The single number insertion loss $\mathcal{N}$ for a traffic barrier can be estimated as follows. The insertion loss spectrum, $IL(f)$, as measured in the scaled $(1:10)$ laboratory experiments, is rescaled from the laboratory frequencies, f, to the field frequencies, $F = f/10$, as $IL(F) = IL(f/10)$. A suitable empirical or analytical profile for a typical A-weighted traffic noise spectrum $S(F)$ is then adopted. In the estimates provided below we use the internationally standardised traffic noise spectrum given by European standard EN 1793-3[32;33]. A single number insertion loss rating, $\mathcal{N}$, (or barrier efficiency) in decibels for

each barrier type can be calculated as follows[33]:

$$\mathcal{N} = 10\log_{10}\frac{\sum_{i=n}^{m} 10^{S(F_i)/10}}{\sum_{i=n}^{m} 10^{S(F_i)/10 - IL(F_i)/10}}, \tag{9}$$

where n and m are the lowest and higher indices taken for the 1/3rd octave band central frequencies, F_i, that are of practical significance (for EN1793-3 the applied range is 100Hz to 5kHz).

After employing this procedure, as well as the above-mentioned averaging over the lateral x-axis, the number of parameters in (2) can be reduced from six to four $IL(F, R, \theta_S, \theta_M, A, x) \rightarrow \mathcal{N}(R, \theta_S, \theta_M, A)$, and the data on $\mathcal{N}$, obtained from the results of all 112 experiments, are presented below. Recall that for field estimates, the lab frequencies f must be divided by ten and any lengths, *e.g.* R, should be multiplied by ten. To further confirm the robustness of the procedure, single-number insertion loss ratings were also calculated using a second traffic-noise spectrum standard from the Acoustical Society of Japan[10] and broadly similar $\mathcal{N}$ values and trends were obtained in this case.

VI. Directivity diagrams for single number insertion loss ratings

The values obtained for $\mathcal{N}$ from our experiments are summarized in Tables I and II. Table I shows the single number insertion loss ratings for all barrier types (S, T, LD, LU, RG, RN) relative to the free (F) signal for all selected configurations of source and microphone position. Table II then shows the single number insertion loss ratings for the homogeneous barrier types T, LD and LU relative to both the free (F) signal and the thin vertical screen (S). Recall, that the notation $\mathbf{S}\theta_S\mathbf{M}\theta_M$ is used. Also, note that the relative values for $\mathcal{N}$, given in Table II, are not simply the differences of $\mathcal{N}$ values from Table I, but the result of separate calculations using different relative insertion losses in (9). The results are discussed below.

Table I: Single number insertion loss ratings, $\mathcal{N}$, relative to the free signal (F) as estimated for various barrier top in different source-microphone positions.

Config	F/S	F/RG	F/RN	F/T	F/LU	F/LD
R=300cm						
S15 M00	10.8	9.8	10.7	12.9	12.5	10.9
S15 M15	14.8	14.1	15.2	19.0	17.4	17.2
S15 M30	17.9	16.9	18.2	22.7	21.9	21.8
S15 M45	19.4	19.2	20.4	25.9	23.1	24.0
S30 M00	14.2	13.4	14.6	17.4	16.9	14.8
S30 M15	17.1	16.5	18.1	22.4	20.7	19.2
S30 M30	19.7	19.1	20.4	26.0	23.3	22.7
S30 M45	21.2	21.3	24.4	29.8	26.1	26.7
R=450cm						
S15 M00	12.0	11.2	12.1	13.5	13.2	12.4
S15 M15	15.9	15.1	16.3	19.5	17.9	17.6
S15 M30	19.1	19.1	19.7	24.4	21.8	22.4
S15 M45	20.6	20.8	21.5	27.1	23.5	25.1
S30 M00	15.7	14.7	16.1	17.8	17.8	15.8
S30 M15	18.6	18.6	19.4	23.4	22.1	21.0
S30 M30	21.0	21.2	21.5	26.4	24.9	24.5
S30 M45	22.5	23.4	25.1	31.7	28.4	28.6

Table II: Single number insertion loss ratings, $\mathcal{N}$, relative to either the free signal (F) or to the thin screen barrier (S) as estimated for homogeneous barrier tops T, LU and LD in different source-microphone positions. Two values of $\mathcal{N}$ are given in each cell corresponding to two different values of R: the first number is for $R = 300$cm, the second number is for $R = 450$cm.

Config	F/T	F/LU	F/LD	S/T	S/LU	S/LD
S15 M00	12.9-13.5	12.5-13.2	10.9-12.4	2.1-1.5	1.8-1.2	0.1-0.2
S15 M15	19.0-19.5	17.4-17.9	17.2-17.6	4.6-3.9	2.8-2.2	2.6-1.9
S15 M30	22.7-24.4	21.9-21.8	21.8-22.4	5.3-6.1	3.9-3.0	4.1-3.8
S15 M45	25.9-27.1	23.1-23.5	24.0-25.1	6.6-6.5	4.2-3.1	4.6-4.7
S30 M00	17.4-17.8	16.9-17.8	14.8-15.8	2.8-1.7	2.4-1.9	0.3-0.0
S30 M15	22.4-23.4	20.7-22.1	19.2-21.0	5.7-5.3	3.9-3.8	2.4-2.9
S30 M30	26.0-26.4	23.3-24.9	22.7-24.5	7.1-5.7	3.6-4.3	3.1-4.1
S30 M45	29.8-31.7	26.1-28.4	26.7-28.6	9.6-9.0	5.6-5.8	5.9-6.0

A. Jagged laterally heterogeneous tops - RG,RN

The data shown in Table I shows that the efficiency of RG and RN barrier types is not significantly different from that of the thin screen S-type barrier. The N values for the RG top, in average, are $0.5-1.0$ dB lower than the values for the S top (see the exact values of $\mathcal{N}$ in Table I). On the other hand, $\mathcal{N}$ values for the RN top appear, on average, to be no more than 1dB higher than the S top values. Thus, the use of RG and RN tops does not appear to improve significantly barrier performance. Only in the laboratory experiments with large angles, e.g. $(\theta S, \theta_M) = (30°, 45°)$, does the RN-top show a significant increase in $\mathcal{N}$, of the order $2-2.5$ dB, compared to the S-top.

This general conclusion does not agree well with the preliminary results reported by Ho *et al.*[34], that barriers with RN-tops are significantly more effective than the thin vertical screen S-type barriers. These particular authors conducted a few laboratory experiments on random-edge barriers and concluded that the more random the edges, the more attenuation it brings. However, the authors did not say anything about the strong sound pressure variability laterally along barrier direction (*i.e.* along the x-axis). This is an important factor, but it remains unclear at what x-values the signal and the reported insertion loss were measured in the their publication. In our approach, to smooth these variations, the along barrier averaging for the insertion loss spectra was used. Note also, that the results reported by Menounou and You[12;15] for jagged tops show only the decrease of the sound pressure peak amplitude level, compare to the S top, and its significant variation in the along barrier direction, but no data is supplied on insertion losses. The lack of sound level calculations in the above-mentioned studies has also been noted previously by Pigasse and Kragh[35].

Further analysis of the RG and RN data also shows that the single number insertion loss rating $\mathcal{N}$ in all experiments increases noticeably with the increase of the source or

microphone angles (about $2-5$ dB for each 15 degrees) and these effects are comparable in the magnitude. A much smaller increase ($1-2$ dB) is also observed with the increase of the distance from the barrier top, R, from 3m to 4.5m. This behavior mimicks the theoretical predictions of the insertion loss function for the S- top given by (4) and (8). For instance, the Fresnel number, $\mathcal{F}_N$, is proportional to the distance R defined in (5). With the increase of the source or microphone angle, as well as R, the value of $\mathcal{F}_N$ in (4) increases and this leads to the increase of the insertion loss function as well as the values of the insertion loss rating, $\mathcal{N}$.

B. Homogeneous tops - T, LU, LD

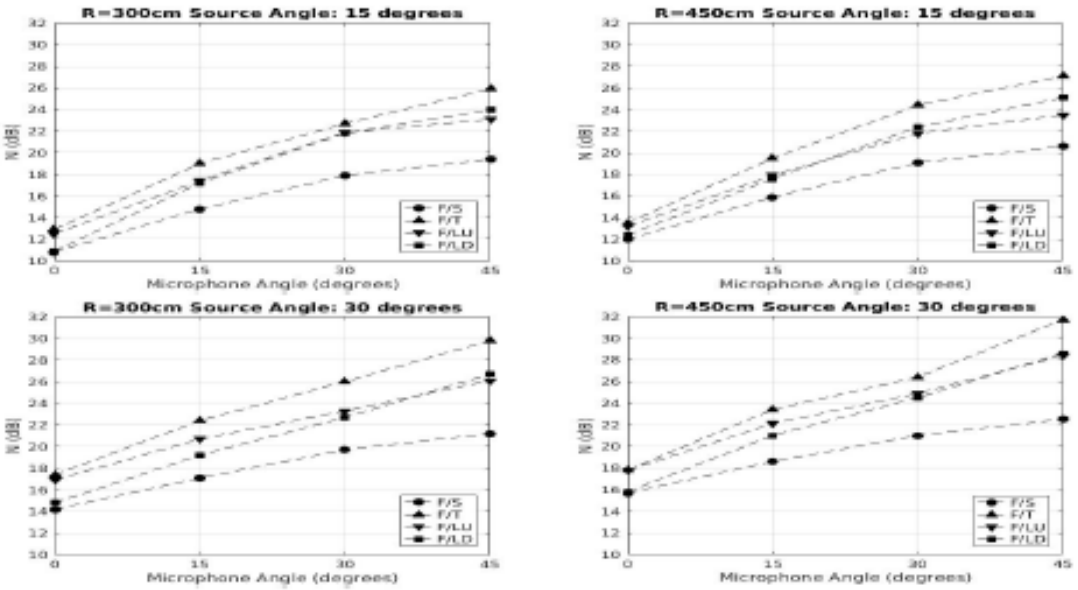

Figure 12: Directivity diagrams (relative to free F signal) for the single number insertion loss rating N as functions of microphone angle, θ_M, for different source angles θ_S and distances from barrier top R. Results for different barrier top geometries S, T, LU and LD are shown.

Directivity diagrams, relative to the free, F, signal, for the barrier top geometries S, T, LU and LD are shown in Fig. 12. The single number insertion loss rating $\mathcal{N}$ is given as a function of the microphone angle, θ_M, for different source angles, θ_S, and two different distances from the barrier top, R. As can be seen, in all experiments the efficiency of the T top is significantly better than the other tops. For example, the $\mathcal{N}$ values for the T top (triangles), at small microphone or source angles, in average, appear to be $2.0 - 2.5$ dB higher than the values for the S top (circles - see also Table I). This difference increases noticeably up to $7 - 9$ dB with the increase of the microphone or source angles and this is broadly in line with predictions from the geometrical theory of diffraction. At smaller angles, the LD top efficiency (squares) is similar to the S-top (circles), while the LU efficiency (inverted triangles) is markedly better than the LD efficiency by about $2 - 3$ dB making it comparable in performance to the T top (triangles) (see Fig. 12 and Table I). At increasing angles, the LU top (inverted triangles) and LD top (squares) efficiencies become more comparable to one another lying approximately $4 - 5$ dB above the S top insertion loss values (circles). However, for these configuration the efficiency of LU and LD tops lie roughly $3 - 4$ dB below the T-top insertion loss values (triangles).

Thus, in all experiments the T-top barrier shows better performance than the other barrier types (see Table I). How much better depends on the barrier top type, angles of measurements and, to a lesser degree, on the distance from the barrier top. As shown in Fig 12, the single number insertion loss rating, $\mathcal{N}$, relative to the free, F, signal, increases monotonically and significantly with increasing θ_M and θ_S. To estimate the effect of the increase in R, we show in Table II relative values, compared to the free F signal and to the S-top, of the single number insertion loss rating, $\mathcal{N}$. In each column two $\mathcal{N}$ values are shown for two different distances, R. As can be seen, the effect of the distance change on $\mathcal{N}$ is small (on average about 0.5-1.5 dB) and may be neglected compared to the effect of a

change in either θ_S or θ_M. This rather unexpected result is in line with the experiments of Okubo and Yamamoto[5]. Thus, to leading order, the effect of the distance change may be neglected and the number of parameters in (2) can be reduced to only three, *i.e* $\mathcal{N}(R, \theta_S, \theta_M, A) \rightarrow \mathcal{N}(\theta_S, \theta_M, A)$, to determine a general barrier top efficiency measure, $\mathcal{N}$.

VII. Conclusions

This research was motivated by the need to develop a methodology for parsimonious scaled acoustic laboratory experiments where the acoustic characteristics of the traffic noise diffracted above sound barriers with different tops may be estimated and compared. Short impulsive spherical sound waves with a broad frequency spectrum were used in experiments as a controllable sound source. A highly stable three-electrode spark discharger was designed and constructed for this purpose. Because the duration of the sound pulse is sufficiently short, the primary signal diffracts from the barrier top and arrives to the receiver earlier than any secondary signals (*e.g.* any signals reflected from surroundings). The latter signals are ignored and only the information from the primary signal is used. This eliminates the need to use expensive acoustic anechoic chambers for experiments. The typical frequency band of the sound source (1–30 kHz) is 10 times the frequency band of typical traffic noise (100–3000 Hz), and the experiments can be considered as 1 : 10 scaled experiments of real traffic sound barriers.

Numerous scaled experiments (112 in total) were conducted with different barrier tops and source-receiver positions. Homogeneous barrier tops that possess no variation of geometry laterally along the barrier, as well as heterogenous jagged tops that do were considered. The results of measurements were processed by using the spectral analyses of the free and diffracted signals. First, frequency spectra were calculated and then the insertion loss spectral functions were estimated for different source-receiver positions and barrier top geometries; these insertion loss functions were subsequently analyzed. Two

different methods were used to calculate frequency spectra, namely, Fourier transforms and a 1/3rd octave filter. Both methods demonstrate satisfactory agreement for all experiments but with an advantage of the 1/3rd octave filter being that its spectrum is less noisy. The experimental data was also validated against theory with very good agreement for a thin vertical screen when compared to a prediction using the geometrical theory of diffraction. However, when the same theoretical approach was applied to a T-top barrier the agreement was not quite good with variations of $1-2$dB between theory and experiments along with a distinct overprediction by the theory of the insertion loss at higher frequencies.

Taking into account the large number of the external parameters and to simplify the analyses, spatial and spectral averaging were applied to the data and the number of external parameters was reduced. The results obtained were rescaled to traffic barriers and, for a typical A-weighted traffic noise spectrum, weighted mean values of the traffic barrier efficiency (a single number rating) were estimated and compared. The main results of this study may be briefly formulated as follows.

A methodology has been developed which enables one to conduct, in a relatively short period of time, a large number of scaled experiments on sound diffraction from a traffic barrier top of arbitrary geometry. Detailed and accurate sound characteristics, *e.g.* spectra, insertion loss functions and single number insertion loss ratings, can be obtained easily. The considered jagged regular (RG) and random (RN) tops, in general, do not appear to improve significantly the barrier performance. Only in the experiments with large microphone-source angles does the RN top show any modest increase in the single number insertion loss rating $\mathcal{N}$ compare to a thin vertical screen. This result does not agree well with the previous preliminary results that such jagged tops are significantly more effective than thin vertical screens[12;15;34]. These authors, however, did not consider the spectrum variability laterally along the barrier. In our approach, this was taken into account and

lateral avaeraging of the insertion loss functions along the barrier was used resulting in relatively low differences in $\mathcal{N}$ values compared to a thin vertical screen. Some of the considered homogeneous tops (T, LU, LD) showed in general significantly better efficiency compare to the thin vertical screen. The best performing appears to be the T top, follow by LU and LD tops. In all cases, the single number insertion loss ratings, $\mathcal{N}$, increase monotonically and significantly (up to 20 dB) with an increase in the angles of sound source and microphone position. In comparison, the effect of the change in microphone and source distance from the barrier top, R, on $\mathcal{N}$ is relatively small (on average about $0.5 - 1.5$ dB) and may therefore be neglected when compared to the effect from a change in angle. This result is in line with previous experiments[5].

Finally, note that parameterizations and/or improved theoretical considerations, similar to (4) and (8) for the thin vertical screen, are obviously needed for other barrier tops. However, this requires conducting a larger number of experiments with differing top geometries. Using the methodology developed and presented here, we plan to work in this direction in the near future.

Acknowledgements

This research was supported by the Arizona Department of Transportation. We are most grateful to Senior Res. Eng. Scott Coppersmith for his assistance in the design and construction of the spark discharger. We are also grateful to Mr. Santiago Espinosa for his help in writing the package of MATLAB programs and last, but not least, to Mr. Patharapong Bhuripanyo for his immense help in data processing and analysis.

Appendix A. MATLAB programs

The pressures signals obtained from the memory of the digital oscilloscope (see Fig.1) were

stored as ".lvm" files using LabVIEW software. To process these data, a custom-built MATLAB software package was used. The program collects the sound pressure signals directly from the ".lvm" files generated by LabVIEW and, to process the initial data, some parameters from the user are required, e.g., oscilloscope sensitivity, time scale, amplification of the preamplifier. The code is used to convert the initial data from these files into a format acceptable to MATLAB. Then the initial pressure signals are graphed, analyzed visually, to exclude obviously erroneous measurements, and processed to obtain the desirable acoustic characteristics, including the frequency spectra, relative insertion loss functions and single number insertion loss ratings. The code is divided into a main program named the "control panel" and supporting programs which are used to calculate the "processing functions" for different barrier top geometries and microphone-source positions. The free signal (no barrier), as well as signals diffracted by different barrier tops, are used in the calculations. The processing functions transform the initial oscilloscope voltage values into the sound pressure and these are used to calculate the appropriate spectra. The main control panel program then collects the relevant information from all processing functions and inputs it into the corresponding spectra analyses. For comparison, two different methods were used to calculate the frequency spectra from the initial data, namely, a standard fast Fourier transform and a 1/3rd octave filter. Additional functions are used to calculate relative insertion losses for each type of tops from the corresponding power spectra and to graph the relevant information. The 1/3rd octave filter was originally designed for MATLAB by Dr. Christophe Couvreur[24] and this code was modified to cover the higher frequency band (up to 80 kHz) required here by Dr. Tamas Zsedrovit. The measured pressure wave signals were input directly into the filter. A "filter function" and its sub functions were then used to calculate pressure power spectra. An additional function "IL" was used to calculate insertion loss spectra for each type of barrier top from

the corresponding power spectra and the relevant insertion loss function was plotted.

Appendix B. Spark Discharger

The spark gap trigger circuit was constructed using an automotive ignition coil as the high voltage source. A variable transformer was employed in this circuit to adjust the trigger voltage for repeatability and to eliminate false triggers. A 400 V TVS and a high voltage capacitor was placed in parallel with the trigger switch contacts as a "snubber" to clamp voltage spikes that could damage the switch contacts. When a pushbutton switch is closed, the automotive ignition coil is energized. When the same pushbutton is then opened, the sudden change of current flow in the primary side of the coil causes a high voltage in the secondary coil following Faraday's law of electromagnetic induction, and this is used to trigger the main spark gap by a partial ionization and breakdown of the air in the gap.

REFERENCES

1. Garai, M. and Guidorzi, P. (**2008**). "In situ measurements of the intrinsic characteristics or the acoustic barriers installed along a new high speed railway line.", Noise Control Eng. J. **56**(5) 342 – 355.

2. Fard, S. M., Kessissoglou, N., Samuels, S. and Burgess, M. (**2013**). "A review of road traffic barriers for low frequency noise", Proceeding of Meetings on Acoustics **19**(1) 040081.

3. May, D. N. and Osman, N. M. (**1980**). "Highway noise barriers - new shapes", J. Sound Vib. **71**(1) 73 – 101.

4. Okubo, T. (**2004**). "Edge-modified noise barrier", J. INCE Japan **28** 317 – 322.

5. Okubo, T. and Yamamoto, K.. (**2007**). "Procedures for determining the acoustic efficiency of edge-modified noise barriers.", Appl. Acoust. **68**(7) 797 – 819.

6. Parnell, J., Samuels, S. and Tsitsos, C. (**2010**). "The acoustic performance of novel noise barrier profiles measured at the roadside.", Acoust. Australia **38**(3) 123 – 129.

7. Shaffer, S. R. (**2014**). *Investigations of environmental effects on freeway acousticsc*, PhD Thesis - Arizona State University

8. Seznec, R. (**1980**). "Diffraction of sound around barriers: use of the boundary-elements technique", J. Sound Vib. **73**(2) 195 – 209.

9. Hothersall, D. C., Crombie, D. H. and Chandler-Wilde, S. N. (**1991**). "The performance of T-profile and associated noise barriers", Appl. Acoust. **32**(4) 269 – 287.

10. Ishizuka, T. and Fujiwara, K.. (**2004**). "Performance of noise barriers with various edge shapes and acoustical conditions", Appl. Acoust. **65**(2) 125 – 141.

11. Fard, S. M., Kessissoglou, N., Samuels, S. and Burgess, M. (**2013**). "Numerical study of noise barrier designs", Proceeding of Acoustics - Victor Harbor 17-20 November 2013

12. Menounou, P. and You, J. H. (**2004**). "Design of the jagged-edge noise barrier: numerical and experimental study.", Noise Control Eng. J. **52**(5) 210 – 224.

13. Koussa, F., Defrance, J., Jean, P. and Blanc-Benon, P. (**2013**). "Acoustic Performance of gabions noise barriers: numerical and experimental approaches", Appl. Acoust. **74**(1) 189 – 197.

14. European Committee for Standardization (**2015**). *EN1793-4 Road traffic noise reducing devices. Test method for determining the acoustic performance. Intrinsic characteristics. In situ values of sound diffraction*, Information on how CEN Standards can be obtained is available at http://www.cen.eu.

15. Menounou, P. and You, J. H. (**2004**). "Experimental study of the diffracted sound field around jagged-edge noise barriers", J. Acoust. Soc. Am. **116**(5) 2843 – 2854.

16. Picaut, J. and Simon, L. (**2001**). "A scale model experiment for the study of sound propagation in urban areas", Appl. Acoust. **62**(3) 327 –340.

17. Lamothe, M. J. R. and Bradley, J. S. (**1985**). "Acoustical characteristics of guns as impulsive sources", Canadian Acoust. **13**(2) 16 – 24.

18. Papadopoulos, A. I. and Don, C. G. (**2001**). "A study of barrier attenuation by using acoustic impulses", J. Acoust. Soc. Am. **90**(2) 1011 –1018.

19. Watts, G. R., Hothersall, D. C. and Horoshenkov, K. V. (**2001**). "Measured and predicted acoustic performance of vertically louvered noise barriers", Appl. Acoust. **62**(11) 1287 – 1311.

20. Qin, Q. and Attenborough, K. (**2004**). "Characteristics and application of laser-generated acoustic shock waves in air spark dischargers", Appl. Acoust. **65**(4) 325 – 340.

21. Yuldashev, P., Ollivier, S., Averiyanov, M., Sapozhnikov, O., Khokhlova, V. and Blanc-Benon, P. (**2010**). "Nonlinear propagation of spark-generated N-waves in air: modeling and measurements using acoustical and optical methods", J. Acoust. Soc. Am. **128**(6) 3321 – 3333.

22. Klinkowstein, R. E. (**1974**). *A study of acoustic radiation from an electrical spark discharge in air.*, Doctoral Dissertation, Massachusetts Institute of Technology. **73**(2) 195 – 209.

23. Ayrault, C., Béquin, P. and Baudin, S. (**2012**). "Characteristics of a spark discharge as an adjustable acoustic source for scale model measurements.", Société Française d'Acoustique. Acoustics 2012, Apr 2012, Nantes, France. ¡hal-00810828¿.

24. Couvreur, C. "Implementation of a one-third-octave filter bank in Matlab". http://citeseer.ist.psu.edu/24150.html

25. Maekawa, Z. (**1968**). "Noise reduction by screens", Appl. Acoust. **1**(3), 157 – 173.

26. Kurze, U. J. and Anderson, G. S. (**1971**). "Sound attenuation by barriers", Appl. Acoust. **4**(1) 35 – 53.

27. Kurze, U. J. (**1974**). "Noise reduction by barriers", J. Acoust. Soc. Am. **55**(3), 504 – 518.

28. Pierce, A. D. (**1974**). "Diffraction of sound around corners and over wide barriers", J. Acoust. Soc. Am. **55**(5), 941 – 955.

29. Pierce, A. D. (**1991**). *Acoustics. An introduction to its physical principles and applications.*, Am. Inst of Physics, New York.

30. Jonasson, H. G. (**1972**). "Sound reduction by barriers on the ground", J. Sound Vib. **22**, 113 – 126.

31. Salomons, E. M. (**1997**). "Sound propagation in complex outdoor situations with a non-refracting atmosphere: model based on analytical solutions for diffraction and reflection", ACUSTICA Acta Acustica **83**, 436 – 454.

32. European Committee for Standardization (**1997**). *EN1793-3 Road traffic noise reducing devices - Test methods for determining the acoustic performance - Part 3: Normalized traffic noise spectrum*, Information on how CEN Standards can be obtained is available at http://www.cen.eu

33. Garai, M. and Guidorzi, P. (**2000**). "European methodology for testing the airborne sound insulation characteristics of noise barriers *in situ*: experimental verification and comparison with laboratory data.", J. Acoust. Soc. Am. **108**(3) 1054 – 1067.

34. Ho, S. S. T., Busch-Vishniac, I. J. and Blackstock, D. T. (**1997**). "Noise reduction by a barrier having a random edge profile", J. Acoust. Soc. Am. **101**(5) 2669 – 2676.

35. Pigasse, G. and Kragh, J. (**2011**). *Optimised noise barriers*, Danish Road Directorate, Ministry of Transport, Report 194 **108**(3) 1054 – 1067.